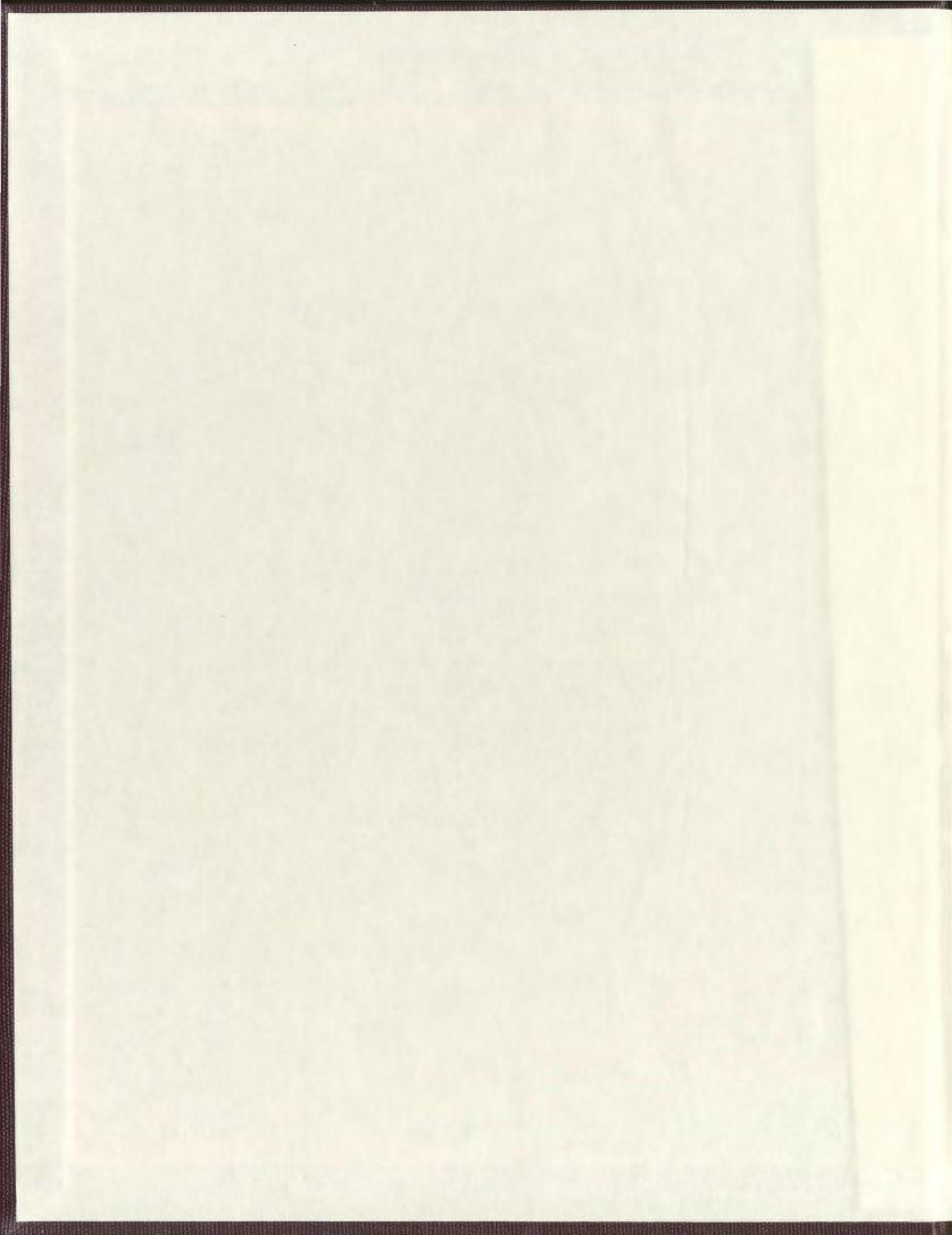


PROVENANCE OF THE BEN NEVIS FORMATION  
SANDSTONES, WHITE ROSE FIELD, JEANNE D'ARC BASIN,  
NEWFOUNDLAND, CANADA

ANGELA DEARIN





**Provenance of the Ben Nevis Formation sandstones, White Rose Field,  
Jeanne d'Arc Basin, Newfoundland, Canada**

by

Angela Dearin

A Thesis submitted to the  
School of Graduate Studies in  
partial fulfilment of the  
requirements for the degree of  
Master of Science

Department of Earth Sciences  
Memorial University of Newfoundland

March 2007

St. John's

Newfoundland



## Abstract

This study focuses on the changes of sediment provenance with time, within and adjacent to selected reservoir intervals of the Aptian Ben Nevis Formation in the White Rose Field, Jeanne d'Arc basin. The field contains both oil and gas, and the reservoir rock is a very-fine- to fine-grained, generally well-sorted sandstone with variable thicknesses of up to 300 m. Average QFL ratios for Ben Nevis sandstones are  $Q_{89}F_3L_8$ , with the major lithic components being detrital carbonate grains and chert. Based on subcrop patterns and relative grain sizes, the Tithonian-Berriasian Hibernia Formation sandstones and the Barremian-Aptian Avalon Formation sandstones are thought to be possible sediment sources.

Tectonic discriminative diagrams as well as petrographic descriptions give evidence of a very small amount of feldspar and indicate that the Ben Nevis Formation is not a first cycle sediment; rather, abraded quartz overgrowths indicate that Ben Nevis Formation sandstones are polycyclic and were sourced from recycled sediments. In addition, the Chemical Index of alteration (CIA) diagram can be used to show that the original basement of igneous and/or metamorphic rocks that acted as sediment source for the Ben Nevis Formation must have been of granodiorite composition.

The Avalon Formation is petrographically and geochemically similar to the Ben Nevis Formation. Cuttings samples show a similar grain size and chemical composition to the Ben Nevis Formation, indicating that the Avalon Formation is a plausible source for the Ben Nevis Formation without requiring significant reworking or alteration.

Possible sources with a higher lithic component, such as the Hibernia Formation, imply geochemical alteration with only limited physical reworking of the rock, which removed a large portion of unstable lithic grains and increased the quartz content relative to feldspars and lithic grains, leading to the quartz-rich composition of the Ben Nevis Formation. This process is supported by trace element data and plots of  $\text{SiO}_2$  against immobile elements, together with common exposures of Hibernia Formation below the Aptian unconformity. Together with erosion of the Upper Hibernia Formation, detrital carbonate grains may have been added from underlying A-marker and/or B-marker units. Based on weathering relationships inferred from CIA diagrams, the remaining (presently preserved) sections of Lower Hibernia Formation were ultimately sourced from a more mafic basement, which is not reflected in the composition of upper Hibernia, Avalon, and Ben Nevis Formation sandstones.

The Ben Nevis Formation is a relatively homogeneous sandstone with very subtle changes both petrographically and geochemically. Grouping of similar Zr concentrations within the Ben Nevis Formation has shown three correlatable units throughout the White Rose Field. Trends on CIA diagrams indicate an increasing amount of weathering moving from the south to north, perhaps due to lower topographic gradients in the north, causing longer residence times and hence increases in chemical weathering. P/K ratios are also lower in the north area, indicating a mature sediment source during early transgression in the north which became progressively less mature as transgression moved southward.

## **Acknowledgements**

I would like to thank my supervisors: Dr. Rudi Meyer and Dr. Michael Enachescu for their help, advice and stimulating discussions and constructive criticism throughout this project; it greatly improved the quality of this manuscript. I would also like to thank Elizabeth Wilson for helping to set up this project, as well as for all of her advice and extensive knowledge of this study area.

Financial support for this project was provided by PetroCanada, the Pan Atlantic Petroleum Consortium (PPSC), and Dr. Rudi Meyer (NSERC grant) and is gratefully acknowledged. Data was provided by PetroCanada, Husky Energy and Canada Newfoundland and Labrador Offshore Petroleum Board (C-NLOPB).

My sincere thanks to Pam King, for all her help with the geochemical sampling. Special thanks to my officemate Erin Gillis for being a sounding board and for all the “networking” sessions. Finally, I would like to thank my parents, Victoria, Leon, Allison, Steve, Nikki and all of my friends and family for their support and encouragement over the past two years.

## Table of Contents

Abstract .....	i
Acknowledgements .....	iii
List of Tables .....	vii
List of Figures .....	viii
List of Plates .....	xii
1. Introduction .....	1
1.1 Thesis Objectives and Purpose .....	1
1.2 Regional Geological Setting .....	2
1.3 Regional Tectonic Evolution .....	7
1.4 Regional Stratigraphy .....	11
1.5 The White Rose Oil Field .....	15
1.5.1 Introduction .....	15
1.5.2 White Rose Structure .....	17
1.5.3 White Rose Stratigraphy .....	19
2. Data Set and Methods .....	25
2.1 Introduction and Data Set .....	25
2.2 Petrography .....	28
2.2.1 Petrographic Samples .....	28
2.2.2 Gazzi Dickinson Point Counting Method .....	34
2.2.3 Assessing Uncertainty in Point Counting Results .....	36
2.2.4 Dickinson Tectonic Setting Criteria .....	36
2.3 Geochemistry .....	40
2.3.1 Geochemical Samples .....	40
2.3.2 The Chemical Index of Alteration .....	43
3. Petrography .....	47
3.1 Introduction .....	47
3.2 Petrographic Description of Framework Grains .....	48
3.2.1 Quartz .....	48
3.2.2 Plagioclase Feldspar .....	50
3.2.3 Potassium Feldspar .....	50
3.2.4 Sedimentary Rock Fragments .....	53
3.2.5 Mineral Grains .....	56
3.2.6 Authigenic Mineral and Cements .....	58
3.3 Petrographic Descriptions of Formations .....	60
3.3.1 Ben Nevis Formation .....	60
3.3.2 Hibernia Formation .....	63

3.3.3	Terra Nova and Lower Tempest Members .....	64
3.4	Quantitative Petrography .....	65
3.4.1	Point Counting Uncertainty .....	66
3.4.2	Ben Nevis Formation .....	67
3.4.3	Hibernia, Rankin and Jeanne d’Arc Formations.....	73
3.5	Grain Size Analysis.....	75
3.5.1	Introduction.....	75
3.5.2	Ben Nevis Formation .....	77
3.5.3	Hibernia Formation.....	81
3.5.4	Terra Nova Member and Lower Tempest Member .....	87
3.5.5	Grain Size Interpretations .....	89
4.	Geochemistry .....	91
4.1	Introduction.....	91
4.2	Contaminated Samples.....	92
4.3	Grain Size.....	97
4.4	Element Mobility .....	98
4.5	Geochemical Abundances .....	111
4.6	Geochemical Correlations.....	114
5.	Provenance of the Ben Nevis Formation .....	121
5.1	Tectonic Provenance.....	121
5.2	Chemical Index of Alteration to Constrain Sediment Source.....	133
5.2.1	Introduction.....	133
5.2.2	Ben Nevis Formation .....	134
5.2.3	Avalon and Eastern Shoals Formations .....	137
5.2.4	Hibernia and Jeanne D’Arc Formations .....	139
5.2.5	Summary of Weathering Trends .....	142
5.3	Potential Sources of Sediment .....	145
5.4	Pre-Mesozoic Basement Rocks as a Possible Primary Sediment Source .....	148
6.	Conclusions.....	156
	References.....	160

Appendix 1	Point Count Data .....	169
Appendix 2	Average Grain Measurements .....	178
Appendix 3	Standard Deviation for all samples .....	213
Appendix 4	X-Ray Fluorescence (XRF) Data .....	216
Appendix 5	Samples that were re-run (due to contamination) .....	239
Appendix 6	Chemical Index of Alteration (CIA) Data .....	242
Appendix 7	Gamma Ray Logs with immobile element values for all samples used in this study .....	253

## List of Tables

### Chapter 2

Table 2.1	Listing of all data and its source that was used in this study.....	26
Table 2.2	Point count data from Wilson and Webb, (1998) and Core Labs, (1982). .....	27
Table 2.3	Listing of all petrographic samples used in this study.....	31
Table 2.4	Grain parameters measured. ....	35
Table 2.5	Primary Detrital grain Parameters .....	38
Table 2.6	Lithic grain types (exclusive of chert and polycrystalline quartz). .....	39
Table 2.7	Number of geochemical samples taken in each formation. ....	41
Table 2.8	List of all major and trace elements measured by XRF technique, along with their associated limits of detection (Poisson limit of detection).....	43

### Chapter 3

Table 3.1	QFL ratios (following Pettijohn, 1975) for all thin sections analysed.....	61
Table 3.2	Classification of detrital sand grains.....	66

### Chapter 4

Table 4.1	List of contaminated samples.....	96
-----------	-----------------------------------	----

### Chapter 5

Table 5.1	QFL values for all samples (from Marsaglia and Ingersoll, 1992) for all samples.....	123
-----------	---	-----

## List of Figures

### Chapter 1

Figure 1.1	Sedimentary basins offshore Eastern Canada.....	3
Figure 1.2	Map of the Jeanne d’Arc Basin showing major structural elements and areas of hydrocarbon production .....	5
Figure 1.3	Significant discoveries map of Jeanne d’Arc Basin .....	6
Figure 1.4	Formal stratigraphy of the Jeanne d’Arc Basin.....	8
Figure 1.5	Map of the White Rose Field showing the three pools and delineation well locations. ....	16
Figure 1.6	Time structure map of the Composite Marker of the White Rose area. ....	18
Figure 1.7	Stratigraphy at the White Rose Field.....	20
Figure 1.8	Wells penetrating the Hibernia Formation at the White Rose Field. ....	22

### Chapter 2

Figure 2.1	Location map of data set and sample distribution.....	29
Figure 2.2	Cross section of wells used in study.....	30
Figure 2.3	Half width of exact upper and lower two-sided 95 percent confidence bound on observed percentage. ....	37
Figure 2.4	A-CN-K diagram with average chemical compositions of igneous rocks .....	46

### Chapter 3

Figure 3.1	QFL plot of Ben Nevis Formation samples.....	68
Figure 3.2	Cross section of the sampled wells in the White Rose Field. ....	69
Figure 3.3	QFL plots of Ben Nevis samples by well. ....	71
Figure 3.4	QPK plot of Ben Nevis samples.....	72

Figure 3.5	QFL plot of Hibernia Formation, Terra Nova Member and Lower Tempest member. ....	74
Figure 3.6	QPK plot of Hibernia, Jeanne d'Arc (Terra Nova Member), and Rankin (Lower Tempest Member) formations. ....	76
Figure 3.7	Grain size of samples from the Ben Nevis Formation in the White Rose Field.....	78
Figure 3.8	Grain size changes through the Ben Nevis Formation. ....	79
Figure 3.9	Width and height values from the Ben Nevis Formation. ....	80
Figure 3.10	Standard deviation of Ben Nevis Formation samples. ....	82
Figure 3.11	Average grain size for Hibernia Formation, Terra Nova Member, and Lower Tempest Member sandstones. ....	83
Figure 3.12	Width and height values from the Hibernia Formation.....	85
Figure 3.13	Standard deviation of the Hibernia Formation, Terra Nova and Lower Tempest Members. ....	86
Figure 3.14	Width and height values from the Terra Nova and Lower Tempest members .....	88
 <b>Chapter 4</b>		
Figure 4.1	$Al_2O_3$ - $K_2O$ and $K_2O$ - $Na_2O$ differences for samples from core.....	93
Figure 4.2	Contamination graphs for samples from cuttings of the Ben Nevis, Avalon, Eastern Shoals and Hibernia formation .....	95
Figure 4.3	Immobile element plots of $TiO_2$ , $Al_2O_3$ , Nb, and Y.....	100
Figure 4.4	Immobile element plots of Zr against Y, Nb, $Al_2O_3$ , and $TiO_2$ .....	101
Figure 4.5	$Al_2O_3$ - $TiO_2$ -Zr ratio diagram.....	104
Figure 4.6	Element plots of $Fe_2O_3$ , Ni, Cr, Mn, and V plotted against immobile element $TiO_2$ .....	105
Figure 4.7	$SiO_2$ plots against immobile elements $TiO_2$ , Y, $Al_2O_3$ and Nb.....	108
Figure 4.8	Harker Diagrams of major elements, $Na_2O$ , $K_2O$ , $MgO$ , $MnO$ , and, $CaO$ . ....	112

Figure 4.9	Cross Section of Ben Nevis Formation samples with associated Zr correlations. ....	116
Figure 4.10	Geochemical values from the Ben Nevis and Hibernia Formations in well K-19. ....	119
<b>Chapter 5</b>		
Figure 5.1	Tectonic setting diagram for samples from the Ben Nevis Formation. ....	122
Figure 5.2	Tectonic setting diagram for samples from the Avalon and Eastern Shoals formations. ....	126
Figure 5.3	Tectonic setting diagram for samples from the Hibernia and Jeanne d’Arc formations (including the Terra Nova Member). ....	128
Figure 5.4	Schematic cartoon depicting Late Triassic - Late Jurassic sediments being eroded off the Central Ridge into the Jeanne d’Arc Basin ....	132
Figure 5.5	Chemical Index of Alteration ternary plot for samples from the Ben Nevis Formation. ....	136
Figure 5.6	A.) $K_2O-Na_2O$ and $Al_2O_3-K_2O$ differences to determine contaminated samples. B.) Chemical Index of Alteration ternary plot for samples from the Avalon and Eastern Shoals Formations. ....	138
Figure 5.7	A-CN-K diagram for samples from the Hibernia, Jeanne d’Arc (Terra Nova Member) and Rankin (Lower Tempest Member) formations. ....	140
Figure 5.8	A-N-K diagram to show trends in the data if CaO was omitted .....	143
Figure 5.9	A-CN-K diagram for samples from all formations studied. ....	144
Figure 5.10	Map of Grand Banks showing infill of basins and basement outcrops (re-produced from Enachescu, 1988). ....	147
Figure 5.11	Map showing likely sediment history of late Triassic-Late Jurassic sediments .....	149

Figure 5.12	Map with 13 wells that penetrated basement rocks .....	152
Figure 5.13	Chromium and nickel values for samples from the Ben Nevis, Hibernia, Jeanne d’Arc (Terra Nova Member) and Rankin Formation (Lower Tempest sandstone). .....	155

## List of Plates

Plate 1. Detrital quartz grains .....	49
Plate 2. Detrital plagioclase feldspar grains.....	51
Plate 3 Detrital potassium feldspar grains .....	52
Plate 4. Detrital carbonate grains .....	54
Plate 5. Detrital rock fragments .....	55
Plate 6. Mineral grains .....	57
Plate 7. Authigenic minerals and cements .....	59

# **Chapter 1**

## **Introduction**

### **1.1 Thesis Objectives and Purpose**

The Ben Nevis Formation is a very important petroleum reservoir within the Jeanne d'Arc Basin, in particular within the White Rose Field. Considerable debate remains as to the depositional model and provenance for the White Rose Reservoir sands (Ben Nevis/Avalon Formation). The Ben Nevis Formation is an Aptian, siliciclastic, marginal marine succession that as a whole has been interpreted as a transgressive shoreface deposit. Overall the sediment source appears to be from the south of the field (E. Wilson, personal communication, 2004). However the influence of provenance and dispersal on reservoir quality (progressive changes in grain size and composition), and the implications of a provenance model on reservoir distribution are not well understood.

There have been numerous studies carried out on the Jeanne d'Arc Basin at a regional scale; however, there are very few published studies focusing on detailed aspects of the White Rose Field. This thesis aims to evaluate and describe the provenance of the Ben Nevis Formation sandstones within the White Rose Field with the premise that provenance and associated sediment transport is reflected in regional mineralogical and chemical trends. This study will investigate the change of provenance with time, within and adjacent to selected reservoir intervals of the Ben Nevis Formation in the White Rose Field, and will also look at how provenance and associated sediment transport is reflected in lateral trends. Questions that will be addressed are whether the sediments have been derived from more than one source area, how the sources may have evolved through time, and whether the sands were deposited directly, or if they are 2<sup>nd</sup> or multi-cycle sediments.

Optical petrography and major/minor element analysis (XRF) will be used to compare Ben Nevis Formation sandstones with underlying clastic deposits such as the Hibernia Formation. In addition, mineral and geochemical composition can be related to overall tectonic setting and/or weathering conditions at the sediment source.

## **1.2 Regional Geological Setting**

The continental margin of the east coast of Newfoundland has an area of approximately 36,000 square kilometres and hosts a series of northeast-trending interconnected Mesozoic rift basins separated by Precambrian and Palaeozoic basement highs (Figure 1.1). The Mesozoic basins of Eastern Canada were formed by rifting and seafloor spreading associated with the break-up of Pangea (Enachescu, 1987 and 1988; Tankard and Welsink, 1987). Rifting began in the central part of Pangea and progressively moved northward reaching Nova Scotia/Morocco and Newfoundland/Iberia/Ireland areas in the Late Triassic. Several parallel rift valleys interrupted by transfer faults were created across the Grand Banks and adjacent areas (Enachescu, 1992; Enachescu and Fagan, 2004).

The Jeanne d'Arc Basin is one of many Mesozoic sedimentary basins and sub-basins located offshore of Newfoundland. The Basin is situated on the northern section of the Grand Banks and contains Mesozoic sediments, preserved as synrift and passive margin sequences (Figure 1.1). This fault-bounded basin has a half graben geometry, plunges to the northeast and has an areal extent of approximately 14,000 square kilometers. It is bounded to the west by the Bonavista Platform, to the east by the Central



Figure 1.1 - Sedimentary basins offshore Eastern Canada (From Enachescu,1992). The Jeanne d'Arc Basin is located approximately 350km from St John's. Mesozoic basins are separated by Precambrian and Paleozoic highs

Ridge Complex, to the south by the Avalon Uplift, and to the north by the Cumberland Belt. During the rifting phase communication existed between the Jeanne D'Arc, Flemish Pass and Orphan basins (Enachescu et al., 2005 and Figure 1.2). It is the deepest basin on the Grand Banks with a Mesozoic-Cenozoic sedimentary succession up to 20 km thick, with 14 km of that being syn-rift sediments (Enachescu, 1987; Keen et al., 1987; Tankard et al., 1989; Driscoll and Hogg, 1995).

There have been a total of 18 significant discoveries within the area of the Jeanne d'Arc Basin and the Central Ridge area (Figure 1.3). The majority of these discoveries were made in the early 1980's, following the discovery of the Hibernia oil field in 1979 (Hibernia P-15 well). Exploration and drilling targets have focused nearly entirely on structural traps such as that mapped at Hibernia, but all other major discoveries including the White Rose field are structural-stratigraphic traps (Enachescu and Fagan, 2004 and 2005). There are three major hydrocarbon-bearing reservoirs: a) the Upper Jurassic Jeanne d'Arc Formation sandstones, b) the Lower Cretaceous Hibernia Formation sandstones and c) the Lower Cretaceous Avalon/Ben Nevis Formation sandstones.

The source rock in the Jeanne d'Arc Basin is the regionally extensive Kimmeridgian Egret Member of the Rankin Formation. The Egret Member is oil prone and predominantly Type II/I kerogen, with lesser amounts of Type III kerogen. It has a gross thickness of 200-300m, an average TOC value of 3-4 % (maximum 8%) and a high hydrogen index of 500-600 mg/g (Williamson, 1992). The oil seen in this basin is sweet (~ 30 °API), with the exception of the Avalon/Ben Nevis reservoir in the Hebron Field, which has sweet and heavy oil of 21 °API (Department of Mines and Energy, 2000).

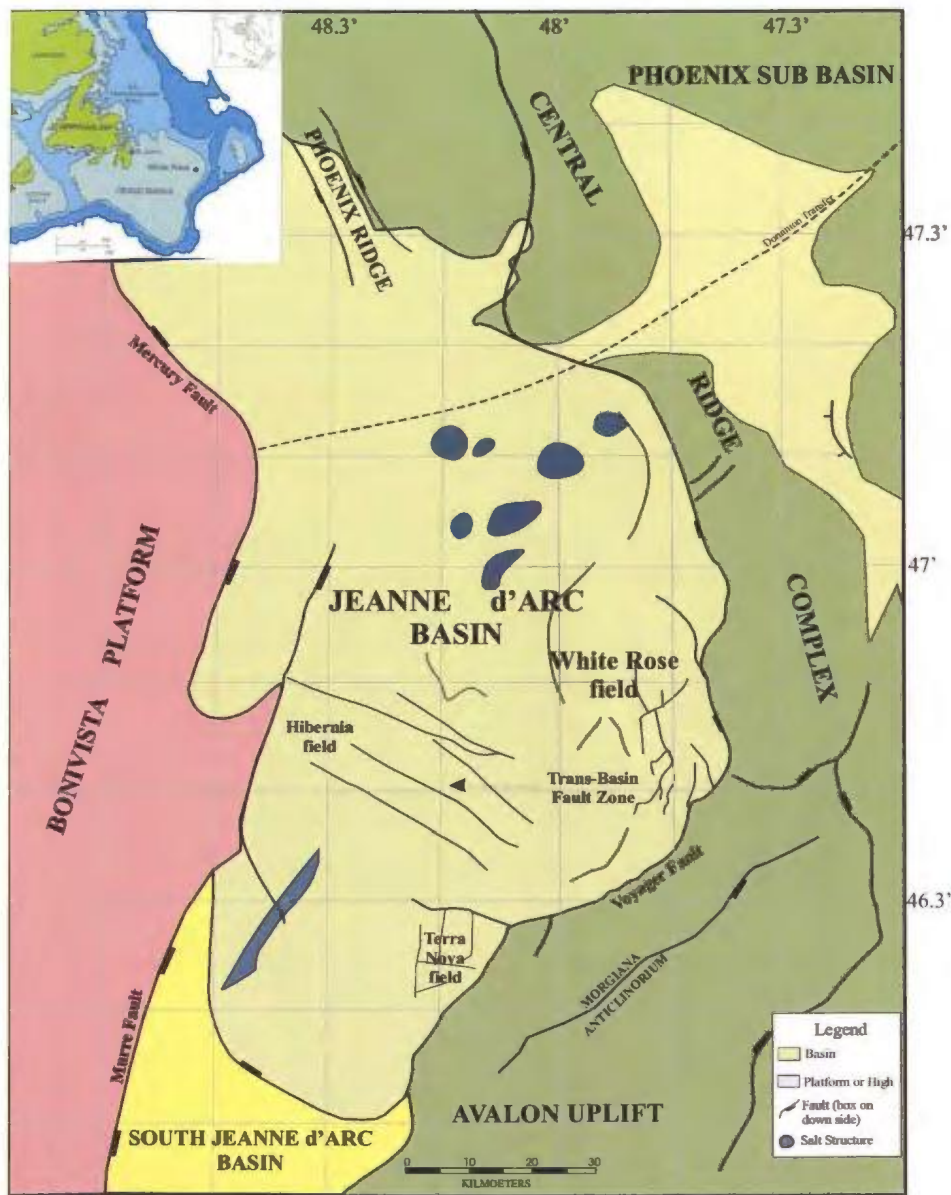


Figure 1.2 - Map of the Jeanne d'Arc Basin showing major structural elements with currently producing fields labelled. The Basin is bounded to the west by the Murre fault, the Mercury Fault, and the Bonavista Platform (Precambrian basement); to the east by the Voyager Fault, the Central Ridge Complex and the Morgania High); and to the south by the Avalon Uplift (modified from Enachescu, 1994).

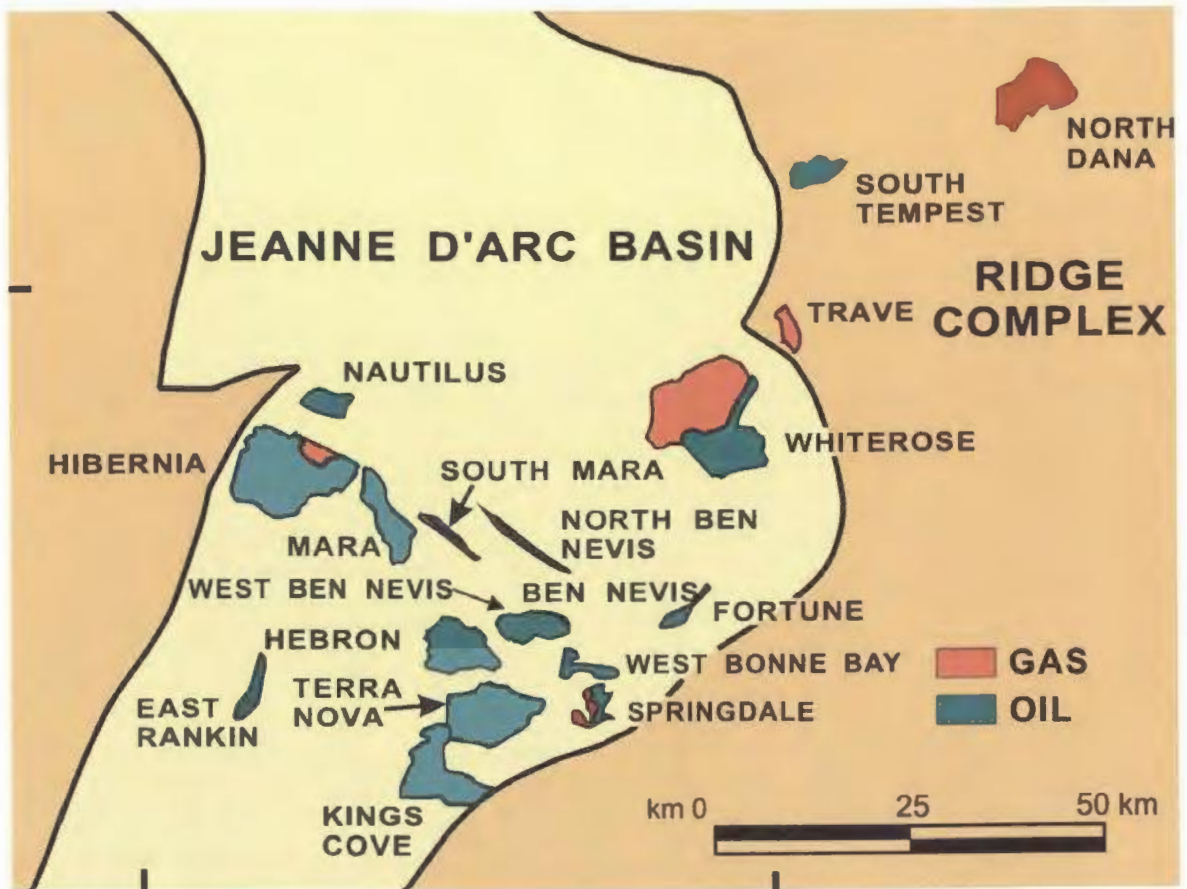


Figure 1.3 - Significant discoveries map of Jeanne d'Arc Basin (from Department of Mines and Energy, 2000).

Heavy oil is also seen in the East Rankin, Springdale and King's Cove discoveries. Oil density in the White Rose Field is 30 °API ([www.huskyenergy.ca](http://www.huskyenergy.ca)).

### **1.3 Regional Tectonic Evolution**

The Jeanne d'Arc Basin is one of several basins that formed during the rifting of North America from Eurasia (Enachescu, 1987). There is general agreement regarding the rifting events that affected the Jeanne d'Arc Basin. However, there are significant differences in the interpretation of the timing, type and range of the third tectonic phase. Several authors have identified two Mesozoic rift phases affecting the Grand Banks (Jansa and Wade, 1975; Wade, 1978; Hubbard et al., 1985; Hubbard, 1988; Tankard and Welsink, 1987, 1988; Tankard et al., 1989; and McAlpine, 1990). However Sinclair (1988), Enachescu (1986, 1987), Hiscott et al. (1990), Driscoll and Hogg (1995) and Driscoll et al. (1995) have identified three rift phases affecting the Grand Banks. Most interpretations of the third tectonic rift phase have been summarized by Sinclair (1993; Figure 1.4). This study will follow the interpretations of Enachescu (1987) and Sinclair (1988, 1993).

Rifting took place during three distinct events: 1) Late Triassic Tethys rift; 2) Iberia-Northern Europe rift at the end of the Jurassic, and; 3) Labrador rift and opening in the Late Cretaceous (Enachescu, 1987). The tectonic style column in figure 1.4 illustrates the various deformation styles related to these rifting stages which includes extension, normal and oblique-slip faulting, halokinesis, uplift and thermal subsidence (Sinclair et al., 1999).

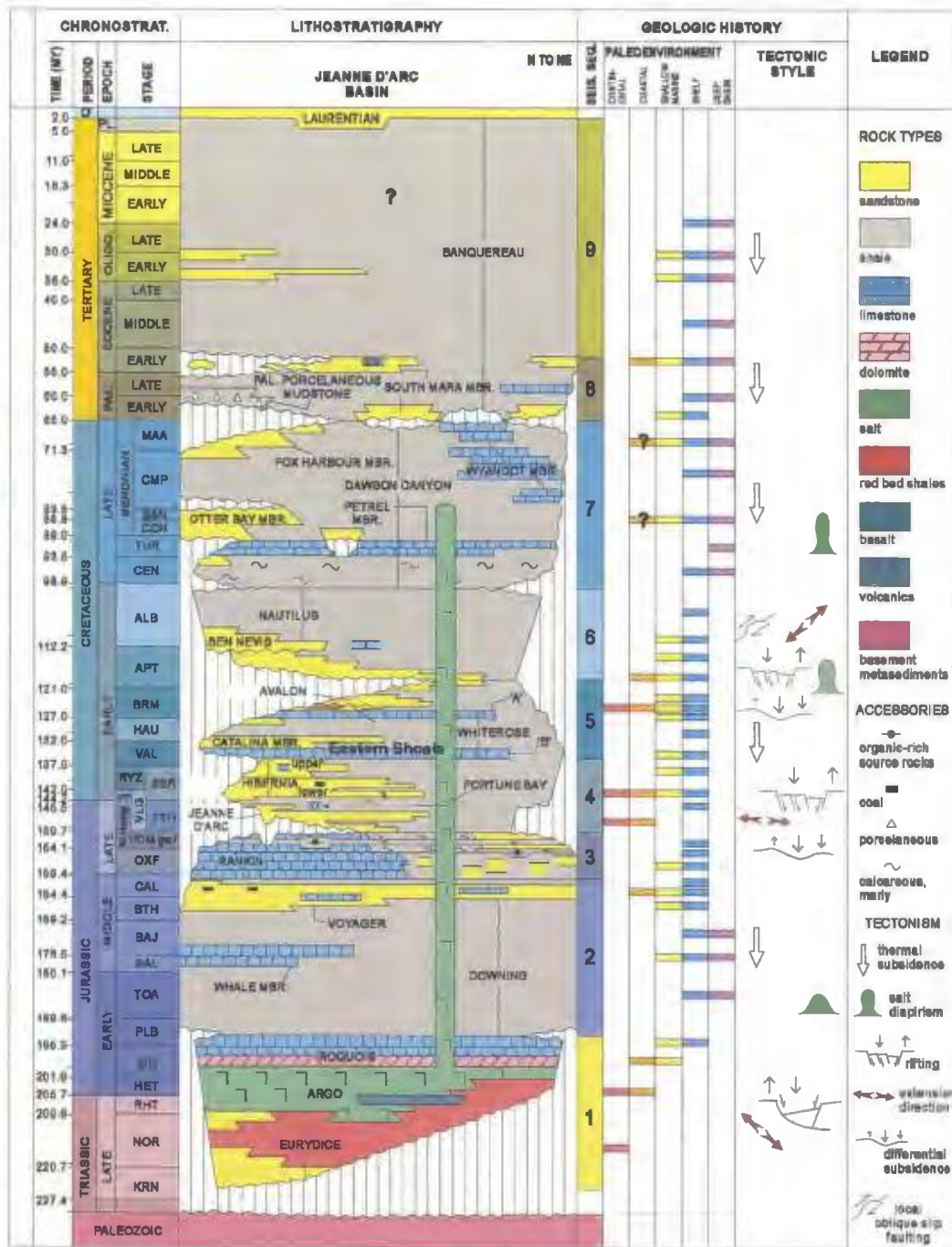


Figure 1.4 - Formal stratigraphy of the Jeanne d'Arc Basin correlated to the numerous tectonic features seen throughout the Mesozoic and Cenozoic, as well as paleoenvironmental interpretations (from Sinclair et al., 1999).

The pre-rift basement consists of Precambrian metamorphic and Palaeozoic metasedimentary and igneous rocks (Enachescu, 1987). These Precambrian rocks are a component of the Avalon terrane of the Appalachian Orogen (Williams and Hatcher, 1983). The Palaeozoic rocks range in age from Cambrian to Devonian or younger, and have an average thickness of 5-8 km (King et al; 1985, 1986).

The first rifting stage occurred in the Late Triassic and into the Jurassic and is known as the Tethys rift (Jenkyns, 1980; Lemoine, 1983; Bernoulli, 1984). During the onset of rifting the basement rocks underwent extensive block faulting, vertical movement and erosion (Enachescu, 1987). Deformation began in the Triassic with NW-SE extension and synchronous sedimentation, resulting in a series of NE-SW trending rift valleys (Arthur et al., 1982; Sinclair, 1988). Continental red beds and evaporites filled the basins of the Grand Banks and the latter are a reflection of repeated influxes of salt water from the Tethys Sea (Tucholke et al; 1989; McAlpine, 1990).

After the initial rift phase, regional thermal subsidence occurred resulting in a marine transgression. This transgression formed a broad epicontinental sea across the Grand Banks, depositing thick accumulations of shale and limestone. Near the end of this thermal subsidence phase (Late Jurassic) the organic-rich shale known as the Egret Member of the Rankin Formation was deposited in restricted anoxic basins.

The second rift phase; known as the North Atlantic rift took place near the end of the Late Jurassic and resulted in the separation of the Eastern Grand Banks from Iberia with separation in the Early Cretaceous (Enachescu and Fagan, 2004, Figure 1.4). This rifting phase rejuvenated extension along major faults as well as created new depositional areas. During this time the continental crust below the Grand Banks began to arch

upwards in a southeasterly direction due to an isostatic response to the changed rift pattern (Kerr, 1985). This is known as the Avalon Uplift and is thought to result in erosion of older, coarse-grained sediments into the basin above the Tithonian Unconformity, a regional, angular unconformity that demarcates this period of renewed uplift/extension.

During the Tithonian – early Valanginian period N-NNE-trending normal faults were common, indicating E-W to ESE-WNW tension across Iberia and the Grand Banks (Sinclair, 1988). The appearance of the Central Ridge structure represents the initial isolation of the Jeanne d’Arc Basin from the northern section of the Flemish Pass area to form two distinct, separate basins (Sinclair, 1988). Other basins that were formed during the Late Jurassic – Early Cretaceous include the Anson Graben and the southern portion of the Flemish Pass Basin. The deposition of the Valanginian “B” marker member limestone above the Hibernia Formation indicates a period of rapid, regional thermal subsidence following a break-up event (Sinclair, 1988)

The third and final rift stage took place during the mid-Aptian to late Albian (Enachescu, 1986, 1987; Sinclair, 1988). During this period NE-SW extension took place, as well as growth on the NW-SE trending (“trans-basin”) normal faults within the Jeanne d’Arc Basin (Enachescu, 1988; Sinclair, 1993, 1994). Seafloor spreading advanced northward, eventually separating Greenland from Labrador during the Campanian (Srivastava, 1978). Through the lower Cretaceous a series of marginal marine and fluviodeltaic sequences were deposited, including the Avalon and Ben Nevis sandstones (Department of Mines and Energy, 2000).

During the Late Cretaceous, tectonic activity was limited to regional thermal subsidence and the relatively undisturbed Cenozoic sediments were deposited across the shelf (Department of Mines, 2000; Enachescu and Fagan, 2004).

Major episodes of basin infill within the Jeanne d’Arc Basin occurred during two event types, extensional phases and thermal subsidence phases (Enachescu, 1987; Figure 1.4). Extensional phases include syn-rift Upper Triassic-Lower Jurassic sediments and Upper Jurassic-Lower Cretaceous failed rift or syn-rift deposits, and each of these are followed by relatively short-lived thermal subsidence phase, including the Upper Cretaceous to Cenozoic marine beds. Formation of the regional Albian–Aptian unconformity appears to coincide with another rifting episode (Sinclair, 1993). This unconformity separates the progradational Avalon Formation from the transgressive Ben Nevis and Nautilus Formations.

#### **1.4 Regional Stratigraphy**

Formal stratigraphy for the Jeanne d’Arc Basin has been proposed and repeatedly revised by Jansa and Wade (1975), Boudreau et al. (1996), Sinclair (1988), Tankard and Welsink (1988), Grant and McAlpine (1990), and McAlpine (1990) as well as numerous others. The stratigraphy used herein is based on McAlpine (1990) and the Canadian Newfoundland & Labrador Offshore Petroleum Board (CNLOPB) publications. The Mesozoic rocks below the Upper Cretaceous Dawson Canyon Formation have been divided into 17 formations, 3 members and 2 markers (McAlpine, 1990). The lithostratigraphic column of the Jeanne d’Arc Basin and general depositional paleoenvironments are also shown in Figure 1.4.

The Eurydice Formation is described as a Triassic red clastic sequence, dominated by reddish siltstone and shales containing scattered anhydrite nodules, with rare feldspathic sandstones (McAlpine, 1990). This is overlain by an evaporite sequence, known as the Argo Formation and followed by marine limestones of the Iroquois Formation. The Eurydice Formation marks the base of the Mesozoic section within the Jeanne d'Arc Basin and is thought to have been deposited in a continental setting during arid climatic conditions (McAlpine, 1990).

The Downing, Voyager and Rankin formations were deposited during the first of three thermal sag events (mid-Pliensbachian to Kimmeridgian). During this time a shallow epicontinental sea covered the Grand Banks and thick successions of shales and limestones from the Downing, Voyager and Rankin formations were deposited (McAlpine, 1990). Environments of deposition range from marginal marine deltaic to deeper marine, the latter providing the setting for the very important organic rich shale of the Egret Member of the Rankin Formation. The Egret Member is interpreted to have been deposited in restricted, anoxic bottom waters and represents the major oil source rock throughout the basin. This period of sag marks a hiatus in extension between the initial rifting and Late Jurassic reactivation of the rift system (Sinclair, 1988). The lower Tempest Member of the Rankin Formation is a thin sandstone reservoir interval with good reservoir quality and localized oil and gas shows (Enachescu, 2006).

Renewed extension and development of the Avalon Uplift during Kimmeridgian time resulted in erosion of rift shoulders and deposition of a large amount of clastic detritus into the basin. Two of the four main reservoir sandstones were deposited during this syn-rift episode – the Jeanne d'Arc and the Hibernia formations. Coarse clastics of

the Jeanne d'Arc Formation were deposited within fluvial-dominated incised valleys and include the coarse-grained Terra Nova Member. The Fortune Bay shales and siltstones were deposited in a marginal marine to neritic environment during a progradational period and may represent delta front and prodelta facies of the overlying Hibernia Formation (McAlpine, 1990). The Hibernia Formation consists of sandstone alternating with shale and siltstone. It was deposited in a northward-prograding deltaic system as medium- to very coarse-grained distributary channel deposits and very fine-to medium-grained delta front sands, including those interpreted for the Hibernia Oil Field (Brown et al., 1989).

The second thermal sag resulted in the deposition of the "B" marker limestone, an informal unit taken to indicate a period of basin stability. The "B" marker type section is described as massive, buff to light grey, oolitic/skeletal, lime grainstones and packstones and is an excellent regional stratigraphic and seismic marker. The fine-grained sandstones, siltstones, shales and minor limestones of the Catalina Formation and the thick silty shales of the White Rose Formation were also deposited during this time. The Catalina Formation is generally comprised of fine-grained clastics and shelly/oolitic limestone, representing marine shelf depositional settings (McAlpine, 1990). The regional "A" marker limestone consists mainly of limestones similar in composition to the "B" marker, with minor beds of calcareous sandstone, siltstone and shale. The "A" marker lies above the White Rose Formation and is seen at the Hibernia and White Rose fields. A thick succession of oolitic and bioclastic sandstones and limestones known as the Eastern Shoals Formation were deposited in the central and southern portions of the Jeanne d'Arc Basin (McAlpine, 1990). The upward-coarsening marine sandstones,

known as the Avalon Formation, were deposited on top of the White Rose and Eastern Shoals Formations. The Avalon Formation represents a period of basin-wide regression, possibly in response to renewed uplift of the southern end of the Jeanne d'Arc Basin (Sinclair, 1988) or a general uplift of the Atlantic Margin (Enachescu, pers comm. 2005). This uplift resulted in the development of the Aptian-Albian unconformity, which is prominently developed in the south and passes laterally into a conformable surface to the north.

The final episode of rifting and deformation to affect the continental crust of the Northern Grand Banks region occurred during Aptian-Albian time. Salt diapirism and fault activity were active during this time, resulting in local initiation of numerous salt ridges and pillars (Enachescu et al., 2000). Faulting during this time had a pronounced effect on the stratigraphic stacking patterns in the Jeanne d'Arc Basin, inducing highly variable rates of creation of accommodation space. This resulted in a long-term transgression above the Aptian-Albian unconformity and deposition of the marginal marine to shallow marine sandstones of the Ben Nevis Formation (Sinclair, 1993). The Ben Nevis Formation grades both laterally and vertically into the Nautilus Shale, which is described as the deposits of a low energy, open marine shelf environment (McAlpine, 1990). The Ben Nevis Formation is the youngest of the prolific hydrocarbon-bearing reservoirs in the Jeanne d'Arc Basin and, being the subject of this study, will be discussed in more detail below.

During Cenomanian time the basin was subsiding and starved of clastic input, leading to the deposition of the lower Dawson Canyon Formation and the Petrel Member lime mudstones. This time also marks the initiation of the final thermal sag over the

basin. The unconformity at the base of the Cenozoic marks the top of the Upper Cretaceous succession. This unconformity exhibits channel forms and canyons on the shelf edge margin and records a significant drop in relative sea level or a regional rebound of the Atlantic margin (Enachescu and Hogg, 2005). Throughout the Cenozoic, depositional patterns are indicative of a passive margin flanking the spreading Atlantic Ocean (Deptuck et al., 2003). Low sediment input and long term subsidence resulted in the deposition of a structurally undisturbed marine succession (McAlpine, 1990); however, some fault readjustment and salt movements affected the Jeanne d'Arc Basin (Enachescu, 1987; Enachescu and Fagan, 2004).

## **1.5 White Rose Oil Field**

### **1.5.1 Introduction**

The White Rose field is one of the largest of eighteen (18) significant discoveries in the area of the Jeanne d'Arc Basin (Figure 1.3). It is located on the northeastern flank of the Jeanne d'Arc Basin (Figure 1.2) approximately 350 km east of St John's, Newfoundland. It is located in 121 m of water and is the fourth largest oil field discovered on the Grand Banks. The White Rose oil and gas field was discovered in November 1984 by the drilling and testing of the Husky-Bow Valley et al. White Rose N-22 well. The field is divided into three pools; the South White Rose pool, the North White Rose pool, and the West White Rose pool (Enachescu et al., 2000; Figure 1.5). The focus of present development is on the South pool, which covers approximately 40 km<sup>2</sup> and contains an estimated 275 million barrels of oil, 2.091 TCF of natural gas and 77 million barrels of natural gas liquids (NGL) (Department of Mines and Energy, 2000).

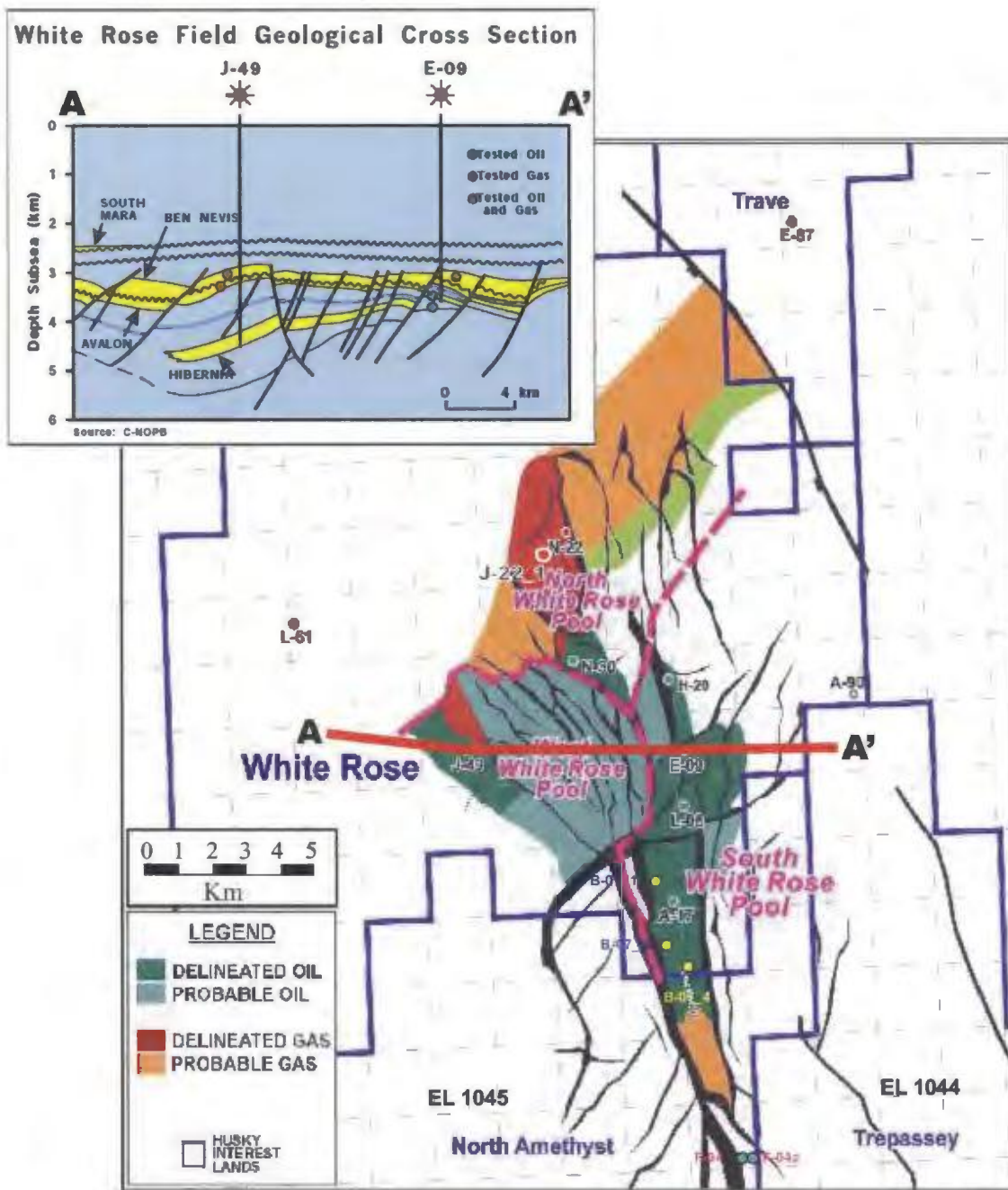


Figure 1.5 - Map of the White Rose Field, showing the three pools and delineation well locations. Cross section A-A' outlines style of trapping mechanism associated with the White Rose Field (From Department of Mines and Energy, 2000; Husky Energy, 2001).

There are currently three exploration wells, six delineation wells and eight scheduled development wells in the White Rose field. Production began in November 2005.

The reservoir is within the Aptian Ben Nevis Formation, which consists of fine-to very fine-grained quartzose sandstones that have a variable thickness of 100 to 300 m. The source rock is the Kimmeridgian marine shale of the Egret Member of the Rankin Formation. The conformably overlying siltstones and calcareous shales of the Nautilus Formation provide the regional seal.

### **1.5.2 White Rose Structure**

The White Rose area was affected by three episodes of rifting. The Osprey/Argo salt beds were deposited in the first phase. Based on structural analysis of seismic data these salt beds are interpreted to have been tectonically mobilized to form elongate walls parallel with the emerging Central Ridge during the second phase (Enachescu et al., 2000; Husky Energy, 2001). During the third rifting phase the salt ridge was divided by salt withdrawal to form the Amethyst ridge and the Northern White Rose diapir (Husky Energy, 2001). Imbricate segments of the Voyager Fault created low blocks and terraces where the Avalon and Ben Nevis formations were deposited, and high blocks where they were subject to erosion (Husky Energy, 2001). Near the end of the extensional stage, two salt withdrawal synclines were formed in the area (Trave syncline and Grand Bruit low), and the Amethyst Ridge and White Rose Diapir were elevated by salt and subjected to erosion (Husky Energy, 2001; see Figure 1.6). Due to lack of a consistent seismic marker in the field, a composite regional marker was interpreted by Enachescu et al., (2000).

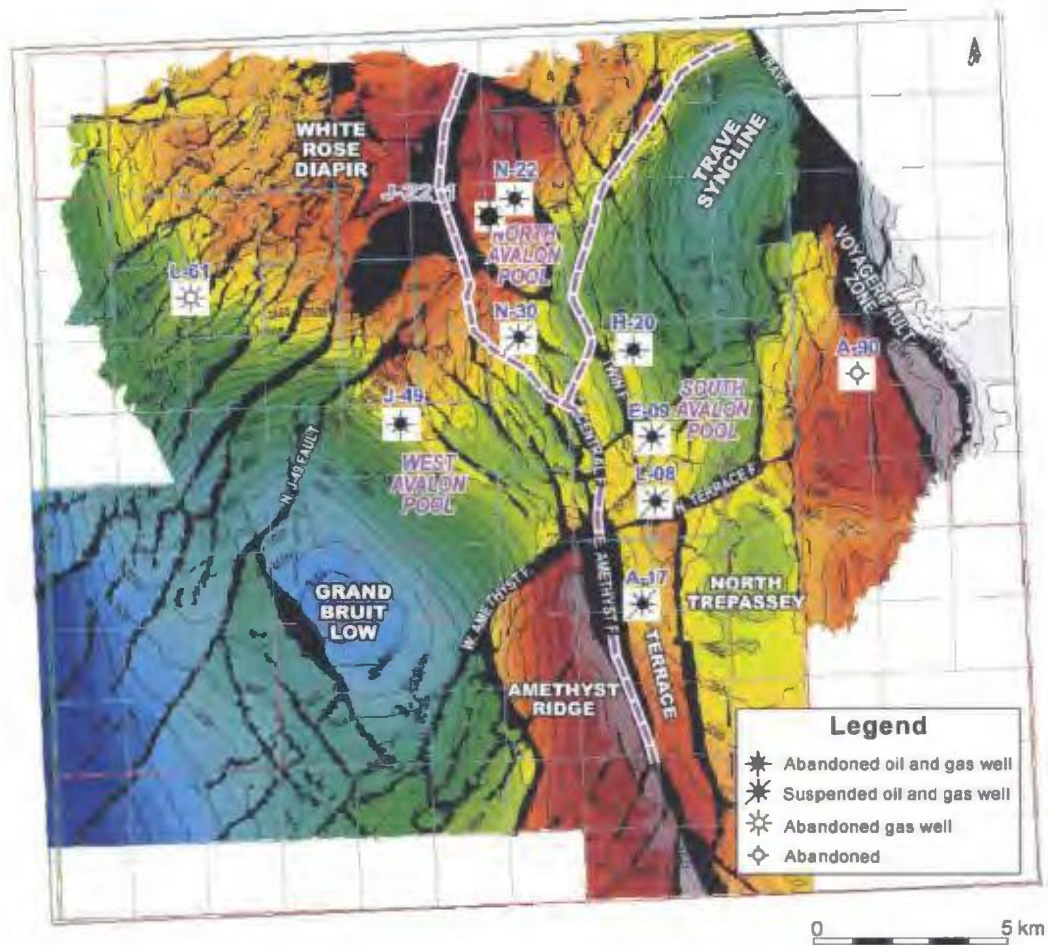


Figure 1.6 - Time structure map of the Composite Marker of the White Rose area (from Husky Energy, 2001). All faults, ridges, diapirs and lows that limit the field and are used to separate the three pools in the White Rose field are shown. The South White Rose Pool is currently the major focus of development; it is limited by the East Amethyst, Central and Twin faults to the west and dip closure to the north and east.

This marker varies from the upper Hauterivian – lower Barremian “A” marker in the west to the base Avalon in the central area. The Mid-Kimmeridgian unconformity to Base Tertiary unconformity markers were mapped in the eastern section of the field. The Regional Composite Marker time structure map shows the main structural elements of the White Rose area that were described above (Figure 1.6). Overall, the White Rose structure consists of faulted Jurassic and Early Cretaceous sediments located on the eastern margin of the Jeanne d’Arc Basin and is draped by Upper Cretaceous and Cenozoic sediments (Figure 1.5). The field resides in a structurally complex faulted area located on the hanging wall of the Voyager Fault and situated above the deep seated Amethyst salt ridge and White Rose Diapir (Husky Energy, 2001). The complex faulting system has compartmentalized the field into three pools, each with a complex structural trapping mechanism with a stratigraphic component seen in the southern and northern part of the field (Husky Energy, 2001).

### **1.5.3 White Rose Stratigraphy**

Wells in the White Rose field have penetrated Cenozoic through Upper Jurassic rocks (Figure 1.7). The oldest rocks are penetrated from the Bathonian to Oxfordian Voyager Formation (Well N-22) and are composed primarily of calcareous shales and siltstones (Husky Energy, 2001). The Oxfordian to Kimmeridgian Rankin Formation unconformably overlies the Voyager Formation. The Egret Member source rock and the Tempest Member sandstones of the Rankin Formation each have been penetrated only once by wells in the field (A-90 and E-09, respectively). The Kimmeridgian to Portlandian Fortune Bay Formation is found throughout the field and has been described

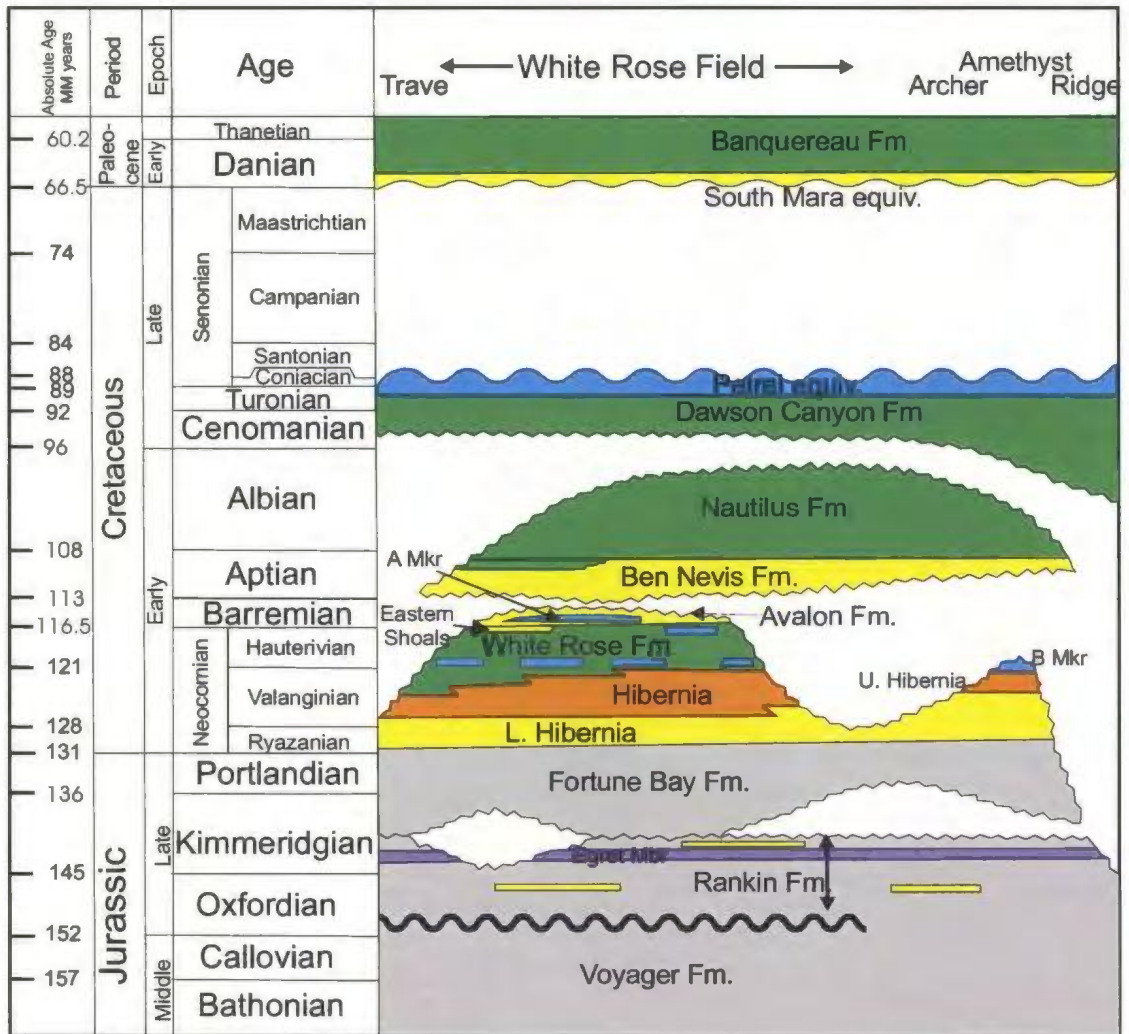


Figure 1.7 - Stratigraphy at the White Rose Field (Modified after Husky Energy, 2001).

White areas in the cross section are gaps along unconformities.

as predominantly grey, silty marine shales deposited as part of a major transgression in the Late Jurassic (Husky Energy, 2001).

The Berriasian Hibernia Formation has been penetrated in the White Rose A-17, E-09, N-22 and J-49 wells, as well as in the Amethyst F-20, Archer K-19, Gross Morne C-17, and Fortune G-57 wells south of the field, and in the Trave E-87 well in the north (Figure 1.8). The Hibernia sandstones form a regressive succession that is separated into an upper and lower member (Husky Energy, 2001). The upper member is not well developed in the White Rose Field and contains siltstones and shales with minor sandstones. The lower member has been penetrated in the E-09 and N-22 wells. It consists of fine-to-medium-grained, light grey/brown silty sandstone. In this part of the Jeanne d'Arc basin is interpreted to have been deposited as a prograding shoreface succession in a regionally regressive package, with only minor occurrence of fluvial and marginal marine deposits (Husky Energy, 2001).

The Hibernia Formation is conformably overlain by a regional transgressive package of marine shales known as the White Rose Formation, which includes the "B" Marker. It is a shelly limestone and is regionally correlatable through most of the Jeanne d'Arc Basin. However, it is thin and poorly developed at White Rose and is only seen in White Rose N-22, B-07-4, and E-09 wells and is eroded in the Archer K-19, White Rose A-17 and Trave E-87 wells (Husky Energy, 2001).

The Hauterivian to Barremian Eastern Shoals Formation unconformably underlies the Avalon Formation. It is present in the J-22-1, N-30, N-22, H-20, J-49 and L-61 wells. It is comprised of interbedded shale, siltstone and sandstone. The A Marker is a shelly

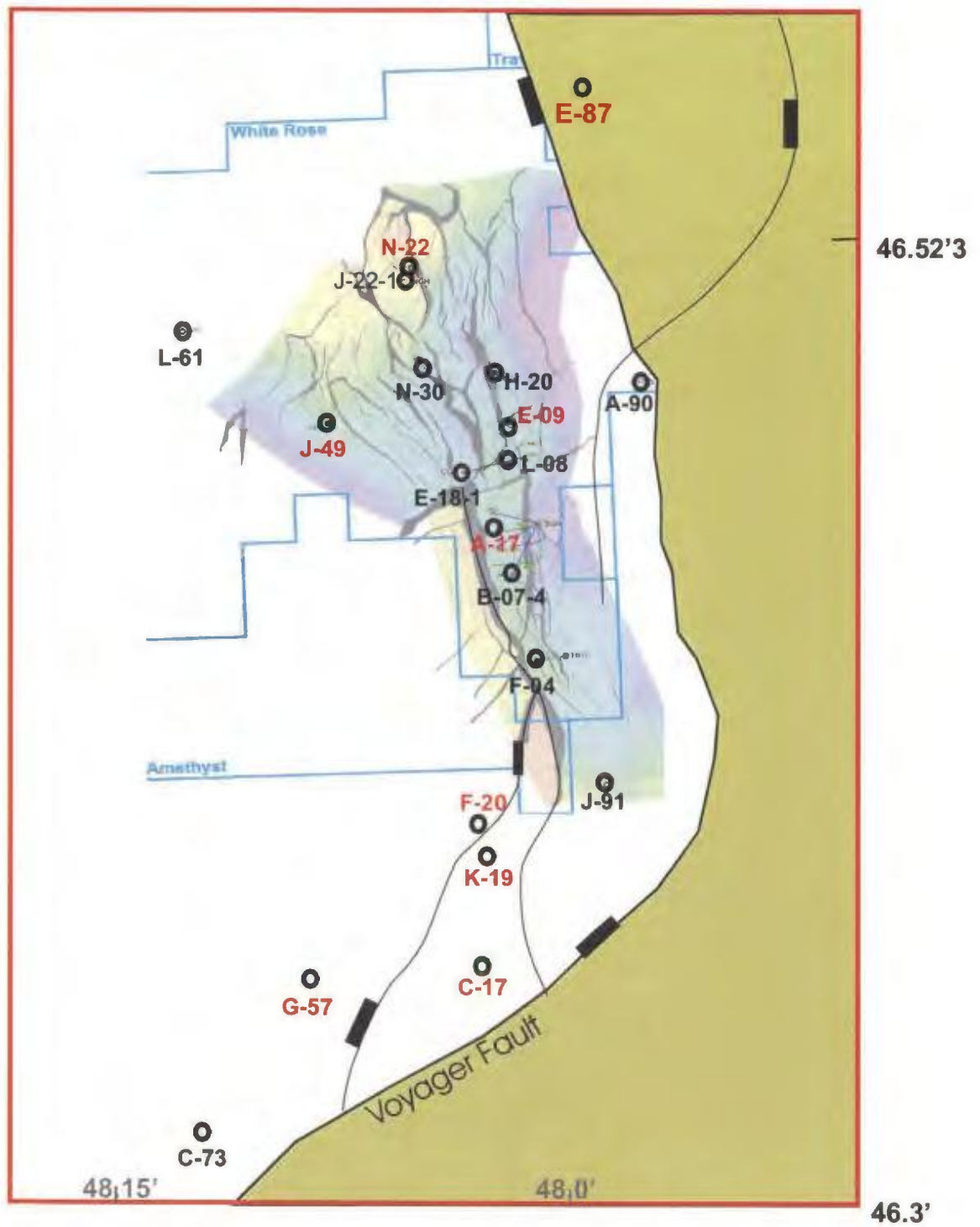


Figure 1.8 - Wells penetrating the Hibernia Formation (red labels) at the White Rose Field.

limestone within the Eastern Shoals Formation and is found in E-09, L-08, E-18-1, J-49 and L-61 wells.

The Aptian/Albian Ben Nevis and Avalon Formations are the most consistent hydrocarbon-bearing reservoirs in the Jeanne d'Arc Basin. The Avalon Formation has been described as a coarsening upward, progradational package, while the Ben Nevis Formation is described as a fining upward, transgressive package (McAlpine, 1990). Previous reports (Husky Energy, 2001) have defined the reservoir at White Rose to be either entirely Avalon Formation, or have assigned the reservoir sandstone to a loosely defined Avalon/Ben Nevis package. However, biostratigraphic data by Riley and Ainsworth (2003) have dated the reservoir sands in the White Rose field as Late Aptian and they have called them the Ben Nevis Formation. Only the lowermost sandstones in the H-20 well have been labelled as possible Avalon Formation sandstones or very lowest Ben Nevis sandstone. In light of this new data, the reservoir sandstones will be referred to as the Ben Nevis Formation in this study.

The Ben Nevis Formation at the White Rose Field represents a marginal marine shoreface succession, consisting of very fine-to fine-grained sandstones, siltstones and shales ranging in thickness from 100 to 400 m. Trace fossils have been used to aid in environmental interpretations. The trace fossil assemblages suggest a variety of brackish, marginal- and shallow-marine environments (Pemberton et al., 2001).

The Base of the Ben Nevis Formation is defined by the widespread, angular unconformity of latest Barremian to mid-Aptian. This unconformity marks the erosion of large amounts of sediment in the southern Jeanne d'Arc Basin, Central Ridge and Flemish Cap areas, and becomes less pronounced within the center of the basin until it

becomes a correlative conformity (Sinclair, 1993; Enachescu and Hogg, 2005). As a result, seismic reflector terminations or bedding dip changes are very difficult to identify in the White Rose Field, and biostratigraphic data becomes a key tool for differentiating the Avalon from the Ben Nevis Formation.

The Albian to Cenomanian Nautilus Formation conformably overlies the Ben Nevis Formation. It consists of grey siltstones and shales with minor sandstones, representing a low-energy open marine shelf environment, and making-up the seal rock over the Ben Nevis reservoir sandstones (Husky Energy, 2001).

The Cenomanian to Coniacian Dawson Canyon Formation unconformably overlies the Nautilus Formation. It consists of marls and calcareous shales and ranges in thickness from 100-500 m in the White Rose Field (Husky Energy, 2001). The Petrel Member occurs within the Dawson Canyon Formation. It consists of a thin light grey to brown argillaceous limestone and is present throughout the White Rose Field (Husky Energy, 2001).

The Banquereau Formation consists of Paleogene to Neogene clastics deposited during the final thermal subsidence stage. It is a marine shale sequence that can be up to 2,500 m thick. Coarser clastics are seen near the base, including the South Mara Member sandstone. The South Mara Member directly overlies the Base Tertiary Unconformity and has tested gas and condensate at the White Rose L-61 well (Husky Energy, 2001).

## **Chapter 2**

### **Data Set and Methods**

#### **2.1 Introduction and Data Set**

The main objective of this study is to investigate the change of provenance with time, within and adjacent to selected reservoir intervals of the Ben Nevis Formation in the White Rose Field. The premise is that provenance and associated sediment transport is reflected in mineralogical and geochemical trends. Optical petrography and major/minor element analysis (X-Ray Fluorescence) are used to compare the Ben Nevis Formation sandstones to those of the underlying Avalon, Eastern Shoals, Hibernia, Jeanne d'Arc (Terra Nova Member), and Rankin (Lower Tempest Member) formations to determine if one or more of these formations were possible sources of sediment for the Ben Nevis Formation at the White Rose Field.

Petrographic thin sections and samples for geochemical analyses were the primary materials for this study. Samples were taken from both cores and drill cuttings. Every effort was made to ensure that all core samples were taken approximately within the same grain size range (fine to very fine grained), as well as within clean sandstones with minimal amounts of mud or bioclastic debris. However this was not always possible due to different environmental settings in different formations (e.g. fluvial and fluvio-deltaic facies in the Hibernia Formation and shoreface facies in the Ben Nevis Formation). Samples were not taken near erosive surfaces or at bed boundaries in an attempt to avoid concentration of heavy minerals that is commonly seen at or near these surfaces.

Petrographic and geochemical samples were obtained from a number of sources (Table 2.1), including C-NLOPB, Husky Energy, Wilson and Webb (1998), and Core Laboratories Petrographic Services for Mobil Oil Canada (Core Laboratories 1982). All geochemical data was obtained from core and cuttings samples made available by CNLOPB.

Table 2.1 – Listing of data types and sources of data used in this study

<b>Data Source</b>	<b>Petrographic Thin sections</b>	<b>Geochemical Data (XRF)</b>
Core (new samples)	21	63
Cuttings (new samples)	70 (limited use)	255
C-NLOPB collection	8	0
Husky Energy collection	40 (Ben Nevis Fm.)	0
Wilson and Webb (1998), Core Laboratories (1982)	35	0
<b>Total</b>	<b>174</b>	<b>318</b>

A total of 174 petrographic thin sections were prepared in this study; however, thin sections of cuttings were not used in point counting due to poor sample quality and contamination. This resulted in 69 thin sections that were used for quantitative petrographic analysis. In addition, 35 samples were integrated into this study from the previous work of Wilson and Webb (1998) and a report by Core Laboratories Petrographic Services for Mobil Oil Canada (Core Laboratories, 1982) (Table 2.2). The study by Wilson and Webb (1998) analysed a number of samples from Jurassic and Cretaceous sandstones throughout the Grand Banks, including samples from the Ben Nevis, Avalon, Eastern Shoals, Hibernia and Jeanne d’Arc Formations and Core

Laboratories (1982) analysed thin sections from the Ben Nevis Formation in well I-13 of the Hebron Field.

Table 2.2 – Distribution of samples analyzed by Wilson and Webb (1998) and Core Laboratories (1982)

Well	Ben Nevis Formation	Avalon Formation	Eastern Shoals Formation	Hibernia Formation	Jeanne d'Arc Formation
I-78				1	
C60			4		
C96		2		3	
P-15					2
L-11		1		4	
K-08	1	2		8	
I-13	7				

A sample interval of 10 m was used to obtain thin sections for petrographic analysis in cored intervals of the Ben Nevis Formation in the White Rose field. Due to the sparse core coverage for the Hibernia Formation in the eastern section of the basin, a smaller, 5 m interval was used for sandstones from this formation. Similarly, a 5 m sampling interval was applied to cuttings samples. Cuttings samples tend to be fine grained and can be classified as siltstones. One shale sample from the Ben Nevis Formation was taken and all other samples are classified as sandstones. Every attempt was made to obtain clean sandstone samples containing minimal mud or bioclastic debris. Thin sections were prepared using 70 samples from cuttings; however, they were not useful for quantitative petrographic analysis due to poor quality (cavings and disaggregation). Sandstone samples were often disaggregated and point counting,

comparable to that of a sample from core was not feasible. Cavings were also present in these thin sections and in the absence of a consistent method to distinguish them from *in-situ* material, point counting of these thin sections was not possible.

A total of 318 samples for geochemical analyses by X-Ray Fluorescence (XRF) were collected from cores and cuttings. Figure 2.1 shows the map distribution of samples from various wells and the number of petrographic and geochemical samples taken from each well. Figure 2.2 is a cross section illustrating stratigraphic distribution of samples in each well, but omitting samples from the studies of Wilson and Webb (1998) and Core Laboratories (1982). Thin sections of cuttings are only shown in Figure 2.2.

## **2.2 Petrography**

### **2.2.1 Petrographic Samples**

Conventional core plugs and rotary sidewall core samples from numerous sources were used to make thin sections (Table 2.3). Samples from White Rose A-17, L-08 and H-20 wells were made available by Husky Energy, samples from well G-57 and C-73 are on-loan from CNLOPB, and remaining samples (wells J-22-1, F-04, and C-17) were cut from conventional core plugs and rotary sidewall cores made available by the CNLOPB. All thin sections were taken from the Ben Nevis, Hibernia, Jeanne d'Arc (Terra Nova Member), and Rankin formations (Lower Tempest Sandstones).

Petrographic samples were prepared by first vacuum impregnating with blue-dyed epoxy. Samples were then mounted on an optical glass slide and cut to a thickness of 30 microns (0.03mm). Samples from A-17, L-08 and H-20 (Husky Energy samples) were half stained with Alizarin Red S to distinguish calcite from dolomite and potassium



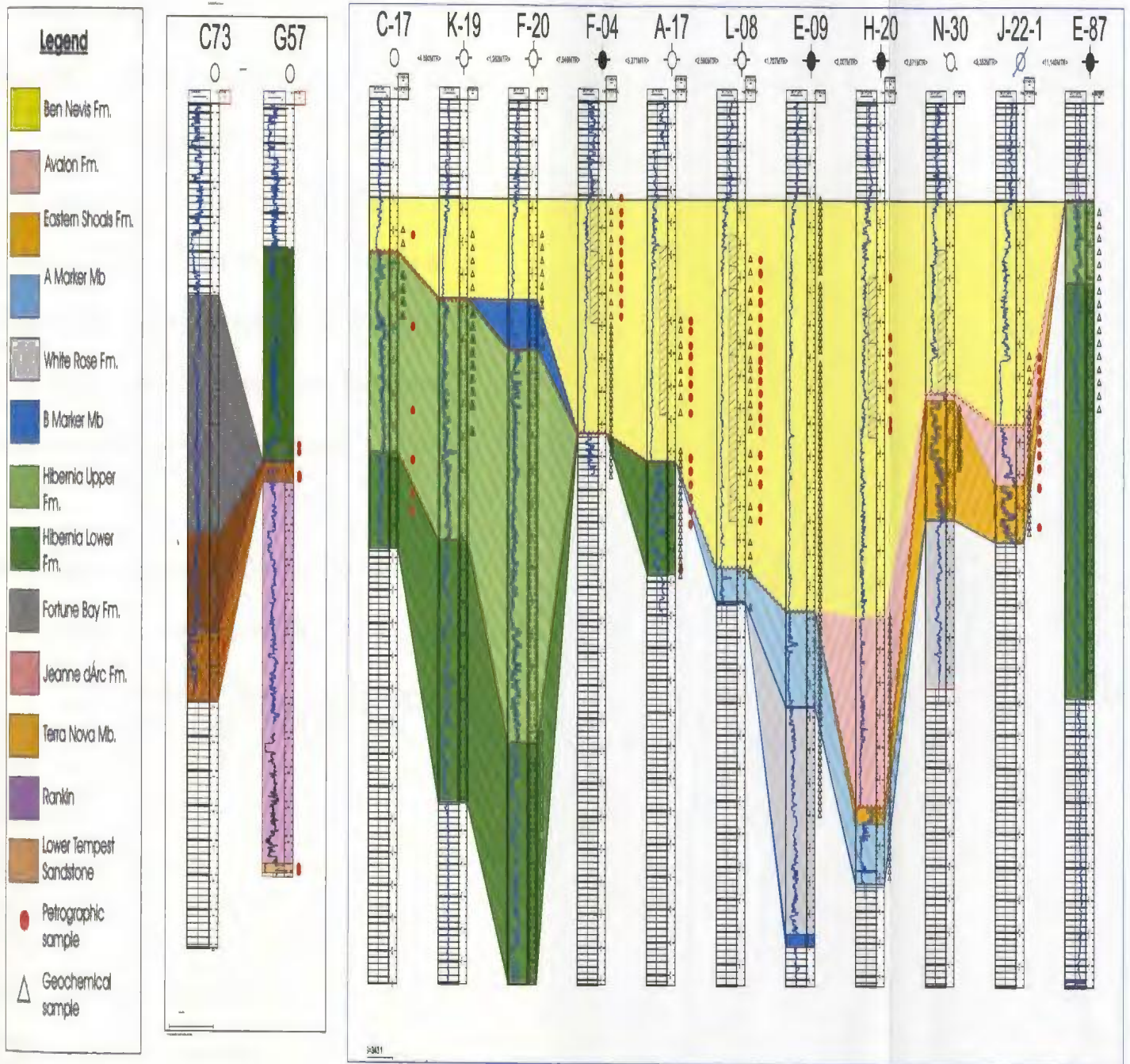


Figure 2.2 - Cross section of wells used in study (Blue line on Figure 2.1). Thin sections represented by red circles, geochemical samples (XRF) represented by black triangles

ferricyanide to distinguish ferroan varieties of calcite/dolomite. Dolomite will appear unstained, ankerite will appear deep turquoise blue, calcite will appear red/pink and ferroan calcite will appear mauve-purple or royal blue with increasing Fe content. Samples from wells J-22-1, F-04, C-17 and all cuttings were stained for calcite and feldspars. Staining for feldspar involves exposing the sample to 55% hydrofluoric acid solution for 1 min, and then treating it with a concentrated solution of sodium cobaltinitrite, about 50 g per 100 ml of distilled water. This reaction forms a yellow stain on the potassium feldspars, a white stain on the plagioclase feldspars, and the quartz is not affected. Samples borrowed from CNLOPB (wells G-57 and C-73) are polished thin sections and were impregnated with blue-dyed epoxy without any staining.

Table 2.3 – Listing of all petrographic samples used in this study. Thin sections prepared from cuttings were not used in point counting analysis.

Formation	From Previous Studies	On-loan		New (this study)	
		Husky	CNLOPB	Core	Cuttings
Ben Nevis	8	40		15	4
Avalon	5				8
Eastern Shoals	4				12
A Marker					10
White Rose					3
B Marker					5
Hibernia	16		2	6	28
Rankin					4
Rankin (L. Tempest)			4		
Jeanne d'Arc (Terra Nova Mb.)	2		2		
Sub-total	35	40	8	21	70
<b>Total</b>		<b>104</b>			<b>70</b>

Thin sections were analyzed using a Nikon Eclipse E600 petrographic microscope. Point counting was performed on all thin sections except cuttings due to their contamination (Appendix 1). Approximately 300 counts were taken for each thin section. Every attempt was made to ensure all samples were taken from clean sandstones with minimal amounts of bioclastic debris (e.g. serpulid worm tubes, mollusc shells) and cementation. All point counting data was plotted on ternary diagrams for rock classification and to derive tectonic setting. The Gazzi-Dickinson point counting method (see Section 2.2.1) was used to determine framework mineralogy.

Grain analysis was performed using commercial image analysis software Simple PCI<sup>®</sup>. This software allows detailed, accurate measurements to be taken of each grain in the field of view. All samples were photographed at 10X magnification, except the channel facies of the Hibernia and Jeanne d'Arc formations (G-57 and C-73 wells). These samples had a much larger grain size and were analysed at 4X magnification. Each grain in the photograph was digitally outlined by hand. After all grains in the photograph had been outlined it was saved as a 'Region of Interest' file (ROI). Simple PCI software was applied to these files in order to measure various parameters. The focus of this grain analysis was on grain size and sorting, and therefore the following parameters were measured:

- a. Length, the longest straight-line length along a curvilinear thin object, computed

$$\text{as: } \frac{1}{4} \left( \text{Perimeter} + \left( \sqrt{(\text{Perimeter})^2 - (16 \times \text{Area})} \right) \right);$$

- b. Width, the maximum dimension of the object in the X axis direction (horizontal on the screen).
- c. Height, the maximum dimension of the object in the Y axis direction (vertical on the screen).
- d. Equivalent circular Diameter of an object assumed to be circular, computed as:

$$\sqrt{\frac{2\pi}{Area}}$$

- e. Perimeter (the distance around the boundary of the object);
- f. Area (The object area is measured by counting the number of pixels in an object);
- g. Equivalent spherical volume of an object assumed to be a sphere, computed as:

$$\frac{4}{3} \left( \frac{\pi Diameter}{2} \right)^3;$$

- h. Elongation, aspect ratio of an object that is long and thin, computed as

$$\frac{Length}{Breadth};$$

- i. Breadth, average straight-line thickness of a curvilinear thin object, computed as

$$\frac{1}{4} \left( Perimeter - \left( \sqrt{(Perimeter)^2 - (16 \times Area)} \right) \right).$$

Although the image analysis program carries out these calculation based on pixels, pixel size is calibrated to a length scale in microns depending on the microscope magnification used. Grain measurements for all samples are listed in microns in Appendix 2.

The standard deviation ( $S_i$ ) of measured grain parameters was used to determine sorting. The inclusive graphic standard deviation was calculated to derive a measure of sorting (Folk, 1974):

$$S_i = \frac{(\phi_{84} - \phi_{16})/2 + (\phi_{95} - \phi_5)/3.3}{2}$$

Where  $\phi$  is the phi value corresponding to the  $n^{\text{th}}$  percentile. All standard deviation results for each sample are listed in Appendix 3.

### **2.2.2 Gazzi-Dickinson Point Counting Method**

Petrographic grain analysis was carried-out using the Gazzi-Dickinson point counting method to determine framework compositions. This method was developed independently by Gazzi (1966) and Dickinson (1970) and emphasises the use of petrography for reconstructing the original detrital composition. One assumption made by the above authors is that mineralogical composition of sand is primarily controlled by the nature of the parent rock; the possible influence of climate is not explicitly considered. The Gazzi-Dickinson method minimizes variation of composition with grain size, thus eliminating the need for sieving and multiple counts of different size fractions (Ingersoll et al., 1984). This method places greater emphasis on using petrographic techniques to reconstruct original detrital compositions independent of grain size (Ingersoll et al., 1984). The primary difference between the Gazzi-Dickinson method and the traditional method is that monomineralic crystals and other grains of sand size (>0.0625 mm) that occur within larger rock fragments are classified in the category of the crystal or grain, rather than in the category of the larger rock fragment (Ingersoll et al., 1984). This is done so modal composition does not change due to simple breakage of polycrystalline rock fragments and so that counting of poorly sorted or coarse-grained sand or sandstone is faster (Ingersoll et al., 1984). Parameters counted are listed in Table

2.4 and the application of these parameters to tectonic provenance is demonstrated by Dickinson (1970), Graham et al. (1976), Ingersoll (1978), Ingersoll and Suczek (1979), Dickinson (1985) and Marsaglia and Ingersoll (1992). For each thin section 300 points were counted (1 mm spacing) so as to cover the entire thin section.

Quartzose sandstones are described using QFL ternary diagrams to graphically represent compositions based on three end members; Quartz, Feldspar, and Lithic grains (Graham et al., 1976). Q is meant to represent the greatest stability and is the sum of monocrystalline quartz and chalcedony grains, and polycrystalline quartzite and chert. F represents the feldspar grains that are the most abundant of the unstable single-crystal grains. L is the sum of all the unstable grains (lithic or rock fragments), which are aphanitic grains excluding chert and quartzite.

Table 2.4 – Grain parameters measured (After Dickinson, 1970; Graham et al., 1976 and Ingersoll and Suczek, 1979).

<b>Sums</b>	<b>Symbols</b>	<b>Grain Types</b>
Q	Q	Total quartzose grains
	Qm	Monocrystalline quartz
	Qp	Polycrystalline quartz
	Qv	Volcanic quartz
F	F	Total Feldspar grains
	P	Plagioclase
	K	Potassium Feldspar
L	L	Total Lithic grains
	Ls	Sedimentary Lithic grains
	Lm	Metamorphic Lithic grains
	Lv	Volcanic Lithic grains
	Misc.	Miscellaneous and unidentified grains

### **2.2.3 Assessing Uncertainty in Point Counting Results**

Howarth (1998) presents charts to estimate upper and lower 95% confidence limits for given proportions based on point count data such as that generated in this study. For example, if we take  $n = 3$  as a commonly counted number of feldspar grains and  $N = 300$  is the total number of grains counted, then the charts shown in Figure 2.3 can be used to estimate the uncertainty for a 95% confidence interval (CI). Entering the observed percentage, 1%, on the ordinate, and  $N = 300$  on the abscissa, the estimated width of the lower half of the CI is 0.8 (Figure 2.3a), whereas that of the upper half is 1.9 (Figure 2.3b). Therefore there is a 95% probability that the true value of the parameter is between 0.2 and 2.9%. Similarly, for  $n = 200$ , a common number of quartz grains counted in the samples of this study, the observed raw proportion is 66.7%, and lower and upper bounds are -5.5% and +5.2%, respectively. The two examples give a good indication for the magnitude of the uncertainty of the point count results.

### **2.2.4 Dickinson Tectonic Setting Criteria**

Sandstone compositions are influenced by the character of the sedimentary provenance, the nature of the sedimentary processes within the depositional basin and the kind of dispersal paths that link provenance to the basin (Dickinson and Suczek, 1979). Dickinson (1970) has classified subquartzosic sandstones into 3 primary grain parameters that are used in provenance determination (Table 2.5). The primary parameters are:

- 1) Q – total quartz grains;
- 2) F – total feldspar grains, and
- 3) L – total unstable lithic fragments (aphanitic rock fragments).

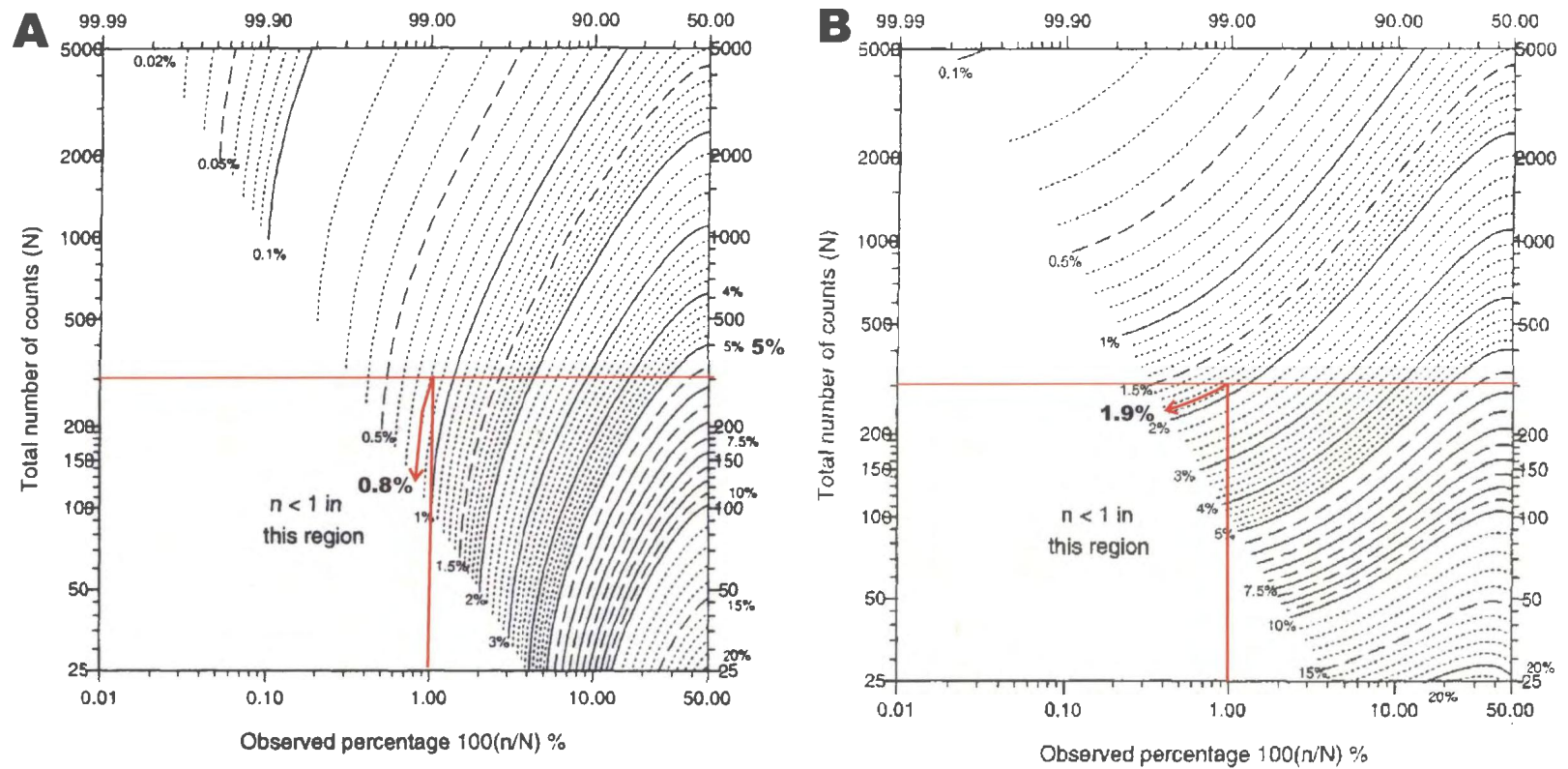


Figure 2.3 - A. Half width of exact lower two-sided 95 percent confidence bound on observed percentage. B. Half-width of exact upper two sided 95 percent confidence bounds on observed percentages (from Howarth, 1998). The lower 95 percent confidence limit is  $1-0.8 = 0.2$  percent, and the upper 95 percent confidence limit is  $1+1.9 = 2.9\%$ .

Table 2.5: Primary Detrital grain parameters (from Dickinson, 1970)

<b>(Q,F,L where Q+F+L=100)</b>	
<b>Q</b>	a) Monocrystalline quartz grains b) Polycrystalline quartz or chalcedony fragments c) cryptocrystalline opaline fragments
<b>F</b>	a) Plagioclase feldspar b) Potassium feldspar
<b>L</b>	Aphanitic rock fragments less quartzose, chalcedony, and opaline aphanitic fragments

Dickinson (1970) based the recognition of lithic fragments mainly on textural criteria. He classified lithic fragments into 5 categories that are independent of degree of alteration (Table 2.6). Heavy mineral grains are excluded because their distribution in detail is closely controlled by hydraulic properties related to the density and shape (Dickinson, 1970). Following Marsaglia and Ingersoll (1992) extrabasinal carbonate grains are included as sedimentary lithic fragments. Note that a number of early classification schemes to assign tectonic setting have excluded carbonate fragments to avoid the often difficult distinction of intra- and extra-basinal grains (*e.g.* Dickinson, 1970; Dickinson, 1985).

Table 2.6: Lithic grain types (exclusive of chert and polycrystalline quartz). Modified after Dickinson (1970).

1	Volcanic rock fragments	a) Felsitic b) Microlitic c) Lathwork d) vitric
2	Clastic rock fragments	a) Silty-sandy b) Calcareous c) Argillaceous d) Volcaniclastic
3	Tectonite rock fragments	a) Metasedimentary b) metavolcanic
4	Microgranular	a) Hypabyssal b) Sedimentary c) hornfelsic
5	Microphanerite	Count each internal crystal, each of sand size

For comparison of sandstone suites, framework modes are calculated into modal proportions of the following categories of grains:

- a) Stable quartzose grains (Q), including both monocrystalline and polycrystalline grains (including chert);
- b) Total feldspar grains (F), including both plagioclase and potassium feldspar, and
- c) Total unstable lithic grains (L), including sedimentary, metamorphic and volcanic lithic grains.

Complementary ternary diagrams are commonly used to emphasise different characteristics (e.g QmFLt, QpLvLs, and QmPK). However, the QFL diagram is adequate to fully explain tectonic setting, hence additional diagrams are not shown in this study. QFL plots are useful to emphasise grain stability and fields on the diagram depend

on weathering, provenance relief, and transport mechanisms as well as sediment source rocks (Dickinson and Suczek, 1979).

## **2.3 Geochemistry**

### **2.3.1 Geochemical Samples**

X-Ray Fluorescence has been used on geological silicate samples for many years. It has several advantages including minimal sample preparation, large sample size (5 g) allowing a representative sample to be easily obtained and non-destructive analysis, allowing numerous analyses to be run on the same pellet (Longerich, 1995).

Geochemical samples were taken from conventional core and cuttings. A sample interval of 5 m for cutting samples and 10 m for core samples was used in this study. Table 2.7 shows the stratigraphic distribution of the geochemical samples taken through the various formations. The cuttings had to be washed of all drilling mud before analysis; this was performed by a well services contractor (East Coast Sample Services, St. John's). Samples were washed under pressure with a varisol solution and then sieved through a 44 micron sieve and finally dried in a vacuum.

Table 2.7 – Number of geochemical samples taken in each formation.

Formation	XRF	
	Core	Cuttings
Ben Nevis	55	82
Avalon		35
Eastern Shoals		19
A Marker Member		46
White Rose		23
B Marker Member		4
Hibernia	2	39
Rankin	2	7
Jeanne d'Arc	4	
<b>Sub-total</b>	<b>63</b>	<b>255</b>
<b>Total</b>	<b>318</b>	

Samples of 5 grams were crushed using a ceramic mortar and pestle and prepared as pressed pellets. 5 g of crushed sample was mixed with 0.7 g of BRP-5933 Bakelite phenolic resin in a 100 ml glass jar. Phenolic resin was used as a binder in this study. Two 0.5 in. diameter stainless steel ball bearings were added and a plastic lid attached. The jar was rolled on a roller mixer for 10 minutes to mix the sample with the resin. The powder was then placed in a 29 mm diameter pellet press and pressed for 5 seconds at a pressure of 20 tonnes. The pellets were then placed in a 200°C oven for 15 minutes (Longerich, 1995).

The following major and trace element abundances were analyzed:

Na, Mg, Al, Si, P, S, Cl, K (semi-quantitative);

Ca, Sc, Ti, V, Cr, Mn, Fe, Ni, Cu, Zn, Ga, As, Rb, Sr, Y, Zr, Nb, Ba, Ce, Pb, Th, U (quantitative).

The analyses of elements labelled as semi-quantitative have greater sources of error, giving less accurate results than those elements labelled as quantitative. Major and most minor elements are reported as oxides in weight percents (wt %); trace elements are reported in parts per million (ppm) of elemental abundances. All geochemical values for each sample are listed in Appendix 4. Detection limits for samples are explained in detail by Longerich (1995) and Poisson limits of detection (recommended as the best estimator of the limit of detection) for major and trace elements are listed in Table 2.8.

A number of samples had to be re-run due to suspected drilling mud contamination (Appendix 5). These samples had very high levels of Barium (Ba) (>5000ppm), Chlorine (Cl) (>10,000 ppm) and in some samples high levels of Na<sub>2</sub>O (>15%). These elements are very common additives in drilling muds and indicate drilling mud contamination. All samples that had to be re-run were from two wells; F-04 and C-17. The drilling report shows that they were drilled with a seawater based mud with Barite and KCl additives. To attempt to reduce the level of contamination, samples were polished with a 30 micron silicon-carbide paper to clean the surface and then re-run; however, these samples still have high Ba-Cl-Na values and are not considered reliable in geochemical plots.

Table 2.8 – List of all major and trace elements measured by XRF technique, along with their associated limits of detection (Poisson limit of detection), (Longerich, 1995).

Element or Oxide	Poisson l.o.d	Element or Oxide	Poisson l.o.d
Na <sub>2</sub> O	0.010%	Ni	5ppm
MgO	0.012%	Cu	4ppm
Al <sub>2</sub> O <sub>3</sub>	0.012%	Zn	3ppm
SiO <sub>2</sub>	0.011%	Ga	2ppm
P <sub>2</sub> O <sub>5</sub>	0.003%	As	13ppm
S	11ppm	Rb	0.7ppm
Cl	20ppm	Sr	1.1ppm
K <sub>2</sub> O	0.002%	Y	0.6ppm
CaO	0.002%	Zr	1.1ppm
Sc	7ppm	Nb	0.6ppm
TiO <sub>2</sub>	0.003%	Ba	21ppm
V	6ppm	Ce	39ppm
Cr	7ppm	Pb	4ppm
MnO	0.002%	Th	3ppm
Fe <sub>2</sub> O <sub>3</sub>	0.005%		

### 2.3.2 The Chemical Index of Alteration (CIA)

Sedimentary rocks contain a record of their provenance, as well as the processes that they have gone through, such as weathering, erosion, and diagenesis. The mineralogical and major-element composition of siliciclastic sediments reflects their source rock composition, conditions during weathering, transport of detritus and burial (Nesbitt, 2003).

Weathering is one of the most significant influences on sediment geochemistry (McLennan et al., 2003). There are three types of weathering that a sediment can be exposed to: physical, biological and chemical weathering. Physical weathering results in the disaggregation and comminution of crystalline rocks without mineral alteration or

formation of any new minerals. Sorting during transport can result in mineralogical differentiation because some minerals (*e.g.* biotite) are more prone to comminution than others (Nesbitt, 2003). These minerals may be preferentially enriched in fine-grained sediment with harder minerals better represented in the coarser sediments (Nesbitt, 2003). Sediments affected primarily by physical weathering are very useful for provenance determination and are themselves indicators of weathering conditions since the inference can be made that physical weathering dominated chemical weathering during production of detritus (Nesbitt, 2003).

Biological weathering includes the mediation by microbes and fungi to dissolve silicate minerals at rates which would otherwise be much slower (Nesbitt, 1997). This type of weathering can be viewed as chemical weathering by biological means (Nesbitt, 2003). Chemical weathering causes exposed rocks to be dissolved or disaggregated through chemical processes. Soil waters enriched in  $H^+$  flow through fractures and around grain boundaries.  $H^+$  diffuses into crystal lattices weakening bonds and promoting preferential liberation of selected elements (Na, K and Ca of feldspars). This loss results in mineral instability and formation of clay minerals (Nesbitt, 2003). Secondary clay minerals form after Al-silicates in weathering profiles and are proof that chemical weathering has occurred. Chemical weathering is only effective when there is sufficient rainfall to transport acids into the soil subsurface and to mineral surfaces in a significant quantity. Production of abundant acids in soils is typically restricted to temperate and tropical regimes.

The most common method to evaluate weathering in the source region of a sedimentary rock is to use the Chemical Index of Alteration or CIA, following Nesbitt and Young (1984) and Nesbitt et al. (1996):

$$CIA = \left( \frac{Al_2O_3}{Al_2O_3 + CaO^* + Na_2O + K_2O} \right) \times 100$$

\* where CaO represents Ca in silicate minerals only.

This equation reflects major element geochemical properties of a rock and allows inferences to be made about the amount and type of mechanical vs chemical weathering a rock has undergone. The extent of weathering a sediment has undergone can be quantified using the CIA diagram which portrays the proportions of  $Al_2O_3$ ,  $Na_2O+CaO$ , and  $K_2O$  on a mole percent basis, plotted on a ternary diagram (A-CN-K diagram). This diagram only plots the CaO associated with silicates and any CaO associated with calcite, dolomite, or apatite should be removed (see Fedo et al., 1995, for a detailed explanation of this process.). Basaltic and gabbroic rocks typically plot close to the A-CN line, near 40%  $Al_2O_3$ , while granites typically have equal amounts of plagioclase, K-feldspar and quartz and typically plot near the midpoint of the plagioclase-potassium feldspar join (Figure 2.4). An increase in the amount of micaceous material within a rock will result in samples plotting with increased amounts of  $Al_2O_3$ .

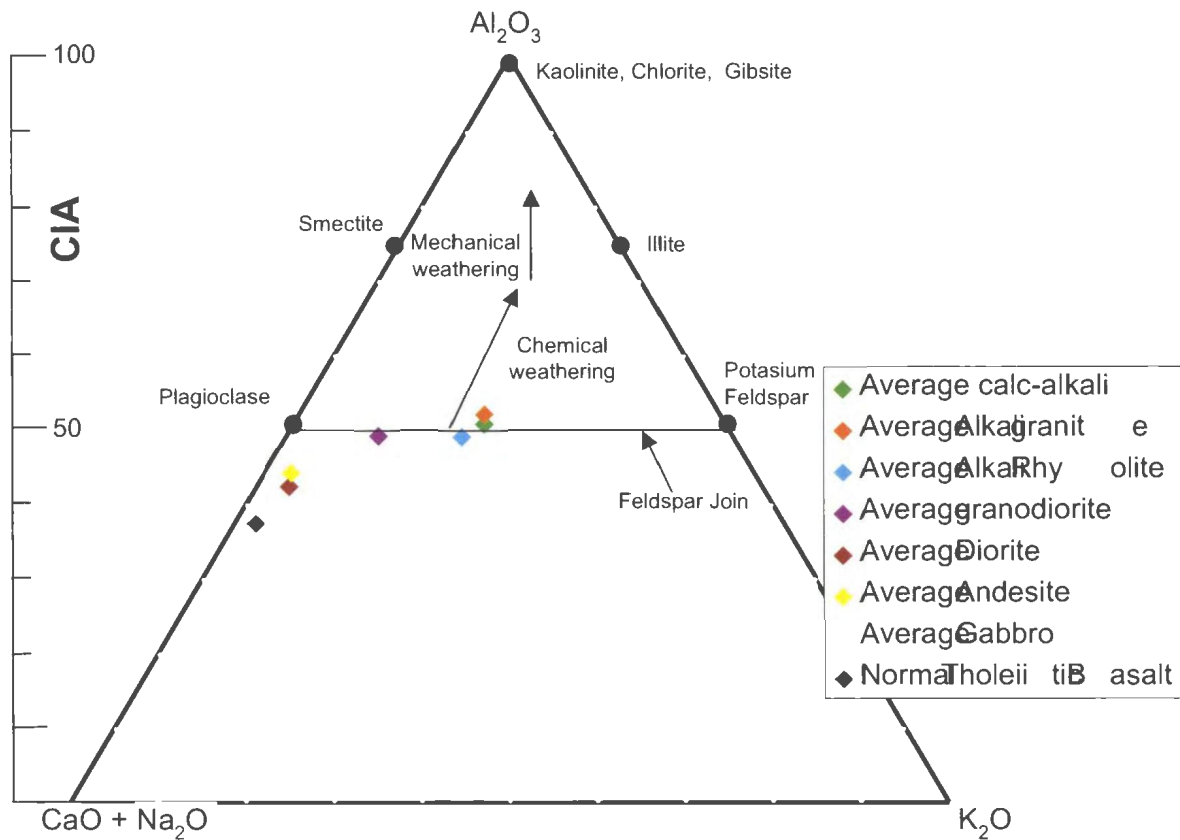


Figure 2.4 - A-CN-K diagram. Average chemical compositions of igneous rocks are plotted to show generalized location (Nockolds, 1954). Chemical weathering is described by trends of increasing  $Al_2O_3$  and a decreasing CN/K ratio. Mechanical weathering is represented by sub-vertical trends of increasing  $Al_2O_3$  at a constant CN/K ratio.

## Chapter 3 Petrography

### 3.1 Introduction

Petrographic and geochemical data are the primary data types used in provenance studies. Petrographic data focus on the detrital constituents of samples based on the assumption that modal detrital composition of given sedimentary rocks is similar to that of the sediment source, or can be linked to a source rock via specified processes.

Provenance studies of detrital components in sandstones began in the late nineteenth century with the first studies of quartz grains by Sorby (1880) and the study of inclusions in quartz and weathering of feldspars by Mackie (1896 and 1899). These methods were not widely used until Krynine was able to apply them effectively (e.g., Krynine, 1937).

Dickinson (1970) proposed simplified grain type classifications to make quantitative detrital modes reproducible. Dickinson and Suczek (1979) and Dickinson and Valloni (1980) showed that plate tectonic setting has a large influence over the modal composition of sand-sized sediments, which was suggested earlier by Crook (1974) and Schwab (1975).

The classification of hybrid arenites by Zuffa (1979) is useful to specify the nature of detrital framework grains. Table 1 from Zuffa (1979) classifies framework components into intrabasinal and/or extrabasinal. Extrabasinal grains are grains that have been brought into the basin from outside sources (*i.e.* quartz weathered from a granitic pluton) and intrabasinal grains are grains that have been formed within the basin (*i.e.* glauconite, rip-up clasts, ooids etc.). Extrabasinal grains are useful in understanding the source area (*i.e.* provenance), whereas intrabasinal grains are useful in understanding

depositional conditions in the sedimentary basin (Zuffa, 1979). Although provenance determination relies on extrabasinal grains, all grains, interstitial components and void spaces were counted during the analysis. The following sections visually describe the framework grains, followed by a petrographic description of each formation to gain an understanding of the framework composition, as well as the diagenetic components seen in each of the formations at and in the vicinity of the White Rose field.

## **3.2 Petrographic Description of Framework Grains**

### **3.2.1 Quartz**

Both monocrystalline and polycrystalline quartz grains are present. Monocrystalline quartz (Qm) is the most abundant form of quartz seen, and displays both straight and undulose extinction (Plate 1). Straight extinction of Qm grains is the most common type of extinction observed. Most of the grains are well rounded with limited grain size variability within the Ben Nevis Formation; however, the Hibernia and Jeanne d'Arc formations contain a broad range of grain sizes ranging from coarse grained to very fine-grained. Some quartz grains (<15%) appear dirty with small needle-like inclusions, as well as carbonate inclusions (Plate 1). Quartz overgrowths are common and typically appear abraded indicating that they are inherited from a prior burial/cementation episode (Plate 1). Some of these quartz overgrowths that cannot be seen under plane-polarized light are visible by catholuminescence within the Ben Nevis Formation (Normore, 2006). Iron-oxide rims and clay rims are commonly seen on numerous grains.

Polycrystalline quartz (Qp) grains such as those shown in Plate 1 are common and tend to exhibit greater than 3 sub-crystals; however, quartz grains with only two subgrains

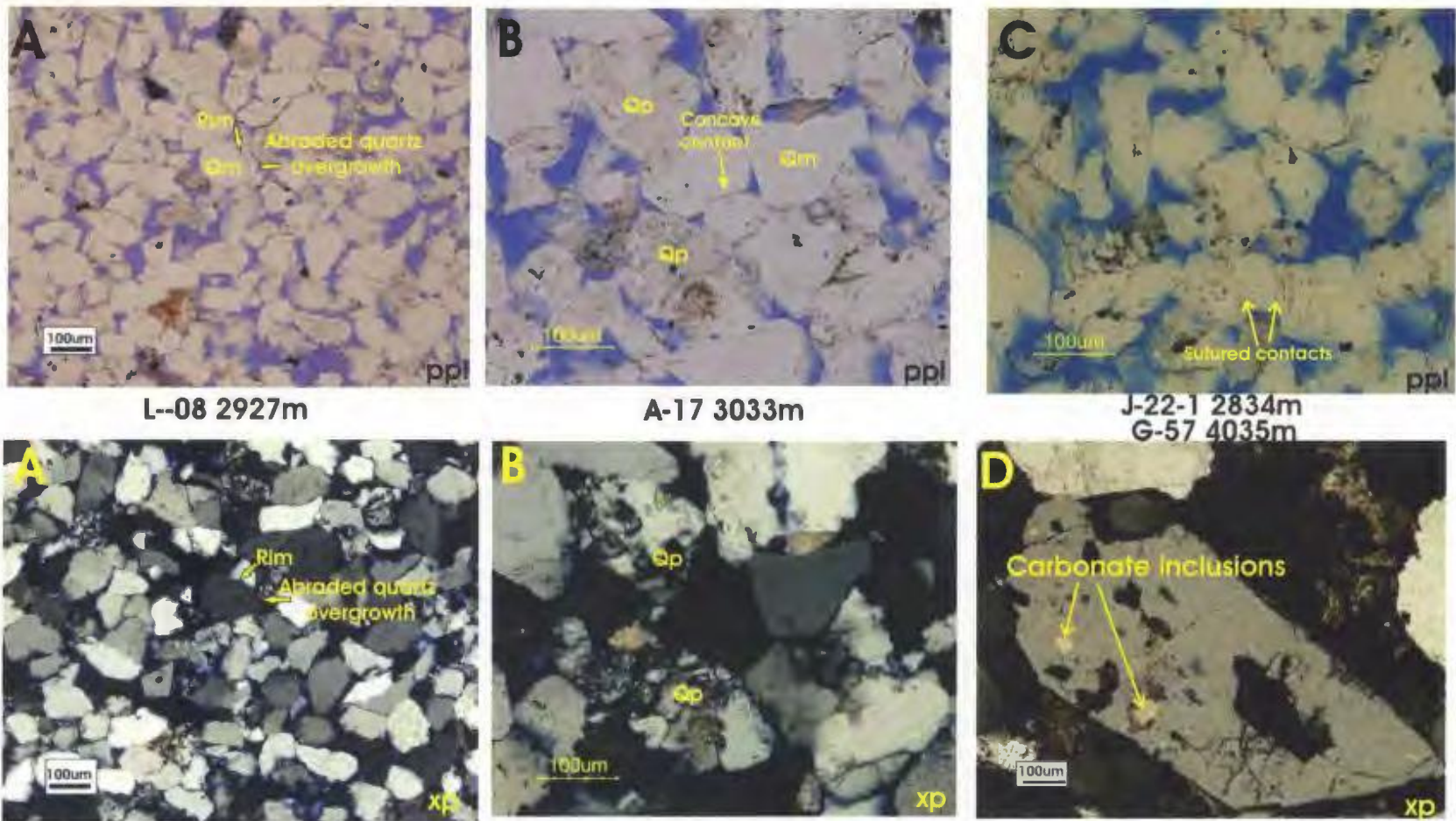


Plate 1: Detrital quartz grains. A. Monocrystalline quartz from L-08 2927m in plane polarized light (ppl) above and cross polarized light (xp) below. Note iron oxide dust rims around grains, as well as quartz overgrowths. Most grains exhibit straight extinction. B. Polycrystalline quartz grain from A-17 3033m in cross polarized light above and cross polarized light below. Grains exhibit more than 3 sub-crystals and appear dirty in plane polarized light. C. Quartz grains from J-22-1 2834m are compacted with sutured and concave contacts. D. Carbonate inclusions from G-57 4035 in xp.

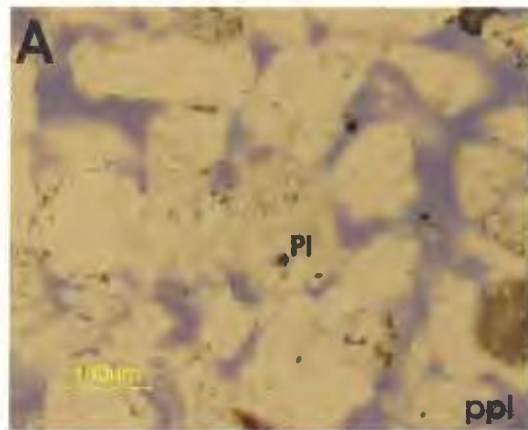
are also common. Boundaries are generally irregularly shaped, with straighter boundaries being more common in smaller grains and grains with a smaller number of subcrystals. Subcrystals exhibit mainly straight extinction; however, undulose extinction is also common. Qp grain size is approximately equal to Qm grain sizes in the Ben Nevis Formation but tends to be coarser in the Hibernia Formation, Terra Nova Member and Lower Tempest Member sandstones.

### **3.2.2 Plagioclase Feldspar**

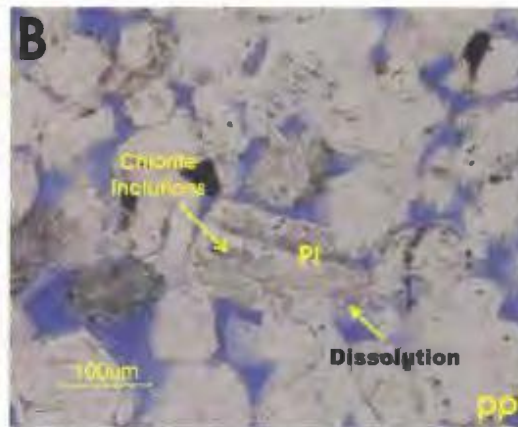
Plagioclase feldspar exhibits albite twinning and most grains are slightly to highly altered with common vacuolization (Plate 2). Grains can also be clear –much like quartz– to cloudy in plain polarized light. Grains tend to be the same grain size as quartz grains, and exhibit a variety of shapes, from equant to elongate (Plate 2). Partially to completely dissolved plagioclase grains with faint remnants of twinning are common. Dissolution generally begins and progresses along twin or cleavage boundaries. Some plagioclase grains that have been nearly or totally replaced by carbonates still exhibit relict albite twinning, not to be confused with lamellar twinning typical of calcite.

### **3.2.3 Potassium Feldspar**

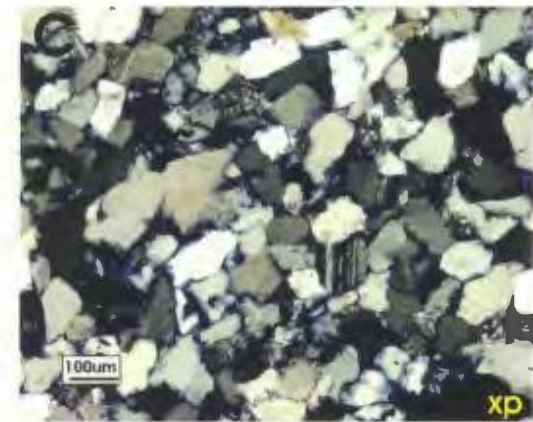
Potassium feldspar can exhibit Carlsbad, albite, and microcline twinning, and is also present without twinning (Plate 3). Potassium feldspars commonly exhibit dissolution effects and microcline grains, recognized by their grid twinning, are occasionally altered (Plate 3). Because potassium feldspars can exhibit numerous styles of twinning or lack thereof it is important to stain thin sections to differentiate potassium



A-17 3033m



H-20 3031m



A-17 3005m

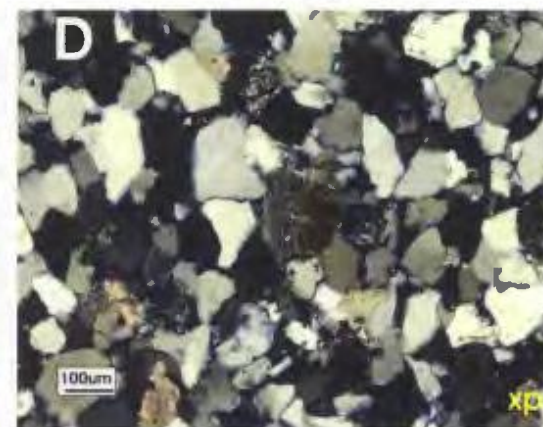
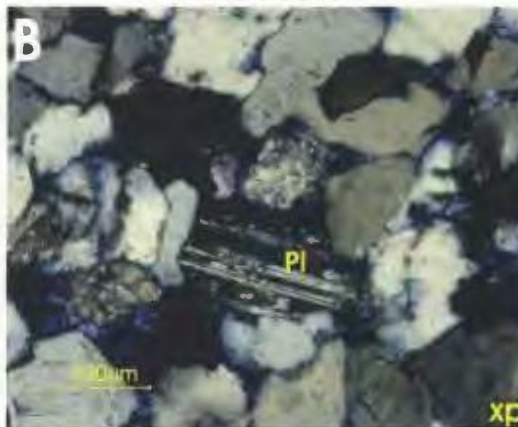
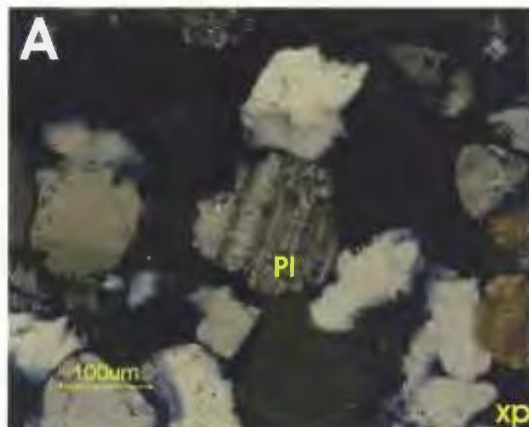


Plate 2: Detrital Plagioclase feldspar grains. A. Plagioclase feldspar (PI) grain in plane polarized and cross-polars (above and below respectively). Grains exhibit albite twinning; note grain is dirty, with small vacuoles/inclusions. B. Chlorite inclusions seen in plagioclase grain as well as partial dissolution. C, D. Plagioclase grains from A-17 3005m. Grains can be sub-rounded and elongate and commonly exhibit inclusions and partial dissolution.

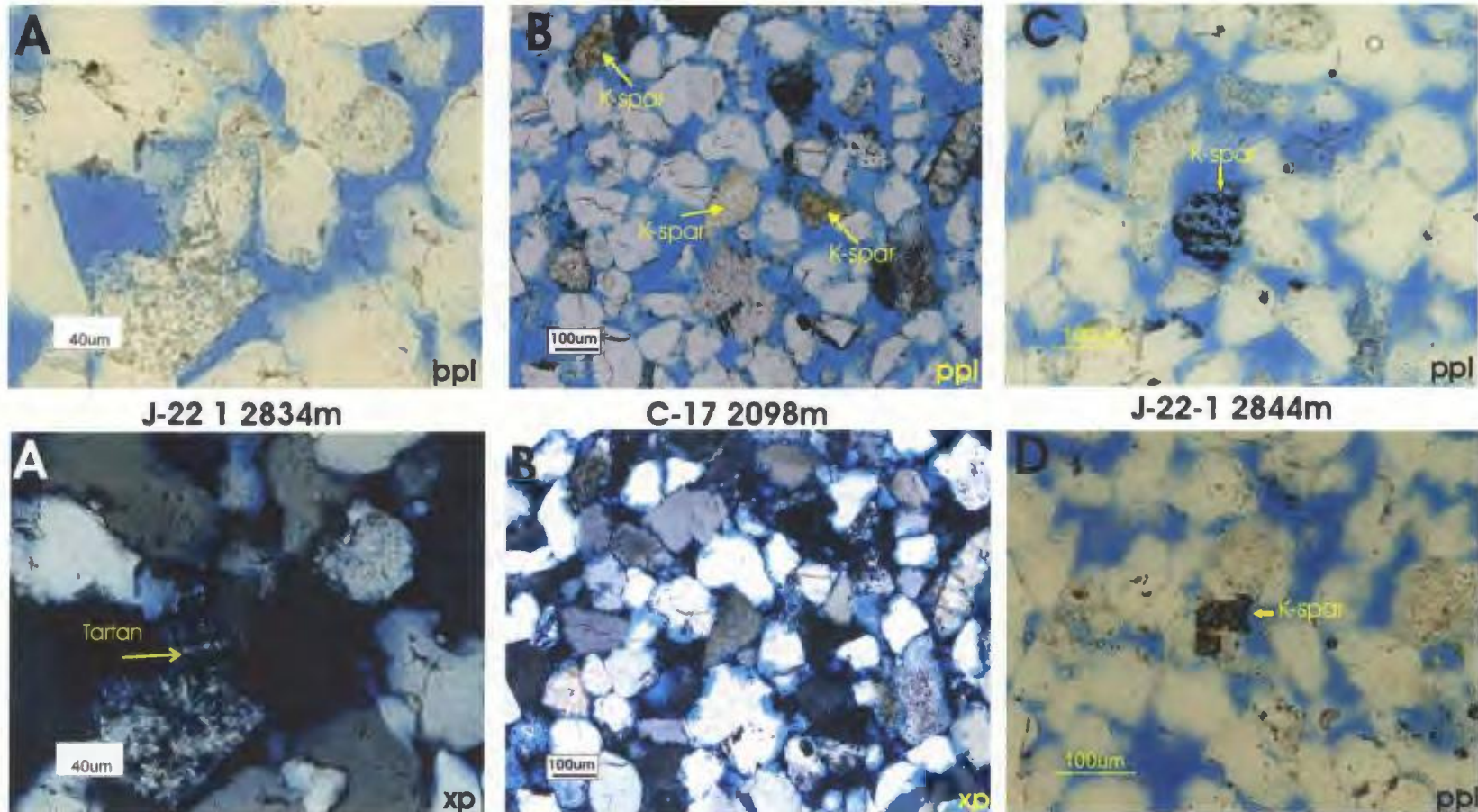


Plate 3: Detrital Potassium Feldspar grains. A. Microcline feldspar grain at 40X magnification in ppl and xpl. Note “plaid” tartan twinning seen in xpl. B. C-17 2098m in the Hibernia Formation, staining shows feldspar grains without twinning at 10X magnification in ppl. C. Partially dissolved stained k-spar grain with opaque mineral replacement (black mineral) at 20X magnification in ppl. D. k-spar grain highly altered, with opaque replacement at 20X magnification in ppl. Parts of the grain that are not stained is indicative of a composition that is not pure end-member potassium feldspar. Note high amount opaque mineral replacement in grain, consistent with its lack of chemical stability compared to the more stable quartz grains surrounding it.

feldspar from quartz and untwinned plagioclase. Thin sections that were stained for feldspar give a much better measure of the amount of potassium feldspars present. In such thin sections, distribution of the yellow K-spar stain is commonly patchy within given grains resulting in a texture lacking any obvious control by cleavage or twinning (Plate 3). Hence, compositionally these grains are not end-member K-feldspar and the unstained, white zones are untwinned and may be the result of diagenetic albitization (Saigal et al., 1988).

### **3.2.4 Sedimentary Rock Fragments**

Sedimentary rock fragments include carbonate rock fragments (macrocrystalline and micritic), chert and shale (Plates 4 and 5). Carbonate rock fragments (Plate 4) are the most common rock fragments observed in the Ben Nevis Formation. Macrocrystalline calcite grains stain pink, however some grains have blue-stained edges indicating a ferroan component to the grain (Plate 4). The grain edges have been rounded (subangular to subrounded), confirming the detrital nature of the grains, rather than authigenic origin as carbonate cements. There is no organic material found within any of the carbonate grains. Micritic carbonate grains are also common. They are generally brownish-red in color and also have rounded edges (Plate 4). Chert is the second most common rock fragment observed in all formations. Note that although strictly speaking chert can be considered a rock fragment, it is included within the parameters Q and Qp of Dickinson and coworkers. However, it is considered a rock fragment (R-or L-pole) in sandstone classification schemes of Folk (1974) and Pettijohn (1975). The detrital chert observed is described as cryptocrystalline quartz (Plate 5). Chert grains tend to be well rounded and

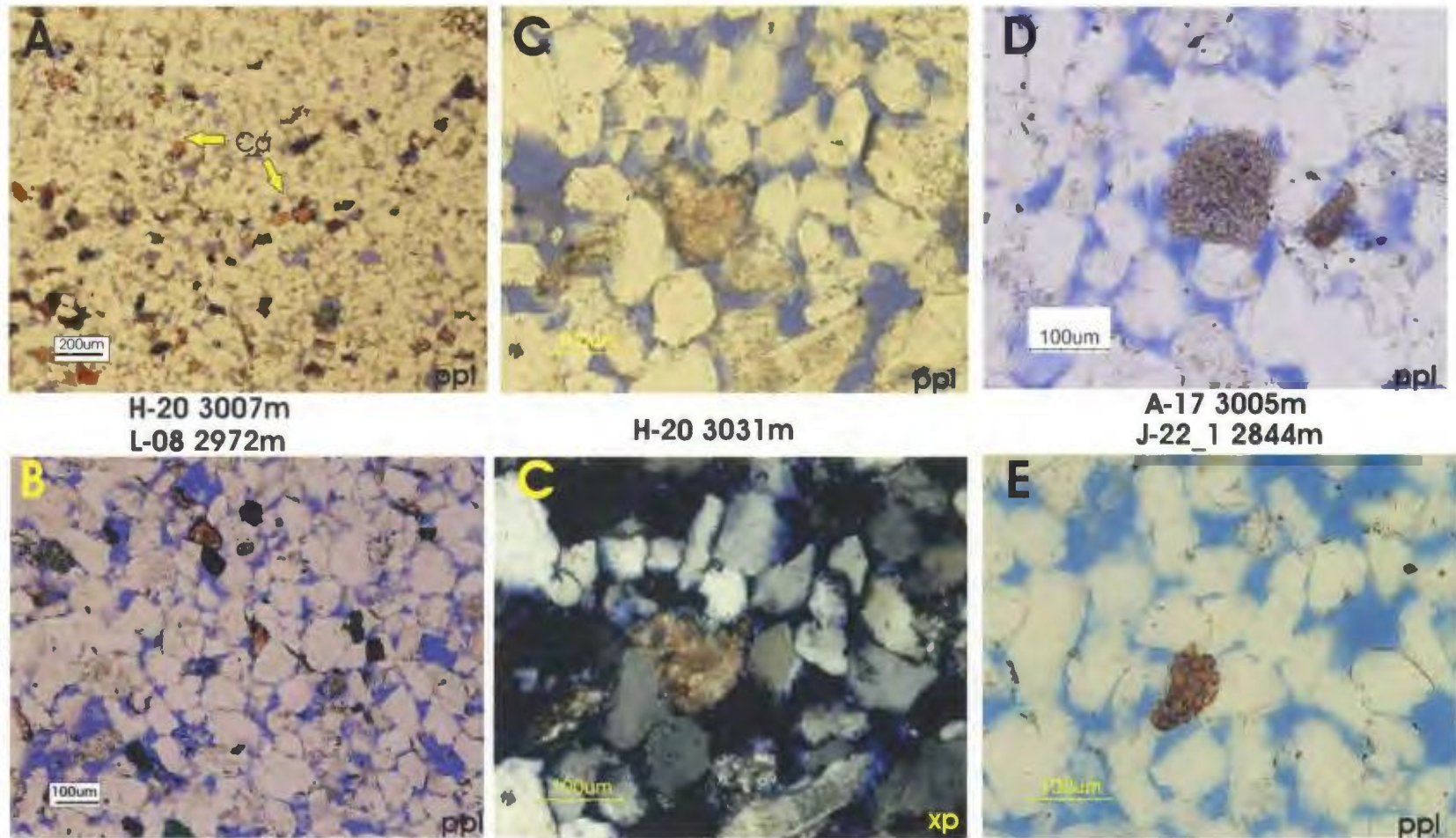
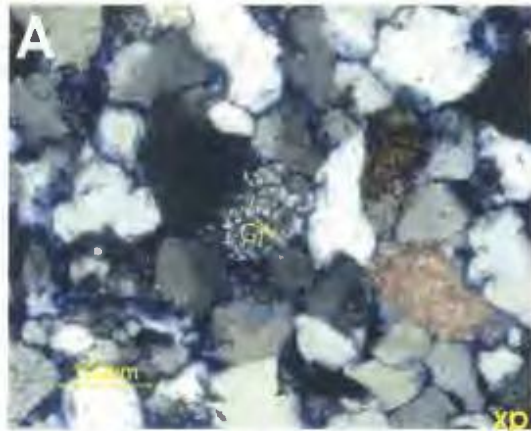
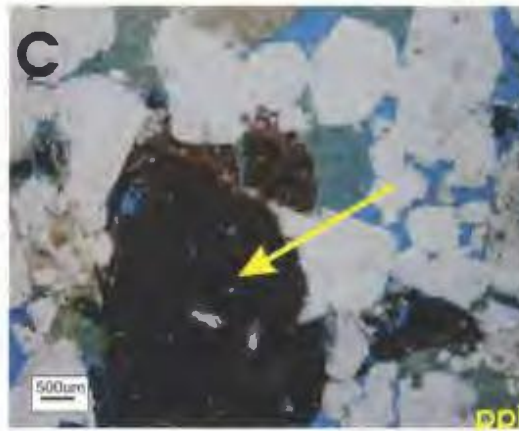


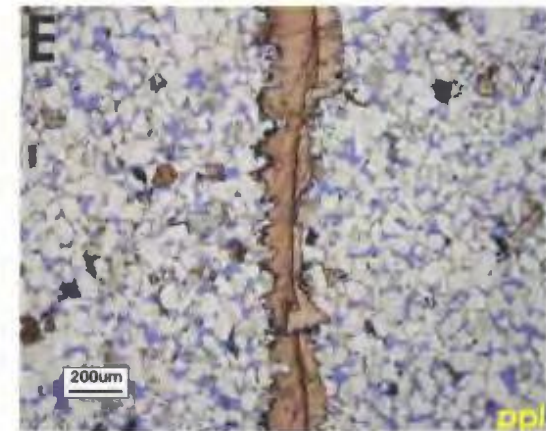
Plate 4. Detrital carbonate grains. A, and B. Detrital carbonate rock fragments stained pink indicating non-ferroan carbonate grains. C. Macrocrystalline carbonate grain with blue stained edges, possibly a cement rim. Edges appear anhedral, consistent with a detrital origin for this grain. Blue carbonate stain indicates early stage ferroan cement. D. Microcrystalline carbonate grain with rounded edges. E. Polycrystalline carbonate grain.



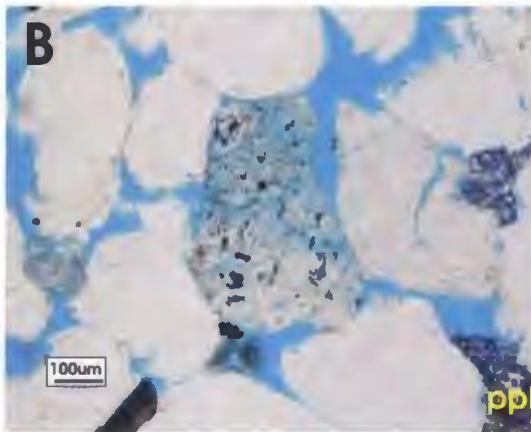
H20 3031m  
G-57 4594m



G-57 4034m



A-17 3012m



C-17 2239m



H-20 2935m

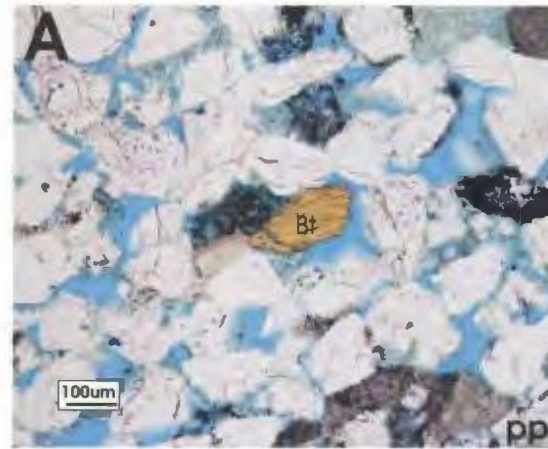
Plate 5. Rock fragments observed in thin section. A. Detrital chert grain with cryptocrystalline texture in xp. B. Partially dissolved chert grain in ppl. C. Large detrital shale clast. D. Peloid grains and molusc shells (broken up) from Hibernia Formation. E. Mollusc shell from Ben Nevis Formation. F. Serpulid worm tube in H-20 2935m.

of similar grain size to the surrounding grains. Partial dissolution of grains is also common (Plate 5).

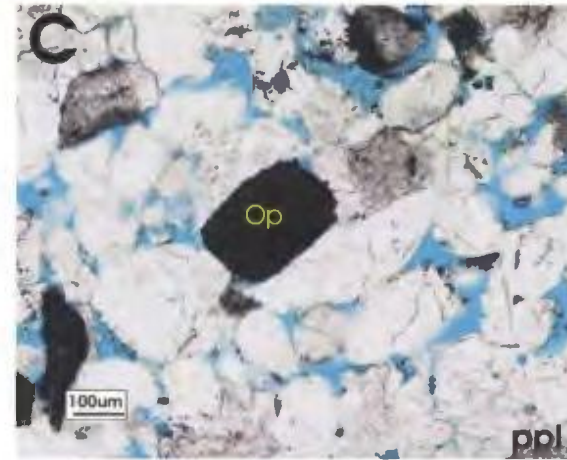
Brown, calcareous and organic-rich shale fragments are mainly restricted to the Hibernia and Jeanne d'Arc formations. They are generally larger than the average grain size and some fragments contain small amounts of silt (Plate 5). The grain size and shape of these fragments indicate they are detrital and not intrabasinal clays seen elsewhere. Intrabasinal bioclastic shells are common to all formations. The Hibernia Formation exhibits abundant calcareous peloidal grains and some oyster and mollusc shells (Plate 5), while the Ben Nevis Formation exhibits oyster and mollusc shells and serpulid worm tubes. Serpulid worm tubes are known to grow on stable "reef" banks in well-oxygenated shallow water marine settings (Ten Hove and van den Hurk, 1993). Although in some cases delicate features are preserved, the shells, and to a lesser extent the worm tubes, have clearly been broken-up, during transport (Ferry, 2005).

### **3.2.5 Mineral Grains**

Detrital biotite (Plate 6) is seen in all formations and is green or brown in color and pleochroic. Muscovite is seen in the Ben Nevis Formation, commonly in clay-rich facies. It occurs as thin elongate strands with high birefringence. Detrital chlorite grains are seen in all formations, but are rare. These grains are green, slightly pleochroic, and show characteristic anomalous bluish-purple interference colours (Plate 6). These minerals are well rounded, with grain size being slightly smaller than the average grain size.



G-57 3995m  
H-20 3031m



G-57 3995m  
A17 3033m

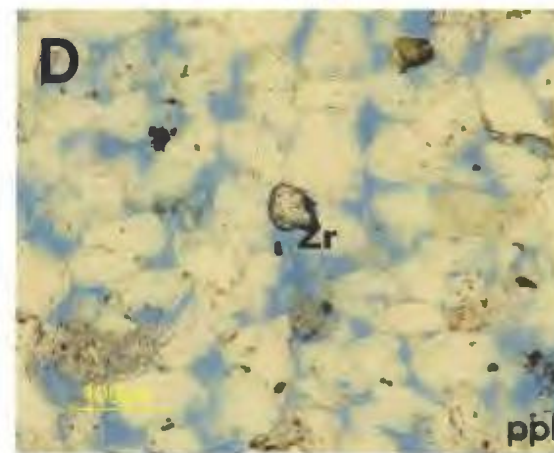
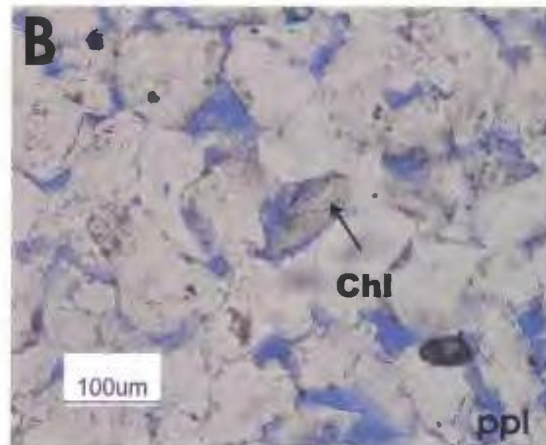


Plate 6. Mineral grains. A. Biotite grain (Bt), highly pleochroic from brown to clear. B. Detrital Chlorite grain. C. Detrital opaque mineral. Grain size of opaques can be highly variable from ~50 microns up to 200 microns. E. Detrital zircon grain from the Ben Nevis Formation.

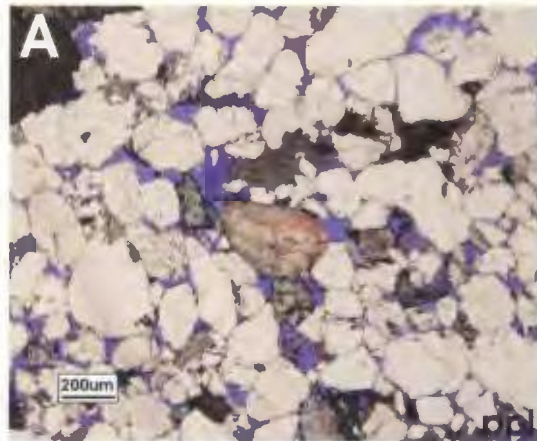
Opaque minerals are seen in all formations. Detrital opaque mineral are generally the same grain size as framework minerals and have rounded edges (Plate 6). Silt-sized opaque flecks that tend to occur as clusters in porous spaces are considered to be an authigenic replacement phase or cement.

Detrital zircons are common in all formations, but are especially abundant in the Ben Nevis Formation. Average grain size is approximately 50-100 $\mu$ m. Zircons are clear with a high relief and birefringence (Plate 6). Grains commonly have opaque, oxidized edges formed as a result of weathering.

### **3.2.6 Authigenic Minerals and Cements**

Small, euhedral opaque minerals occurring in pore-filling clusters may be a replacement phase after pyrite or clay-organic aggregates of pellets or lining from burrowing organisms. Other authigenic phases recognized are the very common replacement of feldspar grains including calcitization, sericitization and chloritization and occasional very thin, highly birefringent (smectite?) rims are seen on feldspar and lithic fragments. Plate 7A shows a detrital feldspar grain completely replaced by carbonate cement.

Numerous types of cement are present in all sedimentary formations studied. The most common types of cements are pore filling carbonate cements, followed by quartz overgrowth cements. Pore filling carbonate cement (Plate 7B) tends to be localized in small areas and concretions. Euhedral rhombic shaped cements are seen at 3995 m in G-57 (Plate 7D). These are thought to be dolomite cement due to the shape and color.



G-57 4035m

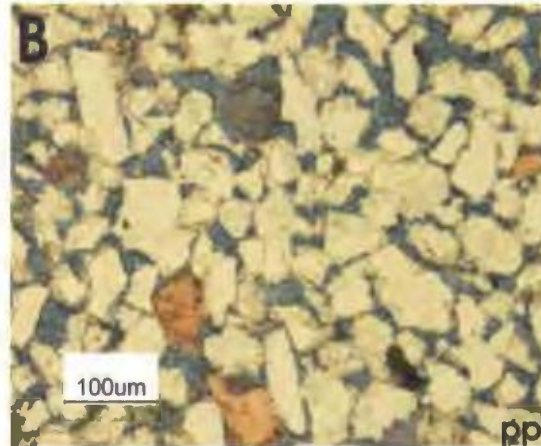
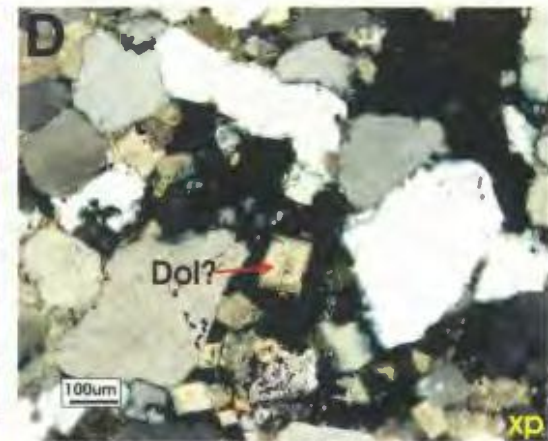
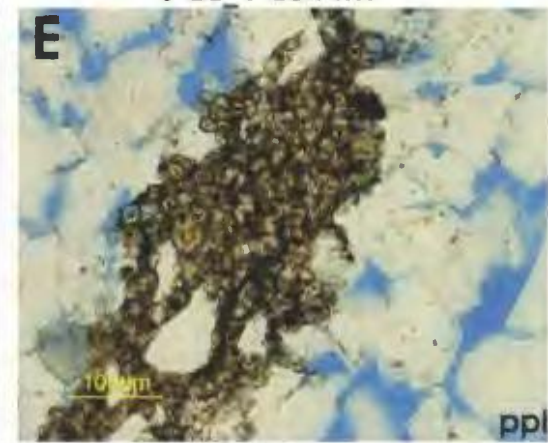
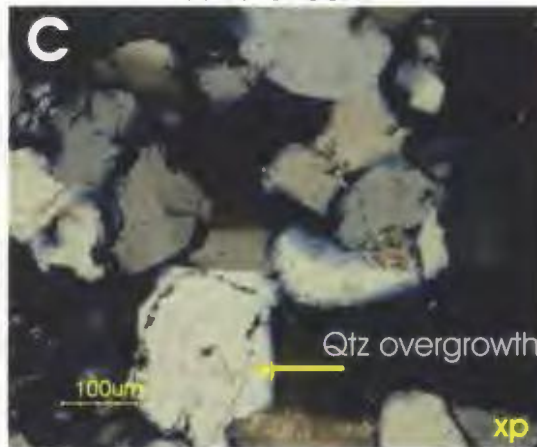
H-20 2995m  
A-17 3033mG-57 3995m  
J-22 1 2844m

Plate 7: Authigenic minerals and cements. A. Carbonate replacing feldspar grain in ppl (above) and xp (below). B. Poikilotopic cement in the Ben Nevis Formation. C. Quartz overgrowth in the Ben Nevis Formation. D. Dolomite cement in xp. E. Siderite cement in ppl.

Siderite cement is common in all formations, especially the Ben Nevis Formation.

Siderite appears as flattened rhombs and is distributed in small patches throughout the Ben Nevis Formation (Plate 7E).

### **3.3 Petrographic Description of Formations**

#### **3.3.1 Ben Nevis Formation**

The Ben Nevis Formation consists mainly of quartz (85%-96%) with common lithic fragments and rare feldspar grains. Quartz grains are both monocrystalline and polycrystalline with a ratio of Qm to Qp of approximately 10 to 1. Both plagioclase and potassium feldspars are seen in the Ben Nevis Formation and make up approximately 1-7% of framework grains (Table 3.1). Most of the samples from the Ben Nevis Formation were not stained for feldspar, making it difficult to differentiate plagioclase from potassium feldspar. Only two wells had samples stained for feldspars (F-04 and J-22-1) and some potassium feldspars that were stained show no twinning, indicating that some feldspars might have been mistaken for quartz grains in unstained samples. Feldspars are generally altered and/or partially dissolved, with common chlorite replacement (Plate 2B). Some feldspars have been replaced with carbonate cement (Plate 7A) or an unidentified opaque mineral (Plate 3D & C). There appears to be a slightly higher value of K-feldspar in stained thin sections, indicating K-feldspars that do not exhibit twinning might have been incorrectly counted as quartz in the grain analysis of wells without the staining (A-17, L-08, and H-20). However the difference is slight (<2%) and does not have a large impact on any petrographic classification schemes.



Table 3.1 - con't.

	Depth (m)	Q%	F%	L%
Hibernia Formation	G-57			
	3985.3	90.72	2.95	6.33
	3995.2	90.20	2.94	6.86
	C-17			
	2028	88.46	4.33	7.21
	2098.5	82.43	10.36	7.21
	2162.5	85.16	10.44	4.40
	2200	90.91	6.49	2.60
	2225	92.75	5.18	2.07
	2239.5	87.15	6.15	6.70
	I-78			
	3270	0.43	0.01	0.56
	C96			
	3870	0.81	0.01	0.18
	3918	0.91	0.01	0.09
	3942	0.78	0.00	0.22
	L11			
	3250	0.86	0.01	0.13
	3290	0.79	0.00	0.21
	3330	0.78	0.04	0.19
	3370	0.68	0.02	0.30
	K-08			
	2900	0.93	0.03	0.05
	2950	0.97	0.01	0.02
	2510	0.75	0.09	0.16
	2550	0.90	0.02	0.08
	2630	0.90	0.03	0.07
	2670	0.98	0.00	0.02
2720	0.97	0.01	0.02	
2800	0.94	0.00	0.06	

	Depth (m)	Q%	F%	L%
Jeanne d'Arc Formation	G-57			
	4029.3	93.80	0.41	5.79
	4035	96.71	0.00	3.29
	C-73			
	4123.8	88.32	0.00	11.68
	4129.6	93.61	0.46	5.94
P15				
	4124.3	0.55	0.00	0.45
	4129.65	0.60	0.00	0.40

Rankin Formation (Lower Tempest Member)	<b>G-57</b>			
	4594.25	93.93	0.00	6.07
	4598	90.52	0.00	9.48

Lithic fragments make up approximately 1-12% of the sandstones (Table 3.1). The most common lithic fragments seen in the Ben Nevis Formation sandstone are carbonate fragments and chert. Other lithic fragments include mica (biotite and muscovite), opaque minerals, and detrital zircons. Note; however, that these monomineralic grains are not included in the calculation of modal proportions of ternary compositional diagrams.

The Ben Nevis Formation has undergone an appreciable amount of diagenesis and compaction with cemented intervals and concretions being common throughout. The cement consists of poikilotopic ferroan calcite (Plate 7B) and small, localized areas of siderite (Plate 7E). In relatively uncemented intervals, grains within the Ben Nevis Formation are often sutured together with elongate and concave-convex contacts, indicating a high degree of compaction (Plate 1C). Quartz overgrowths are common, some being euhedral and others having rounded edges; the latter imply transport following uncertain amounts of weathering (2<sup>nd</sup> cycle). Dissolution and or partial to total replacement of grains is common, especially of feldspars and other less stable lithic fragments such as chert (Plate 3C and 5B).

### **3.3.2 Hibernia Formation**

Hibernia Formation sandstones consist mainly of quartz, feldspars (0%-10%), and a considerable lithic component (1%-47%) (Table 3.1). The quartz is both monocrystalline and polycrystalline with a ratio of Qm to Qp of approximately 5 to 1. Polycrystalline quartz is more common in the coarser sand fraction, but is still present in finer grain sizes. The number of sub-crystals present in polycrystalline quartz grains

ranges from 2 to 20, similar to that seen in the Ben Nevis Formation. Point counting on thin sections that were stained for K-feldspars shows that the ratio of potassium feldspar to plagioclase is approximately 5:1. This relatively high K/P ratio may indicate that some plagioclase grains might have been mistaken for quartz. Lithic fragments in the Hibernia Formation range from 0-10% and include chert, shale fragments, and detrital carbonate (macrocrystalline and micritic grains); chert and shale being the most common. Based on fragments seen in thin section it is difficult to decide whether these shale fragments are intra- or extra-basinal. Herein the shale grains are thought to be derived from older, calcareous and organic rich sedimentary rocks; hence, they are included in the count of extra-basinal lithic fragments. Bioclastic grains are also common in the Hibernia Formation (Plate 5D), particularly in coarser-grained channel facies.

The Hibernia Formation sandstones show evidence of several diagenetic events. Many zones of the Hibernia Formation have been totally cemented with poikilotopic carbonate cement. Euhedral carbonate/dolomite? cements are seen in G-57 at a depth of 3985 m (Plate 7D) with cement boundaries appearing fresh and lacking corroded edges indicating that they were not subjected to subsequent dissolution. This implies a late stage cementation process (with respect to other cements and diagenetic effects seen elsewhere). Chert in the Hibernia Formation is commonly partially dissolved and altered (Plate 5B).

### **3.3.3 Terra Nova and Lower Tempest Members**

The Terra Nova and Lower Tempest members are compositionally very similar. They both consist of quartz and lithic fragments, with very rare feldspars observed (<1%).

The quartz is both monocrystalline and polycrystalline with a Qm:Qp ratio of 5 to 1, similar to that observed in the Hibernia Formation. Lithic fragments make up approximately 0-12% of the framework grains and include chert, shale fragments, and carbonate grains. Except for the relative absence of feldspar, the Terra Nova and Lower Tempest members appear very similar to Hibernia Formation sandstones. Grain alteration increases with depth, in particular there appears to be diagenetic albitization of K-feldspar, and the dissolution of unstable grains. Samples from the Terra Nova and Lower Tempest members are found at much greater depths than samples from the Hibernia and Ben Nevis formations, indicating that albitization and grain dissolution may be depth dependant. Smaller amounts of feldspar (compared to the Ben Nevis and Hibernia formations) may arise from loss by dissolution or are due to different sediment sources.

Diagenetic effects in the Terra Nova and Lower Tempest members are similar to that seen in the Hibernia Formation. Carbonate cement can be completely pore filling, totally destroying the porosity. Partial to total calcite replacement of feldspars is also common.

### **3.4 Quantitative Petrography**

The classification scheme developed by Pettijohn (1975) is a simple way to identify different types of sandstones. A QFL ternary diagram is used with the end members of quartz (Q), feldspar (F), and rock fragments/lithics (L). Sandstones are divided into two major groups based on texture (arenites and wackes). Table 3.2 shows

the classification of sand grain types. In this classification, chert and detrital carbonate grains are categorized as lithic fragments.

Table 3.2: Classification of detrital sand grains (after Pettijohn, 1975).

Quartz Grains ( $Qt=Qm+Qp$ )	Qt – Total quartz
	Qm – Monocrystalline quartz
	Qp – Polycrystalline quartz
Feldspar Grains ( $F=P+K$ )	F – Total feldspar grains
	P- Plagioclase grains
	K- Potassium feldspar grains
Lithic Fragments ( $Lt=Qp+Lvm+Lsm$ )	Lt – Total lithic Fragments
	L- Total unstable lithic fragments ( $Lvm +Lsm$ )
	Lv/Lvm – Volcanic/metavolcanic lithic fragments
	Ls/Lsm – Sedimentary/metasedimentary lithic fragments

### 3.4.1 Point Counting Uncertainty

Two sided 95 percent confidence bounds can be determined for each parameter (e.g. quartz grains) in each thin section. For example point count data for the sample from well A-17 3045.54 m has a total count of 300 of which 206 quartz grains were counted. This gives a quartz percentage of 69% (of all counted parameter, rather than counted parameter based on the Pettijohn, 1975 counting scheme) and when plotted on Figures 2.3 A and B one can determine the upper and lower 95 percent confidence limits,

which are 4.9% and 5.1% respectively; therefore, the confidence % limits for the quartz component of this samples is [64.1, 74.1]. Using this same method the 95 percent confidence intervals for the feldspar and lithic components are [1.0, 5.8] for feldspar and [1.0, 5.8] for lithics. The Ben Nevis Formation does not show a large amount of variability and these values are a good estimate of the amount of uncertainty in the composition of the Ben Nevis Formation samples. A larger number of counts will result in a higher level of accuracy, which is why the uncertainty in feldspar and lithic values is proportionately larger than quartz values, especially on the upper confidence side.

Samples from the Hibernia Formation show similar levels of uncertainty because they have roughly the same number of counts and feldspar and lithic values are similar to that observed in the Ben Nevis Formation. For example the sample from well C-17 2098.5 m has a total of 305 points counted, with 183 (62.2%), 23 (7.8%), and 16 (5.4%) points counted for quartz, feldspar, and lithic fragments, respectively. Accordingly the relative percentages have 95 percent confidence intervals of [55-65.2] for quartz, [4.7-11.4] for feldspars, and [2.6-8.2] for lithics. Note the higher level of uncertainty in the feldspar and lithic values due to the lower number of grains counted.

### **3.4.2 Ben Nevis Formation**

The Ben Nevis Formation is classified as a quartz arenite, sublitharenite, and subarkose using the classification scheme of Pettijohn (1975) (Figure 3.1). There is little variability in framework composition within the Ben Nevis Formation both stratigraphically and laterally (Figure 3.1 and Figure 3.2) with an average QFL ratio of  $Q_{89}F_3L_8$ . Defining this stratigraphic interval remains difficult due to the abundance of

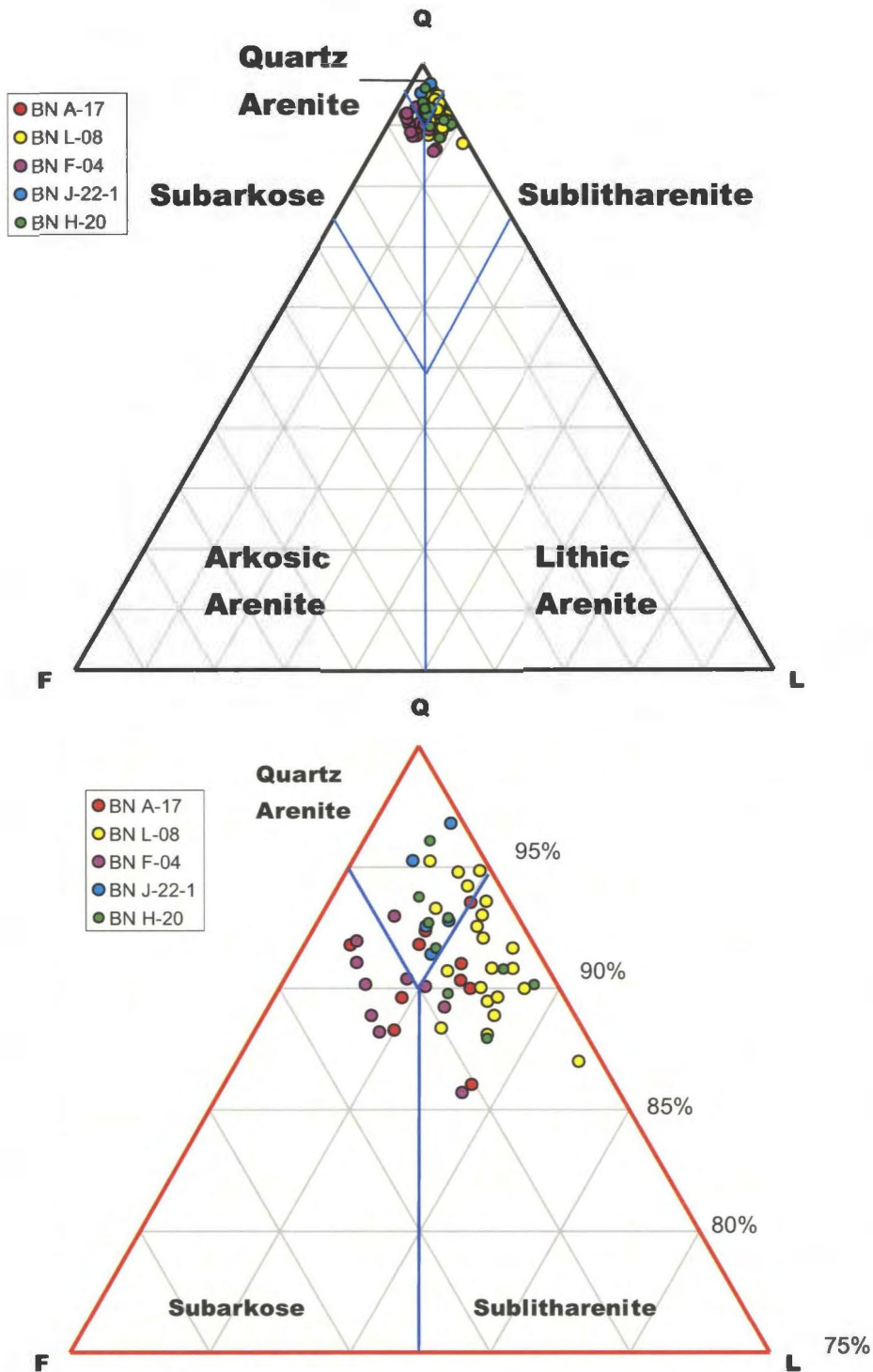


Figure 3.1 - QFL plot of Ben Nevis Formation samples. Ben Nevis Formation sandstones are classified as sublitharenite, subarkose and quartz arenites. Samples from southern wells (F-04 and A-17) plot in the subarkose category.

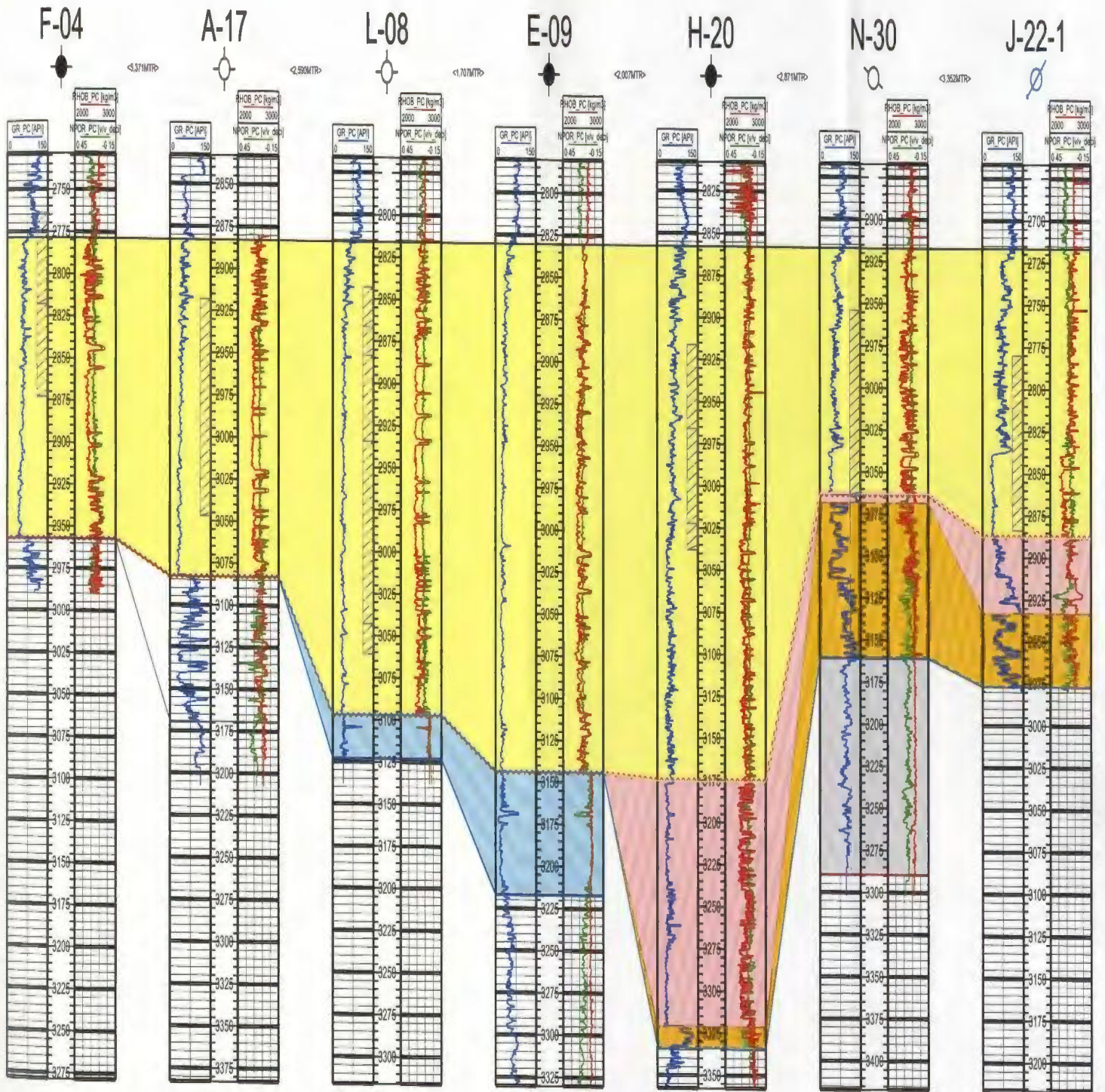


Figure 3.2 - Cross section of the sampled wells in the White Rose Field. Correlations of sand packages is difficult due to the subtle boundaries of the storm deposits. Core indicates Gamma Ray peaks are due to heavily calcite-cemented zones and nodules. See Figure 2.2 for legend.

faulting present in the White Rose Field and the very clean, homogeneous nature of the Ben Nevis Formation. Even with biostratigraphy, correlations within the field remain problematic. Correlating sand packages within the Ben Nevis Formation among the studied wells is difficult due to the clean nature of the sands (Figure 3.2), as well as the amalgamation of storm beds with very subtle boundaries that cannot be picked up by logging tools such as gamma ray logs. Some wells do show weak trends in framework composition, such as wells H-20 and J-22-1. These wells show an overall increase in quartz content moving lower in the section (Figure 3.3). Aside from these weak trends seen in wells H-20 and J-22-1, compositional trends do not appear to be controlled by stratigraphic position.

Samples from wells F-04 and A-17 in the south of the field tend to have slightly higher feldspar content, with most samples from well F-04 and some samples from well A-17 plotting within the subarkose category (Figure 3.3). Wells in the central and northern sections of the field (in particular wells L-08 and H-20) have samples that plot as sublitharenites, with a small number of samples falling into the domain of quartz arenites. All but one sample from well J-22-1 (north end of the field) plot in the quartz arenites category (Figure 3.3). The higher feldspar values observed in the southern area of the field could be interpreted as reflecting shorter transport distance, compared to the northern end of the field, assuming the source was from the south or alternatively the Ben Nevis Formation sandstones are diachronous and are therefore of a different age from the north (early transgression) to south (later transgression).

Figure 3.4 is a QPK plot of all the samples from the Ben Nevis Formation. Samples from wells J-22-1 and F-04 were stained for feldspar but the rest were unstained.

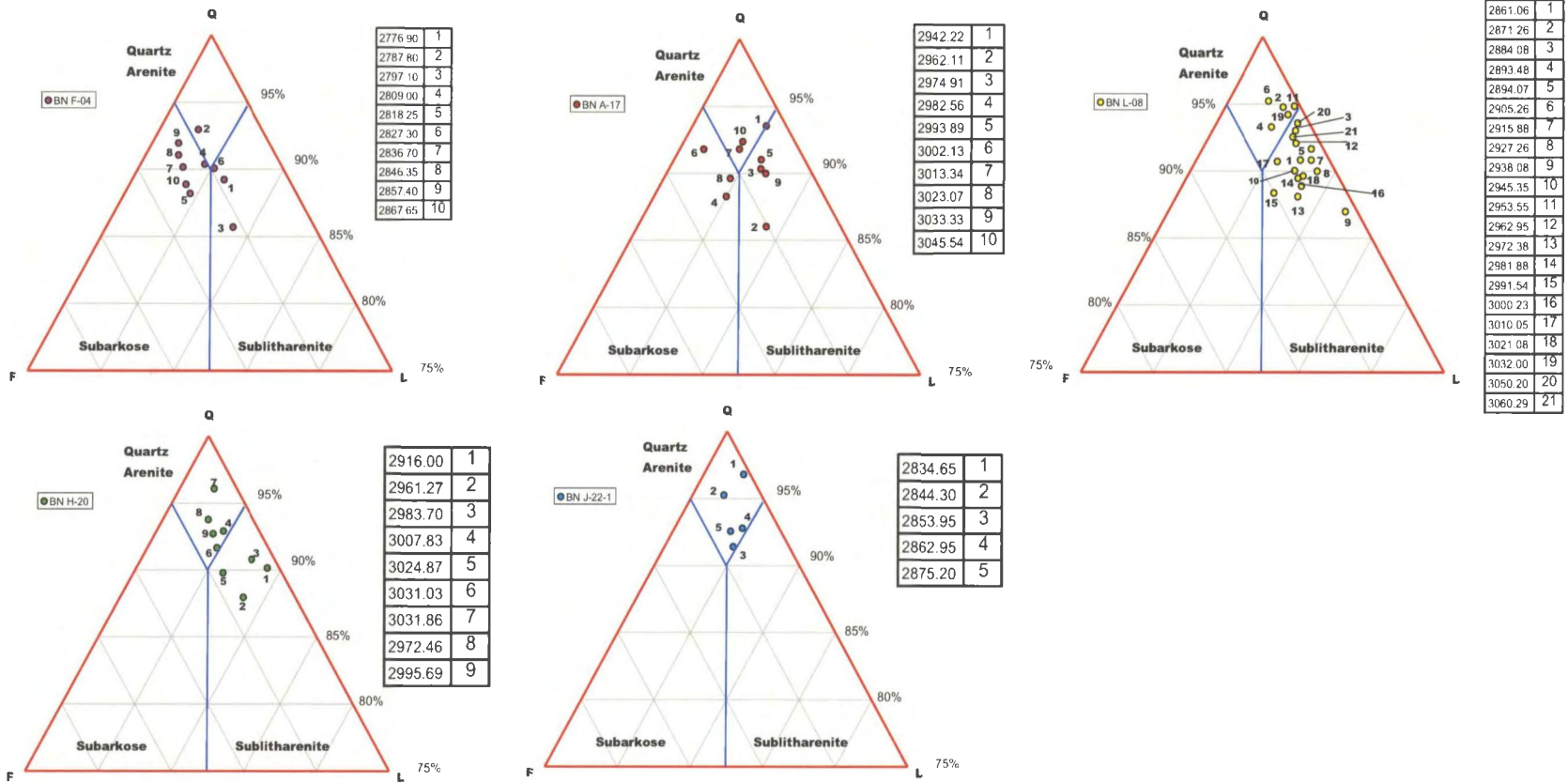


Figure 3.3 - QFL plots of Ben Nevis samples by well. Samples from well F-04 plot in the subarkose field. There appears to be a slightly higher feldspar content in the two southern wells F-04 and A-17. Samples from each well are not taken in the same stratigraphic interval, which might explain the different trends (i.e. increasing quartz moving up section in well J-22-1 and moving down section in well H-20). Aside from these two trends, no other stratigraphic trends are seen within any of the other wells.

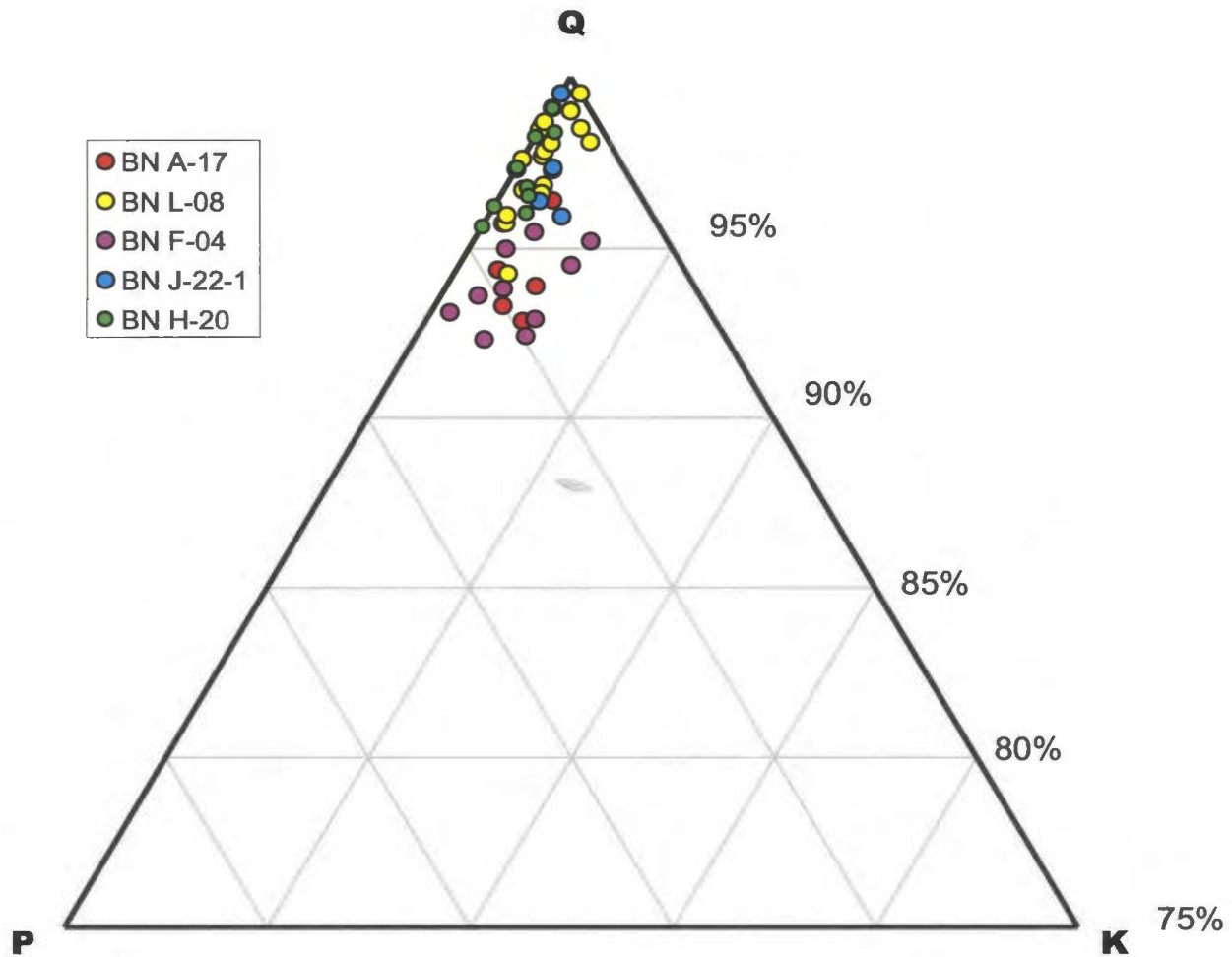


Figure 3.4 - QPK plot of Ben Nevis Formation samples. Samples from J-22-1 and F-04 have been stained for feldspar. F-04 samples show a higher concentration of potassium feldspar than J-22-1 samples. This ternary plot might imply a higher amount of potassium feldspar is found in the southern part of the White Rose Field.

Overall, samples from wells in the southern area of Whiterose field, F-04 and A-17, have higher feldspar (P+K) content than those to the north, L-08, H-20 and J-22. Based on the transgressive nature of the Ben Nevis Formation and a sediment source thought to be located to the south, the compositional trends appear to mimic the diachronous nature of Ben Nevis Formation deposition and temporal compositional variability at the source. During early transgression from the north, composition of lower Ben Nevis sands appears to reflect a more mature (perhaps more highly weathered) sediment source (low P+K), whereas Ben Nevis sands during late transgression in the south reflect a source that is more feldspar-rich, less mature, perhaps corresponding to less deeply-weathered highlands to the south. Note that the samples in well F-04 from the southern area are from the upper part of the formation, enhancing the proposed trend of stratigraphic control. In addition, wells A-17 and F-04 also have overall higher P/K ratios than wells L-08, H-20 and J-22. Based on the relative instability in soil-forming chemical weathering environments of plagioclase compared to K-feldspar (Nesbitt et al., 1996), the difference in P/K ratio is consistent with the proposed trends: a mature sediment source during early transgression in the north (higher P/K), becoming slightly less mature (lower P/K) as transgression progresses to the south

### **3.4.3 Hibernia, Jeanne d’Arc, and Rankin Formations**

The Hibernia, Jeanne d’Arc (Terra Nova Member) and Rankin (Lower Tempest Member) formations sandstones plot in the subarkose and sublitharenite category, with one sample plotting in the quartz arenites category (well G-57 in the Terra Nova Member) based on the Pettijohn (1975) classification scheme (Figure 3.5). All three

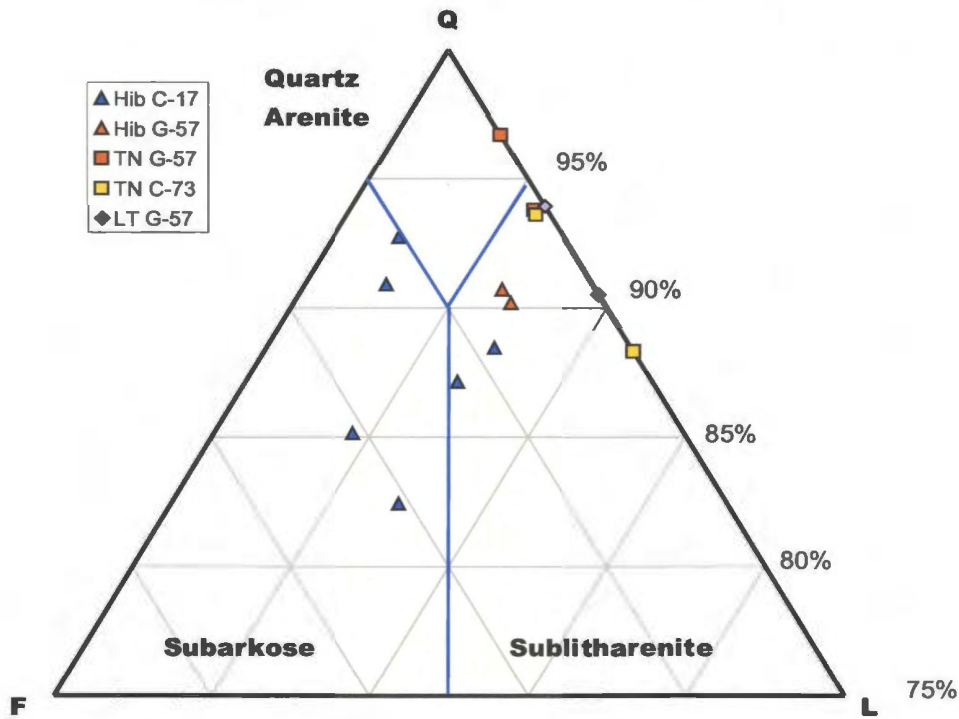
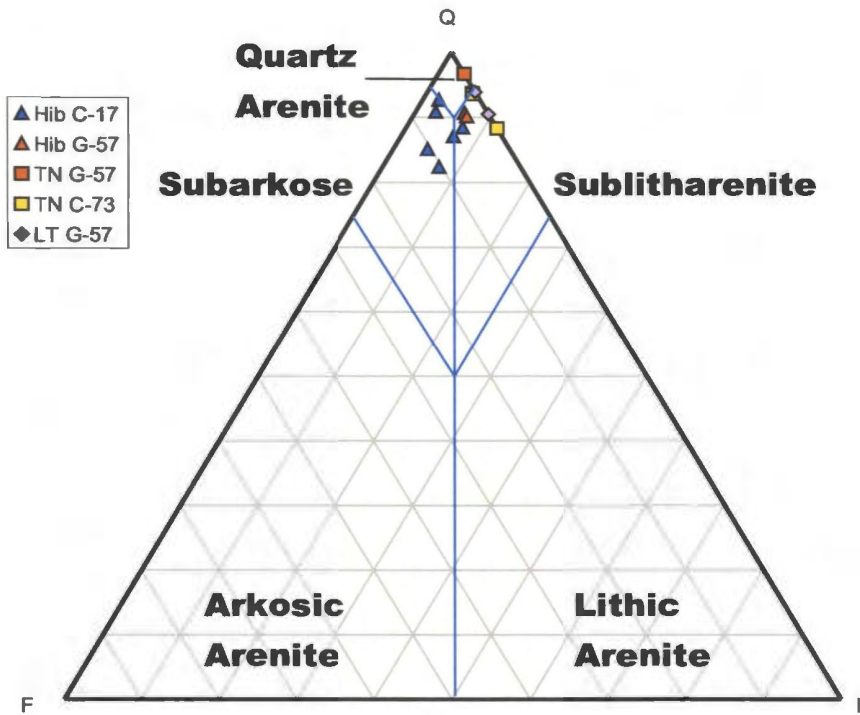


Figure 3.5 - QFL plot of Hibernia Formation (Hib), Terra Nova Member and Lower Tempest Member. Hibernia samples fall in the subarkose and sublitharenite category and samples from the Terra Nova and Lower Tempest members fall in the sublitharenite and quartz arenite category. Samples from the Terra Nova and Lower Tempest members have a very small amount of feldspar, with a number of samples having values of zero.

formations/members are very similar, with the same type of lithics (i.e. shale/mud clasts and carbonate grains). However, the samples from the Terra Nova Member and the Lower Tempest Member have a very small feldspar component (<1%) compared to the Hibernia Formation (0-10%). This is likely due to differences in sediment source for these intervals, although the effect of unstained thin sections on point counts can not be ruled out entirely (see QPK diagram in Figure 3.6)

The Hibernia Formation samples are from two facies. Samples from well G-57 were taken from a medium-to coarse-grained channel facies, while samples from well C-17 were taken from a fine to very fine-grained fluvio-deltaic facies. Samples from well C-17 (fluvio-deltaic facies) have higher feldspar content (4-10%) than samples from the channel facies of well G-57 (3%). In addition, C-17 samples also show a much higher ratio of K-feldspar to plagioclase, which may reflect the greater chemical weathering maturity of fluvio-deltaic (delta front?) facies compared to channel facies. Clearly the results may in part reflect sampling differences because samples from well C-17 (fluvio-deltaic facies) were stained for feldspars and the others not.

### **3.5 Grain Size Analysis**

#### **3.5.1 Introduction**

Grain size analysis was performed on all thin sections used in this study. Detrital grain measurements from digital photographs yield much more accurate values than by visual estimation using a micrometer ocular scale, for example. The best parameters to determine grain size are width and height because other parameters such as length and diameter can yield inaccurate results if the grain is not elongated (for length) or nearly

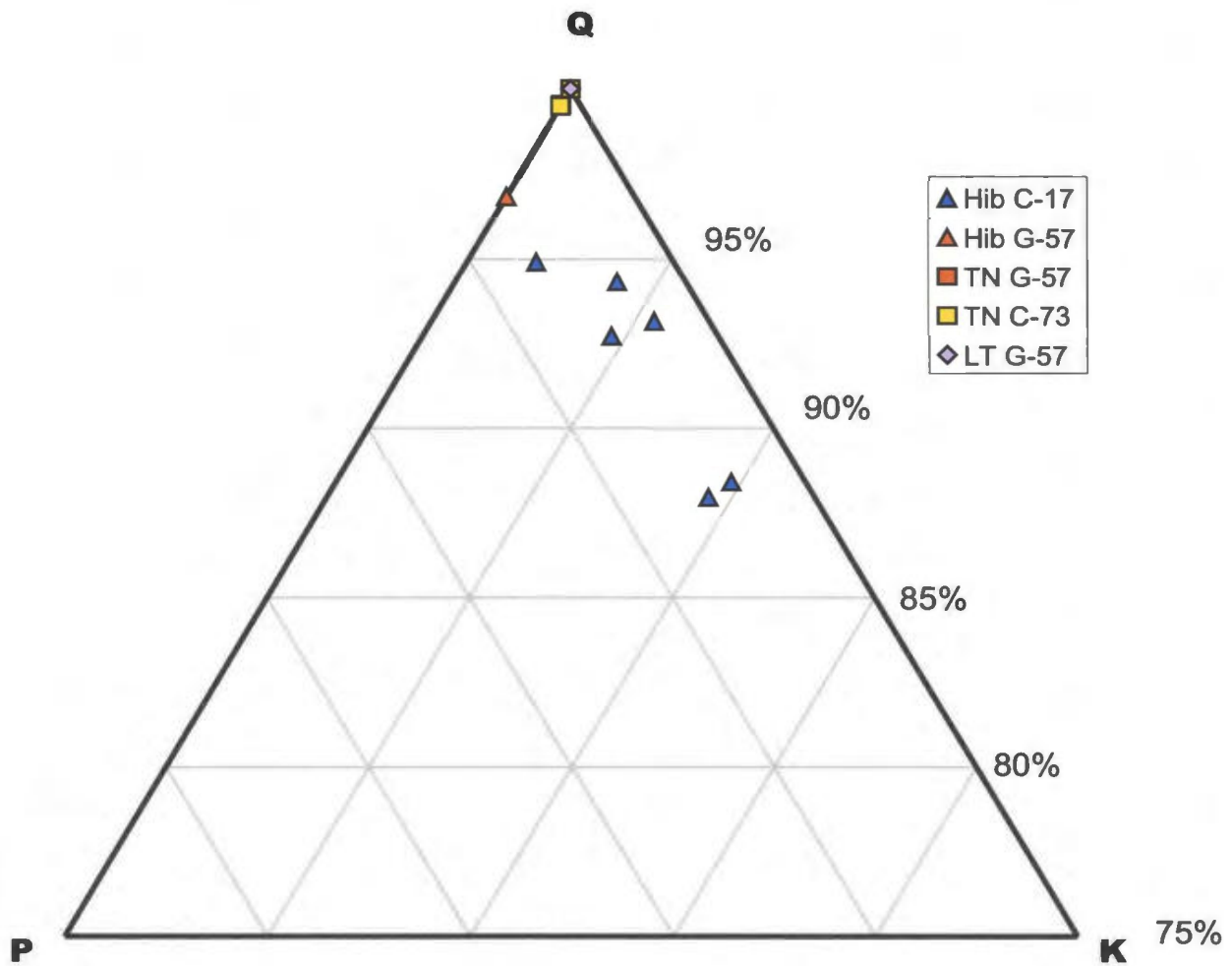


Figure 3.6 - QPK plot of Hibernia, Jeanne d'Arc (Terra Nove Member), and Rankin (Lower Tempest Member) formations. The only samples that show potassium feldspar values are those that were stained. Staining is needed to identify potassium feldspar in these formations

spherical (for diameter). Length values are useful for thin, elongate objects and do not yield accurate results for round or square objects (See Appendix 2 for explanation of all measured parameters). Diameter values can be useful; however, this value is “calculated” from area and assumes the object is a circle.

### **3.5.2 Ben Nevis Formation**

Grain size measurements from the Ben Nevis Formation were taken from 5 wells and 63 samples with a total of 10,025 grains measured. Measurements used to determine grain size are width (dimension parallel to the x-axis) and height (dimension parallel to the y-axis). All grain size data is listed in Appendix 3.

The average width and height values are 86.5 $\mu\text{m}$  and 79.2 $\mu\text{m}$  respectively. Figure 3.7 plots average grain size for all the wells sampled in the Ben Nevis Formation at the White Rose Field. This cross section shows a small amount of grain size variability within each well. Two samples at the top of L-08 have anomalously higher average grain sizes of approximately 220 $\mu\text{m}$  and 207 $\mu\text{m}$  (fine grained sandstone). Grain size is very homogeneous, with a minimal amount of variability between width and height both laterally and vertically. Figure 3.8 is a graph of average grain size with maximum and minimum values plotted. Most samples have maximum values reaching a fine to medium grained sand size range; however samples from wells L-08 and A-17 have values much higher than the average which reach 834 $\mu\text{m}$  (coarse-grained sand size). A bar graph of the frequency of all individual grain measurements (Figure 3.9 A) shows the distribution of grain size. Approximately 90% of all the grains are fine-grained sand to coarse silt

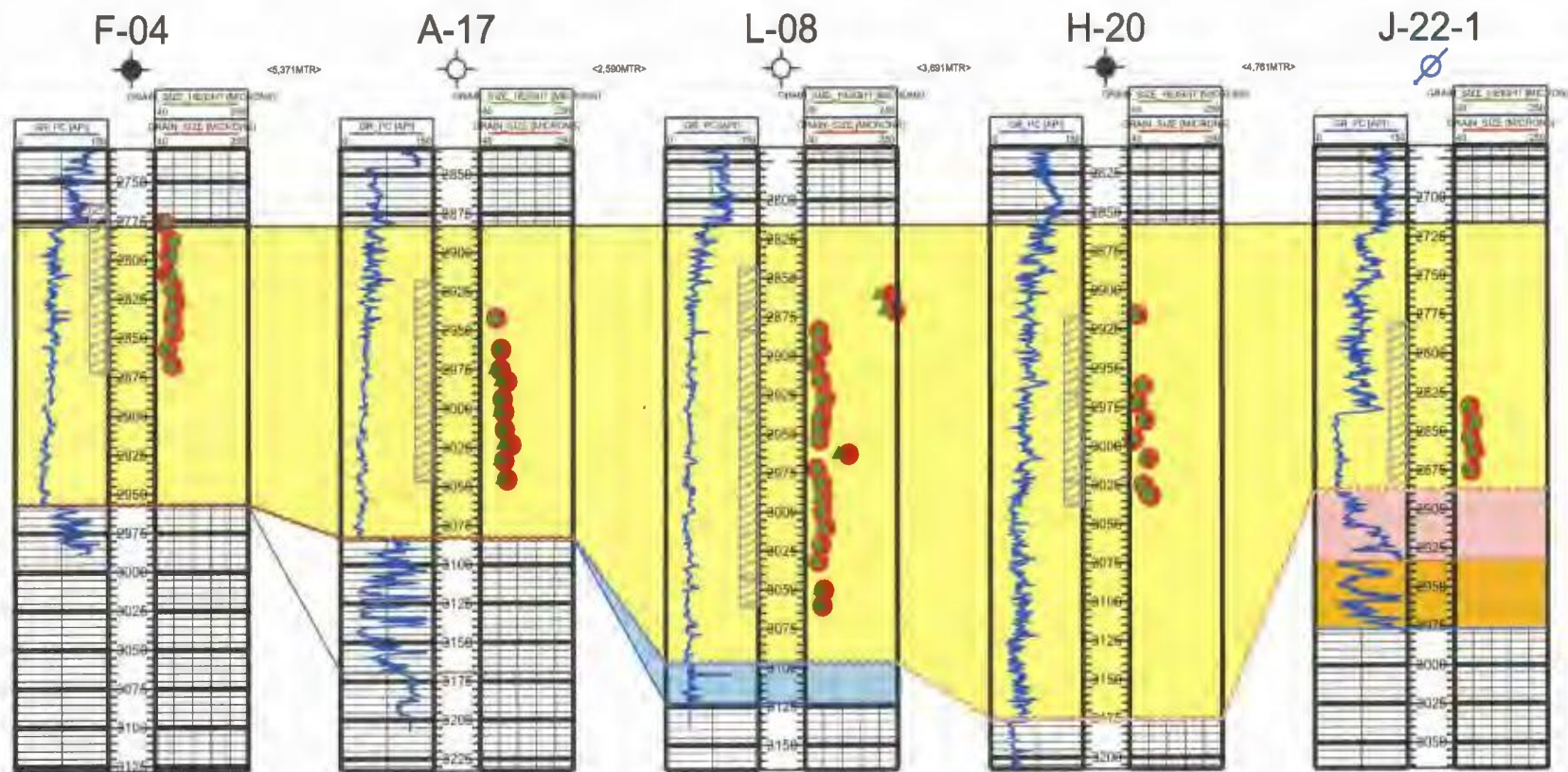


Figure 3.7 - Grain size of samples from the Ben Nevis Formation in the White Rose Field. Minimal grain size changes are seen throughout the wells, except two samples from well L-08 that have larger grain sizes than the rest of the samples. Height values represented by green triangles and width values represented by red circles.

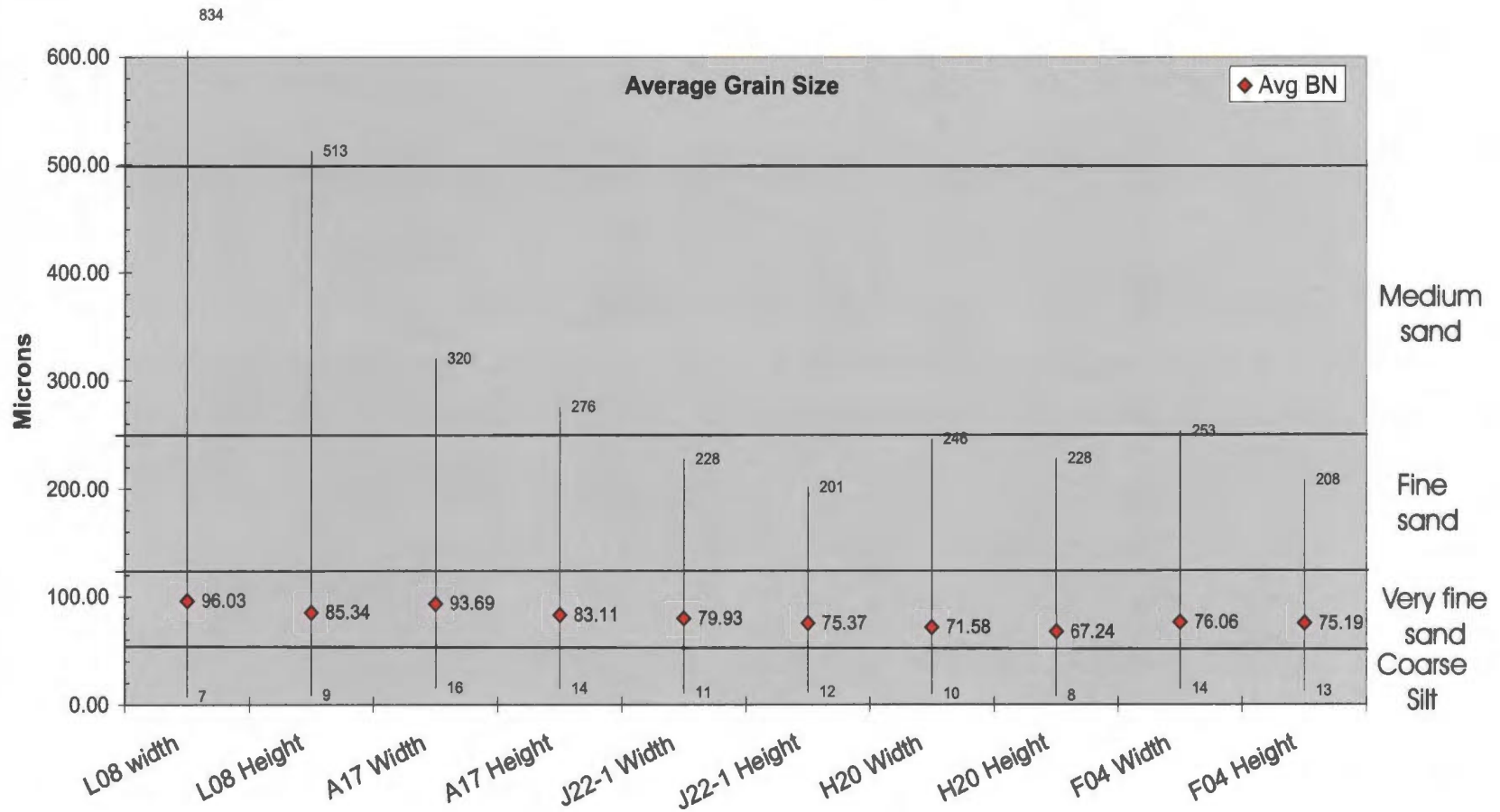


Figure 3.8 - Grain size changes through the Ben Nevis Formation. Diamonds are averages whereas the thin vertical lines join maximum and minimum values. Grain size is relatively homogeneous and is classified as a very fine grained sandstone. Measured parameters width and height are used to determine grain size (see Appendix 2 for definitions). Maximum values are in the fine-to coarse-grained sand range and minimum values are in the coarse silt range.

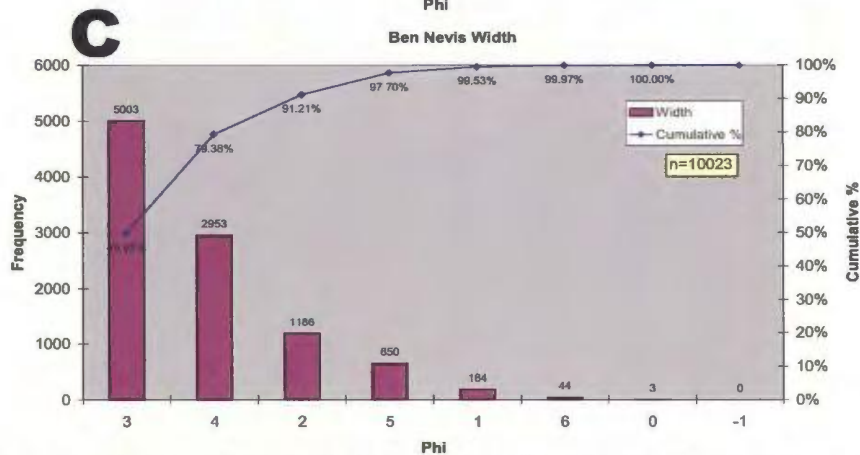
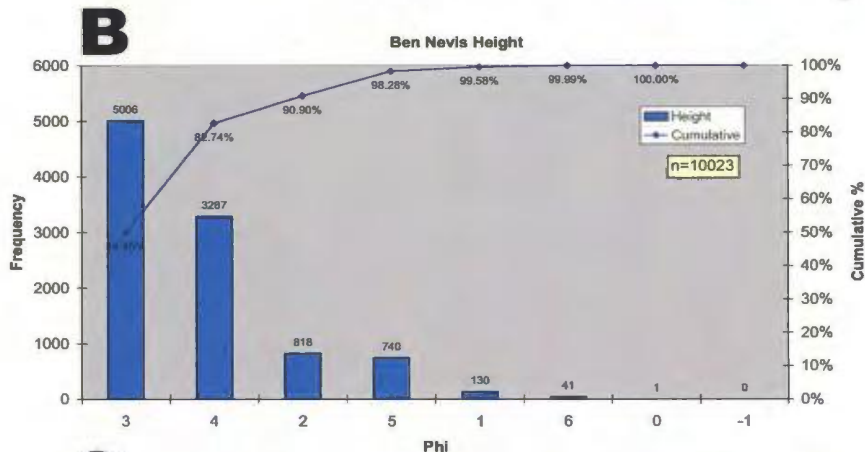
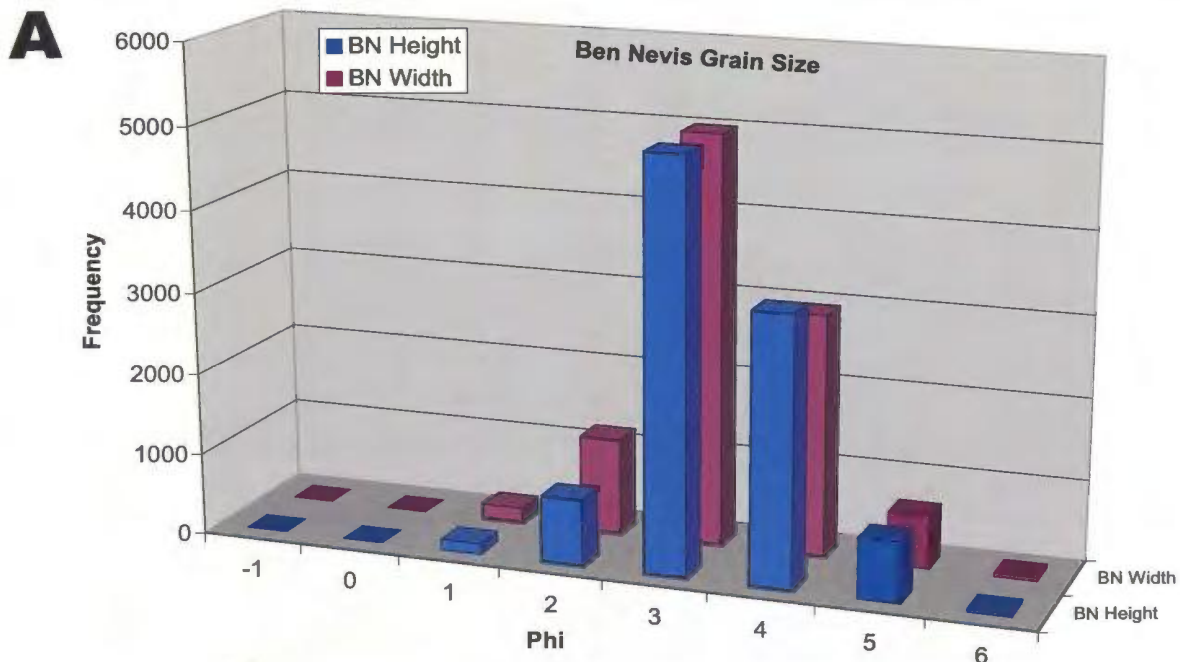


Figure 3.9 - A. - Bar graphs of width and height values from the Ben Nevis Formation (In the above bar graphs each bar represents values from -1 to -0.1; 0 to 0.9; 1 to 1.9 ect.). The plots show normal distributions. B and C. - Sorted histograms of width and height values for all samples taken in the Ben Nevis Formation. Average grain size is very fine-grained.

sized (2-4 phi) and less than 2% are coarse-grained sand (Figures 3.9 B and C). This indicates that the large maximum values seen in L-08 and to a lesser degree in A-17 are merely extreme outliers, and overall grain size in the Ben Nevis Formation is very homogeneous.

Figure 3.10 shows the standard deviations calculated from the measured parameters width and height. The calculated average standard deviation for width and height of the samples from the Ben Nevis Formation are  $0.65\phi$  and  $0.62\phi$  respectively, so the sandstones can be classified as moderately well sorted. Maximum values of the standard deviation of width and height are  $0.84\phi$  and  $0.83\phi$  respectively (moderately sorted). Minimum values of the standards deviation of width and height are  $0.46\phi$  and  $0.45\phi$  respectively (well sorted).

Grain analysis has shown that the Ben Nevis Formation ranges from a coarse silt to a fine-grained sandstone with less than 2% of grain sizes being medium-to coarse grained sand. The Ben Nevis Formation is moderately well-sorted with maximum and minimum values falling into the moderately sorted and well-sorted categories respectively.

### **3.5.3 Hibernia Formation**

Grain size measurements for the Hibernia and Jeanne d'Arc formations were taken from 3 wells and 15 samples (Figure 3.11A) with a total of 2,373 grains measured. There are two different facies that were sampled in the Hibernia Formation and they will be discussed separately.

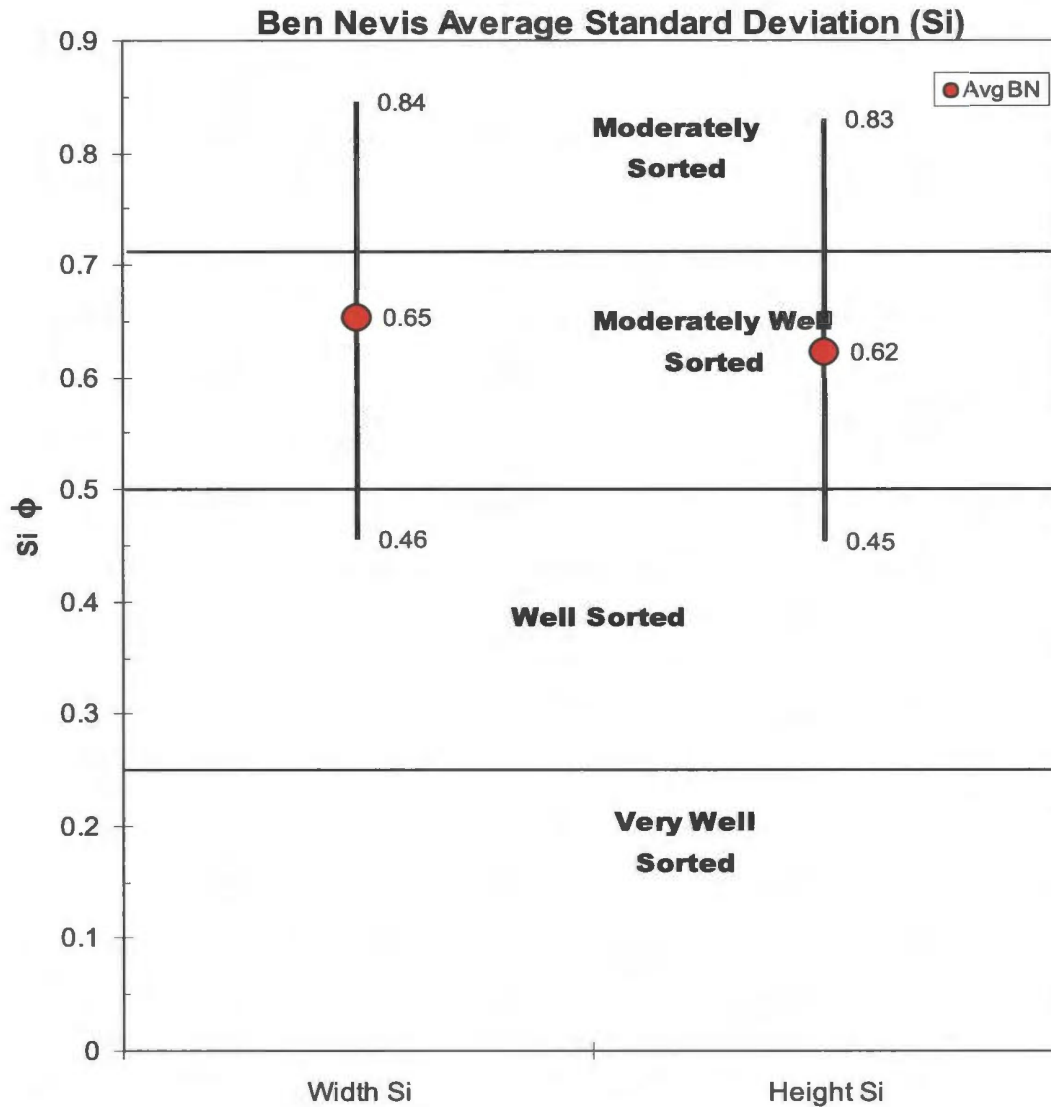


Figure 3.10 - Standard Deviation of the grain size of Ben Nevis Formation samples, with associated maximum and minimum values. The Ben Nevis Formation is moderately well sorted with maximum values plotting in the moderately sorted category and minimum values plotting in the well sorted category.

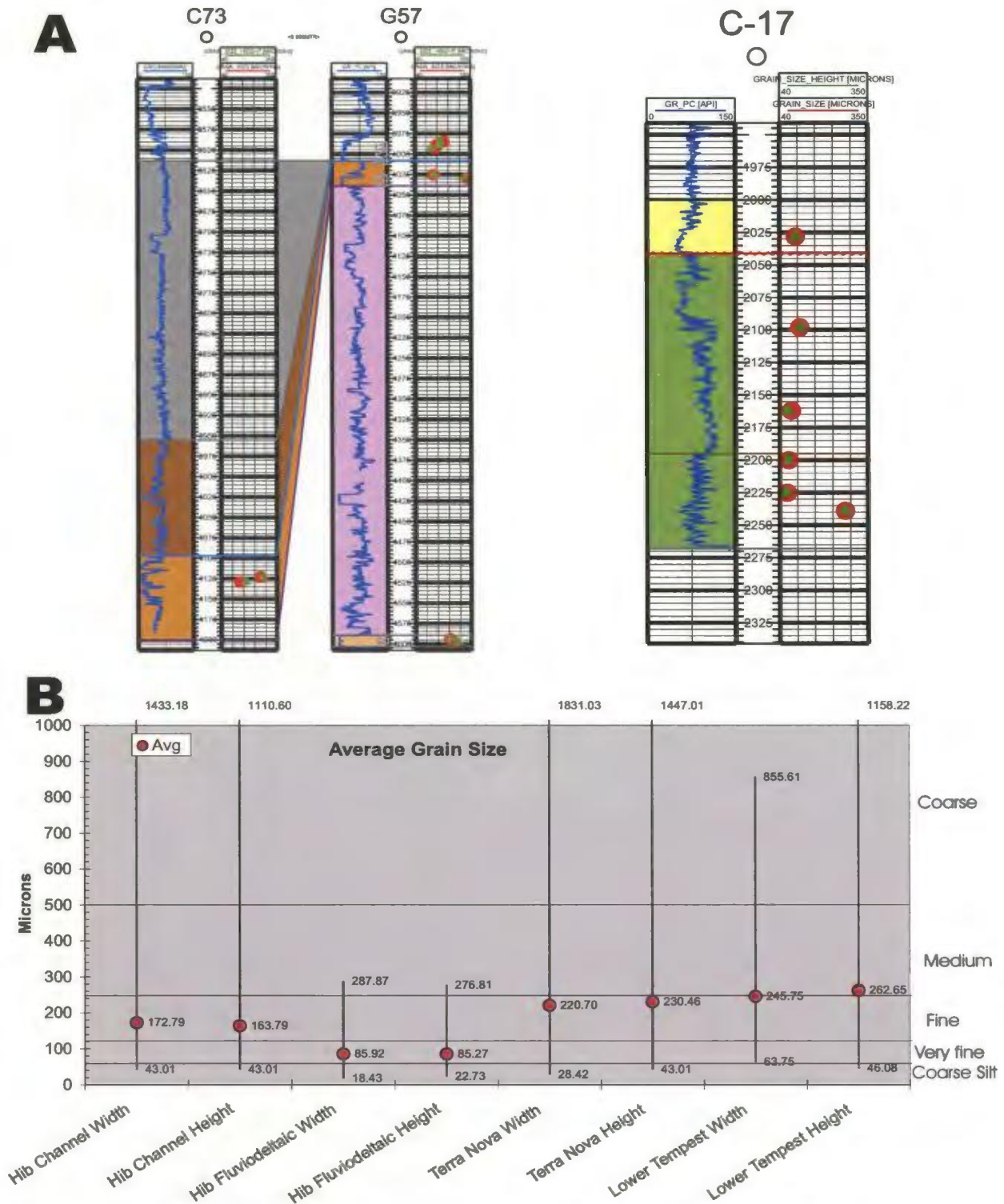


Figure 3.11 - Average grain size for Hibernia Formation, Terra Nova Member, and Lower Tempest Member sandstones. Hibernia Formation samples are fine-grained sandstone, while the Terra Nova and Lower Tempest member sandstones are fine-to medium-grained. There are commonly coarse sand-sized grains seen in all three formations. Red circles represent grain size width and green triangles represent grain size height. Thin vertical lines from B represent maximum and minimum values.

The channel facies of the Hibernia Formation has an average width and height grain size of 172.79  $\mu\text{m}$  and 163  $\mu\text{m}$  respectively (Figure 3.11B). Maximum values reach 772  $\mu\text{m}$  (coarse sand) and minimum values reach 43  $\mu\text{m}$  (coarse silt). A bar graph of width and height measurements (Figure 3.12) shows a unimodal, approximately normal distribution with 95% of all grains being medium to very fine grained sand (Figures 3.12.B and C).

The fluvio-deltaic facies of the Hibernia Formation has an average width and height grain size of 85.92 $\mu\text{m}$  and 85.27 $\mu\text{m}$  respectively (very fine grained). Maximum values reach 287 $\mu\text{m}$  (medium sand) and minimum values reach 18 $\mu\text{m}$  (medium silt). Bar graphs of width and height show a skewed-right bimodal distribution with approximately 98% of the grains being fine-grained sand to coarse silt (Figure 3.12 E and F). Grain size measurements from the Hibernia fluvio-deltaic facies are similar to grain sizes seen in the Ben Nevis Formation.

Standard deviation ( $S_i$ ) values for the Hibernia Formation vary between the two types of facies analysed and are shown in Figure 3.13. Width and height  $S_i$  values for the channel facies are 0.65 $\phi$  and 0.67 $\phi$  respectively. Width and height values for the fluvio-deltaic facies are 0.54 $\phi$  and 0.55 $\phi$  respectively. Both facies are moderately well sorted, however some values for each facies plot at the upper and lower limit of the moderately sorted category. The fluvio-deltaic facies is slightly better sorted than the channel facies.

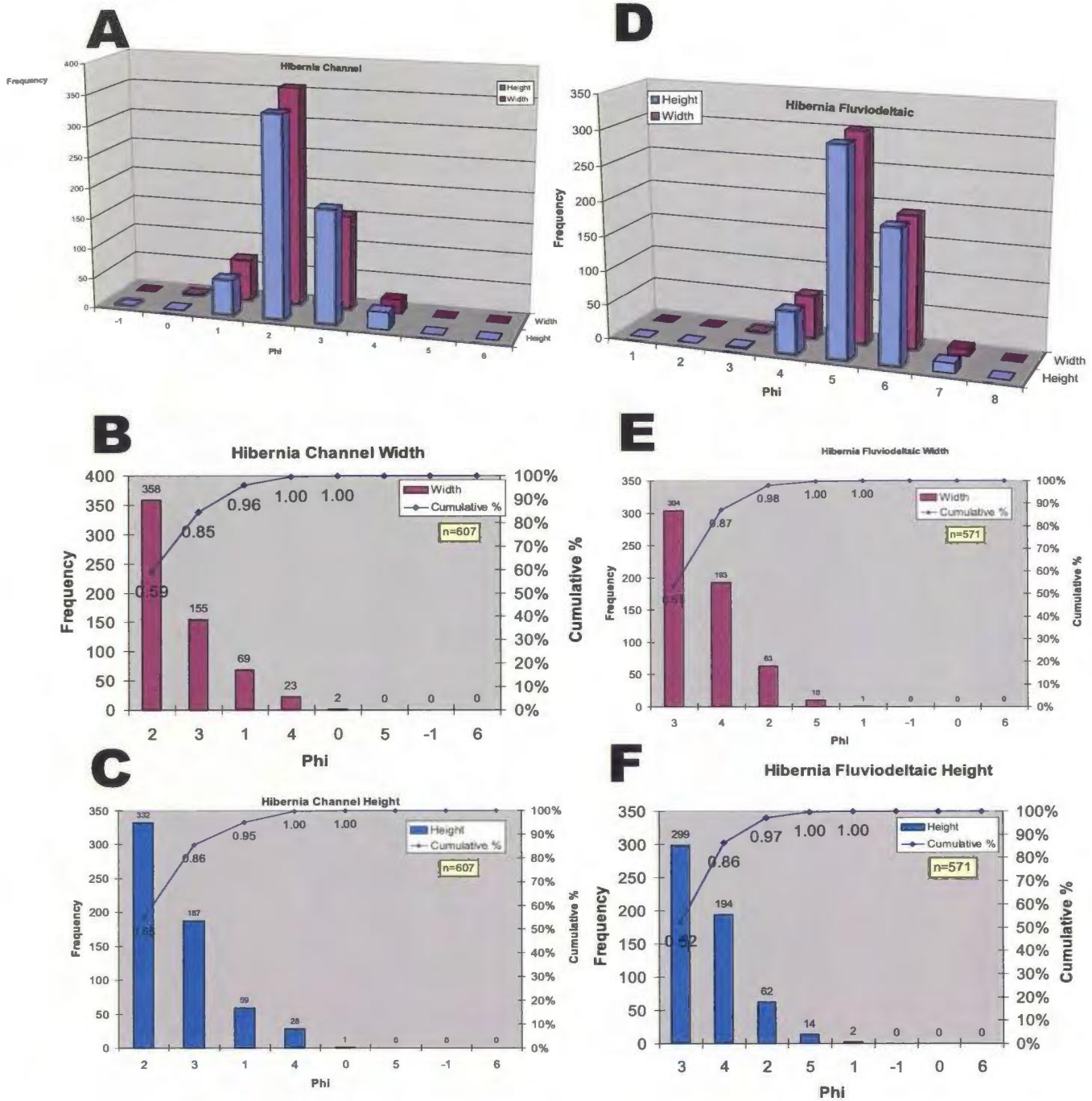


Figure 3.12 - Width and height values from the Hibernia Formation. A and D. - Bar graphs of width and height from the Hibernia channel facies (A) and the Hibernia fluviodeltaic facies (D). B, C, E, and F. - Sorted bar graphs of width and height. Average grain size is fine grained sandstone.

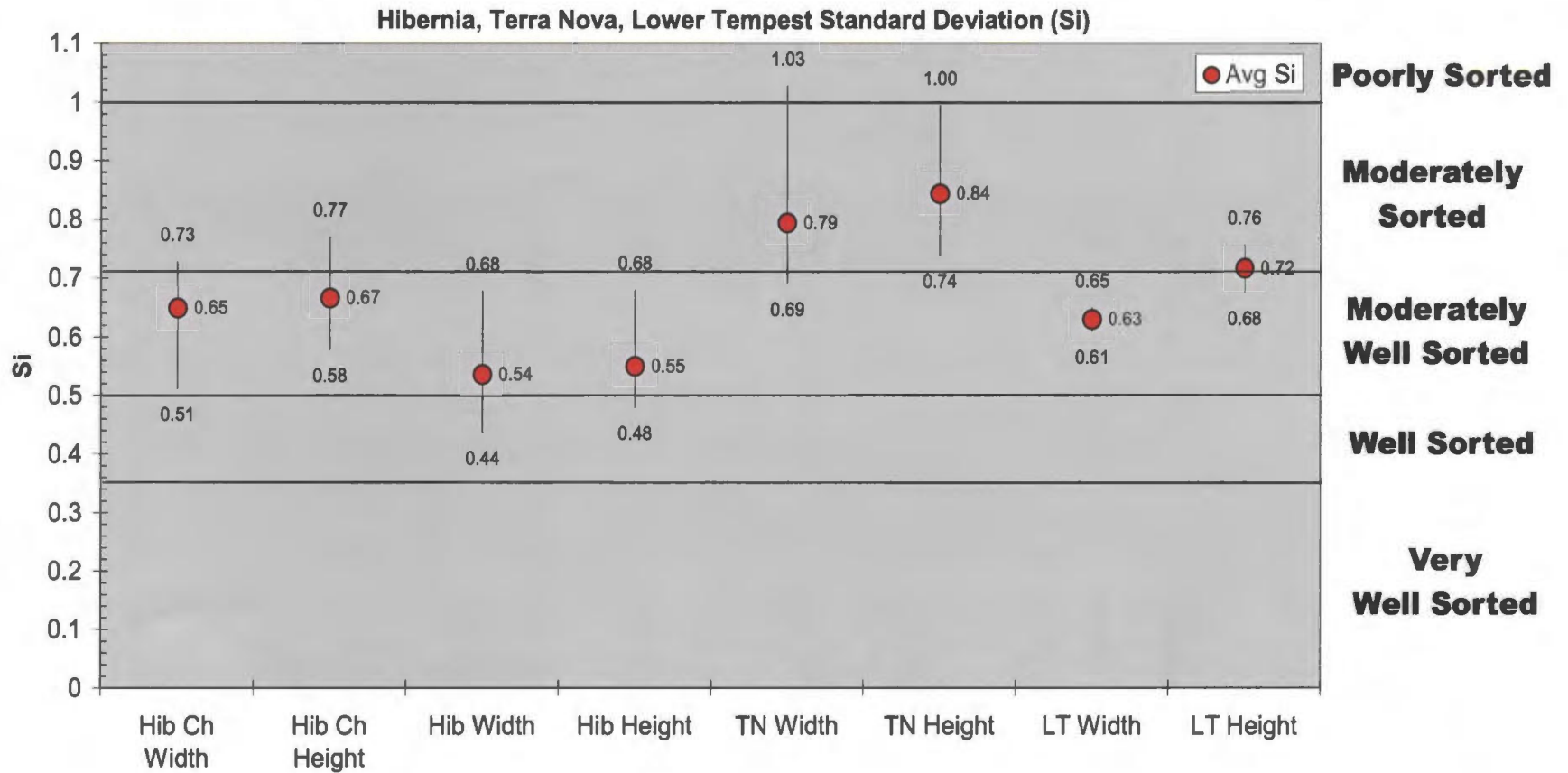


Figure 3.13 - Standard deviation of the Hibernia Formation, Terra Nova and Lower Tempest Members, with maximum and minimum values. Hibernia Formation and Lower Tempest Member are moderately well sorted, while the Terra Nova Member is moderately sorted.

### 3.5.4 Terra Nova and Lower Tempest Members

The Terra Nova Member has an average width and height grain size of 220  $\mu\text{m}$  and 230  $\mu\text{m}$  respectively (Figure 3.11). Maximum values reach 1831  $\mu\text{m}$  (very coarse sand) and minimum values reach 28.42  $\mu\text{m}$ . (medium silt). A bar graph of width and height values (Figure 3.14A) shows a normal distribution of grain sizes with approximately 88% of all grains being medium to very fine grained sand (Figure 3.14 B and C). The Lower Tempest Member has an average width and height grain size of 245.75  $\mu\text{m}$  and 262.65  $\mu\text{m}$  respectively (Figure 3.11). Maximum values reach 1158  $\mu\text{m}$  (very coarse sand) and minimum values reach 46  $\mu\text{m}$  (coarse silt). A bar graph of width and height values (Figure 3.14 D) shows a normal distribution that is slightly skewed left with 83-85% of all grains being medium to fine grained sand, and with approximately 2% of grains being very coarse to coarse grained sand (Figure 3.14 E and F).

Standard deviation values for the Terra Nova and Lower Tempest Members are shown in Figure 3.13. Width and height  $S_i$  values for the Terra Nova Member are 0.79  $\phi$  and 0.84  $\phi$  respectively and classify the Terra Nova Member as moderately sorted. Maximum and minimum values stay in the moderately well sorted category as well. Width and height  $S_i$  values for the Lower Tempest Member are 0.63  $\phi$  and 0.72  $\phi$  respectively and these samples are classified as moderately to moderately well sorted. Compared to the other units, maximum and minimum values are not significantly different and do not deviate far from the average, likely because only two (2) samples of the Lower Tempest Member were measured.

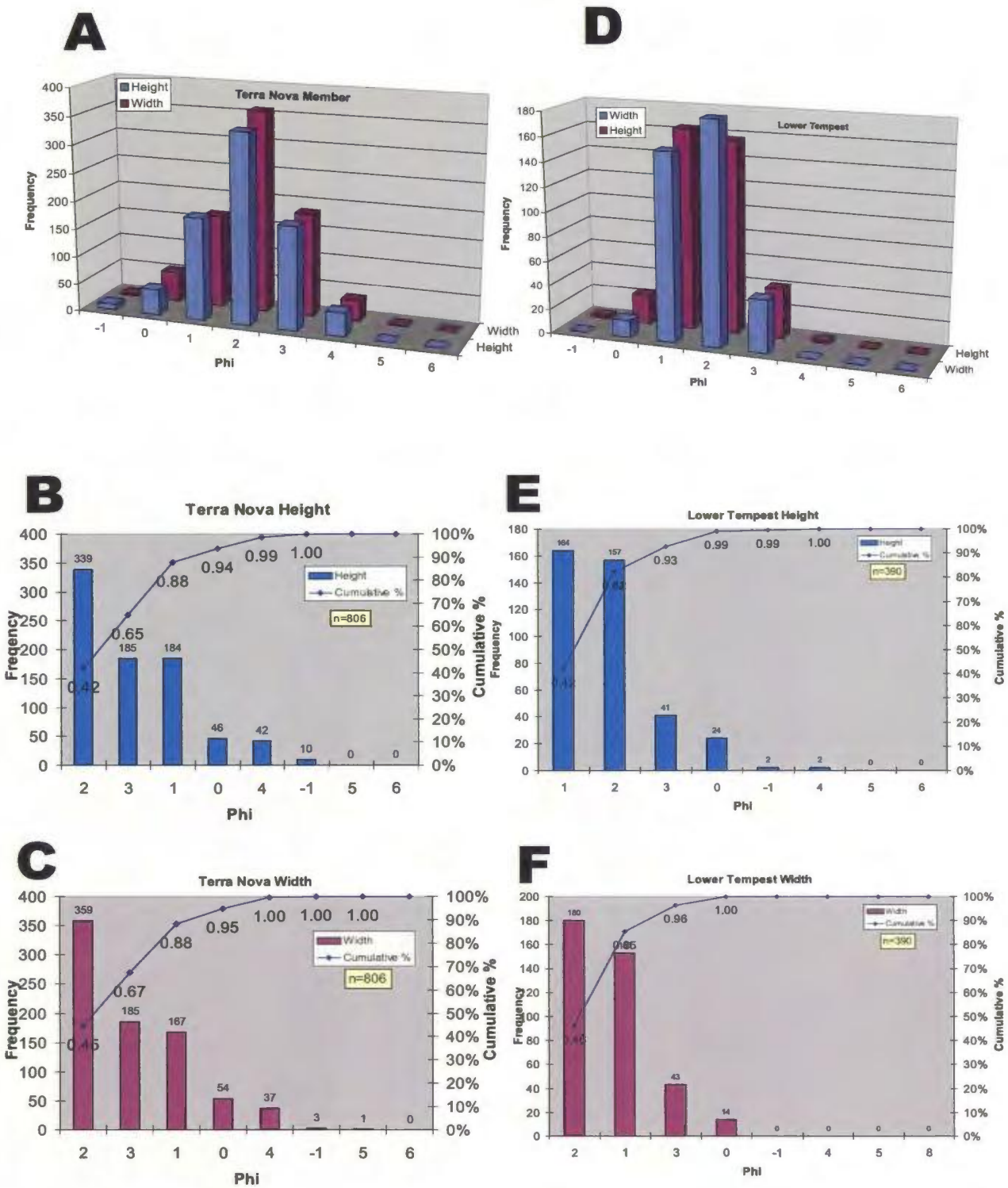


Figure 3.14- Width and height values for the Terra Nova and Lower Tempest members. A and D.- Histograms of width and height from the Terra Nova and Lower Tempest Members. B, C, E, and F. - Sorted histograms of width and height. Average grain size is fine grained.

### 3.5.5 Grain Size Interpretations

The large number of samples taken from the Ben Nevis Formation ensures that the values determined from the grain analysis are reliable. The Hibernia Formation has the second largest number of samples, followed by the Terra Nova and Lower Tempest members; hence, the accuracy of average grain sizes for each formation follows the same order.

Average grain size for samples of the Ben Nevis Formation is very uniform (very fine-grained sand) with only four of 10,023 grains in total being larger than a medium sand grade (1  $\phi$ ) and only 85 grains being smaller than medium silt grade (6  $\phi$ ) (Figure 3.9). Average grain sizes for the Hibernia Formation, Terra Nova and Lower Tempest members are coarser with a higher amount of variability in grain sizes. Average grain sizes for the Hibernia channel facies are larger (fine-grained sand) than the Hibernia fluvio-deltaic facies (very fine grained sand), the latter being in the same range as the Ben Nevis Formation samples. Grain size for the Terra Nova and Lower Tempest members is also relatively large (fine-to medium-grained sand) and is comparable to the Hibernia channel facies. The data indicates that samples taken from channel facies are coarser grained than samples from marginal marine settings (fluvio-deltaic and shoreface).

Standard deviations for the Ben Nevis Formation are uniform and fall into the moderately well sorted category with a small amount of variation (Figure 3.10). Both width and height maximum and minimum standard deviation values fall into the moderately sorted and the well-sorted category respectively. This high level of sorting was likely produced in a shoreface setting in which wave processes reworked and sorted

grains very efficiently (Ferry, 2005). The Hibernia channel facies and the Terra Nova and Lower Tempest members are moderately to moderately well sorted with a higher variability in grain sizes, which is likely due to the fluvial nature and lower amounts of reworking compared to the shoreface samples of the Ben Nevis Formation.

## Chapter 4: Geochemistry

### 4.1 Introduction

Whole rock major and trace-element geochemistry have been more widely applied to the correlation of sedimentary successions in the last few years (North et al., 2005). Variations in chemical abundances can reflect changes in sediment provenance and processes active in the alluvial basins through which sediment is transported to the oceans (Hurst and Morton, 2001). There are a number of factors that control the geochemistry of a sedimentary rock; these include: a) composition of source terrain; b) chemical weathering; c) hydraulic sorting; d) diagenesis; e) metamorphism; and, f) hydrothermal alteration (Fralick and Kronberg, 1997).

The distribution of trace elements is sensitive to the nature of the provenance (McLennan et al., 2003). During most sedimentary processes, elements such as Al, Fe, Ti, Mn, Zr, Hf, Nb, Cr, Ni, V, Co and the rare-earth elements (La-Lu, Y, Sc) are strongly retained in particulate material and not released in solution (McLennan et al., 2003). Using specific trace elements found in sedimentary rock is a well established method for determining provenance. The distribution of ferromagnesian trace elements (Cr, V, Ni, Co) to detect mafic source rocks is another common application that has been used in provenance studies.

Samples were taken from both cores and cuttings from the Ben Nevis, Avalon, Eastern Shoals and Hibernia formations, and the results are presented in Appendix 4. As a general rule, cuttings samples tend to have a higher concentration of trace elements compared to core samples, and whenever possible core samples should be relied on to

obtain the most accurate values. Most samples from the Hibernia Formation are coarse-grained sandstones and problems arise when attempting to correlate these samples with the finer grained Ben Nevis Formation, so attempts must be made to reduce grain size bias between samples. The use of ratio techniques is a common method for evaluating geochemical data in relation to provenance associations and to compensate for differing grain sizes. Plotting specific trace elements against one another has proven useful to minimize grain size biases and to answer specific questions about the provenance of a rock.

#### **4.2 Contaminated Samples**

Cuttings samples are liable to contain varying amount of drilling mud contaminants such as drill bit shavings, and mud invasion into the sample, causing high values of those oxides and elements found in the drilling mud and/or the drill bit. It is therefore necessary to closely examine all cuttings data to eliminate or at least understand levels of contamination.

When correcting for the relative contributions of calcite, dolomite and apatite to CaO, with regards to the CIA equation, most CaO (corrected) values came out to be negative, indicating that none of the CaO in the sample was associated with feldspars. Therefore any negative values were input as zero in the CIA equation.

The difference between  $K_2O$  values and  $Na_2O$  values in the core samples from the Ben Nevis Formation is always lower than one (with the exception of a single sample – F-04 2809m) (Figure 4.1). Thus, all samples that have a difference between  $K_2O$  and  $Na_2O$  greater than one are herein considered contaminated because core samples don't show

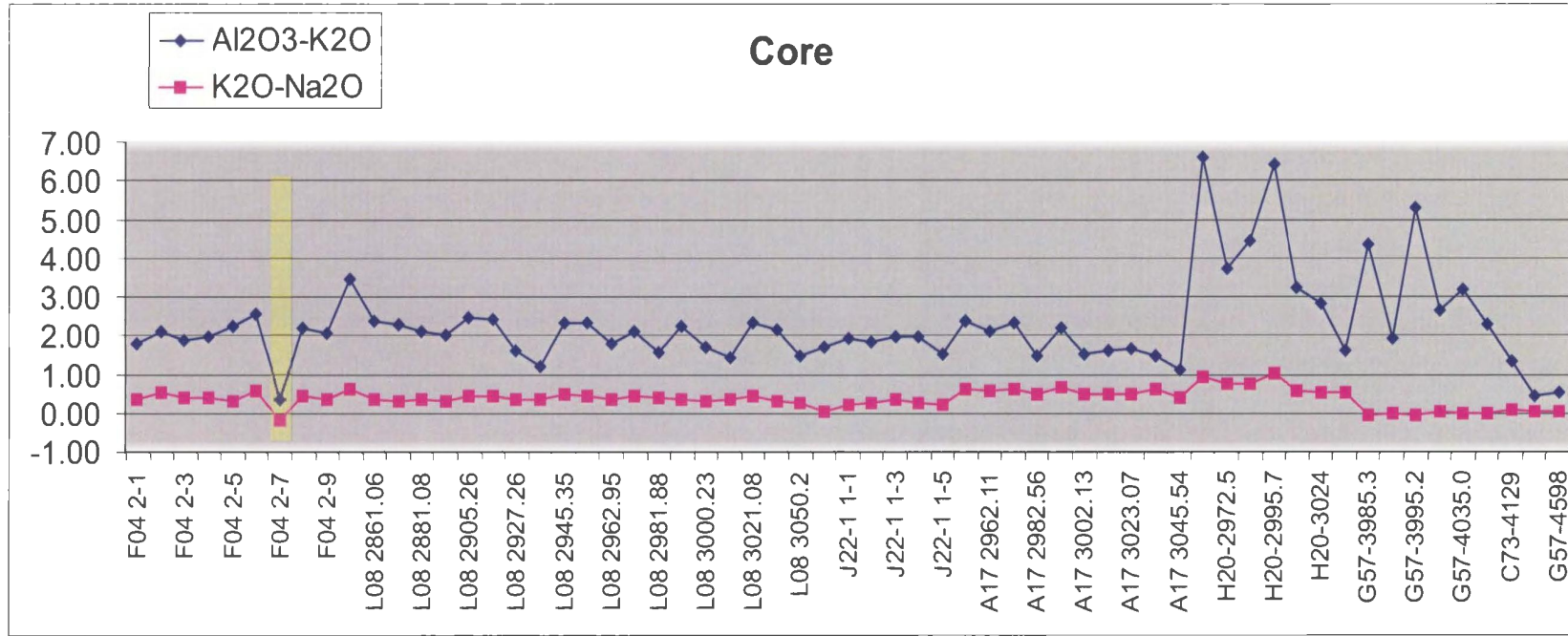


Figure 4.1 -  $\text{Al}_2\text{O}_3\text{-K}_2\text{O}$  and  $\text{K}_2\text{O-Na}_2\text{O}$  differences for samples from cores. All core samples have  $\text{K}_2\text{O-Na}_2\text{O}$  differences less than one, indicating they are not contaminated (except sample F-04 2809m which is due to a very high amount of  $\text{Na}_2\text{O}$ , thought to be due to drilling fluid contamination). All  $\text{Al}_2\text{O}_3\text{-K}_2\text{O}$  values have a difference greater than one, indicating they are not contaminated (except sample F-04 2809m).

such  $\text{Na}_2\text{O}$  or  $\text{K}_2\text{O}$  extremes. It is also observed that samples of core from the Ben Nevis Formation have a difference between  $\text{Al}_2\text{O}_3$  and  $\text{K}_2\text{O}$  greater than one (with the exception of contaminated sample F-04 2809m). Contaminated samples have high concentrations of  $\text{K}_2\text{O}$  because potassium is present in the drilling mud. If  $\text{K}_2\text{O}$  concentrations are high enough to be roughly equal to  $\text{Al}_2\text{O}_3$  concentrations (i.e.  $<1$ ) one can assume the sample has been contaminated. Note that such samples typically result with CIA values less than 50, thereby placing them in the (apparent) compositional domain of various types of igneous rocks, rather than that of sediments or sedimentary rocks which have CIA values  $> 50$ .

Within the Avalon Formation, samples from well J22-1 have  $\text{K}_2\text{O}-\text{Na}_2\text{O}$  differences less than one and are not considered contaminated (Figure 4.2). Samples from well H-20, however, show a difference in  $\text{K}_2\text{O}-\text{Na}_2\text{O}$  greater than one and a difference between  $\text{Al}_2\text{O}_3$  and  $\text{K}_2\text{O}$  less than 1 (Figure 4.2) and are considered contaminated. If the contaminants were eliminated one would expect to see a larger difference in the  $\text{Al}_2\text{O}_3-\text{K}_2\text{O}$  values and a smaller difference between the  $\text{K}_2\text{O}-\text{Na}_2\text{O}$  values. This method works for all samples used in this study (Figure 4.2 – Avalon, Eastern Shoals, Hibernia, and Ben Nevis formation cuttings). Using this method the contaminated samples are identified and not included in any of the trace- and/or major-element plots and subsequent data interpretation presented in this chapter.

Table 4.1 is a list of all samples considered to be contaminated. It is not a coincidence that all of the samples from a specific well interval are contaminated, indicating a type of drilling mud and/or incomplete sieving and flushing of cuttings samples. Cuttings samples from wells J-22-1, K-19, F-20 and E-09 have been determined

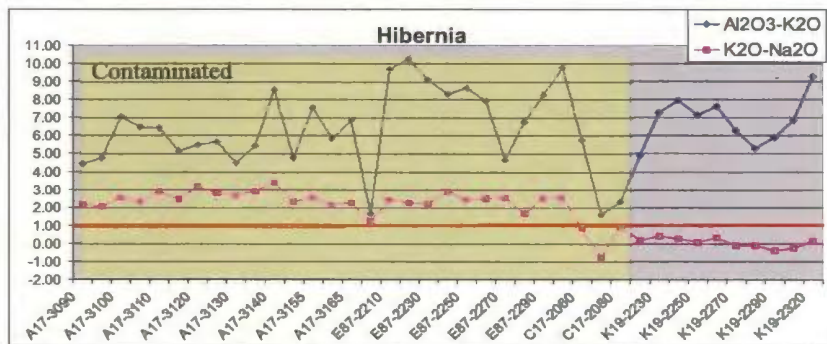
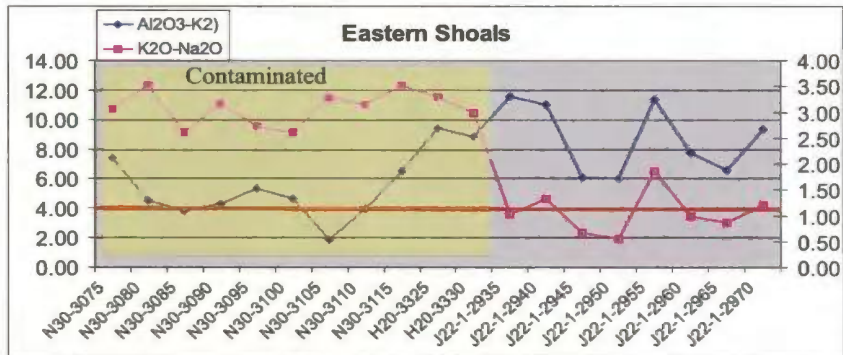
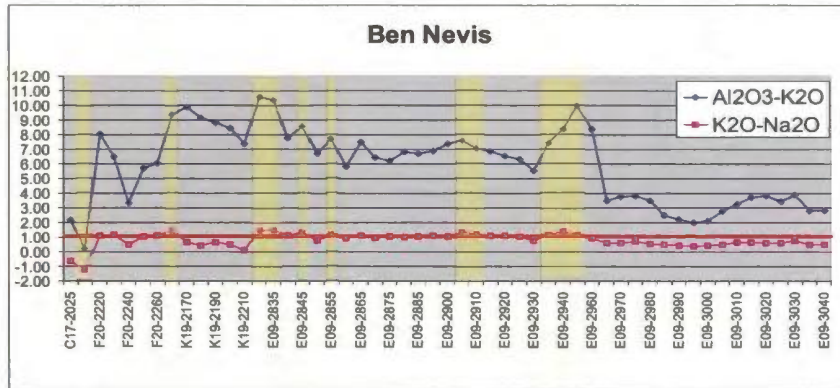
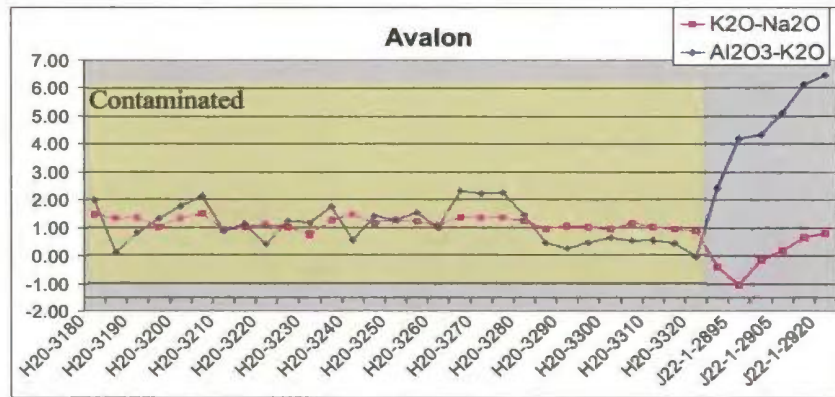


Figure 4.2 - Contamination graphs for samples from cuttings of the Ben Nevis, Avalon, Eastern Shoals and Hibernia formations.

Table 4.1 – List of contaminated samples based on K<sub>2</sub>O-Na<sub>2</sub>O and Al<sub>2</sub>O<sub>3</sub>-K<sub>2</sub>O differences

	Sample	K2O- Na2O	Al2O3- K2O		Sample	K2O- Na2O	Al2O3- K2O		Sample	K2O- Na2O	Al2O3- K2O
Eastern Shoals	N30-3075	<b>3.08</b>	7.39	Ben Nevis cont.	A17-3050	<b>1.58</b>	0.21	Avalon	H20-3180	<b>1.48</b>	1.97
	N30-3080	<b>3.52</b>	4.48		A17-3055	<b>1.70</b>	-0.15		H20-3185	<b>1.32</b>	0.09
	N30-3085	<b>2.62</b>	3.83		A17-3060	<b>1.48</b>	-0.28		H20-3190	<b>1.35</b>	0.82
	N30-3090	<b>3.16</b>	4.31		A17-3065	<b>1.34</b>	-0.38		H20-3195	<b>1.02</b>	1.32
	N30-3095	<b>2.73</b>	5.31		A17-3070	<b>1.34</b>	-0.15		H20-3200	<b>1.32</b>	1.76
	N30-3100	<b>2.61</b>	4.68		A17-3075	<b>0.87</b>	-0.08		H20-3205	<b>1.49</b>	2.11
	N30-3105	<b>3.29</b>	1.85		A17-3080	<b>1.20</b>	-0.23		H20-3210	0.89	<b>0.86</b>
	N30-3110	<b>3.14</b>	3.93		A17-3085	<b>1.96</b>	4.35		H20-3215	<b>1.01</b>	1.10
	N30-3115	<b>3.52</b>	6.54		F04-2875	<b>1.98</b>	5.23		H20-3220	<b>1.12</b>	<b>0.40</b>
	H20-3325	<b>3.31</b>	9.44		F04-2880	<b>2.17</b>	6.94		H20-3225	<b>1.02</b>	1.23
	H20-3330	<b>2.98</b>	8.84		F04-2885	<b>1.82</b>	5.72		H20-3230	0.76	1.16
Hibernia	A17-3090	<b>2.18</b>	4.45	F04-2890	<b>2.11</b>	7.43	H20-3235	<b>1.24</b>	1.73		
	A17-3095	<b>2.04</b>	4.80	F04-2905	<b>2.57</b>	12.91	H20-3240	<b>1.48</b>	<b>0.54</b>		
	A17-3100	<b>2.56</b>	7.04	F04-2945	<b>1.53</b>	2.99	H20-3245	<b>1.17</b>	1.40		
	A17-3105	<b>2.30</b>	6.49	F04-2950	<b>1.25</b>	4.93	H20-3250	<b>1.27</b>	1.27		
	A17-3110	<b>2.90</b>	6.45	F04-2955	<b>2.20</b>	9.31	H20-3255	<b>1.22</b>	1.53		
	A17-3115	<b>2.47</b>	5.15	F20-2250	<b>1.05</b>	5.72	H20-3260	<b>1.04</b>	<b>1.00</b>		
	A17-3120	<b>3.17</b>	5.52	F20-2270	<b>1.50</b>	9.41	H20-3265	<b>1.39</b>	2.30		
	A17-3125	<b>2.79</b>	5.67	E09-2830	<b>1.46</b>	10.60	H20-3270	<b>1.35</b>	2.22		
	A17-3130	<b>2.65</b>	4.52	E09-2835	<b>1.50</b>	10.39	H20-3275	<b>1.37</b>	2.26		
	A17-3135	<b>2.95</b>	5.46	E09-2840	<b>1.13</b>	7.80	H20-3280	<b>1.22</b>	1.44		
	A17-3140	<b>3.41</b>	8.60	E09-2845	<b>1.31</b>	8.60	H20-3285	0.97	<b>0.45</b>		
	A17-3145	<b>2.31</b>	4.80	E09-2855	<b>1.18</b>	7.74	H20-3290	<b>1.05</b>	<b>0.26</b>		
	A17-3155	<b>2.57</b>	7.56	E09-2865	<b>1.10</b>	7.52	H20-3295	<b>1.03</b>	<b>0.45</b>		
	A17-3160	<b>2.12</b>	5.87	E09-2905	<b>1.31</b>	7.62	H20-3300	<b>0.94</b>	<b>0.63</b>		
	A17-3165	<b>2.27</b>	6.86	E09-2910	<b>1.21</b>	7.03	H20-3305	<b>1.17</b>	<b>0.52</b>		
	A17-3175	<b>1.21</b>	1.64	E09-2940	<b>1.39</b>	8.36	H20-3310	<b>1.03</b>	<b>0.55</b>		
	E87-2210	<b>2.42</b>	9.72				H20-3315	<b>0.94</b>	<b>0.43</b>		
	E87-2220	<b>2.25</b>	10.28				H20-3320	<b>0.88</b>	<b>-0.05</b>		
	E87-2230	<b>2.21</b>	9.13	Ben Nevis							
	E87-2240	<b>2.90</b>	8.36	F04 2-7	-0.20	<b>0.34</b>					
	E87-2250	<b>2.43</b>	8.68								
E87-2260	<b>2.50</b>	7.97									
E87-2270	<b>2.55</b>	4.70	Lower Tempest								
E87-2280	<b>1.65</b>	6.77	G57-4594.25	0.02	<b>0.45</b>						
E87-2290	<b>2.51</b>	8.28	G57-4598	0.03	<b>0.54</b>						
E87-2300	<b>2.57</b>	9.80									

to be accurate with minimal contamination and can be used on A-CN-K ternary diagrams for the interpretation of possible weathering trends.

### **4.3 Grain Size**

When using geochemistry for correlations, it is important to ensure that grain size bias is minimized. It is assumed that coarser grained sediments have undergone lesser amounts of weathering/abrasion and are therefore able to retain a larger number of labile, relatively unstable minerals, hence larger elemental values for coarser grained samples (and correspondingly smaller elemental values for finer grained samples). This means that samples with different grain sizes might have different chemistry even from the same sources, so are not useful for comparison purposes. If ratios of immobile elements are compared rather than the concentrations of these and other elements, grain size bias is reduced or eliminated, assuming that the elements in question are contained within the same minerals. For example, if a coarser grained sandstone has higher amounts of zirconium and niobium than a fine-grained sandstone the raw values can not be compared to one another. However, if the two elements are geochemically related, as for example by their characteristic lack of geochemical mobility, the ratio of the two elements should be similar in both rocks and these ratios are comparable.

There is a grain size difference between selected samples, in particular the very fine-grained sandstones of the Ben Nevis Formation and the medium-to fine-grained sandstones of the Hibernia Formation, the Terra Nova and the Lower Tempest members. It is therefore important to use ratios when comparing these formations.

#### 4.4 Element Mobility

The geochemistry of a rock is controlled by many variables other than source rock composition. Initial compositions may be modified by chemical and physical weathering during erosion, transport, and deposition (Sawyer, 1986); as well, diagenesis and hydrothermal alteration may have a large influence on composition after deposition. Determining if an element is in a detrital or diagenetic mineral phase is essential when applying whole rock and trace-element geochemistry. Elements with a low solubility in aqueous fluids are unlikely to become mobile during diagenesis and so are more likely to represent the sediment source area as well as to reflect depositional processes and patterns (Fralick and Kronberg, 1997). There are a number of factors that control the solubility and mobility of elements in sediments, most importantly pH, Eh, and sediment grain size (North et al., 2005).

Fralick and Kronberg (1997) explain that immobile elements will increase or decrease in concentration as mobile elements are lost from, or gained by the rock. When sediment samples from the same source terrain are plotted on an x-y scatter plot one of two patterns will emerge. If both elements are immobile, and their major mineral phases are hydrodynamically similar, the data points will plot on a trend line that points toward the origin. If one or both elements are mobile then the data will be scattered with no obvious trends observed (see Figure 1 from Fralick and Kronberg, 1997). Because anomalous linear arrays can result if element pairs share chemical properties it is necessary to impose conditions to yield accurate results. These conditions include: 1) sediments eroded from different areas of a designated source terrain either have similar compositions or were premixed before entering the basin, and; 2) only elements having

sufficiently different chemical properties should be plotted against one another (significant differences in starting compositions of samples will produce a scattering of points). Based on these conditions, samples from the Rankin Formation and the A Marker Member are not shown on these graphs (Figures 4.3 and 4.4) and are excluded from direct comparison with the Ben Nevis Formation due to their different compositions (both are classified as carbonate rocks).

The first step in determining element mobility is to plot pairs of elements that are suspected of being immobile (*i.e.* Al, Ti, Zr, Nb and Y). Element pairs involving Nb, Y, and TiO<sub>2</sub> from the Ben Nevis, Avalon, Eastern Shoals, White Rose and Hibernia formations form reasonably linear arrays along lines that extend toward the origin (Figure 4.3A-C), with  $r^2$  values ranging from 0.82-0.88. Hence, these can be classified as immobile elements. The trend lines in plots involving Yttrium (Y) intercept somewhere between 0 and 5 ppm Y (not at zero) indicating that Y is contained in a phase lacking Al<sub>2</sub>O<sub>3</sub>, TiO<sub>2</sub> and Nb. This is consistent with trace amounts of monazite, which commonly contains Y and other rare earths (Wedepohl, 1978); the linear trends of Y-Nb and Y-TiO<sub>2</sub> may arise through their association in rutile or zircon. Both of the latter minerals may be present in trace amounts, as indicated by the Nb-TiO<sub>2</sub> plot that could be interpreted as a line with a slight break in slope at about 0.55 % TiO<sub>2</sub> (Figure 4.3.E).

Plots of Al<sub>2</sub>O<sub>3</sub> against Nb, Y and TiO<sub>2</sub> produce linear arrays (Figure 4.3B, C, F) but with more scatter than the plots mentioned above ( $r^2$  values ranging from 0.54-0.75 for Al<sub>2</sub>O<sub>3</sub>/Nb and Al<sub>2</sub>O<sub>3</sub>/TiO<sub>2</sub> plots). The plot of Al<sub>2</sub>O<sub>3</sub>/Y shows comparatively more scatter relative to the other elemental plots with an  $r^2$  value of 0.54. Based on these relationships Al<sub>2</sub>O<sub>3</sub> may not be considered fully immobile, perhaps because of the

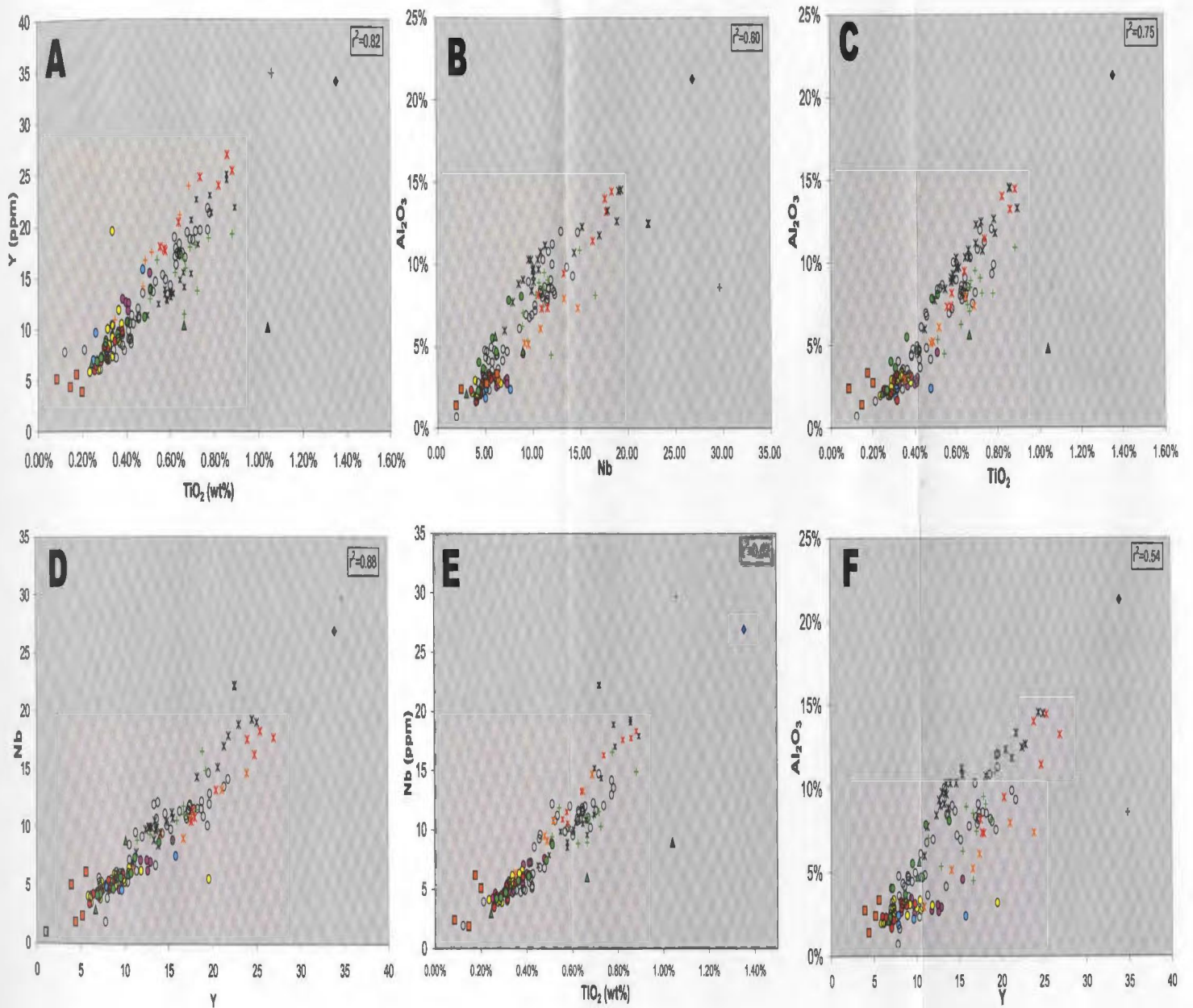


Figure 4.3 - Immobile element plots of  $\text{TiO}_2$ ,  $\text{Al}_2\text{O}_3$ , Nb, and Y. All elements plot along a linear trend line with minimal scatter, indicating these selected elements remained immobile. Samples from cuttings tend to show higher values for all elements plotted, likely due to an increased mud content in the cuttings compared to the samples from core. A large amount of scatter is produced when  $\text{Al}_2\text{O}_3$  is plotted against Y, however this deviation in linearity may be due to differential hydraulic fractionation of the main mineral phase containing  $\text{Al}_2\text{O}_3$ , or minor differences in the source material.

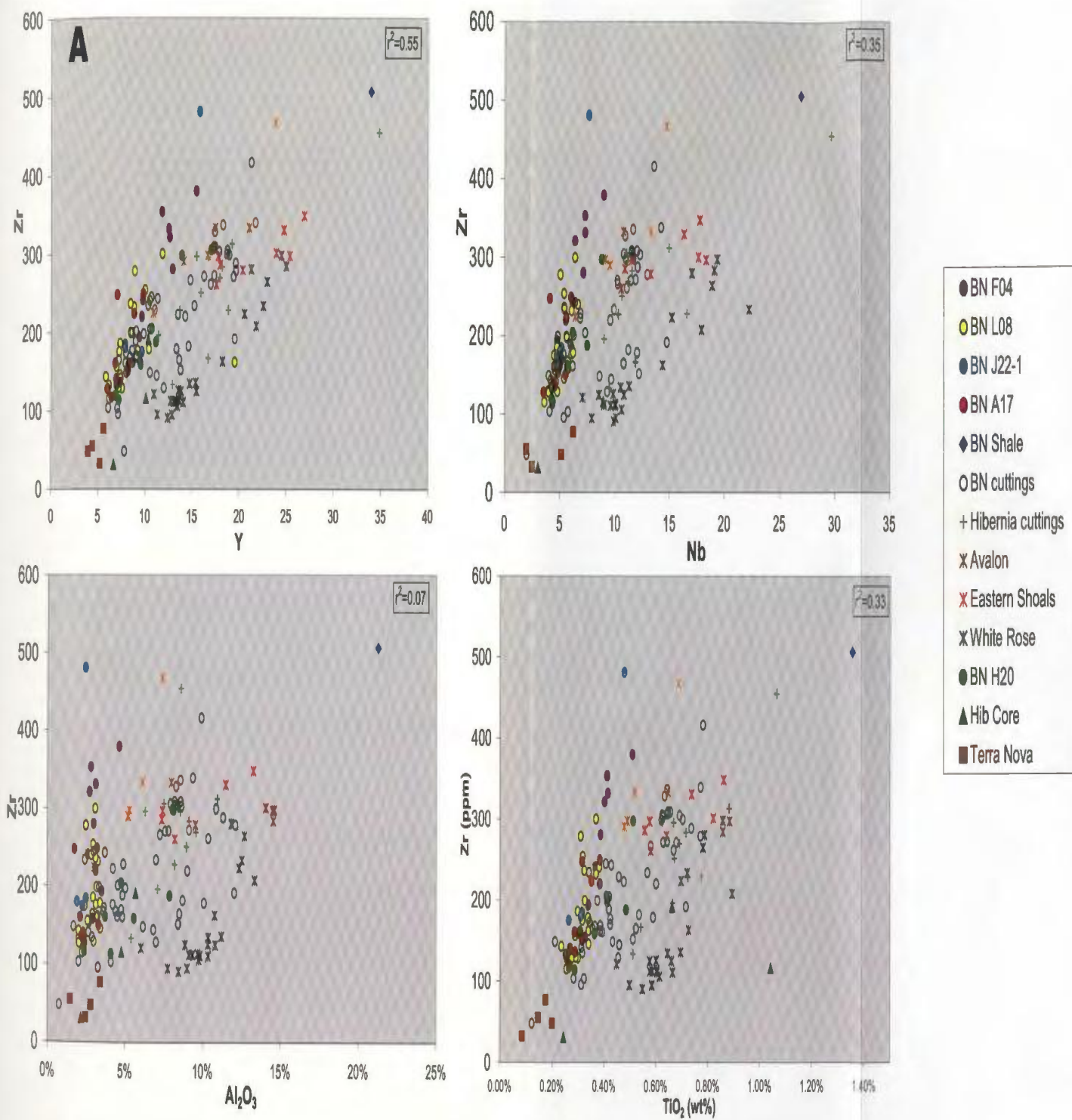


Figure 4.4 - Immobile element plots of Zr against Y, Nb, Al<sub>2</sub>O<sub>3</sub>, and TiO<sub>2</sub> (A-D respectively). Extensive scatter is seen when Zr is plotted against other immobile elements suggesting that Zr may have been physically partitioned during sediment transport.

presence of feldspars (if minor) that are subject to dissolution and replacement reactions.  $\text{TiO}_2\text{-Al}_2\text{O}_3$  may show a stronger correlation than  $\text{Nb-Al}_2\text{O}_3$  and  $\text{Y-Al}_2\text{O}_3$  because of the possible incorporation of  $\text{TiO}_2$  within the structure of feldspars (Wedepohl, 1978).

Rare-earth elements such as Y and Sc, that may have been mobile but behaved in a chemically similar manner to one another, will show a linear pattern and can be mistakenly classified as immobile (Fralick and Kronberg, 1997). To determine if these elements are immobile they must be individually plotted against an immobile element with differing chemical behaviour such as Ti which, in contrast to the rare earths, is preferentially contained in minerals such as rutile and ilmenite (Wedepohl, 1978). When Y is plotted against  $\text{TiO}_2$  (Figure 4.3A) we see a linear plot, with an  $r^2$  value of 0.82 and can conclude that Y was in fact immobile. One Ben Nevis sample (L-08 2945 m) has a high Y value (20 ppm) and also has a high Th value (9 ppm) compared to other samples in the Ben Nevis Formation (average values of Y and Th are 13 ppm and 5 ppm respectively). High values of Y and Th are consistent with traces of monazite in the sample. Two samples from the Hibernia Formation (G-57 3985.3, and G-57 3995.2) plot below the trend lines of  $\text{TiO}_2$  vs Y, Nb, and  $\text{Al}_2\text{O}_3$  (Figure 4.1) and appear enriched in  $\text{TiO}_2$ , which is thought to be due to an enrichment in ilmenite, consistent with the high petrographic count of opaque minerals for these samples (see Appendix 1). Sc and Th values are often below the limit of detection and cannot be tested for element mobility.

Zr shows the largest amount of scatter of all the suspected immobile elements when plotted against other elements (Figure 4.4), in particular when plotted against  $\text{Al}_2\text{O}_3$ .  $R^2$  values range from 0.07 to 0.55 (Figure 4.4) and indicate that Zr was either chemically mobilized or was physically partitioned during sediment transport.

The chemical mobility and hydraulic sorting of Zr can be further explored using an Al-Ti-Zr ratio diagram following Fralick and Kronberg (1997); (Figure 4.5). Omitting the two outlier samples which must have had a different source, the graph shows an approximately linear trend with a negative slope. The trend is interpreted to reflect the concentration by hydraulic sorting of Zr-bearing minerals, particularly in Ben Nevis and Avalon sandstones, and of major Al- and Ti-bearing phases preferentially in the more clay-rich Hibernia and Terra Nova formations. Hence it is proposed that Zr was retained in the same host mineral phase during weathering and diagenesis, indicating that Zr is immobile and was partitioned during sediment transport (Fralick and Kronberg, 1997). Ratios of Al-Ti-Zr in the Ben Nevis samples should be the same as the average ratio for these elements in the source terrain, provided these elements have not been differentially partitioned during weathering and subsequent transport, deposition and diagenesis (Fralick and Kronberg, 1997). Nearly all the samples from suspected sedimentary sources for the Ben Nevis Formation (Avalon, Eastern Shoals, Hibernia cuttings samples and one of the Hibernia core samples) fall along this linear trend and it is expected that the original basement source rocks would also plot along this trend line. Note, however, that cuttings of the Hibernia and Ben Nevis formations account for much of the scatter in the graph, particularly at low  $Zr/Al_2O_3$  ratios, leaving the possibility that at least some of the Zr was mobile, perhaps associated with clay minerals during weathering.

Suspected immobile elements Cr, Fe, Ni and V do not follow a linear array when plotted against  $TiO_2$  and hence are not considered immobile (Figure 4.6). Ni, Mn and Cr all show very different values for samples from the Terra Nova and Lower Tempest members. See for example, particularly high chromium values (300-500 ppm) in samples

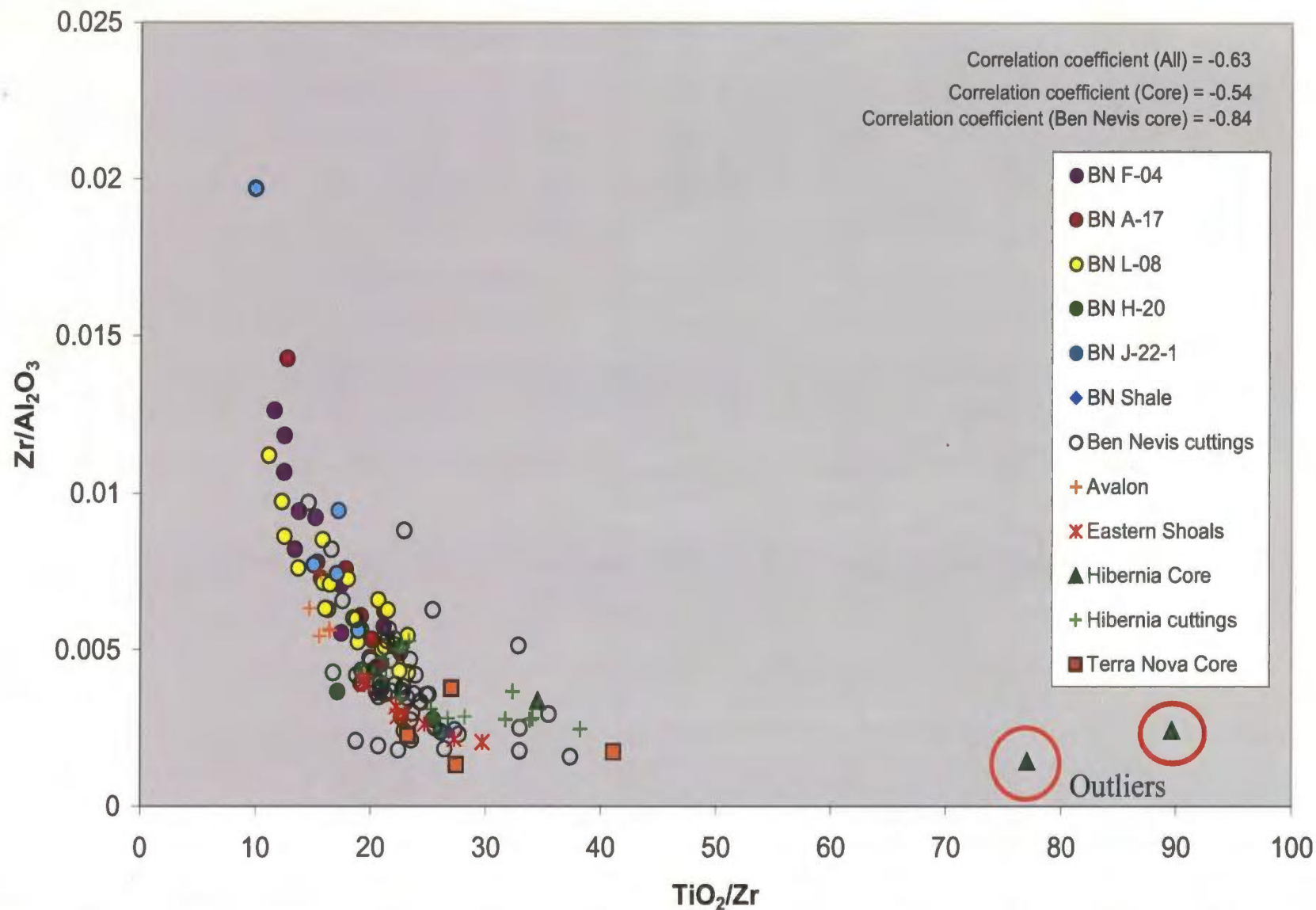


Figure 4.5-  $\text{Al}_2\text{O}_2$ - $\text{TiO}_2$ -Zr ratio diagram (modified after Fralick and Kronberg, 1997). Correlation coefficient for all samples (excluding the two Hibernia outliers) is -0.68. The correlation coefficient is -0.54 for all core samples and is -0.84 for all Ben Nevis core samples. This linear trend indicates that Zr was retained in the same host mineral phases during weathering and diagenesis.

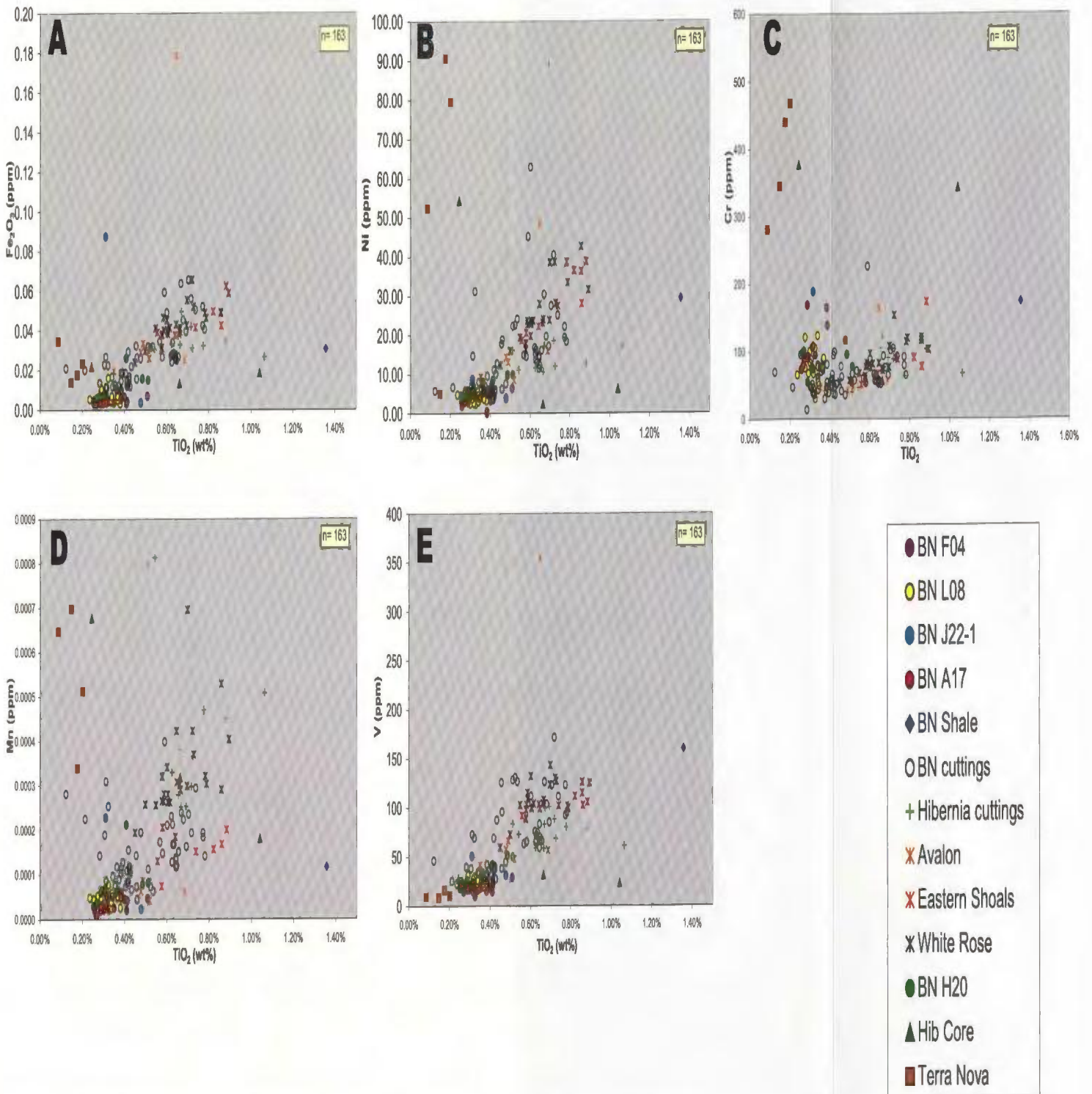


Figure 4.6 - Element plots of Fe<sub>2</sub>O<sub>3</sub>, Ni, Cr, Mn, and V plotted against immobile element TiO<sub>2</sub>. Fe<sub>2</sub>O<sub>3</sub>, Ni, Cr and V show loose correlations with TiO<sub>2</sub> however too much scatter is seen to classify these as immobile. High Cr, Ni and Mn values for the Terra Nova Member and Lower Tempest Member are observed and could be due to a higher amount of spinel in these formations which is present due to their coarser grain size.

from the Terra Nova Member, as well as in one sample from the Hibernia Formation (Figure 4.6.C). High Cr values along with high Ni values may be due to a higher amount of spinel present in these samples and indicate a mafic component to these samples that is not seen in the Ben Nevis Formation samples (Figure 4.6 B,C). One sample from the Hibernia Formation has a high value of chromium, but a very low value of nickel, perhaps due to a Ni-depleted spinel component (Figure 4.6 B,C).

Information about the alteration history of a data set can be determined by plotting an immobile element against  $\text{SiO}_2$ . The premise behind this technique is that chemical and physical weathering act over time to destroy all major mineral phases except quartz (Fralick and Kronberg, 1997). Plotting selected elements against  $\text{SiO}_2$  concentrations for sandstones and shales provides further insight into chemical and hydrodynamic behaviour of their mineral phases. Minimal post-depositional gains or losses of  $\text{SiO}_2$  from the sediment are necessary for this technique to work (Fralick and Kronberg, 1997).

Petrographic data shows quartz overgrowths are common, however, gains of  $\text{SiO}_2$  from this process are thought to be minimal due to the limited extent of these overgrowths seen in thin sections. When samples are plotted against  $\text{SiO}_2$ , positive or negative trend lines are expected, which can indicate if the immobile element was concentrated in the sand or clay fraction. A positive trend line extending from  $\text{SiO}_2$ -rich compositions through a hypothetical clay-rich shale end-member in direction of a y-axis intercept at 0%  $\text{SiO}_2$  indicates that the given immobile element is concentrated in the sand fraction. A negative trend line extending from the shale end-member toward a y-axis intercept at 100%  $\text{SiO}_2$ , indicates that the immobile element is preferentially concentrated in the clay fraction (see Figure 2 in Fralick and Kronberg, 1997).

Immobile elements  $\text{TiO}_2$ , Y, Nb, and  $\text{Al}_2\text{O}_3$  from both cuttings and cores of the Ben Nevis, Avalon, Eastern Shoals, White Rose, and Hibernia formations are plotted against  $\text{SiO}_2$  on Figures 4.7 A-E. A sample of shale from the Ben Nevis Formation is used to establish an end-member shale composition. Immobile element concentrations lying on or near a best-fit tie line from the shale end member to an idealized quartz sandstone end-member at 100%  $\text{SiO}_2$  are then implied to have been concentrated in the clay fraction of sediments (in contrast to the 0%  $\text{SiO}_2$  tie line implying a concentration in the sand fraction). However, a single shale sample is not thought to be truly representative of the shale end member. Instead, a small domain surrounding the shale end member, about  $\pm 10\%$   $\text{SiO}_2$ , is used to extend a “tie block” outlined on the graphs of Figure 4.7. The tie block accommodates some degree of variability around the hypothetical tie line and most of Ben Nevis Formation samples fall into this area. Note that a large proportion of samples, with  $> 80\%$   $\text{SiO}_2$  and  $< 5\%$   $\text{Al}_2\text{O}_3$ , are essentially clay-free as confirmed by petrographic analysis. Of the trace elements plotted only Ti is thought to enter the structure of feldspars (up to 0.04%) or be present as rutile or ilmenite inclusions in quartz or feldspar, respectively (Wedepohl, 1978). However, structural and adsorbed trace elements can account for relative trace element enrichment within even minor amounts of clay minerals present in rock fragments, thin grain rims, and as alteration products. A significant number of silica-rich samples with 5-10%  $\text{Al}_2\text{O}_3$ , reflect not only the presence of clays, both also variable amounts of feldspar. Few samples contain  $> 10\%$   $\text{Al}_2\text{O}_3$ , consistent with the overall quartz-rich nature of Ben Nevis sandstones (Figure 4.5A).

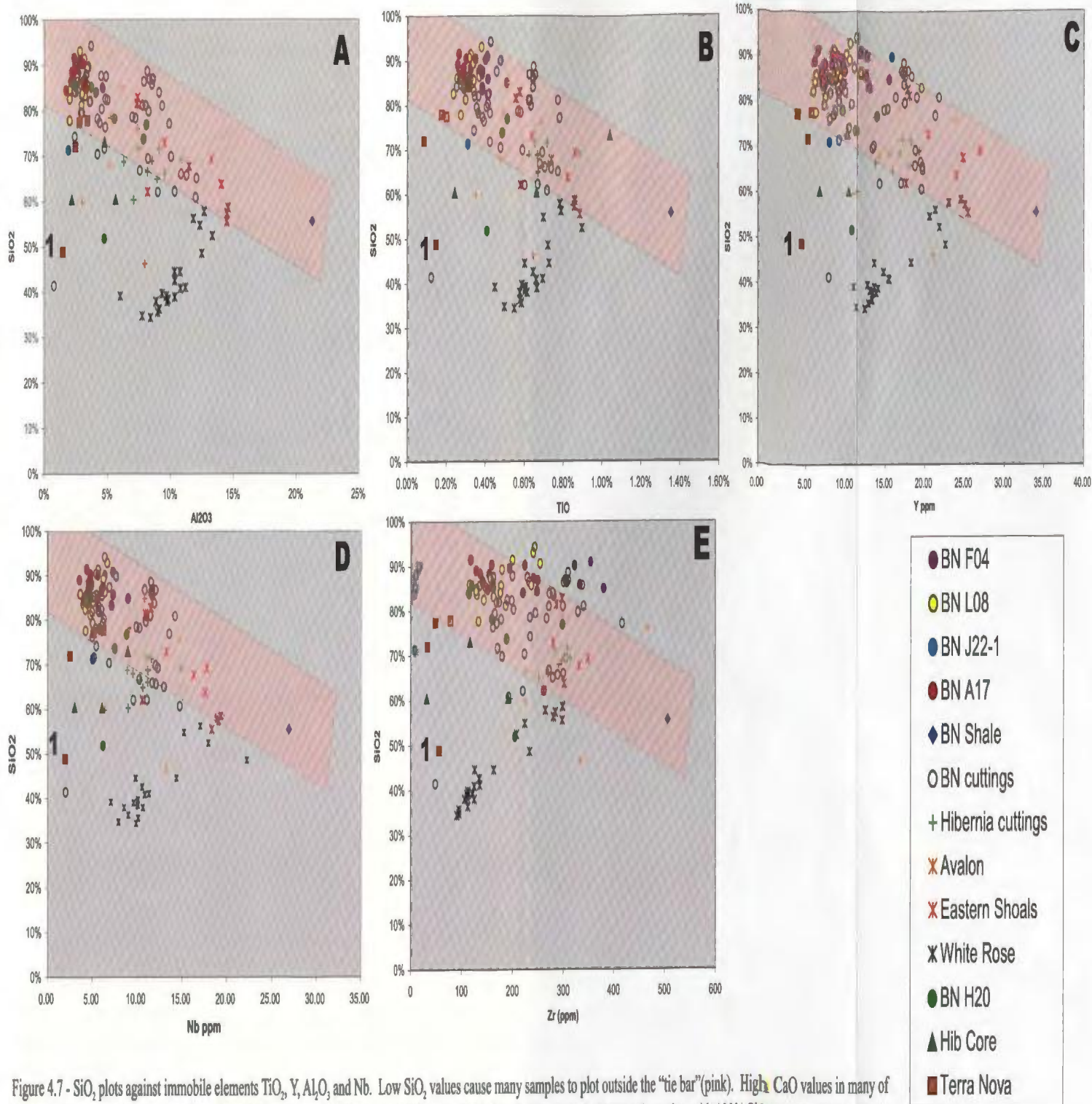


Figure 4.7 - SiO<sub>2</sub> plots against immobile elements TiO<sub>2</sub>, Y, Al<sub>2</sub>O<sub>3</sub> and Nb. Low SiO<sub>2</sub> values cause many samples to plot outside the "tie bar"(pink). High CaO values in many of these samples account for the low SiO<sub>2</sub> values. Most of the immobile elements fall within the tie bar that connects the shale end member with 100% SiO<sub>2</sub> end member (except for samples from the White Rose Formation, which is described by McAlpine, 1990 as a shale). This indicates that these immobile elements concentrate in the clay fraction. Zr abundances plot in a linear type array, indicating that this element is concentrated in both the fine and coarse fractions.

Not all samples lie directly within the “tie block”, rather some surround it in clusters. Ben Nevis samples from cores plot in a tight cluster near the 90% SiO<sub>2</sub> range, while the samples from cuttings have a larger spread (48-90 wt%) and plot into an area similar to the Hibernia samples. One sample from the Ben Nevis Formation in the H-20 well falls near the 50% SiO<sub>2</sub> line due to a high CaO content (27%) caused by a large amount of carbonate cement, which was also seen petrographically (Plate 8). The Hibernia cuttings form a broad cluster and have lower SiO<sub>2</sub> values and generally higher immobile trace element values than the Ben Nevis samples. This is likely due to the difference in grain size and depositional facies, where Ben Nevis samples are from a shoreface setting in which the sands were reworked and segregated from nearly all clay-sized particles and mudstone rock fragments, while the Hibernia samples represent fluvio-deltaic facies, not subjected to the same amount of reworking (hence they have a higher mud content).

Avalon Formation samples have a lower silica content than Ben Nevis Formation samples (46-85 wt% range) and therefore do not fall within the tie block. CaO values for the Avalon Formation are in the range of 10-30 wt%; this component is present almost exclusively in carbonate cement. These high CaO values lower the SiO<sub>2</sub> weight percentages. If one were to correct for the high carbonate cement content one would expect to see an increase in the overall SiO<sub>2</sub> values and Avalon Formation samples would plot in the same general field as Ben Nevis samples. Some samples from the Terra Nova Member also do not fall within the tie block. However, these samples have variable silica values and low immobile element concentrations. Based on petrographic analyses, Terra Nova sample 1 (Figure 4.7) has a high carbonate cement content, which is consistent with

a high CaO value (30%) from XRF results. The remaining Terra Nova Member samples have CaO values ranging from 7%-14%, which lowers the SiO<sub>2</sub> values to bring them out of the tie block.

The Whiterose Formation is described as a medium to dark grey silty, calcareous shale with thin siltstone and limestone beds (McAlpine, 1990) and is expected to have a low SiO<sub>2</sub> content and a significant Al<sub>2</sub>O<sub>3</sub> content (Average SiO<sub>2</sub> value is 44% and average Al<sub>2</sub>O<sub>3</sub> value is 11%). These samples are compositionally dissimilar to the Ben Nevis Formation and hence cannot be compared to sand-prone clastic formations.

Figure 4.7 shows that samples from the Hibernia and Ben Nevis formations cluster within and around the tie block extending from 100% SiO<sub>2</sub> to the shale end-member (negative slope). This indicates that these immobile elements (TiO<sub>2</sub>, Al<sub>2</sub>O<sub>3</sub>, Y, and Nb) are concentrated in the clay fraction. Samples from the Avalon Formation and the Terra Nova and Lower Tempest Members do not plot within this tie block, which is likely due to the high content of carbonate cement.

The data presented above suggests that Al, Ti, Nb, and Y were immobile and affected by chemical and mechanical sorting in a similar manner. The plot of SiO<sub>2</sub> – Zr shows a significant number of data points outside and above the tie block, illustrating that Zr: (1) is likely associated with more than one mineral phase, not only as discrete zircon but also perhaps in Ti-oxides and clay minerals, and (2) is concentrated in both sand- and clay-sized fractions. These immobile elements (Al, Ti, Nb, and Y) are useful for provenance analysis because they are strongly retained in particulate material and not released in solution; hence they reflect the original source-rock composition.

## 4.5 Geochemical Abundances

Major-element distributions reflect the mineralogy of the samples, with sandstones generally having higher  $\text{SiO}_2$  content and lower  $\text{Al}_2\text{O}_3$  content than shales. Variations in major-element geochemistry of the various sandstones are shown on Harker diagrams (Figure 4.8, and Figure 4.7 A and C). Samples taken from cores are more reliable and most useful for comparison purposes.

In general, samples from the Ben Nevis Formation have a slightly higher  $\text{SiO}_2$  content compared to the other formations. Samples from the Ben Nevis Formation plot within a small cluster and have very little variability, with the exception of a few samples taken from cuttings and samples from well H-20. Samples from well H-20 tend to have a larger variability compared to other samples from the Ben Nevis Formation due to the higher clay content seen petrographically (0-16% clay matrix in point counts from H-20 well) and geochemically (higher  $\text{Al}_2\text{O}_3$  values). Samples with low  $\text{SiO}_2$  values have higher CaO values, with loss on ignition (LOI) values corresponding to high amounts of  $\text{CO}_2$ . As stated earlier, correcting for calcite cement should increase the  $\text{SiO}_2$  values to fall closer to the tie blocks of Figure 4.7. Three samples from the H-20 well have slightly higher MgO values than the rest of the Ben Nevis Formation samples due to the high amount of carbonate cement (33-37% seen in the thin sections) (Plate 8A).  $\text{Na}_2\text{O}$  values are approximately the same for all formations, implying that plagioclase feldspar content is relatively constant throughout all formations. A number of samples from cuttings and one sample from well F-04 have significantly higher  $\text{Na}_2\text{O}$  values and this is thought to be due to drilling-mud contamination. One shale sample was taken from the Ben Nevis Formation. This sample shows significantly higher values of  $\text{Al}_2\text{O}_3$ ,  $\text{K}_2\text{O}$ , MgO and  $\text{TiO}_2$

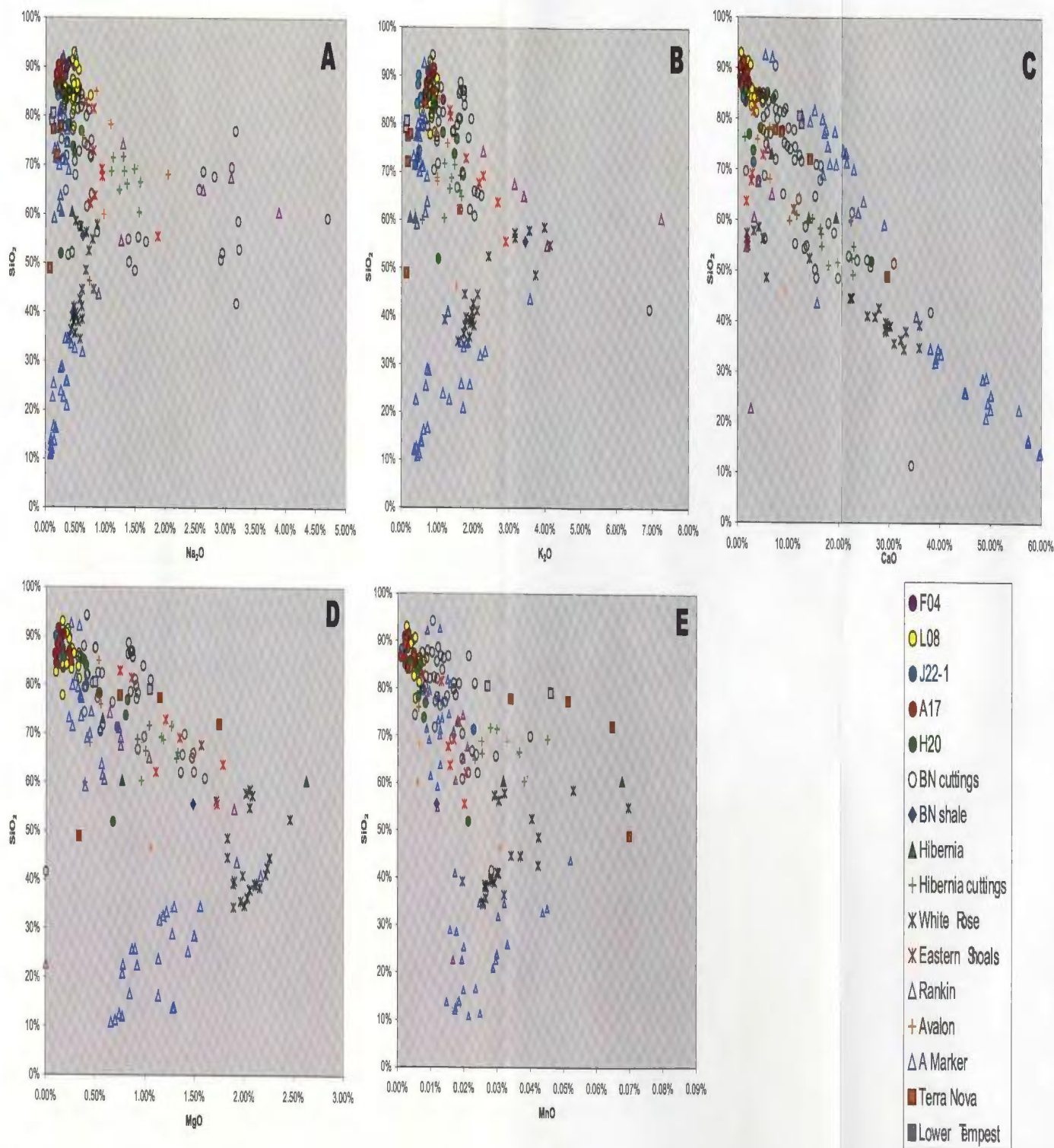


Figure 4.8 - Harker diagrams of major elements,  $Na_2O$ ,  $K_2O$ ,  $MgO$ ,  $MnO$ , and  $CaO$ , (oxides  $TiO_2$  and  $Al_2O_3$  are found on Figure 4.5) plotted against  $SiO_2$ . Samples from each formation tend to cluster. Cuttings samples have a larger spread than core samples, due to higher concentrations of contaminants such as potassium (from  $KCl$ ) and are deemed less accurate. A number of the samples have low  $SiO_2$  values and associated high  $CaO$  values. This is likely due to a high calcite cement component.

compared to the Ben Nevis Formation sandstones, which reflects the tendency of these chemical species to concentrate in the clay fraction.

Samples from the Avalon Formation have similar major-element values to the Ben Nevis Formation and it is not possible to differentiate Ben Nevis samples from Avalon samples. This is an indication of their very similar geochemical composition. Samples from the Eastern Shoals Formation and the Hibernia Formation have a slightly lower SiO<sub>2</sub> content and higher TiO<sub>2</sub>, Al<sub>2</sub>O<sub>3</sub>, K<sub>2</sub>O, MnO and MgO values than the Ben Nevis Formation. This is likely due to an increase in clay content in both mudstone rock fragments as well as authigenic components and reflects a lower mineralogical maturity compared to the Ben Nevis Formation.

Samples from the Terra Nova Member and the Lower Tempest sandstones have slightly lower K<sub>2</sub>O values than the other formations, implying a lower potassium feldspar and K-mica content. Some dissolution and replacement is seen in the deeper samples (Plate 3C, 7A), however the lack of any feldspar grains in thin sections and the low Na<sub>2</sub>O and K<sub>2</sub>O concentrations seen in these samples (especially the Lower Tempest samples) indicates that feldspar abundance is mainly controlled by pre- or syn-depositional processes, with only minor diagenetic replacement. The Lower Tempest sandstones also show lower values of TiO<sub>2</sub> and other immobile elements compared to all other formations and therefore cannot be considered a source sediment for the Ben Nevis Formation. These samples were taken from intervals of a clean massive sandstone with a negligible mud and lithic component (Q<sub>94</sub>F<sub>0</sub>L<sub>6</sub>) and reflect a texturally mature sandstone.

Trace elements Zr, Nb and Y tend to be preferentially partitioned into residual magma during crystallization (Feng and Kerrich, 1990). As a result these elements are

enriched in felsic rather than mafic sources and are thought to reflect provenance composition due to their immobile behaviour (Taylor and McLennan, 1985). The Ben Nevis shale has a much higher Zr concentration (506 ppm) than the average concentration for the Ben Nevis sandstones (208 ppm), reflecting the preference of Zr to concentrate in the shale. These trends in trace elements are similar to what is seen in the major elements. Trace-element concentrations tend to be slightly higher in the Hibernia and Eastern Shoals formations than in the Ben Nevis Formation, likely due to both textural and mineralogical maturity of the latter. Nb and Y values are approximately the same for samples from the Ben Nevis and Hibernia cores, the Avalon Formation and the Terra Nova and Lower Tempest members.

#### **4.6 Geochemical Correlations**

The observed geochemical values in the Ben Nevis Formation remain relatively constant both stratigraphically and laterally (Appendix 7).  $\text{SiO}_2$  values are variable in all formations (41%-93%  $\text{SiO}_2$  for clastic samples) and are lowered in concentration due to high concentrations of CaO (arising primarily from high levels of cementation) and higher  $\text{Al}_2\text{O}_3$  concentrations (in samples from muddier facies with a higher clay content). High  $\text{Al}_2\text{O}_3$  values seen in cuttings may also be due to drilling-mud contamination. Contaminated samples typically have associated high weight percentages of  $\text{K}_2\text{O}$  and  $\text{Na}_2\text{O}$ , and these have been filtered using the methodology described in Section 4.2, above. CaO values are also variable as a result of the different amount of cementation present in each sample. CaO weight percents range from 0.50% to 38% and give an indication of the amount of cement seen in the sample. Calculated CaO for the CIA

diagram showed that in most cases none of the CaO present in the samples was due to CaO found in feldspars, hence it was associated with the carbonate cement. Because of these factors, both SiO<sub>2</sub> and CaO are not useful for well-to-well correlations, but are useful in association with Al<sub>2</sub>O<sub>3</sub> to estimate the degree of contamination due to cementation and drilling muds, especially within cutting samples.

Immobile element concentrations remain relatively constant with little variability; however, some peaks in Al<sub>2</sub>O<sub>3</sub>, TiO<sub>2</sub>, and Zr may be useful to establish stratigraphic trends in the Ben Nevis Formation. Clearly, possible trends are limited by the sampling strategy of 5 to 10 m intervals, and should therefore rely (as much as possible) on sets of contiguous samples with distinct value ranges, rather than individual sample values. On the other hand, visible heavy mineral bands were carefully avoided during sampling, and associated elemental peaks are therefore not associated with hydrodynamic concentrations. Figure 4.9 depicts a cross-section of all the wells that sampled the Ben Nevis Formation in and around the White Rose Field, with concentrations (both weight percent and parts per million) of SiO<sub>2</sub>, CaO, Al<sub>2</sub>O<sub>3</sub>, and minor elements Y, Nb, Zr, and TiO<sub>2</sub>. Samples from cores show relatively little change in SiO<sub>2</sub>, CaO and Al<sub>2</sub>O<sub>3</sub> and these values are not considered contaminated.

At the base of both wells L-08 and E-09 is a carbonate unit (classified as the A Marker), and these wells are relatively close to one another with minimal faulting present between them (Figure 1.8); hence the basal sandstone of both wells can be considered to be in approximately the same stratigraphic interval (informal unit C). The top of unit C in these two wells is suggested to be located at relative peaks of Zr, 300 ppm in L-08 (2991 m) and 200-229 ppm in E-09 (2975-85 m), in contrast to typical concentrations of 115 to

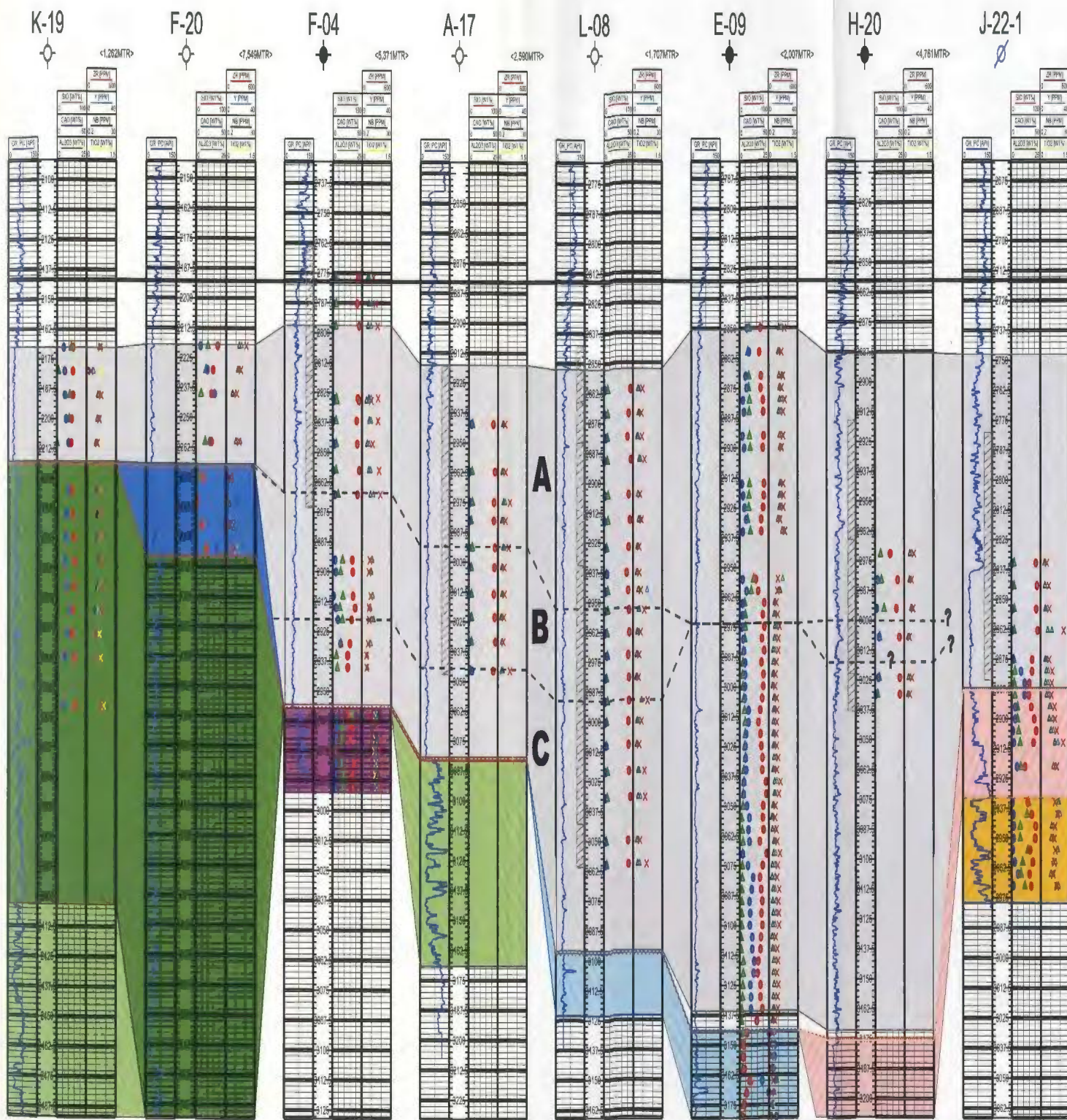


Figure 4.9 - Cross section of Ben Nevis Formation samples with associated Zr correlations. Zr and TiO<sub>2</sub> concentrations are useful for correlating across the Ben Nevis Formation. In total 3 packages of sandstones (A-C) within the Ben Nevis can be picked out based on Zr spikes (contaminated samples have been omitted). Grey and Dark grey fill represents Ben Nevis Formation; Dark blue fill represents B marker member; light blue fill represents A marker Member; Dark green fill represents Upper Hibernia Formation; light green fill represents Lower Hibernia Formation; purple fill represents Rankin Formation; Pink fill represents Avalon Formation; Orange fill represents Eastern Shoals Formation.

< 175 ppm above and below. In well A-17 the Ben Nevis Formation is in contact with the Hibernia Upper Zone, indicating that the base of the Ben Nevis Formation at A-17 is not correlatable to the base at L-08 and E-09. The top of unit C in well A-17 is placed at 3045 m (248 ppm), consistent with southward thinning of the basal interval, but can only be inferred in F-04 (at about 2915 m) due to lack of reliable data (contaminated samples). Northward of E-09, the top of unit C cannot be reliably extended due to insufficient sample coverage in wells H-20 and J-22. However, the Avalon Formation in well H-20 shows major-and trace-element values that are comparable to those observed in the Ben Nevis Formation, with very minor differences. Therefore one can conclude that these two formations are very similar and cannot be distinguished from one another geochemically.

Based on Zr values another correlation surface can be defined separating a middle unit B (with consistently low values) from an upper interval, unit A, with relatively high Zr concentrations (Figure 4.9). Middle unit B is defined at well L-08 (below 2953 m with 134 ppm average Zr) and well A-17 (below 2994 m, 130 ppm average), and inferred to below 2870 m in well F-04. Zr concentrations are significantly higher in the overlying unit A with similar averages of 178 ppm, 189 ppm, and 249 ppm. High Zr concentrations in the upper unit are consistent with high interval concentrations in wells F-20 and K-19 to the south, 314 ppm and 279 ppm, respectively. Cuttings samples in the upper part of Ben Nevis in well E-09 are deemed to be contaminated, making northward extrapolation of units A and B difficult. Based on the 180 ppm Zr average of four samples between 2940 m and 2975 m, this interval in well E-09 is typical of unit A, hence unit B appears to pinch-out between wells L-08 and E-09. North of L-08 the top of middle unit B can again be defined in well H-20, separating relatively low Zr values (average = 132 ppm) from

much higher values in upper unit A (average = 184 ppm). Consistently higher Zr values in the uppermost interval, unit A, are interpreted as resulting from changes in the source area. Increasing Zr concentrations southward from well L-08 toward well K-19 are proposed to reflect distal to proximal relationships in depositional setting.

Both major- and trace-element concentrations for the Hibernia Formation are slightly higher than values from the Ben Nevis Formation.  $\text{Al}_2\text{O}_3$  values are slightly higher in some samples; this is due to the higher mud content from interlaminated sandstone-shale horizons of the Hibernia Formation (seen on gamma ray logs) compared to the very clean Ben Nevis sandstones (seen on both gamma ray logs and in cores). Immobile elements  $\text{TiO}_2$ , Y, Nb and Zr have a range of values and are not considered homogeneous; however, lack of core samples restricts accurate correlations from being made. The Hibernia Formation does not have good core control on the east side of the basin and collecting an abundance of samples like that for the Ben Nevis Formation is not possible. Therefore only inferences about geochemical composition and loose correlations can be made.

Samples from K-19 are particularly useful for comparison purposes because of similar grain sizes in both the Ben Nevis and Hibernia formations. Samples from the Ben Nevis and Hibernia formations within well K-19 have a high  $\text{SiO}_2$  concentration and low CaO and  $\text{Al}_2\text{O}_3$  concentrations, with minimal variability (Figure 4.10). All samples from K-19 were taken from cuttings, hence the lack of variability could, in principle, indicate the degree of drilling-mud contamination remaining the same in both formations. However, the degree of drilling mud contamination is low because values such as  $\text{K}_2\text{O}$  and  $\text{Na}_2\text{O}$  remain constant throughout both formations (Cl and Ba are also found in

# K-19

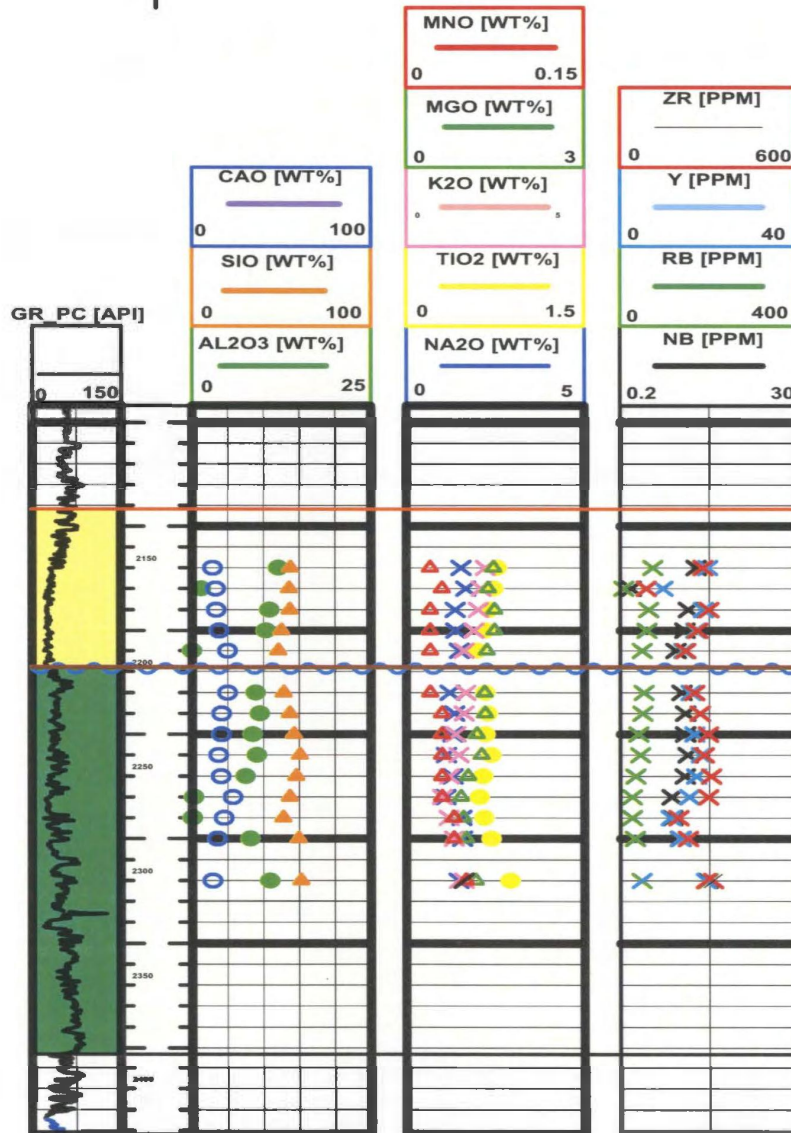
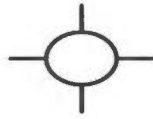


Figure 4.10 - Geochemical values from the Ben Nevis and the Hibernia formations in well K-19.

drilling muds and their values would also be very high in the case of contamination). If drilling mud contamination was present,  $K_2O$ ,  $Na_2O$ , Cl, and Ba concentrations would be atypically high and very chaotic. Since this is not the case, the quality of the data can be assumed to be good. From these values we can interpret the sandstones from both the Ben Nevis and Hibernia formations are compositionally similar, at least for the area of well K-19, without significant changes from the Hibernia Formation, up through the Ben Nevis Formation. Even elements that have been shown to be mobile (*i.e.*  $Na_2O$ ,  $K_2O$ ) do not show major or consistent changes.

## Chapter 5 Provenance of the Ben Nevis Formation

### 5.1 Tectonic Provenance

Dickinson and Suczek (1979) have shown that average compositions of sandstones derived from different tectonic terranes tend to lie in discrete fields within QFL and  $Q_MFL_T$  diagrams. In QFL classification plots presented earlier (Figures 3.1 and 3.5), carbonate fragments are grouped with lithic fragments. Although tectonic QFL diagrams presented by Dickinson and Suczek (1979) and Dickinson et al. (1983) do not include carbonate grains as framework constituent, herein I follow Marsaglia and Ingersoll (1992) to include carbonate grains that appear to be extrabasinal. Figure 5.1 shows all data points for the Ben Nevis Formation plotted on a QFL diagram with subdivisions of provenance type from Dickinson et al., (1983). The average QFL ratio for samples from the Ben Nevis Formation is  $Q_{94}F_3L_3$ . Point count data show the lithic components of samples from Ben Nevis Formation to be almost exclusively clay/mud clasts and detrital carbonate grains. Within the Ben Nevis Formation sandstones there are no obvious trends observed from the QFL diagram of Figure 5.1. All the samples tend to have high amounts of quartz (75%-98%) and low amounts of feldspar (0.5%-8%) and variable amount of lithics (0.5%-21% including carbonate grains) (Table 5.1). All samples from the Ben Nevis Formation plot in the Craton Interior and along the quartz-rich domain of the Recycled Orogenic Province with minimal variability (Figure 5.1). Samples from well A-17 increase slightly (<3%) in quartz moving down the section and quartz content decreases slightly moving down the section in well J-22-1, similar to the trends seen in Figure 3.3. There is not a large or consistent difference

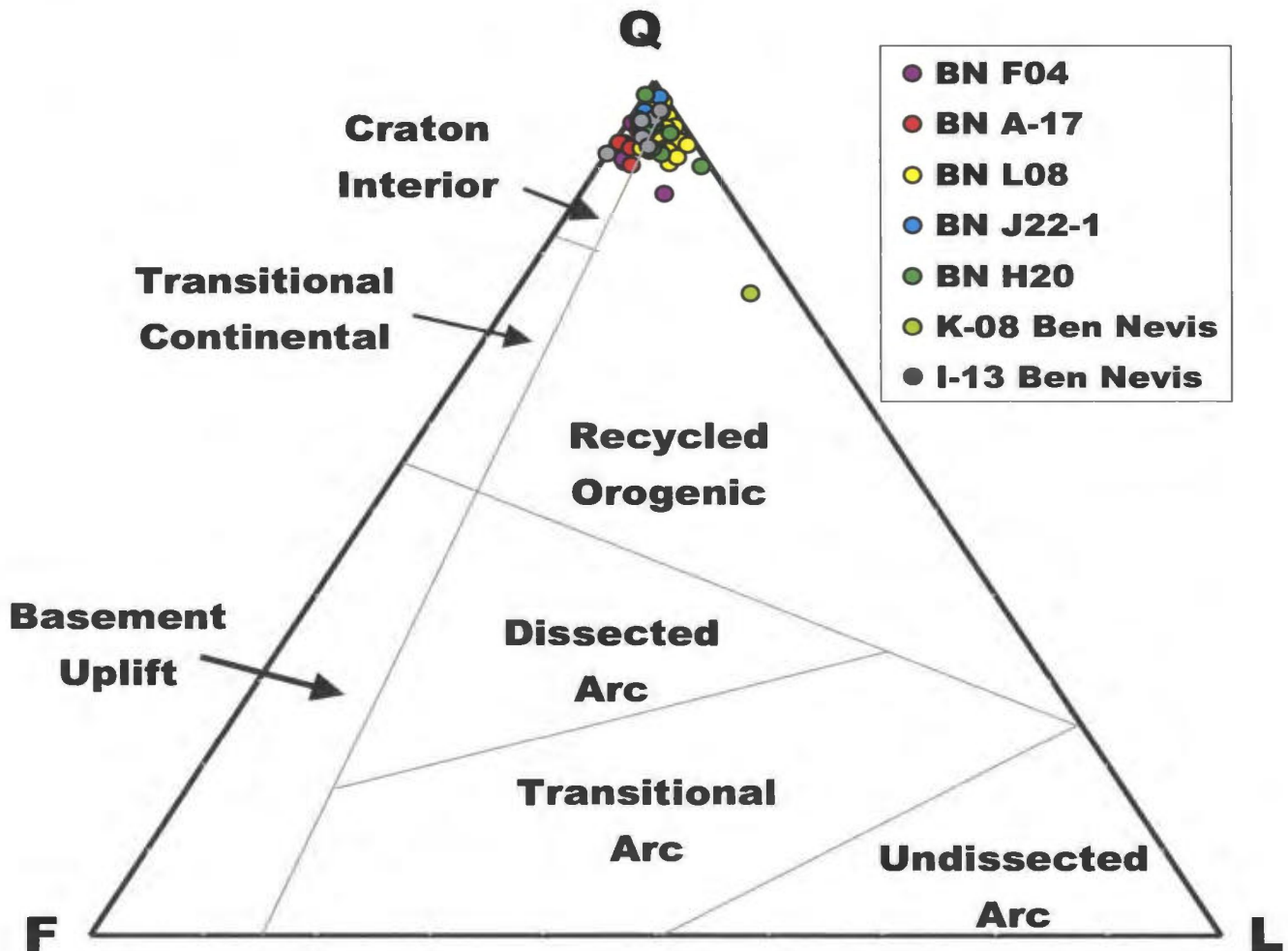


Figure 5.1 - Tectonic setting diagram (from Dickinson et al., 1983) for samples from the Ben Nevis Formation. All samples plot into the Craton Interior and Recycled Orogenic tectonic settings, with a minimal amount of variability. Samples from well I-13 plot in the same general area as samples from wells in the White Rose Field indicating no large difference in composition between the two areas.

Table 5.1 : QFL values (from Marsaglia and Ingersoll, 1992) for all samples

Depth	Q	F	L	Depth	Q	F	L
<b>A-17 Ben Nevis</b>				<b>J-22-1 Ben Nevis</b>			
2942.2	96.77	1.38	1.84	2834.65	98.18	0.45	1.36
2962.1	92.50	5.50	2.00	2844.3	96.57	2.58	0.86
2974.9	93.07	3.46	3.46	2853.95	94.42	3.86	1.72
2982.6	90.32	6.91	2.76	2862.95	94.92	2.54	2.54
2993.9	95.52	3.14	1.35	2875.2	94.55	3.47	1.98
3002.1	92.95	6.64	0.41	Avg	<b>95.73</b>	<b>2.58</b>	<b>1.69</b>
3013.3	94.39	4.21	1.40	<b>H-20 Ben Nevis</b>			
3023.1	92.31	5.98	1.71	2916	90.16	0.82	9.02
3033.3	94.74	3.35	1.91	2961.27	91.57	3.61	4.82
3045.5	94.93	3.23	1.84	2983.7	94.00	1.60	4.40
Avg	93.75	4.38	1.87	3007.83	95.00	2.50	2.50
<b>L-08 Ben Nevis</b>				3024.87	92.24	4.08	3.67
2861.1	94.62	1.92	3.46	3031.03	95.63	3.57	0.79
2871.3	98.46	1.16	0.39	3031.86	98.44	1.56	0.00
2884.1	95.18	1.20	3.61	2972.46	94.82	3.11	2.07
2893.5	96.56	2.67	0.76	2995.69	94.70	3.31	1.99
2894.1	96.00	0.80	3.20	Avg	<b>94.06</b>	<b>2.68</b>	<b>3.25</b>
2905.3	96.05	1.98	1.98	<b>K-08 Ben Nevis</b>			
2915.9	96.44	1.19	2.37	1690	74.36	3.85	21.79
2927.3	93.12	1.21	5.67	<b>I-13 Ben Nevis</b>			
2938.1	92.66	0.77	6.56	1890.39	95.56	2.22	2.22
2945.4	93.23	2.79	3.98	1893.12	95.79	2.11	2.11
2953.6	97.63	0.40	1.98	1895.83	96.63	1.12	2.25
2963	96.81	1.59	1.59	1899.14	95.45	3.41	1.14
2972.4	90.52	3.45	6.03	1904.42	93.55	4.30	2.15
2981.9	92.31	2.83	4.86	1905.58	91.67	8.33	0.00
2991.5	92.25	5.04	2.71	1906.04	92.47	4.30	3.23
3000.2	92.00	2.80	5.20	Avg	<b>94.45</b>	<b>3.69</b>	<b>1.87</b>
3010.1	91.94	3.63	4.44	<b>Ben Nevis Average (Total)</b>			
3021.1	91.24	2.39	6.37	<b>93.65</b>	<b>3.35</b>	<b>3.00</b>	
3032	96.54	1.15	2.31	<b>C96 Avalon</b>			
3050.2	94.80	0.80	4.40	2315	62.69	2.24	35.07
3060.3	94.63	1.65	3.72	2325	78.10	2.92	18.98
Avg	<b>94.43</b>	<b>1.97</b>	<b>3.60</b>	<b>K-08 Avalon</b>			
<b>F-04 Ben Nevis</b>				1760	85.19	2.78	12.04
2776.9	91.93	4.48	3.59	1800	51.96	0.00	48.04
2787.8	95.18	4.39	0.44	<b>L-11 Avalon</b>			
2797.1	87.01	5.63	7.36	3210	89.23	1.54	9.23
2809	92.58	5.24	2.18	<b>Avalon Average (Total)</b>			
2818.3	90.65	7.32	2.03	<b>73.43</b>	<b>1.89</b>	<b>24.67</b>	
2827.3	92.24	4.74	3.02				
2836.7	92.74	6.84	0.43				
2846.4	92.86	6.70	0.45				
2857.4	92.86	6.25	0.89				
2867.7	91.03	7.26	1.71				
Avg	<b>91.91</b>	<b>5.89</b>	<b>2.21</b>				

Table 5.1 :Con't

Depth	Q	F	L	Depth	Q	F	L
<b>C-60 Eastern Shoals</b>				<b>I-78 Hibernia</b>			
3340	66.912	3.6765	29.412	3270	44.03	0.75	55.22
3410	63.91	3.0075	33.083				
3590	69.536	7.2848	23.179				
3710	74.126	3.4965	22.378				
Avg	<b>68.621</b>	<b>4.3663</b>	<b>27.013</b>				
<b>L-11 Hibernia</b>				<b>G-57 Terra Nova</b>			
3250	86.842	1.3158	11.842	4029.3	96.79	0.40	2.81
3290	79.085	0	20.915	4035	97.97	0.00	2.03
3330	80.864	3.7037	15.432	Avg	<b>97.38</b>	<b>0.20</b>	<b>2.42</b>
3370	68.116	2.1739	29.71				
Avg	<b>78.727</b>	<b>1.7984</b>	<b>19.475</b>				
<b>C-17 Hibernia</b>				<b>C-73 Terra Nova</b>			
2028	91.35	4.33	4.33	4123.8	90.37	0.00	9.63
2098.5	85.14	10.36	4.50	4129.6	96.90	0.44	2.65
2162.5	86.81	10.44	2.75	Avg	<b>93.64</b>	<b>0.22</b>	<b>6.14</b>
2200	92.21	6.49	1.30				
2225	93.78	5.18	1.04				
2239.5	87.71	6.15	6.15				
Avg	<b>89.50</b>	<b>7.16</b>	<b>3.35</b>				
<b>G-57 Hibernia</b>				<b>Terra Nova Average (total)</b>			
3985.3	91.18	2.94	5.88		<b>95.508</b>	<b>0.21</b>	<b>4.28</b>
3995.2	91.26	2.91	5.83				
Avg	<b>91.22</b>	<b>2.93</b>	<b>5.86</b>				
<b>K-08 Hibernia</b>				<b>G-57 Lower Tempest</b>			
2510	75.00	8.75	16.25	4594.25	94.78	0.00	5.22
2550	91.84	2.04	6.12	4598	91.04	0.00	8.96
2630	91.30	3.48	5.22	Avg	<b>92.91</b>	<b>0.00</b>	<b>7.09</b>
2670	98.26	0.00	1.74				
2720	98.52	0.74	0.74				
2800	96.35	0.00	3.65				
2900	95.238	2.7211	2.0408				
2950	96.694	0.8264	2.4793				
Avg	<b>92.90</b>	<b>2.32</b>	<b>4.78</b>				
<b>C-96 Hibernia</b>				<b>P-15 Jeanne d'Arc</b>			
3870	81.429	0.7143	17.857	4124.30	59.35	0.00	40.65
3918	90.551	0.7874	8.6614	4129.65	62.77	0.00	37.23
3942	78.351	0	21.649	Avg	<b>61.06</b>	<b>0.00</b>	<b>38.94</b>
Avg	<b>83.443</b>	<b>0.5006</b>	<b>16.056</b>				

petrographically between samples from the White Rose Field compared to samples to the south of the field (wells K-08 and I-13), broadly consistent with a similar tectonic regime for the Ben Nevis sandstones along the eastern margin of the Jeanne d'Arc basin. The lack of samples from the K-08 well makes it difficult to make any conclusions about the lithic content of sandstones from this well, as well as comparisons between the two wells, other than that samples from I-13 appear to be more quartz rich (average: 94%, range: 92-97%) than the single sample from well K-08 (Q = 74).

Samples from the Avalon and Eastern Shoals formations have a higher lithic content than samples from the Ben Nevis Formation with average QFL ratios of  $Q_{73}F_2L_{24}$  and  $Q_{68}F_4L_{27}$  respectively (Table 5.1). Point count data show that the main lithic components are phyllite fragments, mud or shale clasts and detrital carbonate grains. The increase in lithic components seen in the Avalon and Eastern Shoals Formation compared to the Ben Nevis Formation is likely due to a difference in the amount of reworking between the two formations. The Ben Nevis Formation sandstones likely underwent a greater amount of reworking compared to those of the Avalon and Eastern Shoals formations, thus removing most of the clay and unstable minerals from the Ben Nevis Formation. Samples from the Avalon and Eastern Shoals formations plot in the Recycled Orogenic Province with one sample (from well L-11) plotting in the Craton Interior Province (Figure 5.2), indicating a higher lithic content as well as a larger sedimentary component to the source terrain. The higher lithic content also supports the inference of a lower maturity than the samples that plot in the Craton Interior province. However samples that plot in the Craton Interior province do not necessarily indicate that there was not a significant sedimentary component to the source terrane; intense reworking

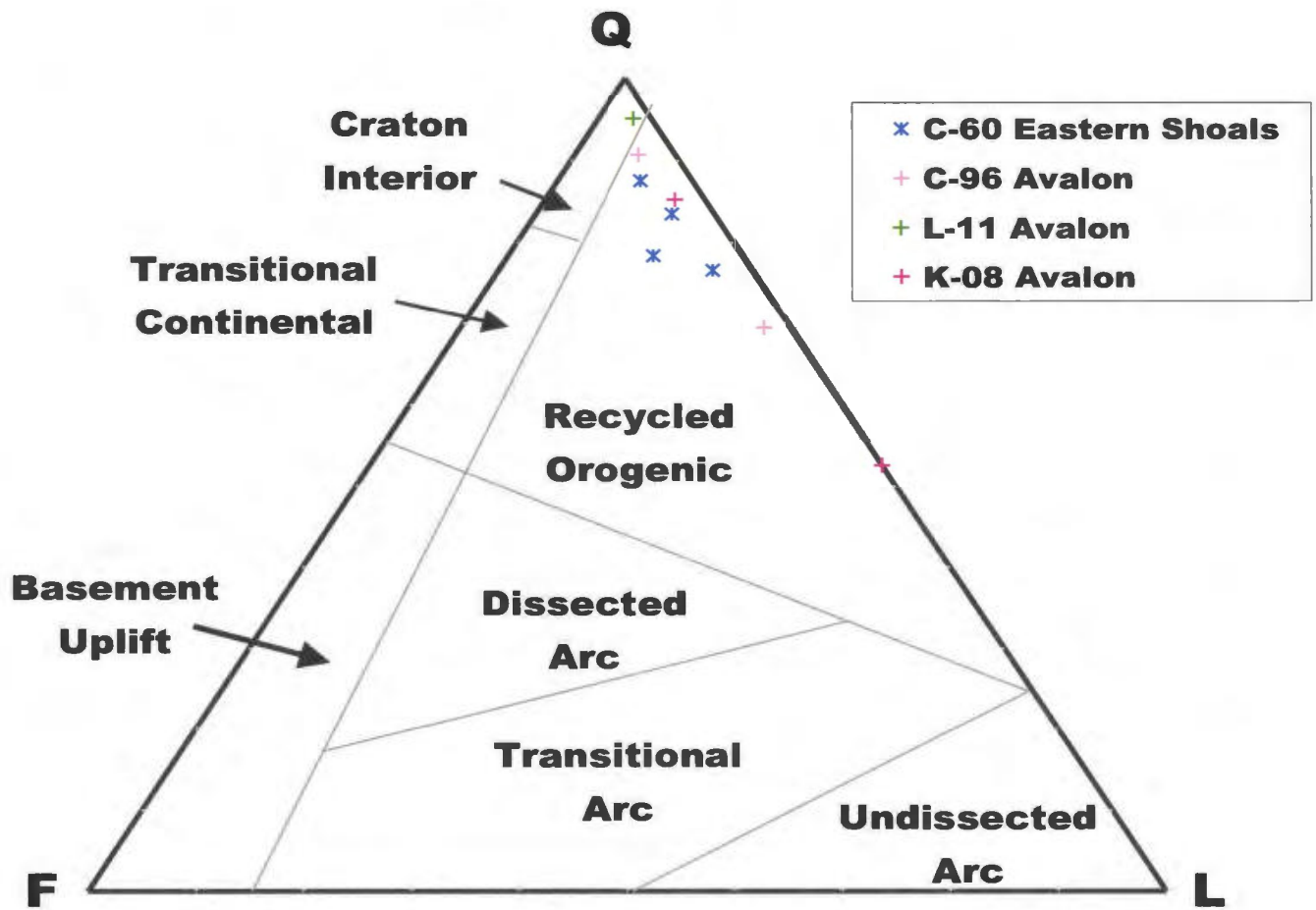


Figure 5.2 - Tectonic setting diagram for samples from the Avalon and Eastern Shoals formations. These formations have a higher lithic content than samples from the Ben Nevis Formation, possibly because the Avalon and Eastern Shoals formations were not exposed to the degree of wave action and reworking that is seen in the Ben Nevis Formation.

of sands can remove a large portion of unstable lithic grains and increase the quartz content relative to feldspars and lithic components, leading to a composition similar to that of the Ben Nevis Formation.

Samples from the Hibernia and Jeanne d'Arc formations (in particular the Terra Nova Member of the Jeanne d'Arc Formation) plot near the boundary between the Craton Interior and Recycled Orogenic provinces (Figure 5.3). Point count data shows a variable amount of feldspars (from 0% to 10%) and a highly variable amount of lithics (1%-55%). Most of the lithics are extrabasinal detrital carbonates and clay/mud clasts. All samples from the Hibernia and Jeanne d'Arc formations plot in the same tectonic provenance terrane as samples from the Ben Nevis Formation (with the exception of three samples), indicating a similar source composition and tectonic setting (Craton Interior/Recycled Orogenic). Two samples from well P-15 and one sample from well I-78 are much more lithic-rich at the expense of the quartz component within the Recycled Orogenic province compared to the other samples from the Hibernia and Jeanne d'Arc formations (Table 5.1). Well P-15 is located in the Hibernia Oil field and well I-78 is located on the western edge of the Flemish Pass area (Figure 2.1). Samples from well P-15 (4124.3 and 4129.65 m) are petrographically described as a medium to coarse-grained, well-sorted, moderately lithic quartzose sandstones (Wilson and Webb, 1998). The main lithic components within these samples are relatively ductile shale/mudstone fragments and argillaceous metasilstone. The single sample from well I-78 (3270m) is petrographically described as a fine-grained quartzose sandstone with common phylitic rock fragments (Wilson and Webb, 1998); it has an abundance of phyllite fragments not seen in any of the other samples. This may be because it is more proximal to the source and underwent less

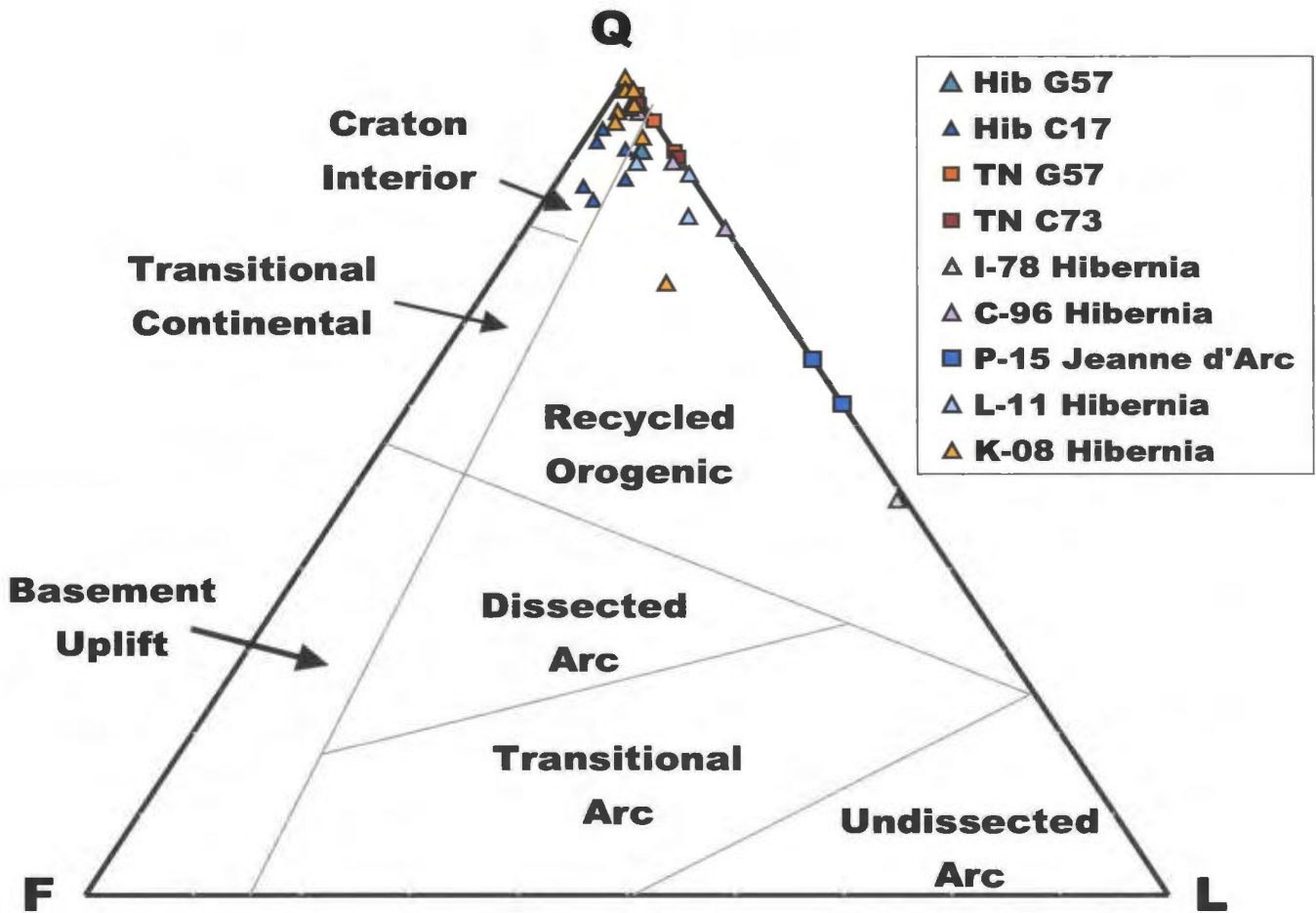


Figure 5.3 - Tectonic setting diagram for samples from the Hibernia and Jeanne d'Arc formations (including the Terra Nova Member of the Jeanne d'Arc Formation). Most of these samples fall in the same tectonic setting as the samples from the Ben Nevis Formation, indicating a similar source. Three samples fall much lower within the Recycled Orogenic category; the sample from well I-78 is located in the northern section of the Flemish Pass and is not likely related to the other samples. Samples from well P-15 have a higher lithic content which may be due to a difference in facies rather than tectonic setting.

mechanical weathering, or it may indicate a different source rock than what is found in the Jeanne d'Arc Basin. The large difference in QFL ratios suggests these samples are not petrographically related to the Ben Nevis Formation, and because of their geographical location, they are not a likely source for Ben Nevis Formation sandstones, in particular well I-78 which is located in the Flemish Pass area (~150 km north-east of the Jeanne d'Arc Basin).

Recycled orogens expose uplifted sedimentary strata (Dickinson et al., 1983). Tectonic settings include subduction complexes of arc orogens, highlands along the suture belts of collisional orogens and thin-skinned foreland fold-thrust belts along the flanks of arc or collision orogens (Dickinson and Suczek, 1979, their figure 7). Sands tend to be low in feldspar because igneous rocks are commonly not the primary sediment sources. Quartzose sandstones can be derived from recycled orogens whose ultimate sources were cratonic, if the recycling of sediment involves deformation and uplift of shallow water sediments from a continental margin succession. One would expect the composition of first- and second-cycle sediments to grade into one another on the QFL plot. In addition, sedimentological factors such as depositional environment may alter framework composition. For example, beach-barrier deposits may be enriched in quartz due to the removal of lithic grains by a large amount of wave action and reworking.

Provenance from Craton Interiors has been described as “*Sands derived from exposed shield areas and recycled from associated platform successions accumulate upon the platform themselves, and along rifted continental margins in shelf, slope and rise environments*” (Dickinson and Suczek, 1979, p. 2175). A subcategory of Craton Interior Provenance is Uplifted Basement Provenance, described as “*Sands shed from fault*

*bounded uplifts of continental basement rocks accumulated mainly in nearby yoked basins without much transport*” (Dickinson and Suczek, 1979, p.2175). Corresponding tectonic settings include incipient rift belts, transform ruptures of continental blocks, and zones of wrench tectonism within continental interiors (Dickinson and Suczek, 1979). Lithic sands reflect a partial derivation from sedimentary cover that masks or shields basement rocks.

The tectonic history of the Jeanne d’Arc Basin has been well documented as an ancient failed rift basin on a passive margin (e.g. Enachescu, 1987 and 1988; Tankard and Welsink, 1987; Sinclair, 1988). This does not fit with the description of a collisional orogen or subduction complexes associated with recycled orogens. However, during Atlantic rifting (Late Jurassic-Early Cretaceous), fault movement and tectonic uplift of the Triassic-Jurassic rift basins resulted in the emergence of the Central Ridge and the Avalon Uplift. Both of these highs were then potential sources and may have shed sediments into the Jeanne d’Arc Basin.

Knowing the tectonic setting of the Jeanne d’Arc Basin (rifted passive margin) one should expect that samples should plot in the Craton Interior Provenance field, however, a significant proportion of the data from this study plots within the Recycled Orogenic provenance field. This might be because the granitic/crystalline basement consists mainly of the Avalon Terrane and partially of the Meguma Terrane, which are part of the Appalachian Orogen (a Palaeozoic collision belt). It is correct to classify these sands as of Recycled Orogenic provenance, with rifted and uplifted blocks of Appalachian rocks acting as a sediment source. Alternatively one could shift the boundaries for each tectonic setting to include a larger lithic component and account for

sands derived from uplifted basement blocks with a thick sedimentary cover that acts as the primary source, with erosion not always reaching the basement. Seismic data shows that the Central Ridge complex is a thick section of sedimentary rocks overlying the Precambrian basement (Enachescu, 1992 and Figure 5.4), which is what Dickinson and Suczek have described as an Uplifted Basement provenance.

The Ben Nevis, Avalon, Eastern Shoals, Hibernia, and Jeanne d'Arc formation sandstones all plot within the same general area, along the boundary between the Craton Interior Province and the Recycled Orogenic Province, indicating that they were all deposited within a similar tectonic domain. There are numerous uplifted blocks found to the east, south and southeast of the eastern margin of the Jeanne d'Arc Basin that could have acted as potential source areas. Samples from the Jeanne d'Arc Formation have a very low feldspar component (lower than the Ben Nevis Formation) and are relatively deep in the section and rarely exposed beneath the Aptian unconformity. It is for these reasons that the Jeanne d'Arc Formation is not a likely sediment source for Ben Nevis Formation sandstones. The Hibernia Formation generally has a higher lithic content than the Ben Nevis Formation; as well, the lithic grains seen in the Hibernia Formation are usually shale/mud grains, which are rare in the Ben Nevis Formation. Most carbonate grains seen in the Hibernia Formation are shell fragments, while carbonate grains from the Ben Nevis Formation appear to be extrabasinal detrital fragments (Plate 4C) and are not merely shell fragments. However it is possible that these carbonate grains were eroded from the underlying A-marker and/or B marker units. The Avalon Formation is very similar both petrographically and geochemically to the Ben Nevis Formation. Cuttings samples of the Avalon Formation show a very fine-grained quartz-rich

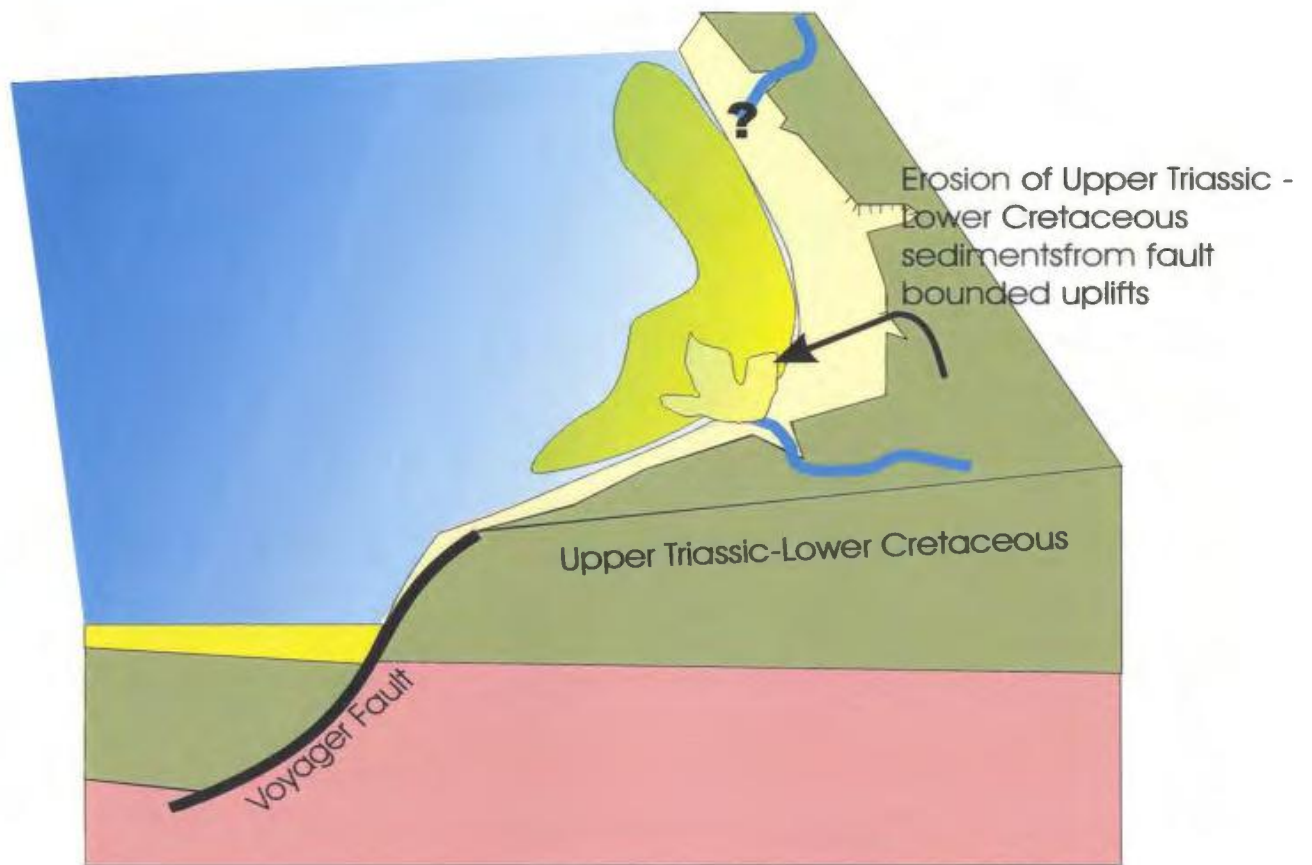


Figure 5.4 - Schematic cartoon depicting Upper Triassic - Lower Cretaceous sediments being eroded off the Central Ridge into the Jeanne d'Arc Basin, in particular into the area of the White Rose Field.

sandstone, similar to that seen in the Ben Nevis Formation, indicating that the Avalon Formation is a potential source for the Ben Nevis Formation sandstones.

## **5.2 Chemical Index of Alteration to Constrain Sediment Source**

### **5.2.1 Introduction**

Aside from the type of sediment source rock, weathering, sediment transport and diagenesis are all significant influences on sediment geochemistry. If diagenetic compositional effects can be accounted for and/or considered to be minor, weathering, and in particular the intensity of chemical weathering may be the most important variable controlling sediment composition. Climatic conditions are in-turn one of the most important factors that determine the rate of chemical weathering (Nesbitt, 2003). The intensity of tectonism is a large factor in the rate of erosion from source lands (i.e. rapid rates of uplift will result in rapid rates of erosion). Therefore the mineralogical and bulk chemical composition of sands and muds are controlled by, and reflect relative rates of chemical weathering and erosion. When rates remain stable over time, the mineralogical and bulk chemical composition remain unchanged (Nesbitt, 2003). When rates of other processes change, the sediment composition reflects those changes.

The Chemical Index of Alteration (CIA) is interpreted as a measure of the amount of weathering a sample has undergone. The CIA value is closely related to the  $\text{Al}_2\text{O}_3$  content of the mineral plotted on the diagram, where the primary minerals have CIA values around 50 or less and secondary clay minerals have CIA values of about 75 or higher (Nesbitt, 2003). Therefore the CIA is a measure of the amount of chemically weathered materials in a siliciclastic sediment or rock and is interpreted to reflect the

relative importance of chemical vs. physical weathering at the source lands (Nesbitt, 2003). It is important to note that this method assumes that the sample consists of framework grains and that the contributions of calcite and dolomite cements, and apatite to %-CaO have been removed.

Diagenetic effects can alter the mineralogy and geochemistry of a rock causing conversion of less stable to more stable mineral assemblages, as well as metasomatism (Nesbitt, 2003). In principle this can occur to such an extent that the effects of previous weathering trends are disguised. Particularly K-metasomatism is a common process of converting clay mineral weathering products of feldspars (kaolinite) to K-rich phases such as illite and muscovite. Another possible diagenetic effect is the albitization of Ca-rich feldspars, or the alteration of albite to K-feldspar (Nesbitt, 2003). Quartz cements on the other hand have little direct effect on the CIA of sedimentary rocks. Although the Ben Nevis Formation in particular has clearly not been altered extensively by diagenesis, the interpretation of CIA values and trends within A-CN-K ternary diagrams must be approached with caution to provide broad estimates and inferences about degrees of weathering.

### **5.2.2 Ben Nevis Formation**

The average CIA value for samples taken from Ben Nevis Formation cores is 65 (Appendix 6), with one outlier (well F-O4, 2809 m). This sample has a high Na<sub>2</sub>O value, possibly caused by drilling mud contamination. Samples from wells in the northern section of the White Rose Field (wells J-22-1 and H-20) on average have slightly higher CIA values (74 and 71 respectively) and plot closer to the Al<sub>2</sub>O<sub>3</sub> apex compared to

samples from wells in the southern section of the field (wells F-04, A-17, and L-08 with average CIA values of 63, 67 and 63 respectively) (Figure 5.5). Within A-CN-K compositional space, samples in the north plot directly above samples from the south, hence Ben Nevis samples from wells J-22-1 and H-20 are mostly more mature than those from the southern area of the field (note that at least 3 samples from well H-20 are scattered at CIA levels comparable to more southern wells). One possible interpretation of these relationships is that Ben Nevis sands in the north represent Ben Nevis sands from the southern area that have been reworked mechanically, producing a vertical trend of constant CN-K ratio. Clearly, this implies that Ben Nevis sands to the south are diachronous and younger relative to those in the north, a relationship at present not supported by any other observations. On the contrary, regional evidence presented earlier is taken to suggest slightly older Ben Nevis sedimentation to the north, younging as overall transgression progressed toward the south. In addition, this explanation is not consistent with the relative composition of Ben Nevis cuttings from well K-19 (one of the southernmost wells in the area) which is located within a chemical weathering trend sub-parallel to the CN-A tie relative to wells J-22-1 and H-20 to the north.

As an alternative explanation it is proposed that Ben Nevis composition in the north reflects extensive chemical weathering at the sediment source, accessed during early, south-directed transgression. This is consistent with petrographic observations, namely lower plagioclase+K-spar contents reflecting a more mature source, as discussed in Section 3.4.2. Chemical weathering may have been enhanced by relatively low topographic gradients, diminishing the effects of mechanical erosion and clastic transport. Subsequent deposition to the south appears to have accessed a less mature sediment

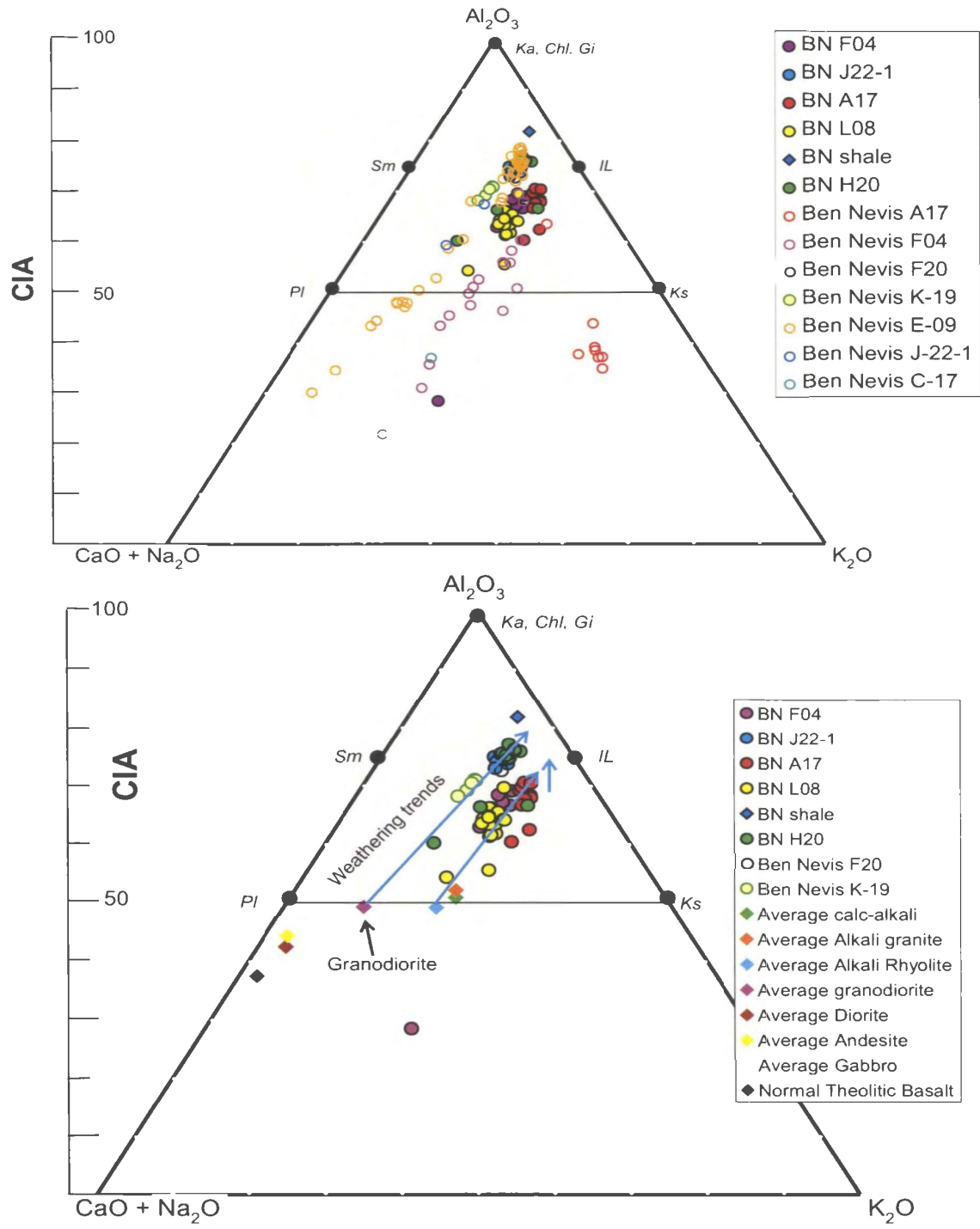


Figure 5.5 - Chemical Index of Alteration (CIA) ternary plot for samples from the Ben Nevis Formation, including samples from cores (filled circles) and cuttings (nonfilled circles). Samples that plot below the 50%  $Al_2O_3$  line are contaminated and should not be used in the analysis. Both the Ben Nevis Formation and Hibernia Formation show that their original source rock was likely a granodiorite however, samples from wells A-17, L-08, and F-04 may have had a more granitic source (more potassium rich).

source (consistent with higher feldspar content of the sands), perhaps aided by a more steeply inclined topographic slope in the source area (Central Ridge?), in turn possibly linked to tectonic activity along the Voyager fault and differential salt movement. Some of the very thick sections of Ben Nevis Formation in the southern block of the Whiterose field must reflect rapid subsidence and creation of accommodation space that accompanied this activity. The uppermost section of Ben Nevis sandstones intercepted in well K-19 may represent a return to the weathering trends observed at the base of the section to the north, although petrographic data is not available from the corresponding cuttings. Possible weathering trends at larger temporal and spatial scales will be further discussed in a subsequent section of this chapter.

### **5.2.3 Avalon and Eastern Shoals Formations**

CIA values for samples from the Avalon and Eastern Shoals formations are very scattered and do not plot in clusters like samples from the Ben Nevis Formation (Figure 5.6). All samples from these formations are cuttings, which may explain the large spread of values. Based on the method described above samples from J-22-1 show reliable geochemical compositions with minimal contamination. These samples plot parallel to the A-CN line, perhaps illustrating the progressive effects of chemical weathering of a common sediment source rock. Within a 30 m-section of the Avalon Formation in well J-22-1 (2890 to 2920 m) the samples show a trend of upward decreasing maturity, coincident with a trend of upward decreasing GR response, that is, an upward increase in relative sand content (Appendix 7, well J-22-1). This very small-scale trend appears to mimic the large, field-scale trends established above for the Ben Nevis Formation and

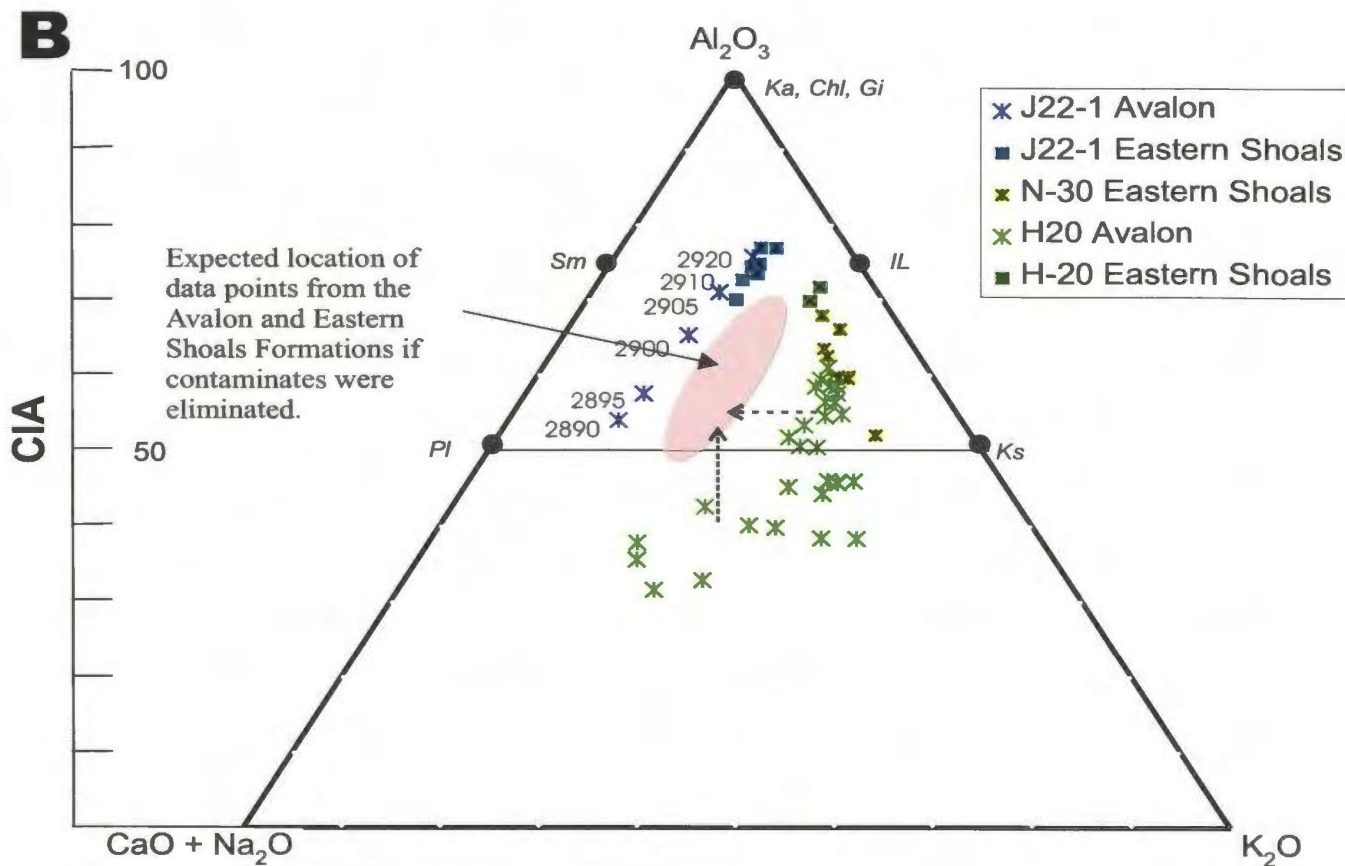
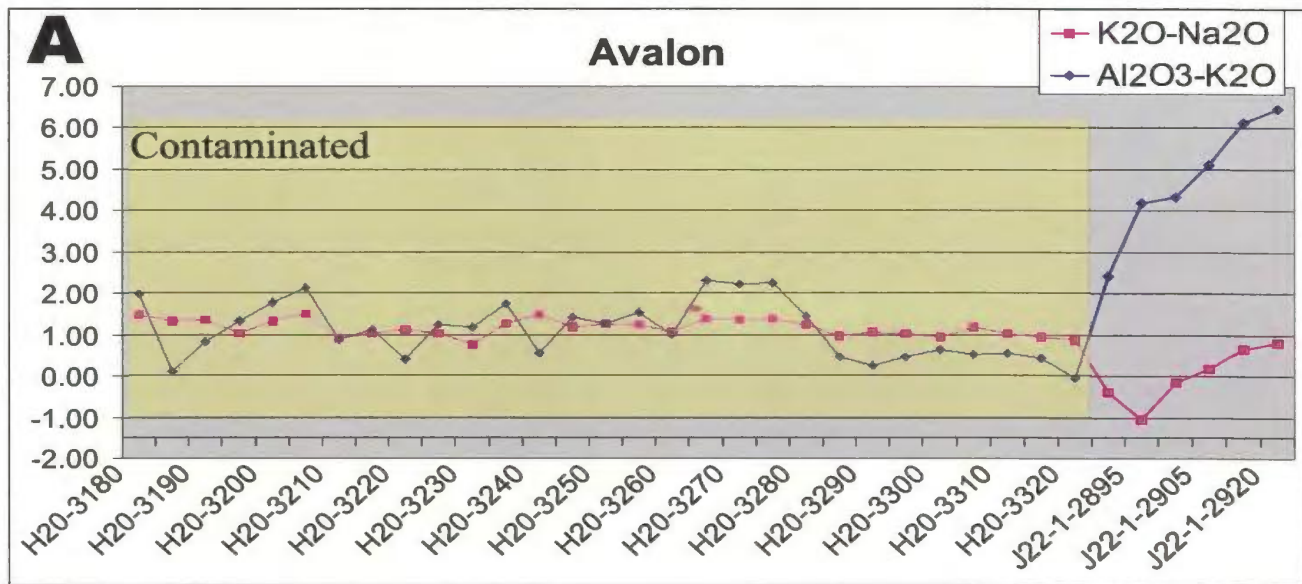


Figure 5.6 - A. K<sub>2</sub>O-Na<sub>2</sub>O and Al<sub>2</sub>O<sub>3</sub>-K<sub>2</sub>O differences determine contaminated samples. B. Chemical Index of Alteration ternary plot for samples from the Avalon and Eastern Shoals formations.

may simply reflect the overall trend of a progradational depositional system.

Alternatively, fault activity may have increased toward the top of the interval, increasing paleo-erosional/depositional slopes and thereby reducing the amount of chemical weathering at the source lands relative to mechanical break-up/erosion.

Samples from the Avalon Formation in well H-20 show a large difference in  $K_2O-Na_2O$  values as well as  $Al_2O_3-K_2O$  values indicating that true values of these samples (without contaminants) should plot slightly higher and to the left on the A-CN-K diagram (“expected” location on Figure 5.6). Such a correction would shift these samples to approximately coincide with the trend of Ben Nevis samples, although many of the Avalon Formation samples would have a lower CIA, indicating provenance from a less mature source, corresponding to shorter or less intense exposure to chemical weathering.

All samples from the Eastern Shoals Formation exhibit a difference between  $K_2O-Na_2O$  that implies contamination ( $Al_2O_3-K_2O$  values don’t indicate contamination). If corrected, they would plot slightly further to the left, that is, approximately coincident and below the composition of Ben Nevis Formation samples. Core samples are needed in both of these formations to say with more certainty where these samples might plot on the A-CN-K diagram.

#### **5.2.4 Hibernia and Jeanne d’Arc Formations**

CIA values for the Hibernia and Jeanne d’Arc formations are also scattered and do not plot within a cluster; however, trends can be picked out within each formation (Figure 5.7). Samples from cores of the Hibernia Formation (and cuttings from well K-19) plot close- and approximately parallel-to the A-CN line, but samples from cuttings have a high

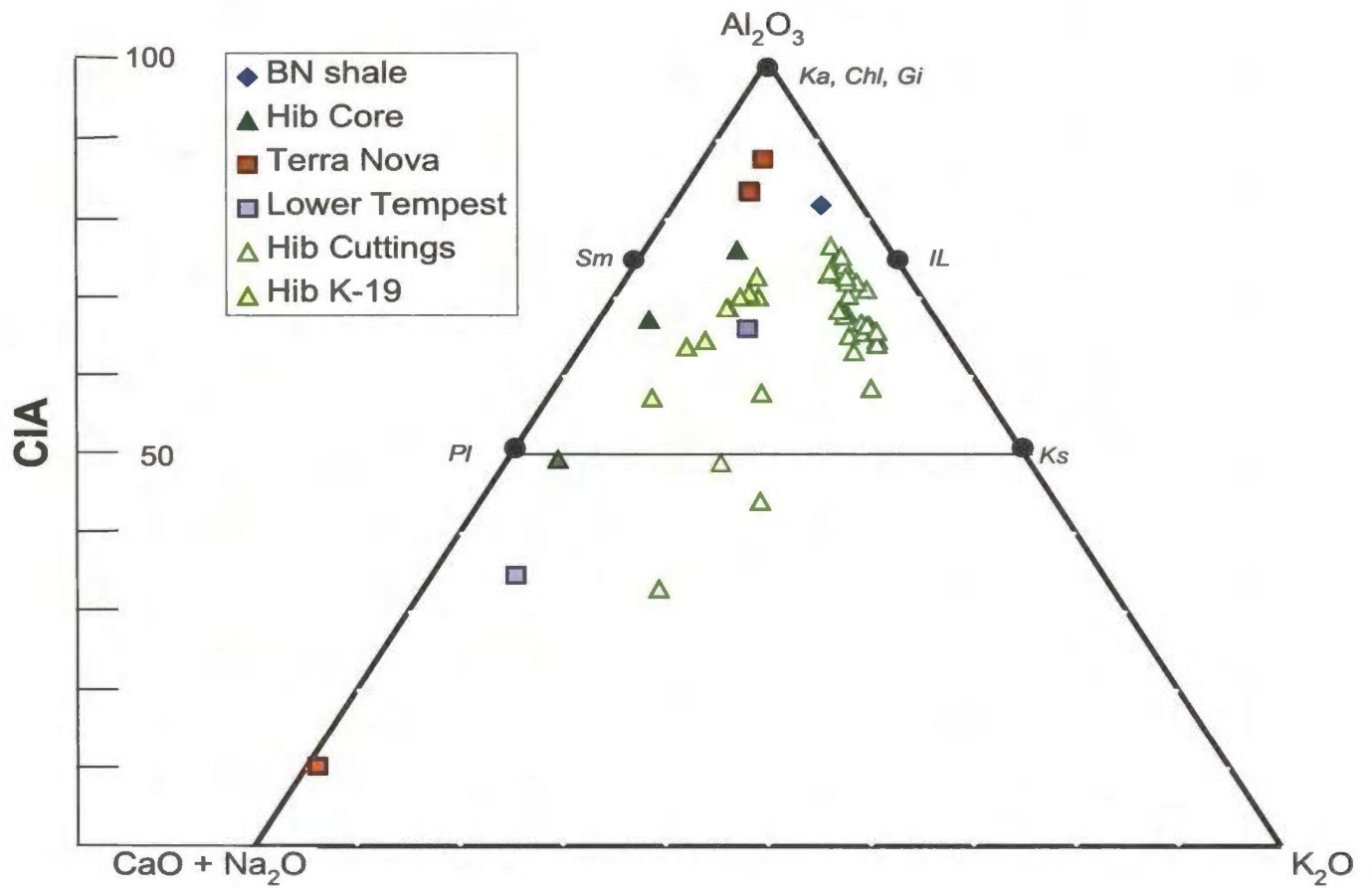


Figure 5.7 - A-CN-K diagram for samples from the Hibernia, Jeanne d'Arc (Terra Nova Member) and Rankin (Lower Tempest sandstones) formations. Core samples are filled and cuttings samples are not filled. Low  $Al_2O_3$ - $K_2O$  values results in samples from the Hibernia Formation (cuttings) plotting on the right side of the diagram.

K/CN ratio and tend to plot closer to the A-K line. Samples from cuttings show trends that are similar to those of contaminated samples of the Avalon and Eastern Shoals Formations (Figure 5.7). If the effects of contamination could be removed, one would expect the difference between  $K_2O$  and  $Na_2O$  to be  $< 1\%$  and the samples would plot on the left side of the A-CN-K diagram, approximately coincident with samples from Hibernia Formation cores (Figure 5.7).

Samples from the Terra Nova Member of the Jeanne d'Arc Formation plot either very high on the A-CN-K diagram (3 samples of CIA of about 85), or plot extremely low near the  $Na_2O$ -CaO apex (sample C-73, 4129 m with CIA=10) (Figure 5.7). The three samples with a high CIA value show high levels of  $Al_2O_3$  compared to  $Na_2O$  and  $K_2O$ . Clearly, the single sample from well C-73 at 4129m has a very high CaO value (30%) and a comparatively low calculated  $CO_2$  value (12%), implying that this may be a bad sample for which all the  $CO_2$  is not accounted for, or alternatively the XRF may have measured an anomalously high CaO value. This sample is clearly an outlier and needs to be re-run before it can be included in any comparisons.

Two samples from the Lower Tempest sandstone of the Rankin Formation have  $Al_2O_3$ - $K_2O$  differences of less than 1% and can be considered contaminated. However sample G-57 4594.25 has a CIA value of 66% and plots in the same range as samples from the Hibernia Formation. This might be due to the very low oxide values for samples from the Lower Tempest sandstone and hence the extreme sensitivity of these weight percents to the CIA formula. It is reasonable to assume sample G-57 4598 should plot in the same area, omitting any contamination.

### 5.2.5 Summary of Weathering Trends

When using the CIA for provenance studies one would expect sediment source rocks to plot close-to or below the 50%  $\text{Al}_2\text{O}_3$  line (due to minimal amounts of weathering) and one would expect that the sediment deposited from that source would plot closer to the  $\text{Al}_2\text{O}_3$  apex (due to the effect of weathering). Samples of the Ben Nevis Formation from wells H-20 and J-22-1 plot above the rest of the samples (wells A-17, L-08, and F-04) and indicate a greater degree of weathering (Figure 5.5). The cluster of samples from A-17, L-08 and F-04 show no linear trends parallel with the A-CN join and indicate that there are minimal differences in the amount of chemical weathering through this area both laterally and vertically. Samples from well E-09 show a linear trend along the A-CN line; however, some of these samples fall well below the 50%  $\text{Al}_2\text{O}_3$  line and nine of them have been classified as contaminated (Table 4.1). Also, these samples have high CaO values and it is thought that not all the CaO in calcite was accounted for. Plotting these values on an A-N-K diagram (eliminating all CaO) shows that samples from the E-09 well plot in the same general area as the core samples, spread between the cluster of wells in the south and the cluster of wells in the north (Figure 5.8). Therefore any lateral trends seen in samples from E-09 are suspect and should be interpreted with caution.

On average the Ben Nevis Formation samples plot closer to the  $\text{Al}_2\text{O}_3$ - $\text{K}_2\text{O}$  line than the Hibernia, Terra Nova and Lower Tempest samples (Figure 5.9). The Avalon and Eastern Shoals formations could also be included in this comparison if the assumption made about contamination is correct. This implies that, at least with regard to

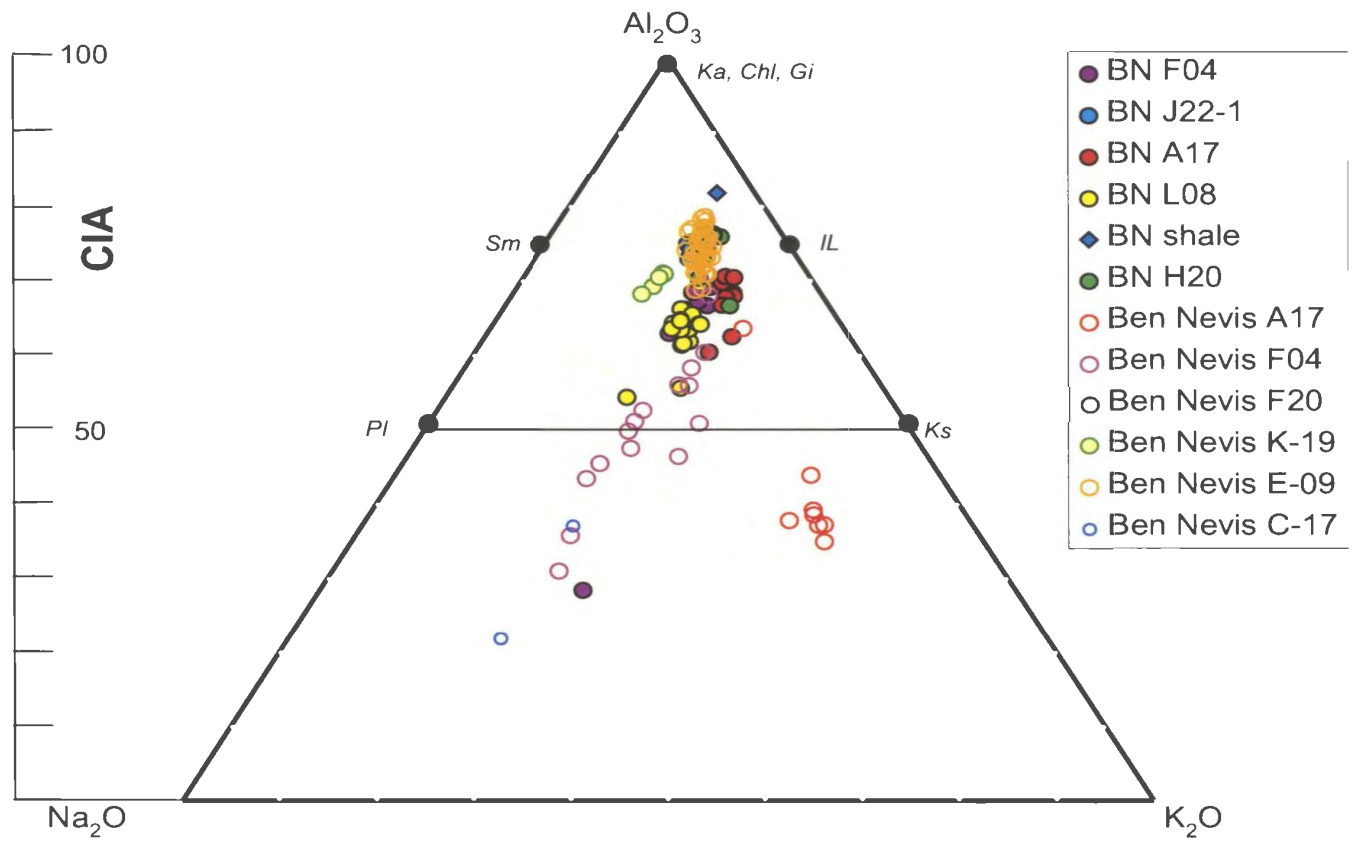


Figure 5.8 - A-N-K diagram to show trends in the data if CaO was omitted. All values from cores have CaO values of zero and therefore this is not an unrealistic assumption. Samples from well E-09 plot in the same area as the samples from cores, with a concentration of samples plotting in the same cluster as the northern wells. Open circles represent samples taken from cuttings and closed circles represent samples taken from cores.

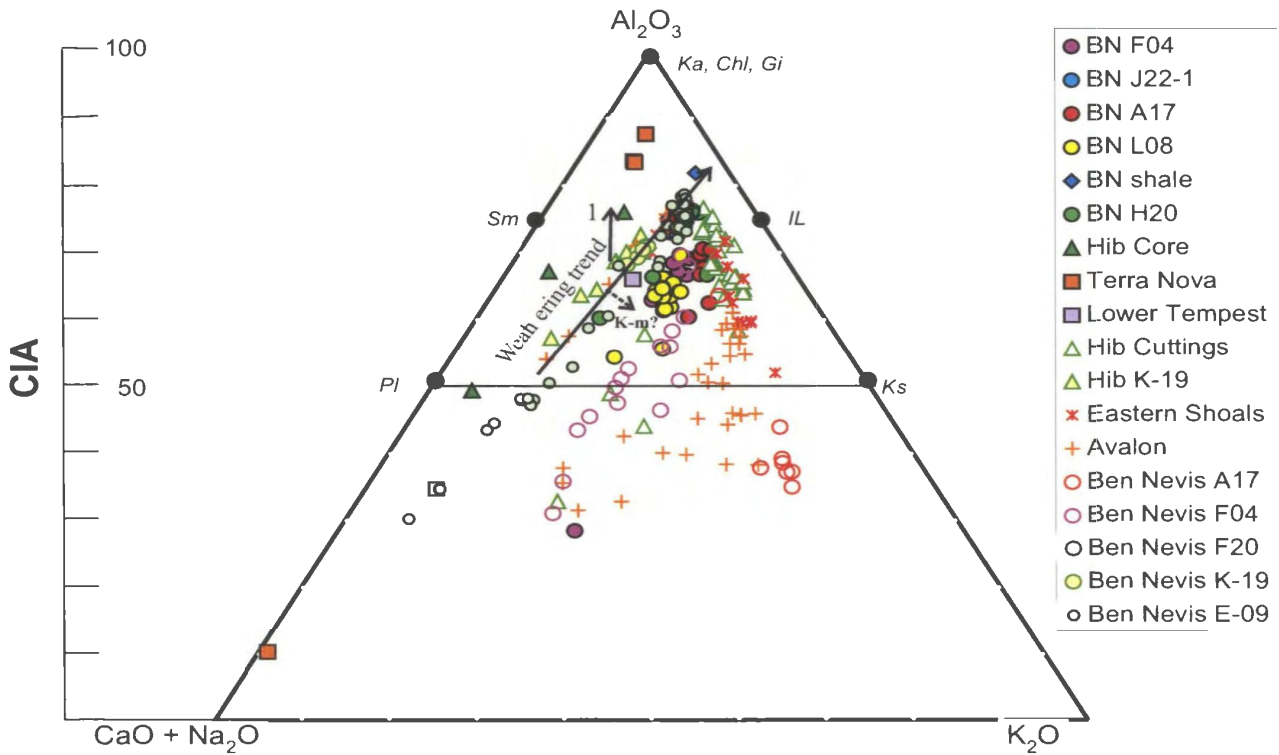


Figure 5.9 - A-CN-K diagram for samples from all formations studied. Source sediments are expected to plot near the 50%  $\text{Al}_2\text{O}_3$  line and weathering trends should move along a trend line from this point. Samples from the Ben Nevis Formation in the north underwent more mechanical weathering than samples from the center of the White Rose Field (Arrow 1). Ben Nevis Formation samples plot to the right of samples from the Hibernia Formation, this may be due to k-metasomatism? (K-m) due to the deep burial the Ben Nevis Formation has been subjected to.

geochemical maturity, all of these formations are possible sediment sources for Ben Nevis Formation sandstones.

To be considered as possible sediment sources, Terra Nova and Lower Tempest sandstones must be shown to have been exposed by the Aptian-age unconformity that pre-dates deposition of the Ben Nevis Formation. This relationship is not seen on any well logs from this study, not even for those wells located on structural highs. The presence of Terra Nova and Lower Tempest equivalent units at the unconformity cannot be ruled-out outside of the study area, but the Hibernia Formation is very commonly exposed below the Aptian unconformity, hence thought to be the more likely sediment source.

### **5.3 Potential Sources of Sediment**

The Central Ridge is located immediately to the east of the Jeanne d'Arc Basin (Figure 1.2) and was an intra-rift high, reaching its maximum elevation during the Early Cretaceous due to increased rotation of its basement core on the basin bounding fault plane (Enachescu, 1988). The ridge was exposed as an island chain or peninsula and hence a large section of Upper Jurassic to Upper Cretaceous sediments are missing due to erosion and non-deposition. Gamma Ray logs from well E-87 show that sedimentary rocks lying immediately below the Aptian unconformity can be assigned to the Hibernia Formation (Appendix 7) and well C-64 shows that an indurated succession approximately 5 km thick of Upper Triassic – Upper Jurassic sedimentary rocks still overlies the Central Ridge Basement (Enachescu, 1988 and 1992). Sedimentary successions tend to get

thinner toward the south of the Central Ridge with intrabasinal basement rocks found approximately 1-2 km below the subsurface (Enachescu, 1988).

To the south of the Jeanne d'Arc Basin is the Morgiana Anticlinorium and the Avalon Uplift, both consisting of Upper Triassic to mid-Jurassic sedimentary rocks (Figure 5.10; reproduced from Enachescu, 1988). Since both the Avalon Uplift basinal areas and the Central Ridge consist of the same type of bedrock (Upper Triassic to mid-Jurassic sediments) it would be difficult to differentiate between the two, either geochemically or petrographically. Point count data shows that samples from the Ben Nevis Formation at well K-08 (Terra Nova Field) have a large detrital carbonate component similar to what is observed in samples at the White Rose Field (Appendix 1), indicating that there is no significant difference in the Ben Nevis framework grains between the two fields, White Rose and Terra Nova. This implies that there is not a large compositional difference between the northeast and southeast sections of the Jeanne d'Arc Basin bordering the Whiterose Field. However it was shown above that samples from wells in the northern part of the White Rose Field (particularly as far north as well J-22-1) have a higher CIA than those in the south, implying slight variations in weathering intensity (as controlled by paleoslopes) and/or sediment source composition during deposition of Ben Nevis sandstones. Clearly, the same fault activity thought to be responsible for changes in paleoslope and consequent chemical weathering, may have controlled the extent to which sediment supply was from the southern or eastern parts of the Central Ridge. Basement maps (Figure 5.10) show that both the Central Ridge and the south Jeanne d'Arc Basin (including the Avalon Uplift) consist of the same strata (Upper Triassic to Upper Jurassic) and one needs to consider if it is relevant to separate

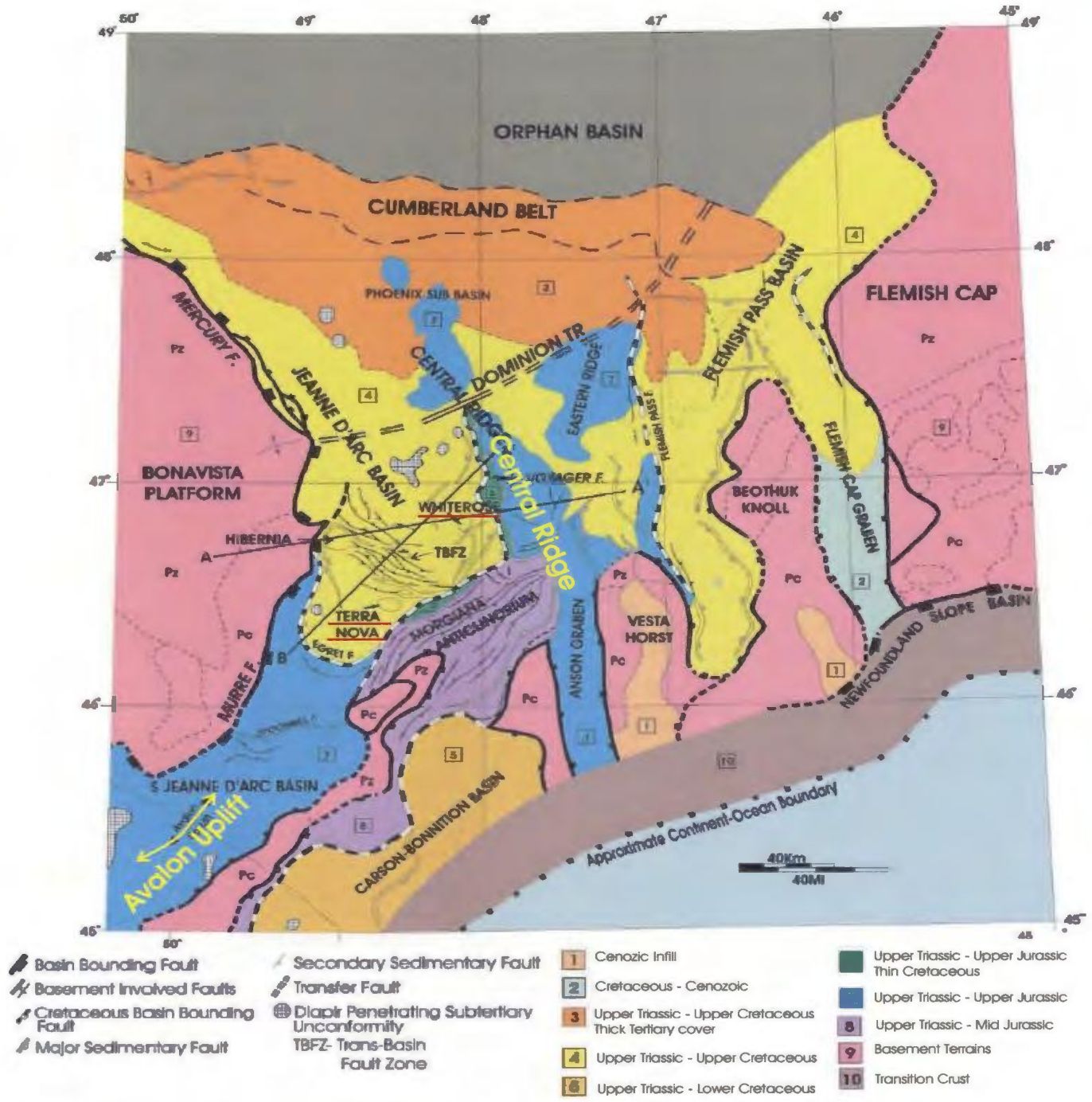


Figure 5.10 - Map of Grand Banks showing infill of basins and basement outcrops (reproduced from Enachescu, 1988). All basement outcrops are shaded pink and include Paleozoic metasedimentary (Pz) basement and Precambrian basement (Pc). The Central Ridge and Avalon uplift consist of Upper Triassic - Upper Jurassic sediments and the Morgiana Anticlinorium consists of Upper Triassic - Mid Jurassic sediments .

these two areas as potential sources for the Ben Nevis Formation sandstones, or if they can be grouped as they are on the basement map (Figure 5.10) as Upper Triassic-Upper Jurassic sedimentary rocks. If compositional differences between these uplifted areas are minor, it is only useful to separate the two in terms of transport distance, which in this case is less than 200 km. This distance is too short to have a noticeable impact on sediment composition due to transport. The Central Ridge is the most proximal location for sediment supply and it is likely that channels were cut through relay ramps along the Central Ridge and brought sediment from this high into the Jeanne d'Arc Basin to deposit sediment into the White Rose Field (Figure 5.11). The Avalon Uplift is a major sediment source for the southern section of the Jeanne d'Arc Basin and it is likely that some of this sediment was transported across the basin by channels and longshore drift to eventually be deposited in the southern section of the Jeanne d'Arc Basin (Terra Nova, Hibernia, and Hebron Fields) (Figure 5.11). Because the Avalon Uplift and Central Ridge both consist of Upper Triassic-Upper Jurassic sedimentary rocks, a large difference in sediment composition is not expected between these two source areas.

#### **5.4 Pre-Mesozoic Basement Rocks as a Possible Primary Sediment Source**

The Chemical Index of Alteration and A-CN-K diagrams are useful tools to estimate the original primary (igneous and/or metamorphic) composition of a sediment source rock. There is no evidence from drilling or seismic mapping of the Ben Nevis Formation sandstone lying directly on top of basement rocks. Overall, there is limited data on basement rocks found in the Grand Banks area and this lack of geochemical analyses on basement rocks prevents a comparison of sedimentary and igneous samples.

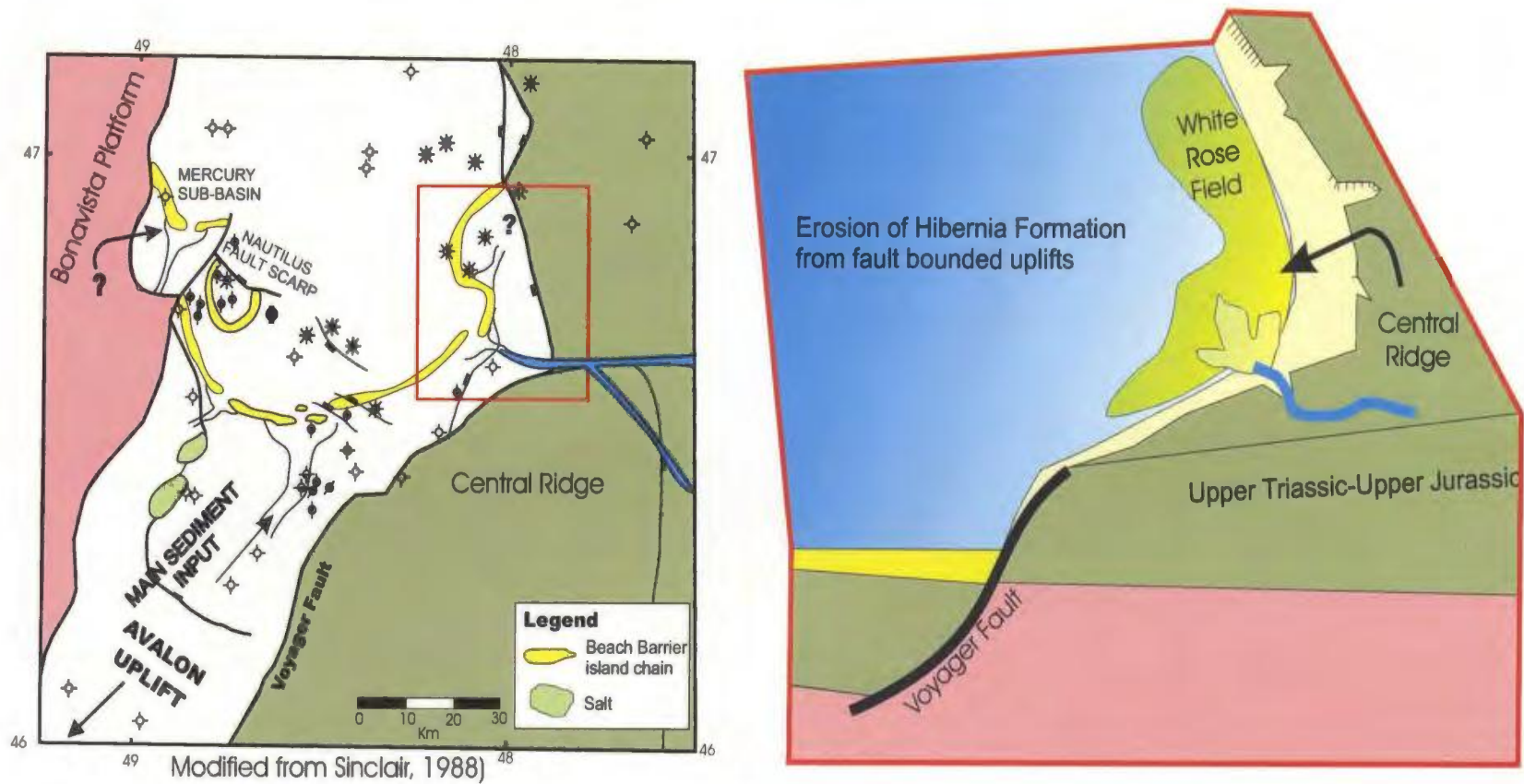


Figure 5.11 - Map showing likely depositional history of Upper Triassic-Upper Jurassic sediments transported from the Avalon uplift into the southern section of the Jeanne d'Arc Basin as well as channels cutting through the Central Ridge to deposit Upper Triassic-Upper Jurassic (i.e. Hibernia Formation) sediments along the eastern edge of the Jeanne d'Arc Basin, in particular in the White Rose oil Field area.

Average compositions of various common igneous rock types are used instead (from Nockolds, 1954) and plotted on Figures 5.5 as a reference. A line representing typical weathering trends can be drawn through the northern Ben Nevis Formation samples (wells J-22-1 and H-20) and the cluster of samples of well K-19, and extrapolated to an average granodiorite composition (Figure 5.5). A similar trend can be drawn to connect the clusters corresponding to wells A-17, F-04, and L-08 to a hypothetical sediment source that is slightly more granitic (Figure 5.5).

Accepting the two trends described above raises the possibility that basement rocks of slightly different compositions were accessed during deposition of the Ben Nevis Formation, perhaps controlled by tectonic activity on faults that also influenced the intensity of chemical vs mechanical weathering on a larger, regional scale. However, lack of basement data and a limited W-to-E distribution of Ben Nevis wells prevent further testing of the hypothesis at this time. Alternatively, a much broader trend can be inferred to encompass all of Ben Nevis samples in A-CN-K compositional space and differences are merely ascribed to local changes in paleoslope and weathering intensity. Importantly, trends inferred from Avalon and Eastern Shoals formation samples are very similar to those of the Ben Nevis Formation (Figure 5.6), in support of a granodiorite-granite sediment source composition. In contrast, trends derived from the very limited number of Hibernia Formation and Terra Nova Member core samples (Figure 5.7), can be inferred to correspond to that of a more mafic source, perhaps distinctive of the older rifting phase.

The Grand Banks can be considered an offshore extension of the Appalachian Orogen and includes the Bonavista Platform, two isolated continental blocks; the Flemish

Pass and the Orphan Knoll, and several other smaller high blocks (Enachescu, 1988 and 1992). The basement rocks that underlie the Mesozoic sedimentary rocks found within the Jeanne d'Arc Basin belong to the Avalon and Meguma Terranes from Palaeozoic orogenic phases (Enachescu, 1988) and include igneous and metasedimentary rocks. The term basement refers to the sequence of rocks that formed the peneplaned cratonic crust prior to the Mesozoic cycle of ocean opening (i.e. the Hadrynian and the Palaeozoic metasedimentary and sedimentary groups) (Enachescu, 1988). The basement rocks were subjected to extension, resulting in intense faulting and major subsidence (Enachescu, 1988). The Upper Devonian to Lower Permian metasedimentary and volcanic rocks of the Avalon Terrane include the sedimentary succession of the Horton, Windsor, Canso-Riversdale and Picto-Cumberland groups (Enachescu, 1988, Howie and Barss, 1975; Schenk, 1978; Williams and Hatcher, 1982, 1983; O'Brien et al., 1983).

There is limited information on the composition of the basement rocks with only 13 wells in the Grand Banks penetrating basement (Figure 5.12). Coring and sampling of these basement rocks indicate the presence of numerous rock types and King et al. (1986) have differentiated the basement into two zones, the Palaeozoic (Pz) and the Precambrian (Pc) based on well-core descriptions and seismic reflection data. Enachescu (1988) has categorized the basement and sedimentary infill areas (Figure 5.10) with all Pre Mesozoic basement rocks shaded pink and categorized as either Precambrian basement (Pc) or Palaeozoic metasediments (Pz).

King et al. (1986) described samples from the Virgin rocks – Eastern Shoals area (Figure 5.12) as pink and white quartzite and tillite with numerous granitic clasts. Two of the thirteen industry wells that reported penetrating the basement include the wells

Linnett	E-63
Cumberland	B-55
Bonavista	C-99
Blue	H-28
Jaeger	A-49
Bittern	M-62
Gannet	O-54
Phalarope	P-62
Razorbill	F-54
Hermine	E-94
Sandpiper	J-77
Murre	G-67
Hibernia	G-55

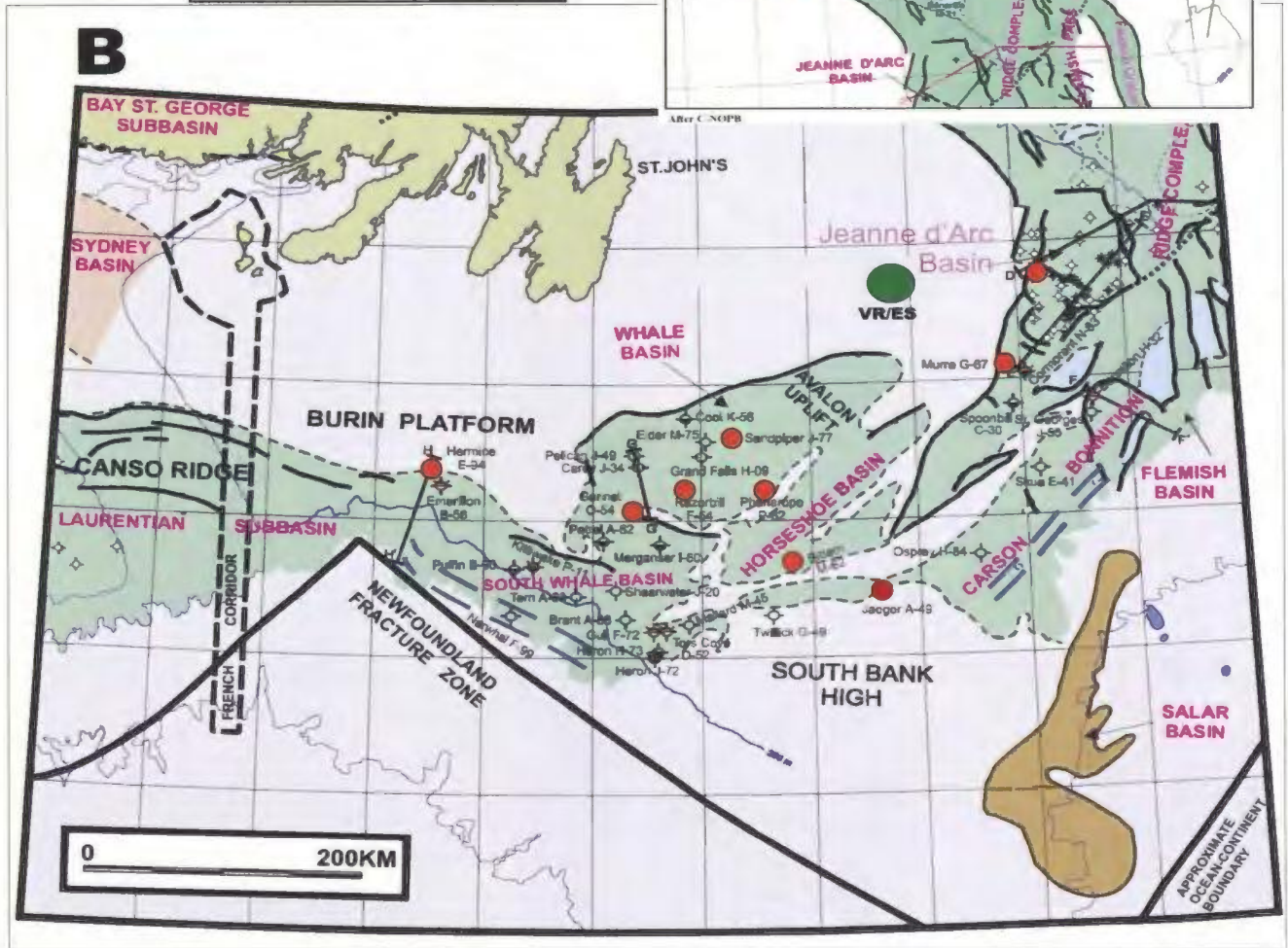
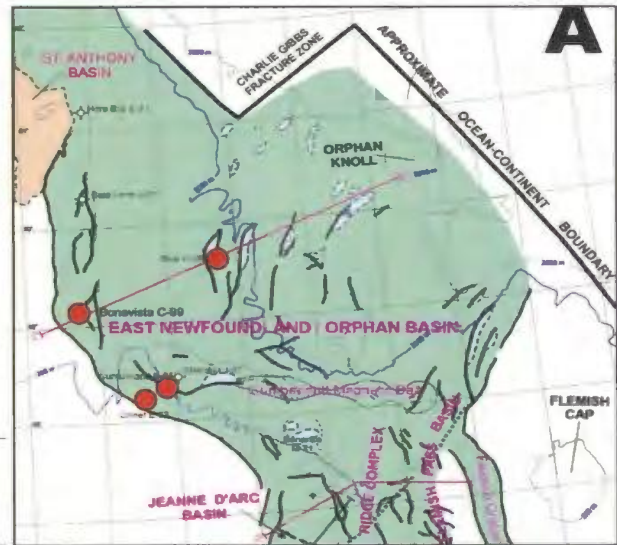


Figure 5.12 - Map with 13 wells that penetrated basement rocks (highlighted in red circles). In the East Newfoundland/Orphan Basin (map A); Linnet E-63, Cumberland B-55, Bonavista C-99, and Blue H-28. In the southern Grand Banks (map B); Jaeger A-49, Bittern M-62, Gannet O-54, Phalarope P-62, Razorbill F-54, Hermine E-94, Sandpiper J-77, Murre G-67, and Hibernia G-55. Virgin rocks-Eastern shoals area (VR/ES) highlighted in green on map B.

Bonavista C-99 and Gannet O-54. The petrographic report from the Bonavista C-99 well history report described the basement rock found between 12,368 and 12,398 feet as:

*Leucocratic granite pegmatite – the rock is composed of equal quantities of interlocking grains of quartz and alkali feldspars, the most abundant feldspar is orthoclase. It occurs clear and unaltered. The less abundant feldspar is plagioclase, occurring mostly as albite. The albite in places is clouded and altered to sericite. Some microcline twinning and perthitic intergrowths are present. Primary ferromagnesian are absent. Chlorite, the alteration product of biotite and secondary oxides (goethite and hematite) are present in sub-parallel lenses that give the rock a false gneissic appearance. Many feldspar grains optically strained but show no preferred direction.*

A small sample of diorite was collected in the Gannet O-54 well at 9750 m and is described as:

*Diorite, gray-green, fine to medium crystalline. Only loose fragments in the sample, a few pieces of very finely crystalline rock of igneous or metamorphic origin are also present (this could be from a cobble xenolith and need not be a part of an igneous body).*

These two samples of basement rocks lie to the north of the Jeanne d’Arc Basin near the Orphan Basin (Figure 5.12) and represent the best available indication of basement rock composition. Seismic regional mapping and potential fields maps indicate that granitic/granodioritic rocks should be widespread within the pre-rift basement of the

Grand Banks and environs (e.g. Enachescu, 1987). Within the limits of this very sparse data, the compositions are consistent with those derived from the A-CN-K diagram of Ben Nevis sandstones.

Tectonic discriminative diagrams, as well as petrographic descriptions, do not show a high amount of feldspars and do not indicate the Ben Nevis Formation is a first cycle sediment; rather, the Ben Nevis Formation sandstones are polycyclic and are sourced from recycled sediments, of Late Triassic – Early Cretaceous age, most likely from the Hibernia Formation. However if one were to trace back the source to the original basement, CIA diagrams show that the original source should be igneous, in particular a granodiorite. Petrographic and geochemical data suggest Ben Nevis Formation sediments were initially sourced from a felsic rock, with a minimal mafic component. Low values of MgO, Fe<sub>2</sub>O<sub>3</sub> and TiO<sub>2</sub> (0.25%, 0.80% and 0.34% respectively) also suggest a minor contribution from mafic source rocks. Chromium and nickel values for samples in the Ben Nevis Formation are low, suggestive of a source (Figure 5.13). However, chromium and nickel values for the Jeanne d’Arc and Rankin formations, and a few samples from the Hibernia Formation (G-57 3985 m, and G-57 3995 m) are much higher and imply a mafic component associated with these formations (Figure 5.13). This increase in Cr and Ni values is consistent with the trend observed on the corresponding A-CN-K diagram (Figure 5.7) and, as mentioned above, perhaps indicative of more mafic basement rocks exposed during the earlier rifting stage.

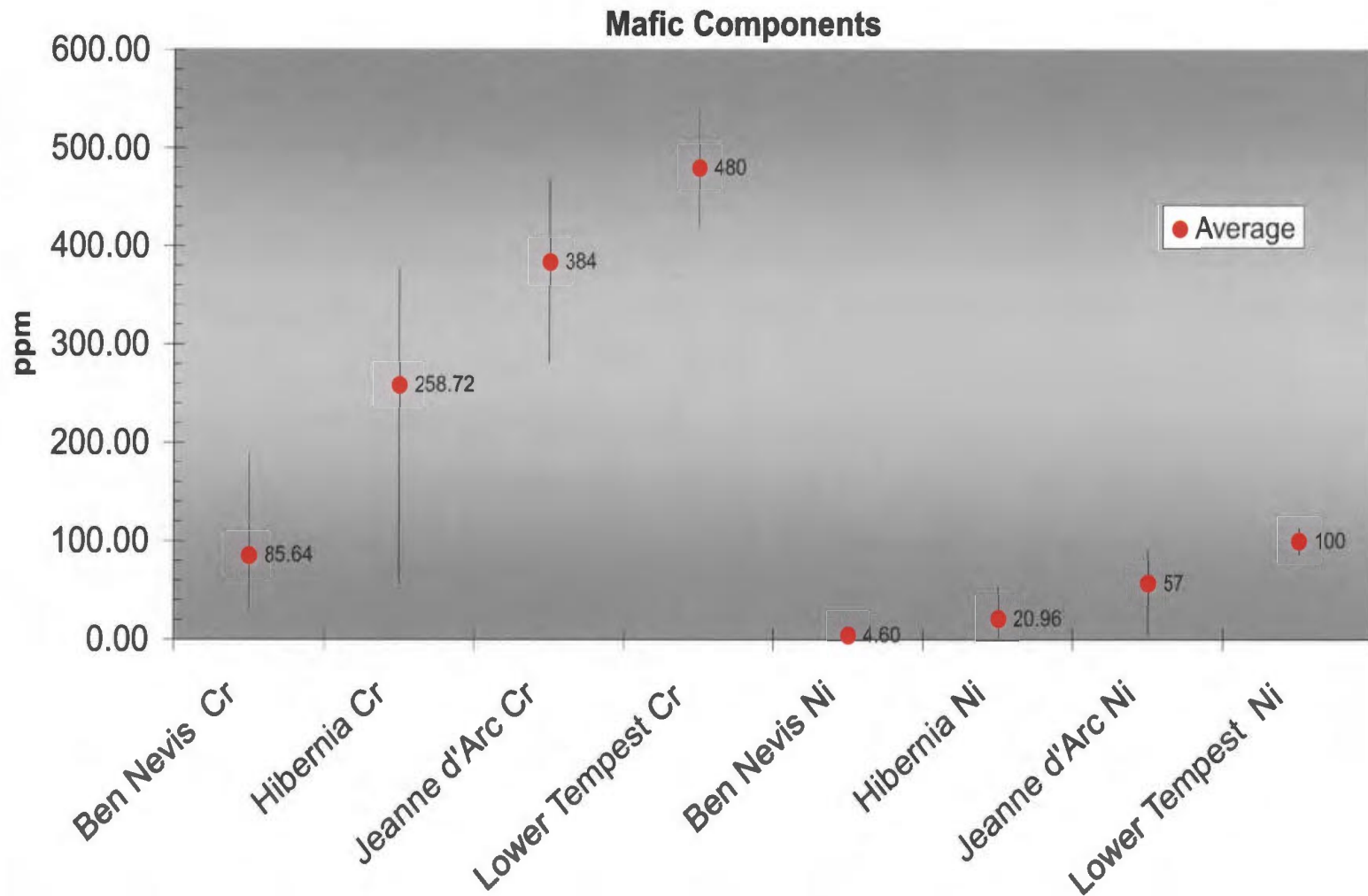


Figure 5.13 - Chromium and nickel values for samples from the Ben Nevis, Hibernia, Jeanne d'Arc (Terra Nova Member) and Rankin Formation (Lower Tempest Member). Chromium values below 200 ppm and nickel values below 50 ppm indicate a rock with a felsic source (van de Kamp and Leake, 1985). Samples from the Ben Nevis Formation are below these values and imply a felsic source; however, samples from the Hibernia, Jeanne d'Arc and Rankin formations are above these values, implying a larger mafic component.

## **Chapter 6**

### **Conclusions**

Provenance of the Ben Nevis Formation sandstones has been investigated using petrographic and geochemical techniques. Petrographic data were analysed to interpret tectonic setting and petrographic difference within the Ben Nevis Formation as well as with possible sediment source rocks. Geochemistry was used to compare geochemical signatures from within the Ben Nevis Formation as well as between possible sources. Anomalously high levels of some trace elements in samples taken from cuttings indicated a high level of contamination from drilling muds and a large number of these samples had to be omitted in the analysis. It is recommended that cutting samples not be used in geochemical analysis due to their high degree of contamination.

The Ben Nevis Formation is a very fine grained, well sorted, quartz arenite to sublitharenite. The major lithic components are carbonate grains and chert. Overall, values of the Chemical Index of alteration (CIA) indicate a higher degree of weathering in Ben Nevis sections to the north, likely due to low topographic gradients that might have caused longer residence times during transport, in-turn inducing increased chemical weathering. Longer transport distances to the northern area may have enhanced this effect. QFL diagrams show that the Ben Nevis Formation sandstones were sourced from a Craton Interior tectonic setting, with some data points falling in the Recycled Orogenic setting. This interpretation indicated that sands were eroded from fault-bounded uplifts and deposited into the basin with relatively little transport.

Both the Avalon and Eastern Shoals formations are classified as fine to very fine grained, well-sorted, sublitharenites. They both have a higher lithic component than samples from the Ben Nevis Formation and an average grain size of fine to very fine grained. They are well-sorted (Wilson and Webb, 1998) and plot lower in the Recycled Orogenic Category. Although only minimal differences in provenance are implied for Ben Nevis and Avalon sandstones, a large portion of cuttings samples were defined as contaminated, and only a few samples were deemed accurate representations of weathering trends.

Samples from the Hibernia Formation have variable grain sizes, ranging from very fine grained in the fluviodeltaic facies to coarse grained in samples from channel facies and are classified as subarkose to sublitharenite. Lithic grains are mainly shale/mud clasts and carbonate grains. Most of the Hibernia Formation samples plot in the Craton Interior category indicative of a similar tectonic setting as the Ben Nevis Formation. However, based on A-CN-K diagrams the sediment source for the few Hibernia Formation cores available for sampling appears to have had a more mafic composition than that inferred for Ben Nevis sandstones. This complicates establishing a clear link between these formations and the sampled Hibernia Formation may not be representative of the upper sections, which is now eroded. Alternatively, the Avalon Formation acted as main sediment source for Ben Nevis sandstones.

The Terra Nova Member of the Jeanne d'Arc Formation is a moderately sorted fine to medium grained sandstone and is classified as subarkose to sublitharenites. The main lithic component is shale/mud clasts and carbonate grains. Samples plot in the Craton Interior and Recycled Orogenic provinces, however a lack of exposure along the

Aptian unconformity, as well as a large difference in grain composition (compared to the Ben Nevis Formation) are the basis to rule-out these sedimentary rocks as potential sources for the Ben Nevis Formation.

The Central Ridge consists of Upper Triassic to Lower Cretaceous sedimentary rocks overlying metasedimentary basement rocks and well E-87 shows the Hibernia Formation lying directly below the Cenozoic sediments. The Ben Nevis Formation sandstones are polycyclic and were likely sourced from recycled sediments of Late Triassic – Early Cretaceous age, most likely from the Hibernia Formation. Chromium and nickel values from the Ben Nevis Formation are consistent with a felsic rather than mafic source. If one were to trace back the source to the original basement, CIA diagrams show that the original source should be of granodiorite composition.

Sediment input to the Ben Nevis Formation was from the south, eroded off the Central Ridge. Based on thickness trends, subsidence was greatest in the northern section of the south pool and the thicker accumulations of sediment are inferred to be the product of fault-induced higher rates of mechanical erosion relative to chemical weathering effects.

The Ben Nevis Formation is relatively homogeneous both petrographically and geochemically, but subtle changes can be demonstrated from north to south in the White Rose Field. Overall, wells in the south have higher P/K ratios than those in the north consistent with a mature sediment source during early transgression in the north (higher P/K), becoming slightly less mature (lower P/K) as transgression progresses to the south. This is consistent with slightly higher CIA values obtained for wells in the north, in turn a reflection of more rapid subsidence in the northern section of the south pool,

accompanied by steeper paleoslopes and diminished rates of chemical weathering. Thick deposits of sediment are not likely to be found in the northern area of the White Rose Field; however, it may be possible that sediments were deposited to the north of the White Rose salt diapir from a potentially new sediment output along the Central Ridge. However, regional trends indicate that more distal environments are found to the north and one could expect to find deeper marine environments including turbidite deposits.

## References

- Arthur, L.R., Cole, D.R., Henderson, G.G.L., and Kushnir, D.W., 1982. Geology of the Hibernia Discovery; *in*: Halbouty, M.T. (ed.) The deliberate search for the subtle trap. American Association of Petroleum Geologists, Memoir 32, p. 181-195.
- Bernoulli, D., 1984. Sedimentary evolution of passive margins of Mesozoic Tethys: American Association of Petroleum Geologists Bulletin, v. 68, p. 793.
- Blatt, H., 1967. Provenance determination and the recycling of sediments. Journal of Sedimentary Petrology, v. 37, p.1031-1044.
- Boudreau, R.R., Meehan, P.J., Wishart, H.A. and Harding, S.C., 1986. Mesozoic stratigraphy of the Jeanne d'Arc Basin. *In*.: Canada's Hydrocarbon Reserves for the 21st Century, August, Canadian Society of Petroleum Geologists. Convention program and abstracts, p. 28
- Brown, D.M., McAlpine, K.D., and Yole, R.W., 1989. Sedimentology and sandstone diagenesis of Hibernia Formation in the Hibernia Oil Field, Grand Banks of Newfoundland. American Association of Petroleum Geology Bulletin, v. 73, no. 5, p. 557-575.
- Core Laboratories, 1982. Reservoir Quality Study for Mobil Oil Canada Limited. Mobil et al. Hebron I-13. Hebron, East Coast Offshore, Core number 2 "Avalon Sand Zone".
- Crook, K.A.W., 1974. Lithogenesis and geotectonics: the significance of compositional variations in flysch arenites (greywackes), *in*: Modern and ancient geosynclinal sedimentation. SEPM Special Publication 19, p. 304-310.
- Davies, D.K. and Etheridge, F.G., 1975. Sandstone composition and depositional environments. American Association of Petroleum Geologists Bulletin v. 59, p. 239-264.
- Department of Mines and Energy. 2000. Sedimentary basins and hydrocarbon potential of Newfoundland and Labrador. Report 2000-01. 61 p.
- Deptuck, M.E., MacRae, R.A., Shimeld, J.W. Williams, G.L. and R.A. Fensome, 2003. Revised Upper Cretaceous and Lower Palaeogene lithostratigraphy and depositional history of the Jeanne d'Arc Basin, offshore Newfoundland, Canada. American Association of Petroleum Geologists Bulletin v. 87, p. 1459-1483.

- Dickinson, W.R., 1970. Interpreting detrital modes of greywacke and arkose. *Journal of Sedimentary Petrology*. v. 40, (2), p. 695-707.
- Dickinson, W.R., 1985. Interpreting provenance relations from detrital modes of sandstone. *In: Zuffa, G.G. (ed), Provenance of arenites: Proceedings of the NATO advanced study institute on reading provenance from arenites. Cozenza, Italy, p. 333-362.*
- Dickinson, W.R. and Suczek, C.A., 1979. Plate tectonics and sandstone composition. *American Association of Petroleum Geologists Bulletin*, v. 63, p.2164-2182.
- Dickinson, W.R., and Valloni, R. 1980. Plate settings and provenance of sands in modern ocean basins. *Geology*, v. 8, (2), p. 82-86.
- Dickinson, W.R., Beard, L.S., Brakenridge, G.R., Erjavec, J.L., Ferguson, R.C., Inman, K.F., Knepp, R.A., Lindberg, F.A., Ryberg, P.T. 1983. Provenance of North American Phanerozoic sandstones in relation to tectonic setting. *Geological Society of America Bulletin*. v. 94, p. 222-235.
- Driscoll, N. W., and Hogg, J. R., 1995. Stratigraphic response to basin formation; Jeanne d'Arc Basin, offshore Newfoundland, *in: J. J. Lambiase (ed), Hydrocarbon Habitat in Rift Basins: Geological Society of London Special Publication 80, p. 145-163.*
- Driscoll, N.W., Hogg, J.R., Christie-Blick, N., and Karner, G.D., 1995. Extensional tectonics in the Jeanne d'Arc Basin, Offshore Newfoundland: Implications for the timing of break-up between Grand Banks and Iberia. *in: Scrutton, R.A., Stoker, M.S., Shimmield, G.B., and Tudhope, A.W. (eds), The Tectonics, Sedimentation and Palaeoceanography of the North Atlantic Region. Geological Society Special Publication 90, p. 1-28.*
- Enachescu, M.E., 1986. Integrated geophysical study of Newfoundland continental margin (East coast Canada); *Society of Exploration Geophysicists, 56<sup>th</sup> Annual International Meeting and Exposition, Expanded Abstracts, November 1986, p.488-492.*
- Enachescu, M.E., 1987. Tectonic and structural framework of the Northeast Newfoundland continental margin, *In: Beaumont, C. and Tankard, A.J. (Eds.), Sedimentary Basins and Basin-Forming Mechanisms, Canadian Society of Petroleum Geologists, Memoir 12, p. 117-146.*
- Enachescu, M.E., 1988. Extended basement beneath the intracratonic rifted basins of the Grand Banks of Newfoundland. *Canadian Journal of Exploration Geophysicists*, v. 24, p. 48-65.

- Enachescu, M.E., 1992. Enigmatic basins offshore Newfoundland. *Canadian Journal of Exploration Geophysics*. v. 28(1) p.44-61.
- Enachescu, M.E. and Dunning, G., 1994. Grand Banks Basin, Canada, Basin Monitor. Book, 85 p., 16 figures, published by PetroConsultants, Geneva, Switzerland.
- Enachescu, M.E., 2006. Newfoundland and Labrador Call for Bids NL06-01, Government of Newfoundland and Labrador, Department of Natural Resources, 55p.
- Enachescu, M.E., Smee, G.W., Meehan, P.J., Hodder, J., Deutsch, K., Emery, D. 2000. White Rose oil field, offshore Newfoundland; from teaser to trophy , *In: American Association of Petroleum Geologists 2000 annual meeting. Annual Meeting Expanded Abstracts - American Association of Petroleum Geologists 2000.* p. 138
- Enachescu, M. and P. Fagan, 2004. Newfoundland and Labrador Call for Bids NF04-01, Government of Newfoundland and Labrador, Department of Natural Resources, 35p.
- Enachescu, M., Fagan, P., and Smee, G., 2005. Exploration opportunities abound in Orphan basin off Newfoundland. *Oil and Gas Journal*, v. 103. no. 30.
- Enachescu M. and P. Fagan, 2005. Newfoundland's Grand Banks presents untested oil and gas potential in eastern North America. *Oil and Gas Journal*, vol. 103, 6, p. 32-39.
- Enachescu, M.E. and J.R. Hogg, 2005. Exploring for Atlantic Canada's next giant petroleum discovery. *CSEG Recorder*, v. 30, no. 5. p.19-30.
- Fedo, C.M., Nesbitt, H.W., Young, G.M., 1995. Unravelling the effects of potassium metasomatism in sedimentary rocks and paleosols, with implications for paleoweathering conditions and provenance. *Geology*, v. 23, p. 921-924.
- Feng, R., and Kerrich, R., 1990. Geochemistry of fine grained clastic sediments in the Archean Abitibi Greenstone belt, Canada; Implications for provenance and tectonic setting. *Geochimica et Cosmochimica Acta*, v. 54, p. 1061-1081.
- Ferry, M. 2005. An Evaluation of the Sedimentology and the Primary Depositional Controls on Permeability for the White Rose A-17 Cored Interval, White Rose Oilfield, Offshore Eastern Newfoundland. MSc. Thesis. Memorial University of Newfoundland
- Folk, R.L. 1974. *Petrology of sedimentary rocks*: Austin, Texas, Hemphill, 184 p.
- Fralick, P.W., and Kronberg, B.I., 1997. Geochemical discrimination of clastic sedimentary rock sources. *Sedimentary Geology*, v. 113, p. 111-124.

- Gazzi, P., 1966. Le arenarie del flysch sopracretaceo dell' appennino modenese; correlazioni con il flysch di monghidoro. *Minerlogica e Petrografica Acta*, v. 12, p. 69-97.
- Graham, S.A., Ingersoll, R.V., and Dickinson, W.R., 1976. Common provenance for lithic grains in carboniferous sandstones from Ouachita mountains and Black Warrior basin. *Journal of Sedimentary Petrology*, v. 46, p. 620-632.
- Grant, A.C., and K.D., McAlpine, 1990. The continental margin around Newfoundland. *in: Keen, M.J. and Williams, G.L. (Eds.). Geology of the Continental Margin of Eastern Canada. Geological Survey of Canada, Geology of Canada 2*, p. 239-292.
- Hiscott, R.N., Wilson, R.C.L., Gradstein, F.M., Pujalte, V., Garcia-Mondejar, J., Boudreau, R.R., and Wishart, H.A., 1990. Comparative stratigraphy and subsidence history of Mesozoic rift basins of North Atlantic. *American Association of Petroleum Geologist Bulletin*, v.74, p. 60-76.
- Howarth, R.J., 1998. Improved estimators of uncertainty in proportions, point-counting and pass-fail test results. *American Journal of Science*, v. 298, p. 594-607.
- Howie, R.D., and Barss, M.S. 1975. Upper Palaeozoic rocks of the Atlantic provinces, Gulf of St. Lawrence, and adjacent continental shelves, *in: van der Linden, W.J.M and Wade, J.A., (eds), Offshore geology of Eastern Canada, 2. Regional Geology: Geological Survey of Canada. Paper 74-30, 2*, p. 35-50.
- Hubbard, R.J., 1988. Age and significance of sequence boundaries on Jurassic and Early Cretaceous rifted continental margins. *American Association of Petroleum Geologists Bulletin*, v. 72, p.49-72.
- Hubbard, R.J., Pape, J., and Roberts, D.G., 1985. Depositional sequence mapping to illustrate the evolution of a passive continental margin, *in: Berg, O.R., and Woolverton, D.C., (eds). Seismic Stratigraphy 2. American Association of Petroleum Geologists, Memoir 39*, p. 93-115.
- Hurst, A.R., and Morton, A.C., 2001. Generic relationships in the mineral-chemical stratigraphy of turbidite sandstones. *Journal of the Geological Society*, v. 158, p. 401-404.
- Husky Energy, 2001.  
[www.huskyenergy.ca/operations/canadaseastcoast/archives/application.asp#Volume2.01-03-04](http://www.huskyenergy.ca/operations/canadaseastcoast/archives/application.asp#Volume2.01-03-04).
- Ingersoll, R.V., 1978. Petrofacies and petrologic evolution of the Late Cretaceous fore-arc basin, northern and central California. *Journal of Geology*, v. 86, p. 335-352.

- Ingersoll, R.V., and Suczek, C.A., 1979. Petrology and provenance of Neogene sand from the Nicobar and Bengal Fans, DSDP sites 211 and 218. *Journal of Sedimentary Petrology*, v. 49, p. 1217-1228.
- Ingersoll, R.V., Bullard, T.F., Ford, R.L., Grim, J.B., Pickle, J.D., and Sares, S.W., 1984. The effect of grain size on detrital modes: A test of the Gazzi Dickinson point-counting method. *Journal of Sedimentary Petrology*, v. 54, pp. 103-116.
- Jansa, L.F., and Wade, J.A., 1975. Geology of the continental margin off Nova Scotia and Newfoundland; *in*: van der Linden, W.J.M., and Wade, J.A. (eds.), *Offshore Geology of Eastern Canada*, Geological Survey of Canada. Paper 74-30, p 51-106.
- Jenkyns, H. C., 1980. Tethys; past and present: Proceedings of the Geologists Association, v.91, Parts 1-2, p. 107-118.
- Keen, C. E., Boutilier R., de Voogd, B., Mudford, B., and Enachescu, M.E., 1987. Crustal geometry and extensional models for the Grand Banks of eastern Canada: constraints from deep seismic reflection data, *in* Beaumont, C. and Tankard, A. J. (eds.), *Sedimentary Basins and Basin-Forming Mechanisms: Canadian Society of Petroleum Geologists Memoir 12*, p. 101-115.
- Kerr and Associates. 1985. Geology and petroleum potential of the western and eastern Grand Banks (2 parts); A Special Report to Industry. Available at the CNLOPB Library.
- King, L.H., Fader, G.B., Poole, W.H., and Wanless, R.K., 1985. Geological setting and age of the Flemish Cap granodiorite, east of the Grand Banks of Newfoundland. *Canadian Journal of Earth Sciences*, v. 22, p.1286-1298.
- King, L.H., Fader, G.B., Jenkins, W.A.M., and King, E.L., 1986. Occurrence and regional geological setting of Paleozoic rocks on the Grand Banks of Newfoundland. *Canadian Journal of Earth Sciences*, v. 23, p.504-526.
- Krynine. P.D., 1946. Microscopic morphology of quartz types. Pan American Congress of Mining and Geological Engineers, *Annals 2<sup>nd</sup> Comm.*, p. 36-49.
- Krynine, P.D. 1937. Petrography and genesis of the Siwalik series. *American Journal of Science*, v. 34, p. 422-446.
- Lemoine, M., 1983. Rifting and early drifting; Mesozoic central Atlantic and Ligurian Tethys. *in*: Initial reports of the Deep Sea Drilling Project covering Leg 76 of the cruises of the drilling vessel Glomar Challenger, Norfolk, Virginia to Fort Lauderdale, Florida, October-December, 1980). *Initial Reports of the Deep Sea Drilling Project (November 1983)*, v. 76, p. 885-895.

- Longerich, H.P., 1995. Analysis of pressed pellets of geological samples using wavelength-dispersive X-Ray Fluorescence spectrometry. *X-Ray Spectrometry*, v. 24, p. 123-136.
- Mackie, W., 1896. The sands and sandstones of eastern Moray. *Edinburgh Geological Society Trans*, v. 7, p. 148-172.
- Mackie, W., 1899. The feldspars present in sedimentary rocks as indications of the conditions of contemporaneous climate. *Edinburgh Geological Society Proc.*, v. 7, p. 443-468.
- Marsaglia, K.M., and Ingersol, R.V. 1992. Compositional trends in arc-related, deep-marine sand and sandstone; a reassessment of magmatic-arc provenance; with Suppl. Data 92-36. *Geological Society of America Bulletin*, v. 104, no. 12, p.1637-1649.
- McAlpine, K. D., 1990. Mesozoic stratigraphy, sedimentary evolution and petroleum potential of the Jeanne d'Arc basin, Grand Banks of Newfoundland: *Geological Survey of Canada, Paper 89-17*, 50 p.
- McLennan, S.M., Bock, B. Hemming, S.R., Hurowitz, J.A., Lev, S.M., McDaniel, D.K., 2003. The role of provenance and sedimentary processes in the geochemistry of sedimentary rocks, *in: Lentz, D.R., ed., Geochemistry of Sediments and Sedimentary Rocks: Evolutionary Considerations to Mineral Deposit-Forming Environments: Geological Association of Canada, GeoText 4*, p. 7-38.
- Nesbitt, H.W., 1997. Bacterial and inorganic weathering processes and weathering of crystalline rocks. *In: Biological-mineralogical interactions. Short Course Handbook*, v. 25, p. 113-142.
- Nesbitt, H.W., 2003. Petrogenesis of siliciclastic sediments and sedimentary rocks. *in: Lentz, D.R., (ed), Geochemistry of Sediments and Sedimentary Rocks: Evolutionary Considerations to Mineral Deposit-Forming Environments. Geological Association of Canada, GeoText 4*, p. 39-51.
- Nesbitt, H.W., and Young, G.M. 1984. Prediction of some weathering trends of plutonic and volcanic rocks based on thermodynamics and kinetic considerations: *Geochimica et Cosmochimica Acta*. v, 97, p.129-147.
- Nesbitt, H.W., Young, G.M., McLennan, S.M., and Keayes, R.R., 1996. Effects of chemical weathering and sorting on the petrogenesis of siliciclastic sediments with implications for provenance studies. *Journal of Geology*, v. 104, p. 525-542.
- Nockolds, S.R., 1954. Average chemical compositions of some igneous rocks. *Bulletin of the Geological Society of America*, v. 65, p. 1007-1032.

- Normore, L., in preparation. Distribution of cements and impact on quality of the Ben Nevis/Avalon reservoir in the White Rose Field, offshore Newfoundland, Canada. M.Sc. Thesis. Memorial University of Newfoundland.
- North, C.P., Hole, M.J., and Jones, D.G., 2005. Geochemical correlations in deltaic successions: A reality check. *Geological Society of America Bulletin*, v. 117, p. 620-632.
- O'Brien, S.J., Wardle, R.J., and King, A.F., 1983. The Avalon Zone: A Pan-African terrane in the Appalachian orogen of Canada. *Geological Journal*, v. 18, p.195-222.
- Pemberton, S. G., Spila, M. V., Pulham, A. J., Saunders, T., Maceachern, J. A., Robbins, D., and Sinclair, I., 2001. Ichnology and sedimentology of shallow and marginal marine systems: Ben Nevis and Avalon reservoirs, Jeanne D'Arc Basin. *Geological Association of Canada Short Course Notes 15*, 353 p.
- Pettijohn, F.J., 1975. *Sedimentary Rocks*. Harper and Row. New York, 628p.
- Riley, N.R., and Ainsworth, L.A., 2003a. White Rose Well A-17 Offshore Eastern Canada Biostratigraphic Report.
- Riley, N.R., and Ainsworth, L.A., 2003b. White Rose Well H-20 Offshore Eastern Canada Biostratigraphic Report.
- Riley, N.R., and Ainsworth, L.A., 2003c. White Rose Well E-09 Offshore Eastern Canada Biostratigraphic Report.
- Saigal, G.C., Morad, S., Bjorlykke, K., Egeberg, P.K., and Aagard, P. 1988. Diagenetic albitization of detrital k-feldspar in Jurassic, Lower Cretaceous, and Tertiary clastic reservoir rocks from offshore Norway; I, textures and origin. *Journal of Sedimentary Research*, v. 58, p. 1003-1013.
- Sawyer, E.W., 1986. The influence of source rock type, chemical weathering and sorting on the geochemistry of clastic sediments from the Quetico metasedimentary belt, Superior Province, Canada. *Chemical Geology*, v. 55, p. 77-95.
- Schwab, F.L., 1975. Framework mineralogy and chemical composition of continental margin-type sandstone. *Geology*, v. 3, p. 487-490.
- Sorby, H.C., 1880. On the structure and origin of non-calcareous stratified rocks. *Geological Society of London Proc*, v. 36, p. 46-92.
- Schenk, P.E., 1978, Synthesis of the Canadian Appalachians. Caledonian Appalachian Orogen of the North Atlantic region. *Geological Survey of Canada. Paper 78-13*, p. 111-136.

- Sinclair, I.K., 1988. Evolution of Mesozoic-Cenozoic sedimentary basins in the Grand Banks area of Newfoundland and comparison with Flavy's (1974) rift model. *Bulletin of Canadian Petroleum Geology*, v. 34, no. 3, p 379-383.
- Sinclair, I. K., 1993, Tectonism: the dominant factor in mid-Cretaceous deposition in the Jeanne d'Arc Basin, Grand Banks. *Marine and Petroleum Geology*, v. 10, p. 530-549.
- Sinclair, I.K., 1994. Tectonism and sedimentation in the Jeanne d'Arc Basin, Grand Banks Newfoundland, Ph.D. Thesis, University of Aberdeen.
- Sinclair, I.K., Evans, J.E., Albrethsons, T.A., and Sydora, L.J. 1999. The Hibernia Oil Field – Effects of episodic tectonism on structural character and reservoir compartmentalization. In: Fleet, A.J., and Boldg, S.A.R. (eds.) *Petroleum Geology of Northwest Europe: Proceedings of the 5<sup>th</sup> conference*, p. 517-528.
- Srivastava, S.P., 1978. Evolution of the Labrador Sea and its bearing on the early evolution of the North Atlantic. *Geophysical Journal of the Royal Astronomical Society*, v. 52, p. 313-357.
- Tankard, A. J., and H. J. Welsink, 1987. Extensional tectonics and stratigraphy of the Hibernia oil field, Grand Banks, Newfoundland. *American Association of Petroleum Geologists Bulletin*, v. 71, p. 1210-1232.
- Tankard, A.J., and Welsink, H.J., 1988. Extensional tectonics, structural styles and stratigraphy of the Mesozoic Grand Banks of Newfoundland. *in: Manspeizer, W. (ed.), Triassic-Jurassic Rifting: Continental Break-up and the Origin of the Atlantic Ocean and Passive Margins, Part A. Development in Geotectonics*, v. 22, p.129-165.
- Tankard, A.J., Welsink, H.J., and Jenkins, W.A.M. 1989. Structural styles and stratigraphy of the Jeanne d'Arc Basin, Grand Banks of Newfoundland. *in: Tankard, A.J., and Balkwill, H.R. (eds.), Extensional Tectonics and Stratigraphy of the North Atlantic Margins. American Association of Petroleum Geologists Memoir 46*, p. 265-282.
- Tankard, A.J. and H.J. Welsink, 1989. Mesozoic extension and styles of basin formation in Atlantic Canada, *in: Tankard, A.J., and Balkwill, H.R. (eds.), Extensional Tectonics and Stratigraphy of the North Atlantic Margins. American Association of Petroleum Geologists Memoir 46*, p. 175-195.
- Taylor, S.R., and McLennan, S.M., 1985. *The continental crust: Its composition and evolution*. Blackwell, Oxford, 312 p.

- Ten Hove, H.A., and van den Hurk, P. 1993. A review of recent and fossil serpulid “reefs”; actuopaleontology and the “Upper Malm” serpulid limestones in north-west Germany. *Geologie en Mijnbouw*. v. 74, p. 23-67.
- Tucholke, B.E., Austin, J.A. Jr., and Uchupi, E. 1989. Crustal Structure and Rift-Drift Evolution of the Newfoundland Basin. In: Tankard, A.J., and Balkwill, H.R. (eds.), *Extensional Tectonics and Stratigraphy of the North Atlantic Margins*. American Association of Petroleum Geologist Memoir 46, p. 247-264.
- Van de Kampe, P.C., and Leake, B.E., 1985. Petrography and geochemistry of feldspathic and mafic sediments of the northeastern Pacific margin. *Transactions of the Royal Society of Edinburgh: Earth Sciences*, v. 76 (4), p.411-449.
- Wade, J.A., 1978. The Mesozoic-Cenozoic history of the northwestern margin of North America. *Offshore Technological Conference Proceedings*, v. 3, p. 1849-1859.
- Wedepohl, K.H., 1978. *Handbook of Geochemistry*. Springer-Verlag Berlin-New York, Volumes II/2 to II/4
- Williams, H., and Hatcher, R.D., 1982. Suspect terranes and accretionary history of the Appalachian orogen. *Geology*, v. 10, p.530-536.
- Williams, H., and Hatcher, R.D., 1983. Appalachian suspect terranes. *in*: Hatcher, R.D. Jr., Williams, H.J., and Zietz, I., (eds.), *Contributions to the tectonics and geophysics of mountain chains*. Geological Society of America, Memoir 159, p33-53.
- Williamson, M.A., 1992. The subsidence, compaction, thermal and maturation history of the Egret Member source rock, Jeanne d'Arc Basin, offshore Newfoundland. *Bulletin of Canadian Petroleum Geology*, v. 40, p. 136 – 150.
- Wilson, M.D., and Webb, J.C. 1998. Reservoir Quality of Jurassic and Cretaceous Sandstones in Ten Wells Grand Banks Area, Offshore Canada.
- Zuffa, G. G., 1979. Provenance of arenites: Proceedings of the NATO advanced study institute on reading provenance from arenites, Cozenza, Italy.

**Appendix 1**  
**Point Count Data**

	A-17	A-17	A-17	A-17	A-17	A-17	A-17	A-17	A-17	A-17	A-17
depth	2942.22	2962.11	2974.91	2982.56	2993.89	3002.13	3013.34	3023.07	3033.33	3045.54	
<b>POINT-COUNTED PARAMETERS</b>											
Detrital	Qm	195	182	201	183	202	202	186	192	178	178
	Qp	8	3	14	13	11	22	16	24	20	28
	k feld	0	2	3	5	2	4	1	5	2	1
	plag	3	9	5	10	5	12	8	9	5	6
	chert	7	15	7	5	11	3	6	7	11	5
	carbonate (det)	4	4	8	6	3	1	3	4	4	4
Authigenic	chlorite	1		5	0	0	2	6	6	2	
	opaque	5	0	3	1	3	2	1	1	1	2
	mica	5	1	3	0	1	1		1	1	
	bioclastic carb					1					8
	Glauc	1									
Cement	Siderite	1					2	1			
	Qtz overgrowth	27	37	16	35	22	13	23	24	31	22
	carb cement	1		6	1	2	1	2			2
	Clay	4	8	5	2						
	Clay rim		5	1	5	5	2	3	5	4	3
	ca rhomb										2
	misc	1	1	2			1				
	porosity	38	33	21	34	32	32	44	22	42	39
<b>Total</b>	<b>301</b>	<b>300</b>	<b>276</b>	<b>300</b>	<b>300</b>	<b>300</b>	<b>300</b>	<b>300</b>	<b>300</b>	<b>301</b>	<b>300</b>

**Calculated Parameters**

(following Pettijohn, 1975)	Q (Qm+Qp)	203	185	215	196	213	224	202	216	198	206
	F	3	11	8	15	7	16	9	14	7	8
	L	11	19	15	11	14	4	9	11	15	9
		217	215	238	222	234	244	220	241	220	223
	Q%	93.55	86.05	90.34	88.29	91.03	91.80	91.82	89.63	90.00	92.38
	F%	1.38	5.12	3.36	6.76	2.99	6.56	4.09	5.81	3.18	3.59
	L%	5.07	8.84	6.30	4.95	5.98	1.64	4.09	4.56	6.82	4.04
(following Nesbitt et al., 1996)	Q (Qm+Qp)	203	185	215	196	213	224	202	216	198	206
	P	3	9	5	10	5	12	8	9	5	6
	K	0	2	3	5	2	4	1	5	2	1
		206	196	223	211	220	240	211	230	205	213
	Q%	98.54	94.39	96.41	92.89	96.82	93.33	95.73	93.91	96.59	96.71
	K%	0.00	1.02	1.35	2.37	0.91	1.67	0.47	2.17	0.98	0.47
	P%	1.46	4.59	2.24	4.74	2.27	5.00	3.79	3.91	2.44	2.82
(following Marsaglia and Ingersoll, 1992)	Q (Qm+Qp+Ch)	210	185	215	196	213	224	202	216	198	206
	F	3	11	8	15	7	16	9	14	7	7
	L	4	4	8	6	3	1	3	4	4	4
		217	200	231	217	223	241	214	234	209	217
	Q%	96.77	92.50	93.07	90.32	95.52	92.95	94.39	92.31	94.74	94.93
	F%	1.38	5.50	3.46	6.91	3.14	6.64	4.21	5.98	3.35	3.23
	L%	1.84	2.00	3.46	2.76	1.35	0.41	1.40	1.71	1.91	1.84

\*\*Ch=chert

	L-08 depth	L-08 3000.2	L-08 2894.1	L-08 2861.1	L-08 2915.9	L-08 2963	L-08 2972.4	L-08 2871.3	L-08 2884.1	L-08 2893.5	L-08 2927.3
<b>Point Counted Parameters</b>											
Detrital	Qm	200	204	205	193	205	180	218	213	216	199
	Qp	16	16	23	25	16	20	19	14	21	17
	k feld	2	1	0	0	1	1	0	1	2	2
	plag	5	1	5	3	3	7	3	4	5	1
	chert	7	10	9	13	11	5	9	5	8	7
	carbonate	13	8	9	6	4	14	1	9	2	14
Authigenic	chlorite (det)	3	3	1	2	3	2	1	3		2
	opaque	4	7	2	4	2	2	1	2	1	3
	mica	2	5	2	1	7	11	4	4	2	4
	bioclastic carb		1	1			3			1	
Cements	Sidinite				2						
	Qtz overgrowth	10	9	9	13	10	14	12	12	14	8
	carb cement					1	1				
	clay (unknown)			1							
	Clay rim	3	1		2	2	2	3		1	6
	misc								1		
	porosity	36	34	32	38	34	42	29	32	27	37
<b>Total</b>	<b>301</b>	<b>300</b>	<b>299</b>	<b>302</b>	<b>299</b>	<b>304</b>	<b>300</b>	<b>300</b>	<b>300</b>	<b>300</b>	<b>300</b>

<b>Calculated Parameters</b>											
(Following Petijohn, 1975)	Q (Qm+Qp)	216	220	228	218	221	200	237	227	237	216
	F	7	2	5	3	4	8	3	3	7	3
	L	20	18	18	19	15	19	10	14	10	21
	Total	243	240	251	240	240	227	250	244	254	240
	Q%	88.9	91.7	90.8	90.8	92.1	88.1	94.8	93.0	93.3	90.0
	F%	2.9	0.8	2.0	1.3	1.7	3.5	1.2	1.2	2.8	1.3
	L%	8.2	7.5	7.2	7.9	6.3	8.4	4.0	5.7	3.9	8.8
(Following Nesbitt et al., 1996)	Q	200	204	205	193	205	180	218	213	216	199
	P	5	1	5	3	3	7	3	4	5	1
	K	2	1	0	0	1	1	0	1	2	2
	Total	207	206	210	196	209	188	221	218	223	202
	Q%	96.62	99.03	97.62	98.47	98.09	95.74	98.64	97.71	96.86	98.51
	P%	2.42	0.49	2.38	1.53	1.44	3.72	1.36	1.83	2.24	0.50
	K%	0.97	0.49	0.00	0.00	0.48	0.53	0.00	0.46	0.90	0.99
(following Marsaglia and Ingersoll, 1992)	Q (Qm+Qp+Ch)	230	240	246	244	243	210	255	237	253	230
	F	7	2	5	3	4	8	3	3	7	3
	L (carb))	13	8	9	6	4	14	1	9	2	14
	Total	250	250	260	253	251	232	259	249	262	247
	Q%(Qm+Qp+C h)	92.00	96.00	94.62	96.44	96.81	90.52	98.46	95.18	96.56	93.12
	F%	2.80	0.80	1.92	1.19	1.59	3.45	1.16	1.20	2.67	1.21
L%(carb)	5.20	3.20	3.46	2.37	1.59	6.03	0.39	3.61	0.76	5.67	

\*\*\*Ch=chert

	L-08	L-08	L-08	L-08	L-08	L-08	L-08	L-08	L-08	L-08	L-08	L-08
	depth	2938.1	2945.4	2953.6	2981.9	2991.5	3010.1	3060.3	3032	3050.2	2905.3	3021.1
<b>Point Counted Parameters</b>												
Detrital	Qm	201	208	215	206	214	215	209	229	223	227	216
	Qp	13	18	25	15	14	10	15	16	11	14	9
	k feld	1	1	1	1	3	1	3	0	0	1	2
	plag	1	6	0	6	10	8	1	3	2	4	4
	chert	13	8	7	7	10	3	5	6	3	2	4
	carbonate (det)	17	10	5	12	7	11	9	6	11	5	16
Authigenic	chlorite	2			1							
	opaque	2	2		4	5	7	2		2	3	3
	mica	5	6	2	6	4	3	6	2	2		2
	bioclastic carb						1			4		1
Cement	Siderite											
	Qtz overgrowth	3	5	4	4	2	3	3	2	3	2	1
	carb cement							1				
	clay (unknown)		2								1	11
	Clay rim	2	1	1	1		3	2	2	2	3	1
	calcite rhomb									5	1	6
	misc											
porosity	40	43	40	37	30	35	44	35	33	38	24	
Total	300	310	300	300	299	300	300	301	301	301	301	300

<b>Calculated Parameters</b>												
(Following Petijohn, 1975)	Q (Qm+Qp)	214	226	240	221	228	225	224	245	234	241	225
	F	2	7	1	7	13	9	4	3	2	5	6
	L	30	18	12	19	17	14	14	12	14	7	20
	Total	246	251	253	247	258	248	242	260	250	253	251
	Q%	87.0	90.0	94.9	89.5	88.4	90.7	92.6	94.2	93.6	95.3	89.6
F%	0.8	2.8	0.4	2.8	5.0	3.6	1.7	1.2	0.8	2.0	2.4	
L%	12.2	7.2	4.7	7.7	6.6	5.6	5.8	4.6	5.6	2.8	8.0	
(Following Nesbitt et al., 1996)	Q	201	208	215	206	214	215	209	229	223	227	216
	P	1	6	0	6	10	8	1	3	2	4	4
	K	1	1	1	1	3	1	3	0	0	1	2
	Total	203	215	216	213	227	224	213	232	225	232	222
	Q%	99.01	96.74	99.54	96.71	94.27	95.98	98.12	98.71	99.11	97.84	97.30
P%	0.49	2.79	0.00	2.82	4.41	3.57	0.47	1.29	0.89	1.72	1.80	
K%	0.49	0.47	0.46	0.47	1.32	0.45	1.41	0.00	0.00	0.43	0.90	
(following Marsaglia and Ingersoll, 1992)	Q (Qm+Qp+Ch)	240	234	247	228	238	228	229	251	237	243	229
	F	2	7	1	7	13	9	4	3	2	5	6
	L (carb)	17	10	5	12	7	11	9	6	11	5	16
	Total	259	251	253	247	258	248	242	260	250	253	251
	Q%(Qm+Qp+Ch)	92.66	93.23	97.63	92.31	92.25	91.94	94.63	96.54	94.80	96.05	91.24
F%	0.77	2.79	0.40	2.83	5.04	3.63	1.65	1.15	0.80	1.98	2.39	
L%(carb)	6.56	3.98	1.98	4.86	2.71	4.44	3.72	2.31	4.40	1.98	6.37	

\*\*\*Ch=chert

	F-04	F-04	F-04	F-04	F-04	F-04	F-04	F-04	F-04	F-04	F-04
depth	2867.7	2857.4	2846.4	2836.7	2827.3	2818.3	2809	2797.1	2787.8	2776.9	
<b>Point Counted Parameters</b>											
Detrital	Qm	199	195	196	201	199	202	192	190	203	189
	Qp	9	11	8	10	10	15	15	8	9	10
	k feld	6	2	1	6	2	4	6	3	3	6
	plag	11	12	14	10	9	14	6	10	7	4
	chert	5	2	4	6	5	6	5	3	5	6
	carbonate (det)	4	2	1	1	7	5	5	17	1	8
Authigenic	chlorite		1	1	1				1		1
	opaque	8	11	6	6	5	1	4	7	3	7
	mica		4	3		1	3	1	1		
	bioclastic carb						1				1
Cement	Qtz overgrowth	3	2	2	3	1	0	2	1	3	0
	carb cement	1	2		1				5		11
	clay (unknown)		3	2		1		2	3	1	2
	Clay rim	5	2	2	2	1				2	1
	calcite rhomb		1								
	misc								1		
porosity	49	50	61	53	59	55	63	58	63	54	
Total	300	300	301	300	300	306	301	308	300	300	

<b>Calculated Parameters</b>											
(Following Petijohn, 1975)	Q (Qm+Qp)	208	206	204	211	209	217	207	198	212	199
	F	17	14	15	16	11	18	12	13	10	10
	L	9	4	5	7	12	11	10	20	6	14
	Total	234	224	224	234	232	246	229	231	228	223
	Q%	88.89	91.96	91.07	90.17	90.09	88.21	90.39	85.71	92.98	89.24
	F%	7.26	6.25	6.70	6.84	4.74	7.32	5.24	5.63	4.39	4.48
L%	3.85	1.79	2.23	2.99	5.17	4.47	4.37	8.66	2.63	6.28	
(Following Nesbitt et al., 1996)	Q	208	206	204	211	209	217	207	198	212	199
	P	11	12	14	10	9	14	6	10	7	4
	K	6	2	1	6	2	4	6	3	3	6
	Total	225	220	219	227	220	235	219	211	222	209
	Q%	92.44	93.64	93.15	92.95	95.00	92.34	94.52	93.84	95.50	95.22
	P%	4.89	5.45	6.39	4.41	4.09	5.96	2.74	4.74	3.15	1.91
K%	2.67	0.91	0.46	2.64	0.91	1.70	2.74	1.42	1.35	2.87	
(following Marsaglia and Ingersoll, 1992)	Q (Qm+Qp+Ch)	213	208	208	217	214	223	212	201	217	205
	F	17	14	15	16	11	18	12	13	10	10
	L (carb+RF)	4	2	1	1	7	5	5	17	1	8
	Total	234	224	224	234	232	246	229	231	228	223
	Q (Qm+Qp+Ch)%	91.03	92.86	92.86	92.74	92.24	90.65	92.58	87.01	95.18	91.93
	F%	7.26	6.25	6.70	6.84	4.74	7.32	5.24	5.63	4.39	4.48
L (carb+RF)%	1.71	0.89	0.45	0.43	3.02	2.03	2.18	7.36	0.44	3.59	

\*\*\*Ch=chert

\*\*\*RF=Rock Fragments

	depth	G-57 3995.2	G-57 3985.3	G-57 4029.3	G-57 4594.25	G-57 4598	G-57 4035	C-73 4123.8	C-73 4129.6
<b>Point Counted Parameters</b>									
Detrital	Qm	174	173	164	190	167	200	167	175
	Qp	10	42	63	42	24	35	22	30
	k feld								
	plag	6	7	1					1
	chert	2	1	7	2	1	3	4	7
	Rock frag			7	7	17	5	21	3
	carbonate det	12	14		6	2			3
Authigenic	opaque	14	11	1			5		1
	mica		2						
	bioclastic carb			3	7	19	1	1	
Cement	Pyrite						2		1
	Qtz overgrowth		1	2	6	4	3		1
	carb cement	71	8	19	24	45	22	88	58
	Ca replacement						2		
	clay (unknown)	1	2		2	5	9	1	4
	Clay rim						3		18
	Chert Precip	3	8	11	4	2			
	porosity	31	33	24	30	18	13		
	Total	324	302	302	320	304	303	304	302

<b>Calculated Parameters</b>									
(Following Petijohn, 1975)	Q (Qm+Qp)	184	215	227	232	191	235	189	205
	F	6	7	1	0	0	0	0	1
	L	14	15	14	15	20	8	25	13
	Total	204	237	242	247	211	243	214	219
	Q%	90.20	90.72	93.80	93.93	90.52	96.71	88.32	93.61
	F%	2.94	2.95	0.41	0.00	0.00	0.00	0.00	0.46
	L%	6.86	6.33	5.79	6.07	9.48	3.29	11.68	5.94
(Following Nesbitt et al., 1996)	Q	184	215	227	232	191	235	189	205
	P	6	7	1	0	0	0	0	1
	K	0	0	0	0	0	0	0	0
	Total	190	222	228	232	191	235	189	206
	Q%	96.84	96.85	99.56	100.00	100.00	100.00	100.00	99.51
	P%	3.16	3.15	0.44	0.00	0.00	0.00	0.00	0.49
	K%	0.00	0.00	0.00	0.00	0.00	0.00	0.00	
(following Marsaglia and Ingersoll, 1992)	Q (Qm+Qp+Ch)	188	217	241	236	193	241	197	219
	F	6	7	1	0	0	0	0	1
	L (carb+Rf)	12	14	7	13	19	5	21	6
	Total	206	238	249	249	212	246	218	226
	Q% (Qm+Qp+Ch)	91.26	91.18	96.79	94.78	91.04	97.97	90.37	96.90
	F%	2.91	2.94	0.40	0.00	0.00	0.00	0.00	0.44
	L% (carb + Rf)	5.83	5.88	2.81	5.22	8.96	2.03	9.63	2.65

\*\*\*Ch=Chert

\*\*\*Rf-Rock fragment

	C-17 depth	Hib 2239.5	Hib 2225	Hib 2200	Hib 2162.5	Hib 2098.5	Hib 2028
<b>Point Counted Parameters</b>							
Detrital	Qm	140	166	204	145	168	168
	Qp	16	13	6	10	15	16
	k feld	7	7	12	16	18	3
	plag	4	3	3	3	5	6
	chert	1	2	3	3	6	6
	carbonate det			1	3	2	5
	Rock frag	2	2		1	3	
Authigenic	Shale det	9		2	1	5	4
	chlorite			2	2		2
	zircon det		2	4	1	1	2
	opaque	2	13	7	6	6	5
	mica		1	2	2	1	
	bioclastic carb	6		1		3	
	peloid	36					
Cement	glauc		1				
	Qtz overgrowth			2		1	3
	carb cement	105					
	clay (unknown)		13	2	8	4	2
	silt/shl matrix		33		119		
	Clay rim				4		
	misc		2				
porosity		52	72	17	67	72	
Total	328	310	323	341	305	294	

<b>Calculated Parameters</b>							
(Following Petijohn, 1975)	Q (Qm+Qp)	156	179	210	155	183	184
	F	11	10	15	19	23	9
	L	12	4	6	8	16	15
	Total	179	193	231	182	222	208
	Q%	87.15	92.75	90.91	85.16	82.43	88.46
	F%	6.15	5.18	6.49	10.44	10.36	4.33
	L%	6.70	2.07	2.60	4.40	7.21	7.21
(Following Nesbitt et al., 1996)	Q	140	166	204	145	168	168
	P	4	3	3	3	5	6
	K	7	7	12	16	18	3
	Total	151	176	219	164	191	177
	Q%	92.72	94.32	93.15	88.41	87.96	94.92
	P%	2.65	1.70	1.37	1.83	2.62	3.39
	K%	4.64	3.98	5.48	9.76	9.42	1.69
(following Marsaglia and Ingersoll, 1992)	Q (Qm+Qp+Ch)	157	181	213	158	189	190
	F	11	10	15	19	23	9
	L (carb+Rf)	11	2	3	5	10	9
	Total	179	193	231	182	222	208
	Q% (Qm+Qp+Ch)	87.71	93.78	92.21	86.81	85.14	91.35
	F%	6.15	5.18	6.49	10.44	10.36	4.33
	L% (carb + Rf)	6.15	1.04	1.30	2.75	4.50	4.33

\*\*\*Ch=Chert

\*\*\* Rf=Rock fragment

	H-20 depth	H-20 2916	H-20 2961.3	H-20 2983.7	H-20 3007.8	H-20 3024.9	H-20 3031	H-20 3031.9	H-20 2972.5	H-20 2995.7
<b>Point Counted Parameters</b>										
Detrital	Qm	98	164	205	175	180	190	222	156	129
	Qp	12	55	22	48	40	41	24	25	11
	k feld		2					1	1	1
	plag	1	7	4	6	10	9	3	5	4
	chert		9	8	5	6	10	6	2	3
	carbonate	11	10	11	6	9	2		3	3
	rock frag		2						1	
Authigenic	chlorite			2		4	2	1		1
	opaque	4	5	11	2	10	4	1	4	4
	mica		7	3	1	3		1		
	bioclastic carb	2							1	
	Siderite	49								2
Cement	pyrite								1	
	Qtz overgrowth		1	2	6	2	5	11		
	carb cement	88			20	2		2	70	71
	clay (unknown)		9		10	17			4	6
	carb rim	26							36	42
	Clay rim			8	1	2	1	1	1	
	Chl cmt		7		9					4
	carb replacement	17						5	5	22
	misc		1							
	porosity	1	23	24	13	22	40	25	3	
<b>Total</b>	<b>309</b>	<b>302</b>	<b>300</b>	<b>302</b>	<b>307</b>	<b>304</b>	<b>303</b>	<b>318</b>	<b>303</b>	

<b>Calculated Parameters</b>										
(Following Petijohn, 1975)	<b>Q (Qm+Qp)</b>	110	219	227	223	220	231	246	181	140
	F	1	9	4	6	10	9	4	6	5
	L	11	21	19	11	15	12	6	6	6
	<b>Total</b>	<b>122</b>	<b>249</b>	<b>250</b>	<b>240</b>	<b>245</b>	<b>252</b>	<b>256</b>	<b>193</b>	<b>151</b>
	<b>Q% (Qm+Qp)</b>	90.16	87.95	90.80	92.92	89.80	91.67	96.09	93.78	92.72
	F%	0.82	3.61	1.60	2.50	4.08	3.57	1.56	3.11	3.31
	L%	9.02	8.43	7.60	4.58	6.12	4.76	2.34	3.11	3.97
(Following Nesbitt et al., 1996)	Q	110	219	227	223	220	231	246	181	140
	P	1	7	4	6	10	9	3	5	4
	K	0	2	0	0	0	0	1	1	1
	<b>Total</b>	<b>111</b>	<b>228</b>	<b>231</b>	<b>229</b>	<b>230</b>	<b>240</b>	<b>250</b>	<b>187</b>	<b>145</b>
	Q%	99.10	96.05	98.27	97.38	95.65	96.25	98.40	96.79	96.55
	P%	0.90	3.07	1.73	2.62	4.35	3.75	1.20	2.67	2.76
	K%	0.00	0.88	0.00	0.00	0.00	0.00	0.40	0.53	0.69
(following Marsaglia and Ingersoll, 1992)	<b>Q (Qm+Qp+Ch)</b>	110	228	235	228	226	241	252	183	143
	F	1	9	4	6	10	9	4	6	5
	L (carb+RF)	11	12	11	6	9	2	0	4	3
	<b>Total</b>	<b>122</b>	<b>249</b>	<b>250</b>	<b>240</b>	<b>245</b>	<b>252</b>	<b>256</b>	<b>193</b>	<b>151</b>
	<b>Q (Qm+Qp+Ch)%</b>	90.16	91.57	94.00	95.00	92.24	95.63	98.44	94.82	94.70
	F%	0.82	3.61	1.60	2.50	4.08	3.57	1.56	3.11	3.31
	L (carb+RF)%	9.02	4.82	4.40	2.50	3.67	0.79	0.00	2.07	1.99

\*\*\*Ch=chert

\*\*\*RF=Rock Fragments

	Sample depth	J22_1-1 2834.7	J22_1-2 2844.3	J22_1-3 2854	J22_1-4 2863	J22_1-5 2875.2
<b>Point Counted Parameters</b>						
Detrital	Qm	201	215	198	215	183
	Qp	12	7	15	4	4
	k feld	0	2	4		2
	plag	1	4	5	6	5
	chert	3	3	7	5	4
	carbonate	3	2	4	6	4
Authigenic	chlorite		1	1	1	16
	opaque	2	2	3	5	2
	mica			2	1	1
	bioclastic carb					
Cement	Glauc					
	Siderite					
	Qtz overgrowth	2	4	0	1	
	carb cement				1	19
	clay (unknown)			1	3	
	Clay rim	2	2	2	1	1
	calcite rhomb	1	2	1		
	misc	1				
	porosity	72	58	57	56	61
	Total	300	302	300	305	302

<b>Calculated Parameters</b>						
(Following Petijohn, 1975)	Q (Qm+Qp)	213	222	213	219	187
	F	1	6	9	6	7
	L	6	5	11	11	8
	Total	220	233	233	236	202
	Q% (Qm+Qp)	96.82	95.28	91.42	92.80	92.57
	F%	0.45	2.58	3.86	2.54	3.47
L%	2.73	2.15	4.72	4.66	3.96	
(Following Nesbitt et al., 1996)	Q	213	222	213	219	187
	P	1	4	5	6	5
	K	0	2	4	0	2
	Total	214	228	222	225	194
	Q%	99.53	97.37	95.95	97.33	96.39
	P%	0.47	1.75	2.25	2.67	2.58
K%	0.00	0.88	1.80	0.00	1.03	
(following Marsaglia and Ingersoll, 1992)	Q (Qm+Qp+Ch)	216	225	220	224	191
	F	1	6	9	6	7
	L (carb+RF)	3	2	4	6	4
	Total	220	233	233	236	202
	Q (Qm+Qp+Ch)%	98.18	96.57	94.42	94.92	94.55
	F%	0.45	2.58	3.86	2.54	3.47
L (carb+RF)%	1.36	0.86	1.72	2.54	1.98	

\*\*\*Ch=chert

\*\*\*RF=rock fragments

Appendix 2  
Average Grain Measurements

\*\* all units are in micrometers

F04_2-1	AREA.1	DIAMETER.1	PERIMETER.1	LENGTH.1	BREADTH.1	ELONGATION.1	ROUNDNESS.1	WIDTH.1	HEIGHT.1
Minimum	279.66	18.87	78.85	28.04	7.35	1.71	0.30	15.67	14.13
Maximum	18485.04	153.41	650.16	270.94	73.46	8.40	0.73	192.93	163.75
Mean	4144.82	67.67	288.53	111.33	32.93	3.52	0.55	79.83	71.53
Smp Std Dev	3103.79	26.43	115.17	46.69	13.40	1.13	0.09	35.16	29.80
Total	746067.33	12180.23	51934.98	20039.41	5928.08	634.04	99.63	14369.60	12875.90
Smp Variance	9633485.05	698.40	13264.48	2180.03	179.49	1.27	0.01	1236.39	887.93
Pop Std Dev	3112.44	26.50	115.49	46.82	13.43	1.13	0.09	35.26	29.88
Pop Variance	9687303.40	702.30	13338.59	2192.21	180.50	1.27	0.01	1243.29	892.89
Std Error	231.34	1.97	8.58	3.48	1.00	0.08	0.01	2.62	2.22
Sqr Total	4826340974.00	949922.43	17372285.41	2623394.14	227542.55	2461.51	56.46	1369691.16	1080875.89
Recip Total	0.09	3.20	0.75	1.99	6.70	55.77	334.17	2.86	3.09
Count	180.00	180.00	180.00	180.00	180.00	180.00	180.00	180.00	180.00

F04_2-2	AREA.1	DIAMETER.1	PERIMETER.1	LENGTH.1	BREADTH.1	ELONGATION.1	ROUNDNESS.1	WIDTH.1	HEIGHT.1
Minimum	221.43	16.79	64.89	21.11	9.76	1.11	0.20	16.59	12.60
Maximum	14767.15	137.12	732.87	341.52	68.96	13.71	0.78	179.72	148.08
Mean	3299.73	59.91	251.69	95.52	30.33	3.30	0.58	69.64	64.20
Smp Std Dev	2604.86	24.75	108.97	44.54	13.39	1.31	0.09	32.42	28.61
Total	765538.49	13898.32	58391.68	22160.01	7035.83	766.02	133.43	16157.31	14895.26
Smp Variance	6785290.31	612.56	11874.67	1983.50	179.17	1.73	0.01	1050.92	818.82
Pop Std Dev	2610.49	24.80	109.21	44.63	13.41	1.32	0.09	32.49	28.68
Pop Variance	6814663.86	615.21	11926.08	1992.09	179.95	1.73	0.01	1055.47	822.36
Std Error	171.02	1.62	7.15	2.92	0.88	0.09	0.01	2.13	1.88
Sqr Total	4100261424.00	974713.88	17451427.25	2576837.53	254942.30	2929.66	78.63	1369067.37	1146296.08
Recip Total	0.16	4.74	1.15	3.11	9.47	78.35	416.47	4.23	4.60
Count	232.00	232.00	232.00	232.00	232.00	232.00	232.00	232.00	232.00



F04 2-5	AREA.1	DIAMETER.1	PERIMETER.1	LENGTH.1	BREADTH.1	ELONGATION.1	ROUNDNESS.1	WIDTH.1	HEIGHT.1
Minimum	645.97	28.68	110.95	38.85	13.06	1.83	0.30	32.57	25.19
Maximum	18009.63	151.43	677.31	276.77	77.77	8.20	0.72	253.15	168.05
Mean	4719.20	74.00	313.39	120.32	36.38	3.40	0.56	87.38	79.04
Smp Std Dev	2984.76	23.07	105.02	44.08	11.40	1.02	0.08	35.17	27.53
Total	651249.22	10212.35	43248.02	16603.99	5020.02	469.39	77.57	12057.77	10908.15
Smp Variance	8908790.13	532.29	11029.74	1942.68	130.02	1.05	0.01	1236.71	758.06
Pop Std Dev	2995.63	23.16	105.41	44.24	11.44	1.03	0.08	35.30	27.63
Pop Variance	8973817.79	536.17	11110.25	1956.86	130.97	1.05	0.01	1245.74	763.59
Std Error	254.08	1.96	8.94	3.75	0.97	0.09	0.01	2.99	2.34
Sqr Total	4302786518.00	829196.25	15075663.68	2265862.16	200555.33	1740.92	44.46	1224215.66	966842.96
Recip Total	0.04	2.06	0.49	1.30	4.24	43.68	251.17	1.83	1.96
Count	138.00	138.00	138.00	138.00	138.00	138.00	138.00	138.00	138.00

F04 2-6	AREA.1	DIAMETER.1	PERIMETER.1	LENGTH.1	BREADTH.1	ELONGATION.1	ROUNDNESS.1	WIDTH.1	HEIGHT.1
Minimum	319.30	20.16	79.50	27.19	10.14	1.61	0.27	18.43	20.58
Maximum	19342.52	156.93	725.38	297.72	68.23	9.42	0.74	206.76	172.96
Mean	3925.70	67.16	281.59	107.02	33.77	3.30	0.57	81.29	70.06
Smp Std Dev	2603.86	22.09	95.79	39.06	12.07	1.06	0.08	32.22	25.08
Total	679146.52	11618.64	48714.83	18515.04	5842.38	571.21	98.90	14063.92	12120.44
Smp Variance	6780064.53	487.92	9175.21	1525.35	145.61	1.13	0.01	1038.12	628.90
Pop Std Dev	2611.41	22.15	96.07	39.17	12.10	1.07	0.08	32.31	25.15
Pop Variance	6819483.51	490.76	9228.55	1534.22	146.45	1.14	0.01	1044.15	632.55
Std Error	197.97	1.68	7.28	2.97	0.92	0.08	0.01	2.45	1.91
Sqr Total	3839078330.00	864716.21	15304852.05	2245427.37	222492.59	2081.47	57.69	1322910.70	957961.79
Recip Total	0.07	2.92	0.70	1.88	5.90	56.82	310.04	2.53	2.84
Count	173.00	173.00	173.00	173.00	173.00	173.00	173.00	173.00	173.00

F04 2-7	AREA.1	DIAMETER.1	PERIMETER.1	LENGTH.1	BREADTH.1	ELONGATION.1	ROUNDNESS.1	WIDTH.1	HEIGHT.1
Minimum	259.27	18.17	68.95	23.39	9.60	1.91	0.37	14.44	22.73
Maximum	16982.44	147.05	684.80	282.22	62.97	6.44	0.71	151.15	208.30
Mean	3881.28	67.34	282.15	107.48	33.60	3.27	0.57	68.15	81.25
Smp Std Dev	2329.81	20.17	88.41	36.15	10.33	0.87	0.07	24.07	28.47
Total	636530.67	11044.25	46273.16	17626.70	5509.88	535.93	93.75	11176.66	13324.44
Smp Variance	5428012.42	406.73	7816.92	1306.93	106.69	0.75	0.00	579.17	810.40
Pop Std Dev	2336.95	20.23	88.68	36.26	10.36	0.87	0.07	24.14	28.55
Pop Variance	5461313.11	409.22	7864.87	1314.95	107.35	0.76	0.00	582.72	815.37
Std Error	181.93	1.57	6.90	2.82	0.81	0.07	0.01	1.88	2.22
Sqr Total	3360750707.00	810456.02	14338102.39	2108852.57	202611.69	1874.83	54.39	856677.23	1215470.12
Recip Total	0.06	2.70	0.65	1.74	5.43	53.15	291.92	2.76	2.31
Count	164.00	164.00	164.00	164.00	164.00	164.00	164.00	164.00	164.00

F04 2-8	AREA.1	DIAMETER.1	PERIMETER.1	LENGTH.1	BREADTH.1	ELONGATION.1	ROUNDNESS.1	WIDTH.1	HEIGHT.1
Minimum	524.21	25.83	97.17	31.10	14.28	1.78	0.35	23.96	28.26
Maximum	11093.53	118.85	504.09	207.14	62.67	6.75	0.72	134.26	163.44
Mean	3952.91	67.82	287.21	110.21	33.40	3.38	0.56	71.73	80.31
Smp Std Dev	2286.24	20.83	93.21	38.88	10.74	1.01	0.08	25.04	29.27
Total	624559.36	10714.98	45378.54	17412.74	5276.53	534.68	89.07	11332.73	12689.42
Smp Variance	5226895.34	433.95	8688.69	1511.86	115.41	1.02	0.01	626.85	856.94
Pop Std Dev	2293.51	20.90	93.51	39.01	10.78	1.01	0.08	25.12	29.37
Pop Variance	5260187.67	436.71	8744.03	1521.49	116.14	1.03	0.01	630.84	862.39
Std Error	181.88	1.66	7.42	3.09	0.85	0.08	0.01	1.99	2.33
Sqr Total	3294674772.00	795213.68	14405802.63	2157883.49	194448.44	1970.41	51.24	911895.54	1154517.70
Recip Total	0.06	2.60	0.62	1.66	5.29	50.44	286.83	2.52	2.29
Count	158.00	158.00	158.00	158.00	158.00	158.00	158.00	158.00	158.00







A17-106	AREA.1	DIAMETER.1	PERIMETER.1	LENGTH.1	BREADTH.1	ELONGATION.1	ROUNDNESS.1	WIDTH.1	HEIGHT.1
Minimum	461.44	24.24	92.70	31.87	13.74	1.18	0.40	27.04	22.73
Maximum	20143.08	160.15	583.53	219.00	112.14	5.68	0.81	212.60	166.51
Mean	5402.38	77.13	313.97	115.78	41.21	2.95	0.60	91.03	83.17
Smp Std Dev	4012.38	30.50	123.84	47.49	17.81	0.90	0.08	36.55	35.23
Total	729321.60	10412.06	42385.77	15630.13	5562.75	398.25	81.37	12289.41	11227.97
Smp Variance	16099170.29	930.05	15336.37	2255.61	317.25	0.81	0.01	1335.55	1241.08
Pop Std Dev	4027.32	30.61	124.30	47.67	17.88	0.91	0.08	36.68	35.36
Pop Variance	16219313.35	936.99	15450.82	2272.44	319.62	0.82	0.01	1345.52	1250.34
Std Error	345.33	2.62	10.66	4.09	1.53	0.08	0.01	3.15	3.03
Sqr Total	6113462051.00	928601.10	15378214.62	2114144.81	272045.03	1284.87	49.97	1299038.50	1101377.82
Recip Total	0.05	2.10	0.52	1.43	4.01	50.23	228.62	1.80	1.98
Count	135.00	135.00	135.00	135.00	135.00	135.00	135.00	135.00	135.00

A17-155	AREA.1	DIAMETER.1	PERIMETER.1	LENGTH.1	BREADTH.1	ELONGATION.1	ROUNDNESS.1	WIDTH.1	HEIGHT.1
Minimum	931.19	34.43	135.40	48.50	18.91	1.15	0.37	29.80	33.79
Maximum	20690.70	162.31	716.55	285.91	101.09	6.39	0.79	264.21	220.89
Mean	5616.78	81.20	334.52	124.61	42.65	3.06	0.59	95.64	89.51
Smp Std Dev	3374.84	23.63	103.50	43.31	14.13	0.98	0.09	34.26	30.65
Total	775116.31	11205.32	46164.32	17196.00	5886.16	421.83	81.92	13198.79	12353.01
Smp Variance	11389526.33	558.40	10713.12	1876.14	199.77	0.95	0.01	1173.80	939.61
Pop Std Dev	3387.13	23.72	103.88	43.47	14.19	0.98	0.09	34.39	30.76
Pop Variance	11472661.56	562.47	10791.32	1889.84	201.23	0.96	0.01	1182.37	946.46
Std Error	287.29	2.01	8.81	3.69	1.20	0.08	0.01	2.92	2.61
Sqr Total	5925416210.00	986908.74	16921488.19	2401678.97	278633.01	1420.88	49.68	1424361.56	1235439.92
Recip Total	0.03	1.85	0.45	1.24	3.60	49.93	238.01	1.64	1.73
Count	138.00	138.00	138.00	138.00	138.00	138.00	138.00	138.00	138.00

A17-209	AREA.1	DIAMETER.1	PERIMETER.1	LENGTH.1	BREADTH.1	ELONGATION.1	ROUNDNESS.1	WIDTH.1	HEIGHT.1
Minimum	0.00	0.00	0.00	0.00	0.00	0.00	0.00	0.31	0.31
Maximum	36941.10	216.88	944.01	372.95	102.03	8.64	0.67	241.78	275.58
Mean	6583.98	83.34	361.42	141.46	39.25	3.81	0.52	100.71	89.36
Smp Std Dev	6135.37	37.91	159.73	62.70	19.59	1.21	0.10	49.11	40.43
Total	737405.51	9334.40	40478.60	15843.10	4396.20	426.93	58.48	11279.58	10008.00
Smp Variance	37642764.94	1436.95	25514.12	3931.44	383.95	1.46	0.01	2411.38	1634.62
Pop Std Dev	6162.94	38.08	160.45	62.98	19.68	1.21	0.10	49.33	40.61
Pop Variance	37981888.95	1449.89	25743.98	3966.86	387.41	1.47	0.01	2433.10	1649.35
Std Error	579.74	3.58	15.09	5.92	1.85	0.11	0.01	4.64	3.82
Sqr Total	9071051135.00	938893.85	17487199.09	2681428.18	215560.57	1790.69	31.55	1406047.55	1077363.76
Recip Total	0.04	1.60	0.37	0.94	3.54	31.20	216.49	4.63	4.75
Count	112.00	112.00	112.00	112.00	112.00	112.00	112.00	112.00	112.00

A17-175	AREA.1	DIAMETER.1	PERIMETER.1	LENGTH.1	BREADTH.1	ELONGATION.1	ROUNDNESS.1	WIDTH.1	HEIGHT.1
Minimum	654.84	28.87	134.06	49.15	11.87	1.59	0.30	38.10	28.26
Maximum	30736.38	197.83	898.05	391.28	113.53	8.30	0.74	320.12	179.11
Mean	6720.47	87.29	368.77	140.49	43.90	3.32	0.57	110.14	91.37
Smp Std Dev	4951.16	30.61	143.03	61.21	16.15	1.25	0.10	47.45	35.48
Total	698928.68	9078.43	38351.82	14610.59	4565.32	345.29	59.71	11454.08	9502.31
Smp Variance	24514019.35	936.76	20457.45	3746.70	260.67	1.56	0.01	2251.56	1259.08
Pop Std Dev	4975.14	30.75	143.72	61.51	16.22	1.25	0.10	47.68	35.66
Pop Variance	24752019.54	945.86	20656.07	3783.08	263.20	1.57	0.01	2273.42	1271.30
Std Error	485.50	3.00	14.03	6.00	1.58	0.12	0.01	4.65	3.48
Sqr Total	7246585932.00	889903.64	16270481.41	2442248.19	227514.79	1308.28	35.22	1495662.27	999155.75
Recip Total	0.03	1.36	0.33	0.89	2.72	35.02	187.27	1.12	1.34
Count	104.00	104.00	104.00	104.00	104.00	104.00	104.00	104.00	104.00

A17-192	AREA.1	DIAMETER.1	PERIMETER.1	LENGTH.1	BREADTH.1	ELONGATION.1	ROUNDNESS.1	WIDTH.1	HEIGHT.1
Minimum	0.00	0.00	0.00	0.00	0.00	0.00	0.00	0.31	0.31
Maximum	14543.56	136.08	667.89	286.90	81.31	9.32	0.77	179.11	172.04
Mean	5258.61	77.34	320.45	119.97	40.25	3.13	0.58	93.91	83.42
Smp Std Dev	3207.81	26.72	113.58	46.15	15.37	1.28	0.12	34.75	33.16
Total	641550.02	9435.42	39094.65	14636.79	4910.53	382.29	70.31	11457.16	10177.58
Smp Variance	10290061.56	714.07	12900.82	2129.74	236.20	1.64	0.01	1207.54	1099.61
Pop Std Dev	3221.04	26.83	114.05	46.34	15.43	1.29	0.12	34.89	33.30
Pop Variance	10375103.39	719.97	13007.44	2147.34	238.15	1.66	0.01	1217.52	1108.69
Std Error	290.42	2.42	10.28	4.18	1.39	0.12	0.01	3.15	3.00
Sqr Total	4629046740.00	816846.85	14101698.53	2015857.93	226466.67	1398.57	42.32	1223274.75	983194.82
Recip Total	0.04	1.73	0.42	1.15	3.44	42.53	211.62	7.97	8.18
Count	122.00	122.00	122.00	122.00	122.00	122.00	122.00	122.00	122.00

A17-128	AREA.1	DIAMETER.1	PERIMETER.1	LENGTH.1	BREADTH.1	ELONGATION.1	ROUNDNESS.1	WIDTH.1	HEIGHT.1
Minimum	953.94	34.85	126.92	39.01	17.50	1.17	0.31	40.86	25.19
Maximum	18335.72	152.79	645.02	250.99	80.99	8.07	0.79	188.63	180.34
Mean	5286.74	78.93	320.70	117.84	42.51	2.90	0.61	94.10	83.28
Smp Std Dev	3093.81	22.40	94.64	38.84	13.31	0.98	0.09	30.70	27.14
Total	745430.33	11128.78	45219.08	16615.82	5993.72	409.30	85.78	13267.60	11742.56
Smp Variance	9571636.89	501.73	8956.50	1508.88	177.20	0.96	0.01	942.29	736.49
Pop Std Dev	3104.84	22.48	94.98	38.98	13.36	0.98	0.09	30.81	27.24
Pop Variance	9640005.72	505.32	9020.47	1519.66	178.47	0.97	0.01	949.02	741.75
Std Error	260.55	1.89	7.97	3.27	1.12	0.08	0.01	2.59	2.29
Sqr Total	5290497099.00	949111.37	15764745.63	2170803.99	279770.80	1323.57	53.22	1381298.05	1081773.20
Recip Total	0.04	1.94	0.48	1.34	3.67	53.63	237.09	1.67	1.89
Count	141.00	141.00	141.00	141.00	141.00	141.00	141.00	141.00	141.00



L08-53	AREA.1	DIAMETER.1	PERIMETER.1	LENGTH.1	BREADTH.1	ELONGATION.1	ROUNDNESS.1	WIDTH.1	HEIGHT.1
Minimum	105.33	11.58	47.65	17.96	5.86	1.43	0.31	10.14	11.37
Maximum	15997.26	142.72	622.41	262.03	74.14	7.94	0.76	188.63	188.94
Mean	3799.76	63.41	272.74	106.07	30.30	3.55	0.55	72.97	69.34
Smp Std Dev	3341.61	28.59	126.84	51.58	13.77	1.01	0.08	35.33	34.32
Total	782750.86	13061.67	56183.46	21850.68	6241.05	731.60	113.03	15031.05	14284.19
Smp Variance	11166331.95	817.66	16088.58	2660.10	189.67	1.03	0.01	1248.55	1177.56
Pop Std Dev	3349.75	28.66	127.15	51.70	13.81	1.02	0.08	35.42	34.40
Pop Variance	11220801.86	821.65	16167.06	2673.08	190.59	1.04	0.01	1254.64	1183.30
Std Error	232.82	1.99	8.84	3.59	0.96	0.07	0.01	2.46	2.39
Sqr Total	5274530901.00	996629.34	18637459.05	2865710.25	228152.80	2810.40	63.27	1353959.49	1233053.70
Recip Total	0.14	4.12	0.98	2.58	8.53	62.45	383.90	3.69	4.01
Count	206.00	206.00	206.00	206.00	206.00	206.00	206.00	206.00	206.00

L08-99	AREA.1	DIAMETER.1	PERIMETER.1	LENGTH.1	BREADTH.1	ELONGATION.1	ROUNDNESS.1	WIDTH.1	HEIGHT.1
Minimum	120.15	12.37	56.31	22.91	5.24	1.32	0.35	14.13	15.67
Maximum	13386.03	130.55	563.90	240.75	74.27	6.92	0.77	170.81	159.45
Mean	3740.95	64.69	279.74	109.22	30.66	3.64	0.54	77.26	68.62
Smp Std Dev	2617.37	24.04	108.55	45.02	11.57	1.06	0.08	32.27	27.39
Total	819267.32	14167.86	61264.09	23918.42	6713.63	797.18	118.81	16919.53	15026.75
Smp Variance	6850641.65	577.88	11783.90	2026.46	133.87	1.13	0.01	1041.36	749.97
Pop Std Dev	2623.37	24.09	108.80	45.12	11.60	1.07	0.08	32.34	27.45
Pop Variance	6882066.61	580.54	11837.96	2035.75	134.49	1.14	0.01	1046.14	753.41
Std Error	176.87	1.62	7.34	3.04	0.78	0.07	0.01	2.18	1.85
Sqr Total	4565125895.00	1043123.55	19718980.19	3056080.67	235129.73	3150.10	65.95	1535229.42	1195308.44
Recip Total	0.12	4.05	0.95	2.51	8.51	65.29	413.95	3.57	3.88
Count	219.00	219.00	219.00	219.00	219.00	219.00	219.00	219.00	219.00









L08-302	AREA.1	DIAMETER.1	PERIMETER.1	LENGTH.1	BREADTH.1	ELONGATION.1	ROUNDNESS.1	WIDTH.1	HEIGHT.1
Minimum	169.51	14.69	55.70	18.87	7.78	1.39	0.23	14.13	12.90
Maximum	34900.89	210.80	884.99	339.78	102.72	11.72	0.76	201.54	240.55
Mean	4433.29	68.98	299.46	116.95	32.78	3.66	0.55	82.75	72.60
Smp Std Dev	4073.80	29.76	135.19	56.24	14.36	1.35	0.09	39.68	33.37
Total	780258.17	12141.13	52704.97	20583.95	5768.53	644.59	96.01	14564.07	12777.59
Smp Variance	16595852.52	885.89	18275.24	3162.48	206.29	1.83	0.01	1574.90	1113.84
Pop Std Dev	4085.42	29.85	135.57	56.40	14.40	1.36	0.09	39.80	33.47
Pop Variance	16690685.96	890.95	18379.67	3180.55	207.47	1.84	0.01	1583.90	1120.21
Std Error	307.07	2.24	10.19	4.24	1.08	0.10	0.01	2.99	2.52
Sqr Total	6379976939.00	993455.56	18999472.29	2963976.91	225374.82	2683.33	53.91	1482364.77	1123688.54
Recip Total	0.10	3.22	0.76	2.03	6.69	53.52	334.26	2.90	3.11
Count	176.00	176.00	176.00	176.00	176.00	176.00	176.00	176.00	176.00

L08-233	AREA.1	DIAMETER.1	PERIMETER.1	LENGTH.1	BREADTH.1	ELONGATION.1	ROUNDNESS.1	WIDTH.1	HEIGHT.1
Minimum	111.56	11.92	56.68	23.61	4.72	1.78	0.25	8.91	18.43
Maximum	24209.34	175.57	760.76	308.26	89.97	10.43	0.72	212.60	209.83
Mean	4533.73	68.52	298.29	117.07	32.07	3.77	0.53	80.36	76.62
Smp Std Dev	4459.35	32.83	144.02	58.08	15.97	1.22	0.08	41.57	38.07
Total	761666.48	11511.22	50113.02	19668.26	5388.25	633.74	89.55	13501.09	12871.60
Smp Variance	19885787.67	1077.65	20742.61	3372.85	255.08	1.48	0.01	1727.84	1449.53
Pop Std Dev	4472.68	32.93	144.45	58.25	16.02	1.22	0.08	41.69	38.19
Pop Variance	20004864.24	1084.10	20866.82	3393.05	256.61	1.49	0.01	1738.18	1458.21
Std Error	344.05	2.53	11.11	4.48	1.23	0.09	0.01	3.21	2.94
Sqr Total	6794001760.00	969783.88	18433061.61	2869261.55	215670.90	2639.66	48.83	1375273.13	1229700.42
Recip Total	0.10	3.13	0.73	1.89	6.73	48.28	324.05	2.83	2.84
Count	168.00	168.00	168.00	168.00	168.00	168.00	168.00	168.00	168.00

L08-A65	AREA.1	DIAMETER.1	PERIMETER.1	LENGTH.1	BREADTH.1	ELONGATION.1	ROUNDNESS.1	WIDTH.1	HEIGHT.1
Minimum	175.08	14.93	57.80	20.26	7.61	1.46	0.27	11.37	18.43
Maximum	23663.61	173.58	734.23	283.71	83.41	9.59	0.76	204.30	178.80
Mean	3547.79	62.34	273.32	107.72	28.94	3.79	0.53	76.53	64.35
Smp Std Dev	2800.03	25.11	115.66	48.44	11.71	1.21	0.09	35.57	27.46
Total	766323.49	13466.36	59037.07	23267.88	6250.66	818.66	115.01	16531.20	13899.56
Smp Variance	7840159.56	630.39	13377.33	2346.12	137.18	1.47	0.01	1264.92	753.96
Pop Std Dev	2806.53	25.17	115.93	48.55	11.74	1.21	0.09	35.65	27.52
Pop Variance	7876625.41	633.32	13439.55	2357.03	137.82	1.47	0.01	1270.80	757.47
Std Error	190.52	1.71	7.87	3.30	0.80	0.08	0.01	2.42	1.87
Sqr Total	4412232267.00	975713.37	19025504.05	3013214.68	210514.36	3419.52	62.87	1538411.11	1057288.54
Recip Total	0.14	4.25	0.99	2.60	9.05	62.39	417.96	3.76	4.12
Count	216.00	216.00	216.00	216.00	216.00	216.00	216.00	216.00	216.00

L08-312	AREA.1	DIAMETER.1	PERIMETER.1	LENGTH.1	BREADTH.1	ELONGATION.1	ROUNDNESS.1	WIDTH.1	HEIGHT.1
Minimum	250.68	17.87	75.14	26.83	8.10	1.84	0.30	15.67	18.43
Maximum	16276.73	143.96	731.24	316.14	62.31	8.28	0.72	216.90	157.91
Mean	4131.44	67.55	291.18	113.40	32.19	3.56	0.55	79.23	71.85
Smp Std Dev	3058.79	26.40	122.54	51.43	12.16	1.09	0.08	36.20	30.15
Total	747789.75	12227.21	52703.64	20524.53	5827.29	643.72	99.48	14340.42	13004.32
Smp Variance	9356186.53	696.81	15015.98	2644.78	147.86	1.20	0.01	1310.18	908.79
Pop Std Dev	3067.27	26.47	122.88	51.57	12.19	1.10	0.08	36.30	30.23
Pop Variance	9408165.34	700.68	15099.40	2659.47	148.68	1.20	0.01	1317.46	913.84
Std Error	227.36	1.96	9.11	3.82	0.90	0.08	0.01	2.69	2.24
Sqr Total	4782914531.00	952115.47	18064156.08	2806087.70	214371.83	2506.01	55.81	1373317.11	1098813.60
Recip Total	0.10	3.26	0.77	2.04	6.73	54.85	337.59	2.90	3.15
Count	181.00	181.00	181.00	181.00	181.00	181.00	181.00	181.00	181.00

L08-250	AREA.1	DIAMETER.1	PERIMETER.1	LENGTH.1	BREADTH.1	ELONGATION.1	ROUNDNESS.1	WIDTH.1	HEIGHT.1
Minimum	186.22	15.40	57.09	18.46	10.09	1.83	0.31	14.44	15.67
Maximum	18856.06	154.95	772.32	335.28	80.75	8.10	0.72	230.72	190.17
Mean	5028.30	73.31	321.22	126.70	33.91	3.75	0.53	87.33	79.47
Smp Std Dev	4417.63	32.07	150.00	62.92	14.24	1.07	0.08	43.40	37.48
Total	764301.02	11142.50	48825.39	19258.08	5154.62	569.69	81.08	13273.75	12079.58
Smp Variance	19515483.97	1028.47	22499.40	3958.62	202.78	1.15	0.01	1883.79	1404.67
Pop Std Dev	4432.24	32.18	150.49	63.13	14.29	1.08	0.08	43.55	37.60
Pop Variance	19644725.59	1035.28	22648.40	3984.83	204.13	1.16	0.01	1896.27	1413.98
Std Error	358.32	2.60	12.17	5.10	1.16	0.09	0.01	3.52	3.04
Sqr Total	6809485496.00	973138.29	19103581.53	3041667.37	205625.97	2309.75	44.22	1445496.63	1173486.36
Recip Total	0.07	2.55	0.60	1.57	5.39	43.68	292.01	2.29	2.43
Count	152.00	152.00	152.00	152.00	152.00	152.00	152.00	152.00	152.00

L08-174	AREA.1	DIAMETER.1	PERIMETER.1	LENGTH.1	BREADTH.1	ELONGATION.1	ROUNDNESS.1	WIDTH.1	HEIGHT.1
Minimum	477.10	24.65	93.63	31.82	11.02	1.79	0.24	23.27	23.27
Maximum	49119.82	250.08	1069.42	423.68	132.47	10.88	0.72	342.64	286.98
Mean	11848.69	112.46	488.56	191.07	53.21	3.82	0.53	138.83	116.59
Smp Std Dev	9938.71	49.38	213.12	85.75	25.28	1.40	0.09	65.72	54.26
Total	1848395.47	17544.10	76215.61	29806.65	8301.15	595.53	83.25	21658.00	18187.33
Smp Variance	98777955.61	2438.47	45418.39	7352.78	638.89	1.97	0.01	4319.36	2944.66
Pop Std Dev	9970.72	49.54	213.80	86.02	25.36	1.41	0.09	65.93	54.44
Pop Variance	99415232.74	2454.20	45711.41	7400.22	643.01	1.98	0.01	4347.23	2963.66
Std Error	795.73	3.95	17.06	6.87	2.02	0.11	0.01	5.26	4.34
Sqr Total	37310423980.00	2353450.21	44321284.71	6842138.96	541391.28	2580.54	45.81	3680672.25	2579745.81
Recip Total	0.03	1.75	0.41	1.06	3.80	45.53	303.37	1.50	1.73
Count	156.00	156.00	156.00	156.00	156.00	156.00	156.00	156.00	156.00



L08-148	AREA.1	DIAMETER.1	PERIMETER.1	LENGTH.1	BREADTH.1	ELONGATION.1	ROUNDNESS.1	WIDTH.1	HEIGHT.1
Minimum	271.35	18.59	75.12	24.77	8.53	1.77	0.31	18.43	16.90
Maximum	12891.93	128.12	543.13	221.33	71.37	8.01	0.72	200.00	138.56
Mean	3767.66	64.58	275.03	106.12	31.40	3.49	0.55	76.68	67.80
Smp Std Dev	2749.78	25.03	108.66	43.82	12.64	1.03	0.08	35.09	26.65
Total	772370.87	13239.38	56381.95	21754.67	6436.31	715.48	113.66	15719.83	13899.25
Smp Variance	7561301.82	626.26	11807.61	1920.40	159.82	1.06	0.01	1231.50	710.47
Pop Std Dev	2756.51	25.09	108.93	43.93	12.67	1.03	0.08	35.18	26.72
Pop Variance	7598367.02	629.33	11865.49	1929.81	160.60	1.07	0.01	1237.54	713.95
Std Error	192.05	1.75	7.59	3.06	0.88	0.07	0.01	2.45	1.86
Sqr Total	4460099826.00	983413.13	17927509.13	2702293.79	234841.76	2714.48	64.32	1457887.38	1088032.57
Recip Total	0.11	3.80	0.90	2.38	7.88	63.34	378.41	3.39	3.65
Count	205.00	205.00	205.00	205.00	205.00	205.00	205.00	205.00	205.00

H20 T82A	AREA.1	DIAMETER.1	PERIMETER.1	LENGTH.1	BREADTH.1	ELONGATION.1	ROUNDNESS.1	WIDTH.1	HEIGHT.1
Minimum	63.90	9.02	35.98	13.12	3.55	1.13	0.27	10.75	8.91
Maximum	8985.75	106.96	445.03	176.11	64.34	9.57	0.79	160.68	146.24
Mean	1747.81	43.99	181.58	67.85	22.94	3.14	0.59	50.31	48.39
Smp Std Dev	1393.94	17.05	71.45	28.30	9.62	1.12	0.09	22.69	20.22
Total	630957.85	15878.72	65550.18	24494.12	8280.97	1132.90	212.43	18161.31	17468.84
Smp Variance	1943055.72	290.66	5104.41	800.89	92.46	1.26	0.01	515.03	408.72
Pop Std Dev	1395.87	17.07	71.54	28.34	9.63	1.13	0.09	22.73	20.24
Pop Variance	1948453.09	291.47	5118.59	803.12	92.72	1.27	0.01	516.46	409.86
Std Error	73.37	0.90	3.76	1.49	0.51	0.06	0.00	1.19	1.06
Sqr Total	1804234837.00	803360.49	13745254.25	1951067.00	223334.57	4011.57	127.98	1099592.27	992867.59
Recip Total	0.40	9.66	2.35	6.40	19.13	127.74	631.09	8.86	9.03
Count	361.00	361.00	361.00	361.00	361.00	361.00	361.00	361.00	361.00



H20 119	AREA.1	DIAMETER.1	PERIMETER.1	LENGTH.1	BREADTH.1	ELONGATION.1	ROUNDNESS.1	WIDTH.1	HEIGHT.1
Minimum	585.56	27.30	103.31	34.86	7.70	1.26	0.24	27.04	22.73
Maximum	14501.08	135.88	708.51	307.03	75.03	10.79	0.80	179.11	227.96
Mean	4709.78	73.61	308.94	117.51	36.95	3.30	0.57	83.57	81.16
Smp Std Dev	2996.94	24.06	107.39	44.60	12.75	1.11	0.08	29.82	33.64
Total	697046.76	10893.61	45722.96	17392.20	5469.28	488.66	84.69	12368.06	12011.69
Smp Variance	8981639.03	578.91	11532.22	1988.88	162.69	1.24	0.01	889.12	1131.35
Pop Std Dev	3007.11	24.14	107.75	44.75	12.80	1.12	0.08	29.92	33.75
Pop Variance	9042738.62	582.85	11610.67	2002.41	163.79	1.25	0.01	895.17	1139.05
Std Error	246.35	1.98	8.83	3.67	1.05	0.09	0.01	2.45	2.76
Sqr Total	4612216240.00	887507.50	15832367.74	2338196.09	226192.30	1796.54	49.46	1165163.85	1142309.30
Recip Total	0.05	2.26	0.54	1.45	4.58	48.82	265.27	2.02	2.17
Count	148.00	148.00	148.00	148.00	148.00	148.00	148.00	148.00	148.00

H20 111	AREA.1	DIAMETER.1	PERIMETER.1	LENGTH.1	BREADTH.1	ELONGATION.1	ROUNDNESS.1	WIDTH.1	HEIGHT.1
Minimum	211.42	16.41	66.06	23.18	8.69	1.15	0.33	18.43	12.90
Maximum	19649.27	158.17	707.70	284.87	72.89	7.41	0.78	174.81	186.18
Mean	3398.62	61.31	256.88	97.62	30.82	3.26	0.57	72.18	64.49
Smp Std Dev	2662.45	23.84	102.87	41.37	12.41	0.95	0.08	31.46	27.41
Total	683121.98	12323.53	51632.02	19621.14	6194.87	654.89	115.40	14508.77	12963.46
Smp Variance	7088617.50	568.20	10581.39	1711.31	154.01	0.91	0.01	990.03	751.52
Pop Std Dev	2669.09	23.90	103.12	41.47	12.44	0.96	0.08	31.54	27.48
Pop Variance	7124060.59	571.04	10634.30	1719.86	154.78	0.92	0.01	994.98	755.28
Std Error	187.79	1.68	7.26	2.92	0.88	0.07	0.01	2.22	1.93
Sqr Total	3746481986.00	869777.92	15389871.88	2259340.70	221883.30	2316.89	67.54	1246282.86	987131.77
Recip Total	0.12	3.88	0.94	2.52	7.76	66.83	357.69	3.42	3.88
Count	201.00	201.00	201.00	201.00	201.00	201.00	201.00	201.00	201.00

H20 97	AREA.1	DIAMETER.1	PERIMETER.1	LENGTH.1	BREADTH.1	ELONGATION.1	ROUNDNESS.1	WIDTH.1	HEIGHT.1
Minimum	477.39	24.65	92.45	30.64	12.26	1.88	0.28	16.90	23.96
Maximum	14658.42	136.62	580.42	237.17	70.59	8.96	0.71	169.28	153.92
Mean	4386.78	70.94	298.38	113.87	35.32	3.31	0.57	83.74	74.23
Smp Std Dev	2833.75	23.50	103.15	42.20	12.22	1.01	0.08	31.59	28.67
Total	723818.44	11705.76	49232.89	18789.13	5827.31	546.66	93.98	13817.53	12248.25
Smp Variance	8030140.57	552.37	10640.85	1780.69	149.32	1.02	0.01	998.01	821.97
Pop Std Dev	2842.38	23.57	103.47	42.33	12.26	1.01	0.08	31.69	28.76
Pop Variance	8079104.84	555.74	10705.73	1791.55	150.23	1.03	0.01	1004.10	826.98
Std Error	220.61	1.83	8.03	3.29	0.95	0.08	0.01	2.46	2.23
Sqr Total	4500204311.00	921594.26	16445907.13	2433399.30	230440.61	1979.49	54.48	1321787.15	1044834.65
Recip Total	0.06	2.64	0.63	1.69	5.33	53.38	296.04	2.34	2.61
Count	165.00	165.00	165.00	165.00	165.00	165.00	165.00	165.00	165.00

H20 71	AREA.1	DIAMETER.1	PERIMETER.1	LENGTH.1	BREADTH.1	ELONGATION.1	ROUNDNESS.1	WIDTH.1	HEIGHT.1
Minimum	601.42	27.67	110.95	36.90	12.62	1.50	0.31	23.96	23.96
Maximum	14786.97	137.21	581.58	258.36	70.30	7.97	0.75	207.07	163.75
Mean	3873.06	67.23	280.36	105.93	34.25	3.17	0.58	76.13	73.24
Smp Std Dev	2289.78	20.28	92.34	39.09	10.68	1.03	0.08	27.57	27.52
Total	720389.18	12505.31	52147.51	19702.61	6371.14	589.52	108.53	14160.08	13622.44
Smp Variance	5243083.89	411.08	8526.78	1528.29	114.08	1.05	0.01	760.02	757.49
Pop Std Dev	2295.96	20.33	92.59	39.20	10.71	1.03	0.08	27.64	27.60
Pop Variance	5271424.89	413.30	8572.87	1536.55	114.70	1.06	0.01	764.13	761.58
Std Error	167.89	1.49	6.77	2.87	0.78	0.08	0.01	2.02	2.02
Sqr Total	3765324209.00	917227.99	16206208.57	2371320.38	239453.40	2064.64	64.58	1219363.28	1138585.94
Recip Total	0.07	3.06	0.75	2.03	6.01	63.84	326.38	2.80	2.95
Count	186.00	186.00	186.00	186.00	186.00	186.00	186.00	186.00	186.00















C73 4123	AREA.1	DIAMETER.1	PERIMETER.1	LENGTH.1	BREADTH.1	ELONGATION.1	ROUNDNESS.1	WIDTH.1	HEIGHT.1
Minimum	3470.98	66.48	254.53	87.68	39.59	1.17	0.31	67.59	69.12
Maximum	714867.78	954.04	3791.28	1426.40	529.07	7.91	0.79	986.18	1258.07
Mean	59937.74	243.75	990.63	365.43	129.89	2.89	0.61	261.37	276.62
Smp Std Dev	79945.57	130.01	538.25	206.37	70.08	0.83	0.07	136.14	166.74
Total	16363004.16	66543.09	270443.33	99761.83	35459.84	789.48	165.76	71354.92	75516.21
Smp Variance	6391293754.00	16902.22	289713.96	42589.82	4910.60	0.70	0.01	18533.53	27801.46
Pop Std Dev	80092.39	130.25	539.24	206.75	70.20	0.84	0.08	136.39	167.04
Pop Variance	6414791157.00	16964.36	290779.08	42746.40	4928.65	0.70	0.01	18601.67	27903.67
Std Error	4838.53	7.87	32.58	12.49	4.24	0.05	0.00	8.24	10.09
Sqr Total	2725584752000	20834023.97	347002516.10	48082779	5946454.04	2473.14	102.18	23709926	28478804.97
Recip Total	0.01	1.40	0.35	0.96	2.65	101.54	457.40	1.32	1.29
Count	273.00	273.00	273.00	273.00	273.00	273.00	273.00	273.00	273.00

G57 4598	AREA.1	DIAMETER.1	PERIMETER.1	LENGTH.1	BREADTH.1	ELONGATION.1	ROUNDNESS.1	WIDTH.1	HEIGHT.1
Minimum	4112.79	72.36	280.07	98.12	40.42	1.32	0.41	69.12	78.34
Maximum	654971.61	913.20	3874.30	1500.71	436.44	5.53	0.77	855.61	1158.22
Mean	60312.83	249.25	993.61	358.71	138.09	2.63	0.63	256.91	283.25
Smp Std Dev	70799.43	121.12	500.79	192.20	64.83	0.67	0.07	117.62	163.94
Total	17249469.37	71284.34	284172.45	102592.05	39494.18	752.53	180.59	73476.27	81010.84
Smp Variance	5012559547.00	14669.14	250786.15	36939.04	4202.42	0.45	0.00	13835.55	26875.13
Pop Std Dev	70923.53	121.33	501.66	192.53	64.94	0.67	0.07	117.83	164.22
Pop Variance	5030147475.00	14720.61	251666.10	37068.65	4217.16	0.45	0.00	13884.10	26969.43
Std Error	4186.46	7.16	29.61	11.36	3.83	0.04	0.00	6.96	9.69
Sqr Total	2473956343000	21962706.52	354081420.40	47365715	6655701.82	2108.04	115.30	22833761	30632988.28
Recip Total	0.01	1.41	0.36	1.01	2.55	115.60	458.41	1.37	1.32
Count	286.00	286.00	286.00	286.00	286.00	286.00	286.00	286.00	286.00

G57 4594	AREA.1	DIAMETER.1	PERIMETER.1	LENGTH.1	BREADTH.1	ELONGATION.1	ROUNDNESS.1	WIDTH.1	HEIGHT.1
Minimum	2129.54	52.07	215.65	81.78	26.04	1.59	0.40	63.75	46.08
Maximum	190625.27	492.66	1985.54	803.66	276.42	5.63	0.74	566.82	583.72
Mean	44134.08	219.80	905.24	339.68	112.94	3.05	0.59	234.59	242.05
Smp Std Dev	35273.16	88.77	374.75	146.52	45.86	0.69	0.06	103.07	105.92
Total	4589944.59	22859.38	94145.46	35326.77	11745.96	317.18	61.31	24397.88	25173.61
Smp Variance	1244195933.00	7880.46	140436.83	21466.71	2102.69	0.47	0.00	10623.34	11219.33
Pop Std Dev	35443.98	89.20	376.56	147.22	46.08	0.69	0.06	103.57	106.43
Pop Variance	1256275505.00	7956.97	141800.30	21675.13	2123.10	0.48	0.00	10726.48	11328.26
Std Error	3458.82	8.70	36.75	14.37	4.50	0.07	0.01	10.11	10.39
Sqr Total	331969370200	5844098.95	99830128.22	14232351	1545291.80	1016.63	36.54	6828446.56	7260180.81
Recip Total	0.01	0.57	0.14	0.38	1.12	35.71	178.54	0.54	0.54
Count	104.00	104.00	104.00	104.00	104.00	104.00	104.00	104.00	104.00

G57 4029	AREA.1	DIAMETER.1	PERIMETER.1	LENGTH.1	BREADTH.1	ELONGATION.1	ROUNDNESS.1	WIDTH.1	HEIGHT.1
Minimum	106.77	11.66	164.69	57.53	0.70	1.78	0.00	39.17	36.10
Maximum	623456.74	890.96	4108.18	2053.35	413.12	2780.00	0.72	761.91	1159.76
Mean	19009.99	110.45	662.72	275.65	55.71	160.60	0.43	144.43	147.97
Smp Std Dev	62863.37	109.57	518.91	238.09	57.62	329.53	0.28	97.16	132.69
Total	3916057.81	22752.01	136519.39	56783.22	11476.47	33083.08	88.35	29751.95	30480.83
Smp Variance	3951803250.00	12005.80	269265.93	56689.04	3320.58	108590.82	0.08	9440.73	17606.45
Pop Std Dev	63016.51	109.84	520.17	238.67	57.76	330.33	0.28	97.40	133.01
Pop Variance	3971080339.00	12064.37	270579.42	56965.58	3336.78	109120.53	0.08	9486.78	17692.34
Std Error	4379.90	7.63	36.15	16.59	4.01	22.96	0.02	6.77	9.24
Sqr Total	888515686900	4986079.66	145942292.40	27330051	1323406.41	27682767.94	53.93	6241774.26	8137031.82
Recip Total	0.29	4.78	0.41	1.05	84.75	53.16	10678.74	1.88	1.99
Count	206.00	206.00	206.00	206.00	206.00	206.00	206.00	206.00	206.00

G57 3995	AREA.1	DIAMETER.1	PERIMETER.1	LENGTH.1	BREADTH.1	ELONGATION.1	ROUNDNESS.1	WIDTH.1	HEIGHT.1
Minimum	1110.19	37.60	139.14	44.77	22.12	1.14	0.30	34.56	39.17
Maximum	50256.60	252.96	1107.62	442.54	139.08	8.45	0.79	338.71	269.59
Mean	13863.56	125.99	524.82	198.03	64.39	3.14	0.59	152.66	130.24
Smp Std Dev	8906.54	42.17	188.01	78.43	21.43	1.04	0.09	61.91	48.93
Total	4006569.24	36410.52	151673.85	57229.23	18607.69	906.19	169.73	44118.33	37638.29
Smp Variance	79326526.57	1778.67	35349.17	6151.12	459.42	1.09	0.01	3832.36	2393.68
Pop Std Dev	8921.99	42.25	188.34	78.57	21.47	1.04	0.09	62.01	49.01
Pop Variance	79601965.90	1784.85	35471.91	6172.48	461.01	1.09	0.01	3845.66	2401.99
Std Error	523.91	2.48	11.06	4.61	1.26	0.06	0.01	3.64	2.88
Sqr Total	78470684860.00	5101322.40	89817832.05	13110494	1330855.58	3155.48	101.92	7842592.26	5593645.50
Recip Total	0.04	2.62	0.64	1.77	5.05	101.67	504.78	2.29	2.60
Count	289.00	289.00	289.00	289.00	289.00	289.00	289.00	289.00	289.00

G57 3990	AREA.1	DIAMETER.1	PERIMETER.1	LENGTH.1	BREADTH.1	ELONGATION.1	ROUNDNESS.1	WIDTH.1	HEIGHT.1
Minimum	233.60	17.25	200.28	75.55	0.70	1.84	0.00	56.84	39.17
Maximum	71461.77	301.64	1836.97	917.75	154.52	1243.72	0.72	339.48	398.62
Mean	18846.45	142.38	683.54	270.23	71.54	70.13	0.53	164.17	176.52
Smp Std Dev	13504.70	61.03	249.56	123.92	34.42	213.66	0.18	54.71	69.49
Total	3147357.45	23776.84	114151.25	45129.17	11946.46	11711.02	87.73	27416.31	29479.30
Smp Variance	182376921.80	3725.04	62279.37	15355.24	1184.52	45651.79	0.03	2993.63	4828.66
Pop Std Dev	13545.32	61.22	250.31	124.29	34.52	214.31	0.18	54.88	69.70
Pop Variance	183475577.90	3747.48	62654.54	15447.74	1191.65	45926.80	0.03	3011.66	4857.75
Std Error	1045.03	4.72	19.31	9.59	2.66	16.53	0.01	4.23	5.38
Sqr Total	89773466560.00	4007339.97	88427652.79	14759786	1052412.22	8445094.94	51.75	5000859.47	6010151.47
Recip Total	0.06	1.84	0.28	0.75	23.61	50.81	3850.22	1.16	1.14
Count	167.00	167.00	167.00	167.00	167.00	167.00	167.00	167.00	167.00

Appendix 3  
Standard Deviation of all samples used in grain analysis (units in  $\phi$ )

	Sample	Length	Width	Height	Diameter	
		Si	Si	Si	Si	
Ben Nevis	A-17	2962.11	0.63	0.71	0.59	0.60
		2974.91	0.55	0.59	0.48	0.48
		2982.56	0.52	0.57	0.49	0.46
		2942.11	0.66	0.73	0.65	0.65
		2993.89	0.68	0.62	0.66	0.61
		3013.34	0.46	0.49	0.49	0.39
		3045.54	0.61	0.73	0.60	0.63
		3023.07	0.59	0.56	0.57	0.48
		3033.33	0.50	0.57	0.62	0.49
		3002.13	0.48	0.46	0.45	0.41
		L-08	2894.07	0.55	0.60	0.54
	2861.06		0.62	0.66	0.59	0.59
	2871.26		0.55	0.64	0.52	0.52
	2884.08		0.76	0.73	0.77	0.69
	2905.26		0.67	0.69	0.59	0.58
	2915.88		0.64	0.67	0.64	0.60
	2927.26		0.65	0.71	0.60	0.61
	2938.08		0.82	0.82	0.73	0.73
	2945.35		0.66	0.69	0.62	0.60
	2953.55		0.82	0.82	0.75	0.74
	2962.95		0.77	0.78	0.71	0.67
	2972.38		0.69	0.69	0.71	0.66
	2981.88		0.81	0.82	0.74	0.74
	2991.54		0.66	0.65	0.60	0.60
	3010.05		0.74	0.73	0.66	0.65
	3021.08		0.86	0.84	0.80	0.77
	3032.00		0.53	0.57	0.53	0.49
	3050.20		0.75	0.78	0.70	0.67
	3060.29		0.70	0.68	0.69	0.64
	3000.23	0.78	0.77	0.76	0.69	
	2893.48	0.74	0.78	0.65	0.65	
	J-22-1	2834.65	0.96	0.77	0.70	1.41
		2844.30	0.57	0.53	0.55	0.50
		2853.95	0.73	0.73	0.68	0.61
		2862.95	0.57	0.56	0.59	0.52
		2875.20	0.66	0.67	0.65	0.60
	F-04	2867.65	0.66	0.69	0.67	0.62
		2857.40	0.73	0.69	0.69	0.66
		2846.35	0.53	0.58	0.53	0.46
		2836.70	0.53	0.56	0.52	0.49
		2827.30	0.48	0.54	0.47	0.45
		2818.25	0.52	0.57	0.52	0.48
2809.00		0.50	0.49	0.53	0.44	
2797.10		0.57	0.54	0.57	0.48	
2787.80		0.50	0.46	0.56	0.43	
2776.90		0.54	0.56	0.52	0.47	

	Sample	Length Si	Width Si	Height Si	Diameter Si
H-20	2972.46	0.86	0.84	0.83	0.79
	2995.69	0.61	0.65	0.61	0.57
	3031.86	0.61	0.65	0.61	0.57
	3031.03	0.53	0.52	0.60	0.49
	3024.87	0.66	0.65	0.67	0.60
	3007.83	0.54	0.58	0.58	0.49
	2983.70	0.53	0.51	0.57	0.47
	2961.27	0.64	0.61	0.62	0.55
	2916.00	0.81	0.79	0.83	0.76

Hibernia	G57 3995	0.64	0.63	0.58	0.51
	G57 3990	0.62	0.51	0.60	0.80
	G57 3985	0.71	0.72	0.71	0.68
	C17 2239	0.71	0.73	0.77	0.36
	C17 2028	0.43	0.44	0.48	0.22
	C17 2098	0.45	0.50	0.54	0.22
	C17 2162	0.66	0.68	0.68	0.34
	C17 2200	0.50	0.56	0.56	0.25
	C17 2225	0.44	0.51	0.49	0.23

Terra Nova	C73 4129	0.82	0.76	0.86	0.77
	C73 4123	0.72	0.70	0.74	0.69
	G57 4029	0.75	0.69	0.78	1.43
	G57 4035	1.05	1.03	1.00	1.00

Lower Tempest	G57 4598	0.69	0.65	0.76	0.65
	G57 4594	0.63	0.61	0.68	0.61

Appendix 4  
X-ray Fluorescence (XRF) Data

	Na <sub>2</sub> O wt%	MgO wt%	Al <sub>2</sub> O <sub>3</sub> wt%	SiO <sub>2</sub> wt%	P <sub>2</sub> O <sub>5</sub> wt%	S ppm	Cl ppm	K <sub>2</sub> O wt%	CaO wt%	Sc ppm	TiO <sub>2</sub> wt%	V ppm	Cr ppm	MnO wt%	Fe <sub>2</sub> O <sub>3</sub> T wt%	Ni ppm
Ben Nevis Core																
F04 2831.08	0.62%	1.48%	21.28%	55.58%	0.03%	6038	749	3.45%	1.84%	11	1.36%	160	174	0.01%	3.07%	29.37
F04 2867.65	0.45%	0.17%	2.61%	87.36%	0.01%	5738	4763	0.81%	1.17%	0	0.37%	20	88	0.00%	0.76%	6.23
F04 2857.40	0.34%	0.17%	2.98%	83.42%	0.02%	6018	3436	0.86%	1.56%	4	0.39%	24	139	0.01%	1.01%	4.29
F04 2846.35	0.48%	0.15%	2.72%	90.16%	0.01%	5339	5424	0.86%	0.47%	1	0.40%	18	55	0.00%	0.66%	3.29
F04 2836.70	0.32%	0.15%	2.68%	88.23%	0.01%	2392	3334	0.72%	0.42%	<LD	0.33%	10	95	0.00%	0.47%	2.33
F04 2827.30	0.55%	0.20%	3.11%	85.84%	0.01%	676	5429	0.86%	1.06%	1	0.41%	22	52	0.00%	0.43%	3.58
F04 2818.25	0.34%	0.23%	3.50%	89.63%	0.01%	1354	3665	0.93%	1.89%	<LD	0.34%	17	62	0.00%	0.41%	3.80
F04 2809.00	2.69%	0.13%	2.83%	82.08%	0.01%	2104	44972	2.49%	0.82%	<LD	0.50%	27	128	0.00%	0.43%	<LD
F04 2797.10	0.48%	0.26%	3.11%	84.05%	0.01%	977	5682	0.94%	3.47%	<LD	0.38%	22	165	0.01%	0.59%	<LD
F04 2787.80	0.39%	0.20%	2.80%	90.92%	0.01%	605	3612	0.73%	0.78%	<LD	0.41%	15	47	0.00%	0.33%	6
F04 2776.90	0.54%	0.38%	4.62%	85.01%	0.01%	970	4130	1.15%	3.53%	2	0.51%	29	55	0.00%	0.70%	6.46
L08 2861.06	0.45%	0.22%	3.17%	91.42%	0.01%	458	2279	0.81%	2.01%	<LD	0.33%	23	30	0.00%	0.43%	2.41
L08 2871.23	0.51%	0.21%	3.13%	85.71%	0.01%	302	3419	0.83%	0.98%	2	0.34%	23	81	0.00%	0.47%	5.26
L08 2881.08	0.46%	0.33%	2.95%	81.25%	0.02%	543	3170	0.83%	3.63%	7	0.30%	21	101	0.01%	0.96%	5.39
L08 2993.48	0.47%	0.16%	2.83%	93.01%	0.01%	225	3113	0.79%	0.64%	1	0.38%	19	42	0.00%	0.32%	3.22
L08 2905.26	0.52%	0.22%	3.42%	85.50%	0.01%	411	3390	0.94%	1.34%	3	0.34%	25	78	0.00%	0.44%	2.98
	Cu ppm	Zn ppm	Ga ppm	As ppm	Rb ppm	Sr ppm	Y ppm	Zr ppm	Nb ppm	Ba ppm	Ce ppm	Pb ppm	Th ppm	U ppm	total wt%	
Ben Nevis Core																
F04 2831.08	19.21	18.07	17.77	16.71	134.37	139.77	33.98	506.34	26.92	961	174.13	19.05	15.75	4.09	90.62%	
F04 2867.65	10.12	<LD	0.89	4.72	13.39	43.46	9.77	241.19	6.19	928	69.09	2.90	5.58	0.18	95.78%	
F04 2857.40	3.15	<LD	2.74	3.85	17.39	48.84	12.93	280.78	7.12	586	27.05	5.82	3.77	0.87	92.74%	
F04 2846.35	4.32	<LD	1.77	8.89	12.79	29.39	12.62	321.56	6.38	376	65.97	1.81	4.50	2.07	97.90%	
F04 2836.70	3.50	<LD	1.62	<LD	13.39	31.55	8.21	154.20	4.87	465	38.13	1.43	2.77	0.05	94.37%	
F04 2827.30	3.55	<LD	2.32	6.71	15.85	36.77	12.52	331.97	7.28	144	54.85	1.71	3.83	0.25	93.27%	
F04 2818.25	5.13	<LD	3.04	2.57	15.53	53.18	9.39	194.07	4.75	1143	43.48	3.20	2.69	<LD	98.18%	
F04 2809.00	7	<LD	<LD	<LD	17.0	38.3	12.4	330.1	7.7	167	63	<LD	<LD	<LD	97.11%	
F04 2797.10	5	<LD	<LD	<LD	16.0	73.9	9.7	220.2	5.5	153	<LD	5	<LD	<LD	94.20%	
F04 2787.80	6	<LD	<LD	<LD	12.9	36.6	11.8	353.7	7.3	108	<LD	<LD	<LD	<LD	97.16%	
F04 2776.90	5.59	3.53	2.12	<LD	23.34	111.11	15.45	379.98	8.97	600	52.66	1.73	3.72	<LD	97.28%	
L08 2861.06	3.69	0.08	3.07	<LD	16.83	53.64	8.49	199.73	5.61	141	12.17	2.32	3.60	0.40	99.26%	
L08 2871.23	3.76	1.83	1.66	<LD	16.66	38.54	9.22	176.99	6.05	150	57.64	2.15	2.54	<LD	92.69%	
L08 2881.08	2.01	<LD	1.72	<LD	18.12	69.69	7.37	186.15	4.76	162	17.20	4.47	3.32	0.46	91.26%	
L08 2993.48	2.72	<LD	2.19	8.50	15.66	28.56	10.51	240.78	6.63	132	22.50	2.42	4.03	1.80	99.05%	
L08 2905.26	4.46	0.64	1.92	0.04	18.97	39.80	7.36	146.21	5.40	181	45.39	3.65	2.84	1.30	93.24%	

	Na2O wt%	MgO wt%	Al2O3 wt%	SiO2 wt%	P2O5 wt%	S ppm	Cl ppm	K2O wt%	CaO wt%	Sc ppm	TiO2 wt%	V ppm	Cr ppm	MnO wt%	Fe2O3T wt%	Ni ppm
Ben Nevis Core																
L08 2915.88	0.55%	0.23%	3.40%	89.35%	0.01%	305	4240	0.98%	0.74%	<LD	0.34%	23	124	0.00%	0.48%	5.64
L08 2927.26	0.39%	0.13%	2.36%	85.04%	0.04%	569	3393	0.76%	2.05%	0	0.30%	17	84	0.00%	0.37%	2.49
L08 2938.08	0.46%	0.16%	2.02%	77.80%	0.01%	581	7082	0.79%	5.00%	<LD	0.27%	21	76	0.01%	0.62%	5.74
L08 2945.35	0.44%	0.25%	3.23%	83.22%	0.29%	564	2904	0.91%	2.92%	1	0.34%	26	55	0.01%	0.69%	4.66
L08 2953.55	0.52%	0.23%	3.25%	86.57%	0.01%	270	3490	0.94%	2.12%	1	0.37%	20	90	0.01%	0.48%	4.25
L08 2962.95	0.45%	0.26%	2.60%	87.32%	0.01%	319	3896	0.82%	2.13%	2	0.29%	23	93	0.00%	0.93%	2.87
L08 2972.38	0.46%	0.32%	2.99%	83.73%	0.02%	952	3318	0.90%	4.92%	4	0.29%	31	68	0.01%	1.06%	3.72
L08 2981.88	0.31%	0.13%	2.24%	86.02%	0.02%	379	1963	0.69%	2.63%	1	0.26%	25	74	0.00%	0.47%	3.25
L08 2991.54	0.47%	0.28%	3.08%	86.42%	0.02%	302	3108	0.84%	1.93%	2	0.37%	29	91	0.01%	0.68%	3.70
L08 3000.23	0.39%	0.20%	2.41%	84.13%	0.03%	419	2759	0.70%	2.67%	3	0.32%	24	68	0.01%	0.68%	2.91
L08 3010.05	0.28%	0.14%	2.04%	84.54%	0.01%	872	2446	0.63%	3.69%	2	0.27%	19	121	0.00%	0.52%	5.18
L08 3021.08	0.32%	0.35%	3.11%	85.80%	0.02%	735	1099	0.77%	2.77%	3	0.32%	30	105	0.01%	1.61%	4.61
L08 3032.0	0.50%	0.20%	2.94%	90.61%	0.01%	750	2916	0.80%	2.49%	<LD	0.32%	28	47	0.01%	0.66%	2.62
L08 3050.2	0.31%	0.10%	2.02%	82.54%	0.01%	765	2615	0.55%	2.70%	<LD	0.24%	23	66	0.00%	0.54%	4.80
L08 3060.	0.75%	0.16%	2.48%	84.17%	0.01%	901	7617	0.79%	3.25%	0	0.31%	19	77	0.00%	0.43%	3.79
	Cu ppm	Zn ppm	Ga ppm	As ppm	Rb ppm	Sr ppm	Y ppm	Zr ppm	Nb ppm	Ba ppm	Ce ppm	Pb ppm	Th ppm	U ppm	total wt%	
Ben Nevis Core																
L08 2915.88	2.52	0.52	1.69	2.39	19.14	33.31	10.42	178.87	6.20	135	54.83	4.98	2.56	0.62	96.66%	
L08 2927.26	3.58	<LD	1.15	9.44	13.81	48.25	7.57	129.16	4.78	123	44.81	2.55	2.24	0.54	91.99%	
L08 2938.08	2.21	<LD	<LD	3.74	13.46	84.66	6.18	132.92	4.22	116	60.05	2.97	2.24	1.34	88.07%	
L08 2945.35	4.43	1.33	2.45	6.18	19.08	66.23	19.52	162.35	5.67	172	69.52	5.21	8.55	1.64	92.81%	
L08 2953.55	5.19	<LD	1.48	<LD	18.60	49.21	8.83	232.51	6.07	210	19.75	2.89	3.19	0.05	95.01%	
L08 2962.95	4.41	<LD	2.10	7.05	14.81	49.22	6.99	156.38	4.56	109	28.86	5.63	2.43	<LD	95.34%	
L08 2972.38	4.45	<LD	1.86	5.64	16.32	78.14	7.23	129.66	3.96	137	51.20	3.94	3.02	2.86	95.33%	
L08 2981.88	3.19	<LD	1.19	3.67	13.25	50.69	6.20	115.60	3.61	113	20.11	2.18	1.94	1.24	93.12%	
L08 2991.54	3.11	<LD	1.38	4.63	15.57	45.46	11.87	300.24	6.38	130	51.11	5.14	4.16	0.73	94.57%	
L08 3000.23	2.68	<LD	2.99	8.02	12.67	48.46	7.29	175.47	4.50	109	34.18	2.45	2.12	0.32	91.97%	
L08 3010.05	3.57	<LD	1.10	0.06	11.21	58.53	6.07	128.13	4.00	130	10.98	0.61	2.29	1.36	92.66%	
L08 3021.08	3.66	<LD	1.24	3.26	16.09	58.22	8.46	236.55	5.41	119	49.41	2.88	5.90	0.42	95.45%	
L08 3032.0	3.28	<LD	<LD	<LD	15.87	61.44	10.02	254.13	5.40	124	64.51	4.51	2.82	0.43	99.12%	
L08 3050.2	4.48	20.58	1.22	1.98	11.08	50.82	5.86	143.45	4.19	84	51.59	3.17	2.19	0.72	89.52%	
L08 3060.	3.18	<LD	2.30	<LD	13.74	64.27	8.92	278.41	5.05	109	28.83	3.94	4.39	0.15	93.41%	

	Na2O wt%	MgO wt%	Al2O3 wt%	SiO2 wt%	P2O5 wt%	S ppm	Cl ppm	K2O wt%	CaO wt%	Sc ppm	TiO2 wt%	V ppm	Cr ppm	MnO wt%	Fe2O3T wt%	Ni ppm
Ben Nevis Core																
J22-1 2834.65	0.20%	0.12%	2.37%	84.15%	0.01%	1083	1856	0.43%	1.07%	0	0.25%	18	96	0.00%	0.42%	4.55
J22-1 2844.30	0.18%	0.12%	2.27%	88.16%	0.01%	657	2074	0.46%	1.06%	<LD	0.26%	23	99	0.00%	0.42%	3.60
J22-1 2853.95	0.19%	0.14%	2.49%	85.38%	0.01%	979	1439	0.53%	1.46%	2	0.31%	21	189	0.00%	0.45%	6.89
J22-1 2862.95	0.21%	0.10%	2.44%	89.99%	0.01%	404	963	0.47%	1.16%	3	0.48%	31	117	0.00%	0.36%	3.92
J22-1 2875.20	0.18%	0.72%	1.91%	71.35%	0.02%	689	948	0.38%	3.10%	2	0.31%	51	107	0.02%	8.76%	8.76
A17 2942.22	0.29%	0.25%	3.31%	84.88%	0.01%	925	1446	0.92%	4.50%	5	0.32%	22	108	0.01%	0.51%	5.51
A17 2962.11	0.24%	0.17%	2.92%	90.39%	0.01%	405	1854	0.81%	1.09%	3	0.30%	19	48	0.00%	0.35%	4.44
A17 2974.91	0.24%	0.23%	3.20%	86.94%	0.02%	599	1969	0.87%	2.18%	2	0.38%	16	47	0.00%	0.54%	0.49
A17 2982.56	0.17%	0.09%	2.12%	86.33%	0.04%	475	2038	0.65%	1.54%	2	0.29%	24	170	0.00%	0.34%	5.97
A17 2993.89	0.21%	0.18%	3.07%	90.33%	0.01%	453	1955	0.88%	0.48%	2	0.35%	18	77	0.00%	0.36%	4.11
A17 3002.13	0.18%	0.11%	2.19%	88.40%	0.01%	451	1781	0.68%	1.31%	1	0.29%	17	90	0.00%	0.31%	3.46
A17 3013.34	0.21%	0.12%	2.31%	86.64%	0.01%	484	1914	0.70%	0.65%	<LD	0.27%	15	88	0.00%	0.31%	2.85
A17 3023.07	0.24%	0.13%	2.40%	89.12%	0.01%	267	2902	0.74%	1.80%	2	0.26%	20	74	0.00%	0.29%	1.96
A17 3033.33	0.28%	0.12%	2.38%	91.52%	0.01%	235	4209	0.90%	1.20%	<LD	0.26%	19	79	0.00%	0.32%	4.02
A17 3045.54	0.27%	0.10%	1.74%	84.43%	0.01%	644	4579	0.64%	5.52%	<LD	0.31%	15	75	0.00%	0.37%	4.82
	Cu ppm	Zn ppm	Ga ppm	As ppm	Rb ppm	Sr ppm	Y ppm	Zr ppm	Nb ppm	Ba ppm	Ce ppm	Pb ppm	Th ppm	U ppm	total wt%	
Ben Nevis Core																
J22-1 2834.65	3.17	<LD	1.71	<LD	10.34	48.46	7.00	133.35	4.30	1494	56.54	4.00	3.47	<LD	89.70%	
J22-1 2844.30	3.78	0.40	2.35	<LD	11.03	38.17	9.66	175.25	4.72	410	28.72	2.27	1.22	<LD	93.41%	
J22-1 2853.95	4.13	<LD	1.63	0.76	13.23	59.50	7.89	184.85	5.15	1156	54.15	1.32	3.03	<LD	91.56%	
J22-1 2862.95	5.97	<LD	1.87	8.51	11.43	42.39	15.79	481.29	7.63	485	57.28	4.23	4.06	<LD	95.58%	
J22-1 2875.20	5.56	1.14	<LD	4.96	9.44	68.02	7.89	180.68	5.02	779	43.95	4.64	4.67	0.37	87.18%	
A17 2942.22	2.91	0.63	1.29	<LD	18.85	78.70	8.18	150.87	5.51	169	27.30	<LD	0.97	<LD	95.43%	
A17 2962.11	3.43	<LD	1.81	3.39	14.57	32.79	8.26	158.76	4.77	132	38.41	1.98	3.19	<LD	96.62%	
A17 2974.91	1.84	<LD	2.03	<LD	15.85	48.63	9.82	249.35	6.03	135	40.24	2.50	2.47	<LD	95.03%	
A17 2982.56	3.65	<LD	1.42	<LD	11.74	40.19	6.86	161.05	4.50	132	33.67	2.27	1.44	0.38	91.96%	
A17 2993.89	2.63	<LD	1.33	3.19	16.16	28.98	8.85	223.86	5.59	140	22.09	3.12	4.96	3.65	96.26%	
A17 3002.13	4.28	<LD	0.70	<LD	12.63	35.46	7.34	136.41	4.55	112	24.04	1.66	1.23	<LD	93.82%	
A17 3013.34	3.50	<LD	2.46	1.47	12.69	28.97	6.97	140.84	4.49	157	33.21	3.42	2.21	0.90	91.60%	
A17 3023.07	4.04	<LD	0.21	<LD	11.84	36.63	6.02	128.12	3.53	92	49.48	3.47	3.04	<LD	95.42%	
A17 3033.33	2.55	<LD	1.71	<LD	12.46	37.41	6.44	117.25	4.35	114	46.72	<LD	2.24	<LD	97.53%	
A17 3045.54	5.44	<LD	1.79	9.45	9.15	82.46	7.08	248.05	4.10	108	25.83	2.17	<LD	0.11	94.09%	

	Na2O wt%	MgO wt%	Al2O3 wt%	SiO2 wt%	P2O5 wt%	S ppm	Cl ppm	K2O wt%	CaO wt%	Sc ppm	TiO2 wt%	V ppm	Cr ppm	MnO wt%	Fe2O3T wt%	Ni ppm
Ben Nevis Core																
H20-2161.3	0.59%	0.82%	8.12%	76.90%	0.02%	2860	1944	1.54%	2.24%	7	0.51%	50	78	0.01%	1.52%	9.88
H20-2972.5	0.25%	0.68%	4.75%	51.93%	0.03%	1492	372	1.02%	26.46%	14	0.41%	41	49	0.02%	2.62%	7.70
H20-2983.7	0.40%	0.53%	5.57%	78.21%	0.01%	1534	1332	1.15%	4.49%	6	0.36%	34	77	0.01%	1.10%	8.10
H20-2995.7	0.46%	0.80%	7.88%	73.76%	0.02%	2981	1126	1.47%	3.08%	5	0.49%	51	96	0.01%	1.58%	9.86
H20 3007.8	0.33%	0.40%	4.10%	83.99%	0.01%	1176	704	0.89%	7.02%	4	0.29%	26	55	0.01%	0.69%	4.15
H20-3024	0.37%	0.37%	3.72%	85.18%	0.01%	790	1294	0.89%	5.83%	4	0.31%	21	76	0.01%	0.72%	5.36
H20-3031	0.22%	0.18%	2.36%	85.71%	0.01%	350	2146	0.76%	1.59%	<LD	0.27%	15	101	0.00%	0.57%	4.08
Hib Core																
G57-3985.3	0.48%	0.57%	4.78%	73.07%	0.03%	19297	2965	0.44%	6.71%	3	1.04%	23	343	0.02%	1.84%	6.30
G57-3990	0.26%	2.63%	2.17%	60.51%	0.03%	17359	1644	0.24%	19.43%	5	0.24%	27	377	0.07%	2.19%	54.29
G57-3995.2	0.44%	0.77%	5.68%	60.41%	0.03%	10756	2017	0.38%	14.04%	7	0.66%	32	56	0.03%	1.33%	2.29
	Cu ppm	Zn ppm	Ga ppm	As ppm	Rb ppm	Sr ppm	Y ppm	Zr ppm	Nb ppm	Ba ppm	Ce ppm	Pb ppm	Th ppm	U ppm	total wt%	
Ben Nevis Core																
H20-2161.3	2.66	1.97	4.68	<LD	34.89	78.89	13.91	298.12	8.81	219	79.97	8.01	6.29	0.91	93.29%	
H20-2972.5	7.03	<LD	2.05	<LD	27.57	412.37	10.73	204.80	6.16	173	48.77	5.77	1.24	<LD	88.70%	
H20-2983.7	5.03	<LD	2.92	2.74	25.58	93.37	9.54	159.20	5.77	190	44.68	4.83	3.65	0.10	92.42%	
H20-2995.7	6.22	1.27	3.76	11.42	34.53	86.06	11.16	187.98	7.49	225	44.06	7.29	4.70	<LD	90.49%	
H20 3007.8	2.16	<LD	3.57	6.29	19.09	114.55	7.21	114.18	4.34	164	7.99	4.21	2.82	<LD	98.16%	
H20-3024	2.30	<LD	1.02	7.51	18.84	113.90	8.69	161.77	4.79	186	33.57	4.90	3.02	<LD	97.82%	
H20-3031	2.02	<LD	2.74	1.12	13.41	41.78	6.87	119.63	4.26	155	12.32	2.87	2.15	0.46	92.04%	
Hib Core																
G57-3985.3	26.91	<LD	0.69	5.11	5.01	41.92	10.13	116.09	8.94	438	38.50	11.12	3.99	1.22	94.24%	
G57-3990	6.05	<LD	0.86	11.75	3.43	78.12	6.69	31.16	3.04	317	31.90	9.67	2.63	<LD	92.39%	
G57-3995.2	3.74	<LD	1.01	17.37	5.85	72.72	10.36	191.44	6.07	142	75.49	5.45	2.68	1.58	86.75%	

	Na2O wt%	MgO wt%	Al2O3 wt%	SiO2 wt%	P2O5 wt%	S ppm	Cl ppm	K2O wt%	CaO wt%	Sc ppm	TiO2 wt%	V ppm	Cr ppm	MnO wt%	Fe2O3T wt%	Ni ppm
Terra Nova Core																
G57-4029.3	0.13%	1.15%	2.80%	77.41%	0.03%	2959	787	0.17%	8.65%	2	0.20%	11	468	0.05%	2.35%	79.53
G57-4035.0	0.25%	0.74%	3.41%	77.85%	0.03%	3506	2563	0.24%	7.41%	4	0.18%	16	440	0.03%	1.78%	90.61
C73- 4123	0.18%	1.75%	2.46%	72.06%	0.05%	1589	1827	0.18%	14.27%	8	0.09%	10	281	0.06%	3.47%	52.34
C73-4129	0.07%	0.33%	1.47%	48.93%	0.03%	1070	514	0.14%	29.60%	15	0.15%	9	346	0.07%	1.39%	5.05
Lower Tempest Core																
G57-4594.25	0.10%	1.05%	0.57%	79.13%	0.03%	2864	1541	0.12%	12.60%	6	0.03%	11	541	0.05%	1.83%	113.43
G57-4598	0.12%	0.49%	0.69%	80.58%	0.02%	2764	1868	0.15%	12.27%	2	0.03%	6	419	0.03%	0.90%	87.22

	Cu ppm	Zn ppm	Ga ppm	As ppm	Rb ppm	Sr ppm	Y ppm	Zr ppm	Nb ppm	Ba ppm	Ce ppm	Pb ppm	Th ppm	U ppm	total wt%
Terra Nova Core															
G57-4029.3	14.67	<LD	1.07	8.91	7.47	2221.89	3.95	48.67	5.14	2348	19.61	7.77	0.27	<LD	94.38%
G57-4035.0	20.41	<LD	<LD	9.40	3.57	894.67	5.62	77.60	6.24	2604	48.70	11.93	2.83	<LD	93.56%
C73- 4123	4.05	<LD	<LD	0.33	4.16	88.75	5.20	32.87	2.49	678	21.63	6.48	1.89	0.08	95.29%
C73-4129	4.72	5.31	0.20	2.46	4.06	194.97	4.42	55.59	1.95	912	49.19	5.44	2.18	0.38	82.70%
Lower Tempest Core															
G57-4594.25	16.37	13.77	<LD	8.97	1.82	426.49	4.25	22.41	3.24	4880	22.70	17.23	<LD	<LD	97.07%
G57-4598	10.59	8.59	<LD	12.08	1.93	338.86	3.62	17.49	2.43	3850	31.98	19.79	<LD	<LD	96.72%

ppm rock	Na2O wt%	MgO wt%	Al2O3 wt%	SiO2 wt%	P2O5 wt%	S ppm	Cl ppm	K2O wt%	CaO wt%	Sc ppm	TiO2 wt%	V ppm	Cr ppm	MnO wt%	Fe2O3T wt%	Ni ppm
Eastern shoals cuttings																
N30-3075	0.73%	1.42%	11.20%	60.65%	0.05%	1540	22741	3.80%	6.16%	17	0.71%	87	94	0.02%	4.29%	22
N30-3080	0.76%	1.15%	8.76%	55.91%	0.06%	2288	37647	4.29%	12.89%	17	0.63%	76	129	0.02%	4.27%	18
N30-3085	0.74%	0.98%	7.18%	67.49%	0.04%	1883	28253	3.36%	7.20%	12	0.52%	69	76	0.02%	3.27%	14
N30-3090	0.82%	1.23%	8.29%	67.14%	0.03%	2209	32868	3.99%	9.92%	14	0.60%	74	68	0.02%	3.26%	18
N30-3095	0.78%	1.29%	8.82%	67.70%	0.04%	2004	25262	3.51%	7.30%	<LD	0.59%	75	86	0.02%	3.42%	18
N30-3100	0.73%	1.22%	8.01%	66.19%	0.04%	2381	24831	3.34%	10.47%	18	0.58%	73	86	0.02%	3.51%	21
N30-3105	0.66%	0.95%	5.80%	57.57%	0.04%	3105	40222	3.96%	17.90%	14	0.48%	67	90	0.03%	3.10%	16
N30-3110	0.70%	0.91%	7.77%	61.43%	0.03%	3060	36608	3.84%	12.95%	17	0.59%	66	90	0.02%	2.81%	14
N30-3115	0.62%	1.70%	10.68%	46.05%	0.05%	8153	26475	4.13%	17.87%	26	0.70%	103	101	0.04%	5.01%	26
H20-3325	0.63%	1.89%	13.39%	51.17%	0.06%	4344	11366	3.94%	12.29%	19	0.79%	117	107	0.03%	4.88%	33
H20-3330	0.83%	1.93%	12.65%	47.75%	0.05%	4064	15348	3.81%	10.85%	16	0.77%	109	130	0.03%	5.47%	32
J22-1-2935	1.87%	1.73%	14.50%	55.58%	0.06%	5389	17317	2.90%	1.93%	13	0.88%	106	174	0.02%	6.25%	39
J22-1-2940	0.94%	1.35%	13.28%	69.22%	0.07%	4846	12733	2.27%	2.84%	11	0.86%	103	78	0.02%	4.26%	28
J22-1-2945	0.67%	0.75%	7.42%	82.87%	0.03%	5274	12064	1.34%	3.42%	<LD	0.58%	90	55	0.01%	3.01%	18
	Cu ppm	Zn ppm	Ga ppm	As ppm	Rb ppm	Sr ppm	Y ppm	Zr ppm	Nb ppm	Ba ppm	Ce ppm	Pb ppm	Th ppm	U ppm	total wt%	
Eastern Shoals cuttings																
N30-3075	21	669	9	<LD	61.9	105.4	16.9	210.3	11.2	546	96	21	7	<LD	91.93%	
N30-3080	18	554	7	<LD	50.8	180.9	14.4	165.9	10.2	546	63	19	7	<LD	93.32%	
N30-3085	16	167	6	22	37.1	101.0	11.9	145.6	7.8	545	59	13	6	<LD	94.25%	
N30-3090	11	166	6	<LD	43.3	173.9	14.6	185.9	8.6	428	71	14	5	<LD	99.31%	
N30-3095	14	223	4	23	47.8	140.2	14.8	191.1	9.1	436	61	16	<LD	<LD	96.66%	
N30-3100	14	215	7	19	44.9	201.7	15.0	230.1	9.2	367	77	23	5	<LD	97.37%	
N30-3105	17	79	4	<LD	33.3	252.3	11.9	178.4	7.3	593	74	12	6	<LD	95.47%	
N30-3110	13	62	7	<LD	39.2	149.4	15.2	177.0	9.5	447	92	14	6	<LD	95.61%	
N30-3115	16	121	11	<LD	76.9	385.1	16.6	157.4	12.9	511	104	19	7	<LD	91.75%	
H20-3325	26	74	13	22	103.3	318.9	20.8	188.5	15.4	436	113	23	10	<LD	91.49%	
H20-3330	26	59	14	21	108.1	294.7	20.3	187.8	15.9	473	88	19	9	<LD	86.89%	
J22-1-2935	18	33	9	<LD	114.6	384.6	25.4	297.4	18.3	17584	<LD	22	7	<LD	90.92%	
J22-1-2940	15	17	5	30	87.4	343.0	26.9	348.6	17.8	12816	80	19	9	<LD	99.17%	
J22-1-2945	15	13	<LD	19	51.3	396.4	17.8	297.2	11.5	15010	<LD	18	8	<LD	104.42%	

	Na2O wt%	MgO wt%	Al2O3 wt%	SiO2 wt%	P2O5 wt%	S ppm	Cl ppm	K2O wt%	CaO wt%	Sc ppm	TiO2 wt%	V ppm	Cr ppm	MnO wt%	Fe2O3T wt%	Ni ppm
Eastern Shoals cuttings																
J22-1-2950	0.80%	0.87%	7.38%	81.51%	0.03%	4672	11373	1.36%	3.11%	<LD	0.56%	92	51	0.01%	3.92%	19
J22-1-2955	0.82%	1.78%	14.06%	63.74%	0.03%	4260	5904	2.68%	1.69%	<LD	0.82%	112	91	0.02%	4.97%	37
J22-1-2960	0.80%	1.21%	9.53%	72.91%	0.03%	5238	9896	1.79%	4.98%	<LD	0.64%	104	67	0.02%	3.78%	22
J22-1-2965	0.75%	1.11%	8.21%	62.18%	0.03%	7249	12227	1.62%	11.08%	11	0.58%	103	77	0.02%	3.82%	21
J22-1-2970	0.94%	1.57%	11.49%	67.75%	0.05%	5852	8047	2.15%	2.66%	<LD	0.74%	102	88	0.02%	4.16%	27
White Rose cuttings																
E87-2150	0.78%	2.05%	12.34%	54.88%	0.08%	6375	18641	4.13%	1.97%	19	0.70%	143	108	0.07%	5.54%	39
E87-2160	0.50%	2.06%	14.60%	58.59%	0.08%	6734	13391	3.98%	4.17%	16	0.86%	115	121	0.05%	4.89%	43
E87-2170	0.67%	1.83%	12.51%	48.61%	0.08%	17776	15405	3.73%	5.70%	14	0.72%	130	154	0.04%	6.57%	39
E87-2180	0.58%	2.08%	14.53%	57.37%	0.06%	12371	3820	3.16%	1.82%	12	0.86%	126	117	0.03%	4.93%	36
E87-2190	0.68%	1.72%	11.83%	56.30%	0.06%	12179	12054	3.16%	5.08%	16	0.79%	100	120	0.03%	4.64%	33
E87-2200	0.86%	2.02%	12.69%	57.84%	0.06%	12266	15300	3.56%	3.18%	11	0.78%	102	115	0.03%	4.89%	39
E09-3220	0.52%	1.89%	6.03%	39.27%	0.03%	8563	5277	1.21%	35.95%	21	0.45%	60	55	0.02%	2.40%	12
E09-3225	0.40%	2.00%	7.77%	34.80%	0.04%	8213	2347	1.58%	35.93%	23	0.50%	73	57	0.03%	2.97%	16
E09-3230	0.47%	2.05%	8.87%	38.03%	0.07%	7476	2759	1.77%	33.29%	22	0.58%	89	64	0.03%	3.15%	16
	Cu ppm	Zn ppm	Ga ppm	As ppm	Rb ppm	Sr ppm	Y ppm	Zr ppm	Nb ppm	Ba ppm	Ce ppm	Pb ppm	Th ppm	U ppm	total wt%	
Eastern Shoals cuttings																
J22-1-2950	13	18	<LD	<LD	52.0	345.1	18.0	286.3	10.9	12267	<LD	19	10	<LD	103.34%	
J22-1-2955	17	23	9	20	111.8	285.5	23.9	301.3	17.6	10500	83	20	9	<LD	93.59%	
J22-1-2960	15	16	<LD	19	74.0	408.6	20.4	279.4	13.3	13143	<LD	17	9	<LD	99.59%	
J22-1-2965	19	20	<LD	<LD	61.3	614.3	17.6	261.2	10.6	21154	<LD	18	6	<LD	94.94%	
J22-1-2970	16	27	<LD	<LD	89.5	345.2	24.7	330.6	16.3	14127	65	20	10	<LD	95.53%	
White Rose cuttings																
E87-2150	22	112	16	<LD	96.1	89.3	20.6	223.8	15.2	1030	133	31	11	5	86.27%	
E87-2160	31	62	17	<LD	93.8	127.8	24.5	298.1	19.3	1287	98	28	9	<LD	93.08%	
E87-2170	55	186	<LD	21	95.0	1413.2	22.6	233.7	22.2	54847	<LD	242	6	<LD	92.90%	
E87-2180	38	132	<LD	<LD	100.9	862.7	25.0	284.2	19.1	34353	<LD	164	9	<LD	92.98%	
E87-2190	40	123	<LD	26	82.2	1154.2	21.3	280.3	17.0	42546	<LD	180	<LD	<LD	93.55%	
E87-2200	41	124	<LD	<LD	89.5	975.7	23.0	264.6	18.9	37040	<LD	187	5	<LD	94.88%	
E09-3220	8.10	7.33	2.26	19.19	41.63	643.68	10.98	121.53	7.06	2940	12.90	24	4.98	2.63	90.90%	
E09-3225	13.82	10.72	6.09	7.54	57.97	781.37	11.33	95.17	7.91	3799	35.67	29	5.29	2.99	88.87%	
E09-3230	10.53	11.16	5.22	7.12	65.49	781.91	13.83	125.07	8.54	3097	41.59	23	7.55	5.34	90.95%	

	Na2O wt%	MgO wt%	Al2O3 wt%	SiO2 wt%	P2O5 wt%	S ppm	Cl ppm	K2O wt%	CaO wt%	Sc ppm	TiO2 wt%	V ppm	Cr ppm	MnO wt%	Fe2O3T wt%	Ni ppm
Whiterose cuttings																
E09-3235	0.47%	1.98%	10.81%	40.91%	0.06%	5952	2220	1.96%	27.18%	21	0.66%	104	75	0.03%	3.99%	23.18
E09-3240	0.45%	2.12%	10.35%	39.01%	0.05%	6113	1737	1.97%	30.18%	24	0.66%	108	72	0.03%	4.13%	24.05
E09-3245	0.60%	2.22%	11.21%	41.15%	0.05%	5717	3800	2.10%	25.67%	28	0.70%	124	77	0.03%	4.27%	23.84
E09-3250	0.43%	2.03%	9.13%	36.37%	0.05%	6950	1574	1.73%	32.31%	23	0.58%	98	59	0.03%	3.78%	17.77
E09-3255	0.57%	2.23%	10.36%	42.63%	0.05%	8195	5530	2.00%	27.95%	26	0.65%	99	83	0.04%	4.31%	27.98
E09-3260	0.61%	2.16%	9.82%	38.53%	0.05%	7067	7357	1.93%	29.20%	18	0.60%	100	75	0.03%	3.86%	22.81
E09-3265	0.47%	2.10%	9.68%	39.26%	0.05%	7278	3411	1.92%	29.57%	22	0.60%	100	76	0.03%	4.03%	23.52
E09-3270	0.80%	1.83%	10.34%	44.62%	0.05%	7766	8129	1.76%	22.61%	20	0.60%	132	97	0.03%	4.53%	19.79
E09-3275	0.50%	1.90%	9.35%	39.78%	0.05%	7243	3685	1.80%	29.30%	19	0.59%	109	78	0.03%	4.01%	22.77
E09-3280	0.54%	2.06%	9.76%	38.03%	0.06%	8417	9031	2.02%	29.36%	13	0.61%	104	82	0.03%	4.15%	23.66
E09-3285	0.58%	1.89%	8.46%	34.47%	0.05%	7539	10180	1.86%	32.89%	14	0.55%	103	68	0.03%	4.11%	19.40
E09-3290	0.49%	1.96%	9.00%	35.67%	0.07%	7574	6532	1.90%	30.99%	21	0.59%	115	83	0.03%	4.65%	23.64
E09-3295	0.61%	2.26%	10.78%	44.59%	0.08%	7240	5031	2.12%	22.29%	13	0.73%	127	91	0.04%	5.20%	28.18
E09-3300	0.72%	2.46%	13.32%	52.48%	0.06%	5648	3809	2.42%	14.21%	11	0.89%	125	103	0.04%	5.89%	31.58

	Cu ppm	Zn ppm	Ga ppm	As ppm	Rb ppm	Sr ppm	Y ppm	Zr ppm	Nb ppm	Ba ppm	Ce ppm	Pb ppm	Th ppm	U ppm	total wt%
White Rose cuttings															
E09-3235	12.62	12.54	8.31	19.62	76.07	709.27	15.48	125.05	10.86	3192	48.47	26.19	8.31	1.78	90.29%
E09-3240	12.59	10.73	7.43	12.79	75.30	780.69	14.07	111.05	9.61	2735	59.19	24.46	7.44	3.50	91.13%
E09-3245	11.50	15.12	8.01	15.19	82.37	727.24	15.39	135.98	11.32	2718	123.60	25.57	8.40	1.07	90.28%
E09-3250	13.21	7.62	9.51	8.48	64.34	834.61	13.34	112.40	9.00	2841	63.06	21.47	6.39	<LD	88.82%
E09-3255	15.60	61.45	9.19	11.26	74.07	821.75	14.76	134.66	10.56	5039	60.07	42.91	6.52	0.32	94.15%
E09-3260	17.70	13.31	7.02	7.05	73.19	773.87	13.09	111.19	10.07	5244	41.37	36.64	7.21	3.93	90.04%
E09-3265	13.68	14.97	7.57	24.28	73.71	821.83	13.61	113.89	10.04	3970	43.63	40.61	6.23	0.14	90.48%
E09-3270	18.22	24.29	8.18	12.69	64.85	504.99	13.57	125.85	9.83	7061	36.00	44.96	6.54	3.50	90.86%
E09-3275	17.73	16.43	9.16	11.85	68.56	1292.22	12.75	112.48	10.09	4304	59.52	34.59	5.88	<LD	90.18%
E09-3280	20.64	18.06	3.67	19.25	77.96	2107.46	13.45	106.12	10.64	11309	43.19	64.31	3.91	<LD	91.21%
E09-3285	17.23	17.81	6.15	19.07	70.35	1920.51	12.41	90.97	9.89	6519	28.20	49.89	4.69	<LD	88.81%
E09-3290	17.73	16.08	6.84	27.08	72.15	1880.05	12.88	95.14	10.11	6585	101.64	48.81	6.30	1.02	88.94%
E09-3295	15.83	20.50	10.14	31.09	84.15	1015.02	18.23	163.08	14.38	5682	47.98	45.97	9.01	1.99	91.84%
E09-3300	17.50	28.83	12.16	29.23	102.08	629.34	21.80	207.83	17.92	6359	66.89	53.79	8.03	2.77	95.20%

	Na2O wt%	MgO wt%	Al2O3 wt%	SiO2 wt%	P2O5 wt%	S ppm	Cl ppm	K2O wt%	CaO wt%	Sc ppm	TiO2 wt%	V ppm	Cr ppm	MnO wt%	Fe2O3T wt%	Ni ppm
Hibernia cuttings																
A17-3090	0.72%	1.07%	7.34%	66.28%	0.18%	4230	20256	2.89%	14.46%	11	0.86%	59	69	0.03%	2.80%	16
A17-3095	0.67%	1.09%	7.51%	77.37%	0.07%	2849	16072	2.71%	8.16%	<LD	0.78%	54	68	0.03%	2.87%	16
A17-3100	0.77%	1.42%	10.37%	69.53%	0.05%	2872	17186	3.33%	8.16%	14	0.85%	75	86	0.03%	3.60%	21
A17-3105	0.71%	1.27%	9.50%	67.34%	0.07%	3480	14978	3.01%	9.27%	13	0.85%	62	84	0.04%	3.47%	20
A17-3110	0.69%	1.27%	10.04%	62.77%	0.07%	6493	20546	3.59%	12.34%	16	0.79%	71	92	0.05%	4.26%	22
A17-3115	0.61%	1.08%	8.23%	65.29%	0.04%	6692	19139	3.09%	14.32%	11	0.71%	60	63	0.04%	3.37%	14
A17-3120	0.62%	1.17%	9.30%	55.64%	0.04%	5207	25251	3.78%	16.98%	12	0.68%	75	83	0.05%	3.42%	18
A17-3125	0.57%	1.41%	9.04%	49.32%	0.04%	4772	20856	3.37%	20.85%	20	0.65%	84	80	0.07%	4.03%	21
A17-3130	0.54%	1.14%	7.71%	53.38%	0.04%	6329	20355	3.19%	18.88%	15	0.62%	79	89	0.07%	3.60%	20
A17-3135	0.56%	1.10%	8.97%	58.22%	0.05%	6822	23312	3.51%	15.24%	<LD	0.61%	67	81	0.05%	3.25%	20
A17-3140	0.52%	1.38%	12.53%	55.93%	0.05%	13352	17948	3.94%	10.70%	14	0.72%	91	92	0.06%	4.96%	31
A17-3145	0.50%	0.83%	7.61%	74.29%	0.04%	9749	16369	2.81%	8.95%	<LD	0.54%	58	62	0.04%	3.12%	19
A17-3155	0.66%	1.03%	10.79%	66.76%	0.04%	10838	15829	3.22%	6.52%	15	0.78%	71	104	0.03%	3.56%	22
A17-3160	0.68%	0.97%	8.67%	72.56%	0.04%	7360	15678	2.80%	7.52%	11	0.74%	59	68	0.04%	2.99%	17
A17-3165	0.79%	1.15%	9.92%	70.94%	0.05%	5652	16716	3.06%	7.46%	16	0.78%	76	87	0.04%	3.41%	19
	Cu ppm	Zn ppm	Ga ppm	As ppm	Rb ppm	Sr ppm	Y ppm	Zr ppm	Nb ppm	Ba ppm	Ce ppm	Pb ppm	Th ppm	U ppm	total wt%	
Hibernia cuttings																
A17-3090	10	24	6	<LD	45.7	177.6	29.9	673.8	14.4	365	120	9	9	<LD	99.91%	
A17-3095	9	26	7	<LD	44.9	113.2	25.7	592.6	14.2	334	57	12	10	<LD	103.77%	
A17-3100	13	36	8	21	68.8	124.2	26.6	470.5	19.9	385	67	14	9	<LD	100.74%	
A17-3105	12	39	9	<LD	63.3	152.8	28.9	563.1	22.5	406	97	11	9	<LD	98.10%	
A17-3110	15	34	9	<LD	67.6	200.7	24.2	369.7	17.3	480	119	13	9	<LD	99.73%	
A17-3115	11	36	6	<LD	50.9	163.5	20.5	323.4	13.9	477	80	13	7	<LD	100.53%	
A17-3120	12	31	7	<LD	60.9	202.4	19.9	245.8	12.2	471	81	14	6	<LD	95.68%	
A17-3125	11	29	9	25	65.5	268.2	17.9	164.3	10.9	419	84	11	5	<LD	92.79%	
A17-3130	10	21	6	<LD	58.4	251.5	17.4	190.3	10.0	388	86	15	7	<LD	92.95%	
A17-3135	13	37	8	<LD	65.6	186.3	18.0	224.8	13.1	535	<LD	11	6	<LD	95.76%	
A17-3140	13	49	13	20	100.4	189.2	21.4	241.2	18.7	537	96	17	8	<LD	96.10%	
A17-3145	11	31	8	<LD	57.2	150.1	18.6	259.3	12.9	345	62	13	9	5	102.96%	
A17-3155	12	23	11	<LD	76.5	128.7	23.6	390.2	19.4	359	89	14	10	5	97.84%	
A17-3160	11	22	6	<LD	55.2	133.6	22.8	404.3	16.5	323	82	15	6	<LD	100.59%	
A17-3165	11	23	10	<LD	62.2	134.5	22.8	401.6	18.0	338	87	11	7	<LD	100.86%	

	Na2O wt%	MgO wt%	Al2O3 wt%	SiO2 wt%	P2O5 wt%	S ppm	Cl ppm	K2O wt%	CaO wt%	Sc ppm	TiO2 wt%	V ppm	Cr ppm	MnO wt%	Fe2O3T wt%	Ni ppm
Hibernia cuttings																
A17-3175	0.36%	0.38%	3.21%	69.66%	0.02%	2918	10742	1.57%	13.19%	<LD	0.33%	28	72	0.02%	1.75%	10
E87-2210	0.61%	1.88%	12.75%	61.28%	0.06%	10418	6333	3.03%	4.75%	<LD	0.78%	119	122	0.03%	4.73%	39
E87-2220	0.58%	1.84%	13.11%	62.49%	0.05%	10281	3949	2.83%	3.82%	<LD	0.81%	109	128	0.03%	4.82%	36
E87-2230	0.77%	1.81%	12.12%	61.98%	0.06%	11569	9531	2.99%	2.34%	<LD	0.82%	96	128	0.02%	4.64%	33
E87-2240	0.54%	1.60%	11.80%	65.41%	0.05%	13379	8317	3.44%	1.76%	<LD	0.75%	88	1260	0.02%	3.90%	28
E87-2250	0.53%	1.35%	11.65%	70.16%	0.04%	7981	10168	2.96%	1.24%	12	0.83%	85	359	0.03%	4.21%	26
E87-2260	0.59%	1.50%	11.06%	56.66%	0.05%	10680	10595	3.09%	8.40%	<LD	0.77%	87	451	0.04%	4.65%	25
E87-2270	0.47%	0.97%	7.72%	67.68%	0.04%	14296	11331	3.03%	2.95%	<LD	0.59%	68	2118	0.01%	3.05%	21
E87-2280	0.54%	1.10%	8.96%	74.68%	0.04%	11926	5631	2.19%	4.03%	12	0.78%	74	228	0.03%	3.48%	23
E87-2290	0.58%	1.49%	11.36%	61.81%	0.07%	12041	10131	3.09%	5.11%	<LD	0.79%	77	551	0.05%	5.03%	30
E87-2300	0.54%	1.69%	12.91%	55.86%	0.04%	14426	5386	3.11%	2.27%	17	0.81%	93	404	0.02%	4.66%	36
C17-2060	1.97%	0.65%	8.60%	76.36%	0.06%	4770	28917	2.82%	1.36%	6	1.06%	61	67	0.05%	2.66%	17.13
C17-2070	3.73%	0.44%	4.55%	49.28%	0.03%	10568	55510	2.95%	22.82%	15	0.54%	73	47	0.08%	3.09%	11.12
C17-2080	2.14%	0.66%	5.40%	52.56%	0.05%	7200	40301	3.09%	22.60%	11	0.51%	84	40	0.08%	2.88%	16.13
C17-2090	3.06%	0.67%	8.18%	59.86%	0.07%	8279	43046	3.24%	10.27%	13	0.78%	80	64	0.05%	3.24%	19.43
	Cu ppm	Zn ppm	Ga ppm	As ppm	Rb ppm	Sr ppm	Y ppm	Zr ppm	Nb ppm	Ba ppm	Ce ppm	Pb ppm	Th ppm	U ppm	total wt%	
Hibernia cuttings																
A17-3175	38	41	<LD	<LD	20.6	244.9	9.2	173.8	5.3	405	72	7	5	<LD	92.43%	
E87-2210	32	89	<LD	<LD	84.8	583.0	22.8	295.0	16.7	22304	<LD	97	7	<LD	95.83%	
E87-2220	36	96	4	<LD	86.0	600.0	22.1	305.5	17.9	23029	<LD	109	7	<LD	96.12%	
E87-2230	37	115	<LD	<LD	79.4	1020.0	23.7	345.4	18.5	37113	<LD	182	6	<LD	95.79%	
E87-2240	41	174	<LD	24	72.2	1060.5	22.5	369.8	16.9	41472	<LD	223	7	<LD	98.50%	
E87-2250	31	85	<LD	<LD	71.4	720.0	24.3	371.4	17.7	24577	<LD	145	6	<LD	99.01%	
E87-2260	30	93	<LD	<LD	70.3	849.3	22.3	316.1	16.3	30965	<LD	141	<LD	<LD	94.26%	
E87-2270	43	127	<LD	18	49.8	1126.1	17.7	282.1	12.1	45258	<LD	251	<LD	<LD	96.82%	
E87-2280	27	90	<LD	<LD	53.1	822.0	21.5	425.4	16.1	28095	<LD	127	<LD	<LD	102.75%	
E87-2290	30	99	<LD	<LD	73.5	782.1	23.6	360.6	16.3	28587	<LD	127	8	<LD	96.88%	
E87-2300	49	215	<LD	32	95.6	1506.3	23.9	292.8	18.5	55000	<LD	255	6	<LD	92.56%	
C17-2060	13.42	25.11	3.43	8.52	64.55	176.15	34.83	454.81	29.69	6396	90.58	8.78	8.73	2.60	100.53%	
C17-2070	10.67	7.20	0.53	14.69	40.57	433.82	16.71	167.13	11.90	8906	27.10	5.46	4.96	<LD	96.80%	
C17-2080	14.03	9.96	0.24	4.16	44.24	411.65	12.93	133.62	9.48	9913	38.88	7.56	4.81	<LD	97.01%	
C17-2090	10.77	16.99	6.00	10.02	67.77	280.55	18.84	229.14	16.57	8163	40.53	7.92	7.16	2.71	96.81%	

	Na2O wt%	MgO wt%	Al2O3 wt%	SiO2 wt%	P2O5 wt%	S ppm	Cl ppm	K2O wt%	CaO wt%	Sc ppm	TiO2 wt%	V ppm	Cr ppm	MnO wt%	Fe2O3T wt%	Ni ppm
Hibernia cuttings																
K19-2230	1.23%	1.32%	8.96%	51.63%	0.05%	3841	8068	1.67%	19.76%	13	0.67%	100	77	0.02%	4.97%	17
K19-2240	1.36%	1.33%	9.56%	54.87%	0.10%	5206	9635	1.62%	16.60%	16	0.69%	101	91	0.03%	4.40%	89
K19-2250	1.31%	1.19%	8.55%	57.30%	0.05%	5489	10039	1.39%	16.49%	19	0.67%	83	76	0.03%	3.80%	17
K19-2260	1.12%	1.27%	9.12%	60.34%	0.09%	5781	7705	1.47%	14.73%	13	0.72%	89	89	0.03%	4.21%	19
K19-2270	1.30%	1.04%	7.51%	58.41%	0.05%	5972	10335	1.20%	16.32%	11	0.65%	69	105	0.03%	3.72%	12
K19-2280	1.10%	0.92%	6.30%	54.89%	0.13%	5345	8420	1.00%	22.96%	17	0.62%	59	66	0.03%	3.34%	12
K19-2290	1.56%	0.96%	7.10%	51.07%	0.04%	6311	14099	1.19%	17.92%	20	0.66%	59	122	0.04%	3.30%	11
K19-2300	1.58%	1.01%	8.20%	59.82%	0.04%	5466	12934	1.34%	14.01%	13	0.72%	69	104	0.04%	3.11%	12
K19-2320	1.48%	1.17%	10.94%	61.03%	0.05%	5849	11615	1.63%	11.66%	12	0.88%	79	103	0.05%	3.47%	13
Rankin cuttings																
F04-2960	1.26%	1.90%	17.14%	54.64%	0.07%	12202	17333	4.05%	1.65%	18	0.77%	221	110	0.01%	5.49%	37.83
F04-2965	2.62%	1.04%	8.86%	65.06%	0.05%	9499	40454	3.40%	6.73%	12	0.68%	125	82	0.02%	4.04%	25.42
F04-2970	3.88%	0.59%	7.68%	60.52%	0.03%	7217	115068	7.24%	3.22%	1	0.69%	72	70	0.02%	3.39%	19.07
F04-2975	7.70%	0.00%	2.27%	22.62%	0.01%	9857	428118	31.75%	2.60%	<LD	0.52%	68	47	0.02%	3.28%	14.98
F04-2980	1.29%	0.64%	7.83%	74.27%	0.04%	10565	21932	2.27%	5.95%	2	0.73%	73	59	0.02%	3.05%	17.79
F04-2985	3.09%	0.76%	9.45%	67.55%	0.05%	11249	42417	3.14%	4.04%	11	0.76%	98	70	0.02%	4.01%	19.83
	Cu ppm	Zn ppm	Ga ppm	As ppm	Rb ppm	Sr ppm	Y ppm	Zr ppm	Nb ppm	Ba ppm	Ce ppm	Pb ppm	Th ppm	U ppm	total wt%	
Hibernia cuttings																
K19-2230	10	68	6	<LD	53.9	365.9	15.9	251.2	10.6	848	71	16	6	<LD	92.28%	
K19-2240	11	38	8	<LD	51.2	361.7	18.0	269.9	11.2	1632	96	16	6	<LD	93.16%	
K19-2250	12	29	4	<LD	42.6	368.5	16.7	296.1	11.2	3403	<LD	18	<LD	<LD	93.66%	
K19-2260	15	25	5	<LD	45.9	384.1	18.2	283.6	11.6	4340	56	25	8	<LD	95.94%	
K19-2270	14	45	<LD	<LD	35.5	387.8	17.1	306.5	11.1	5299	73	25	<LD	<LD	93.49%	
K19-2280	11	105	<LD	<LD	26.7	436.6	15.5	296.9	8.9	3953	55	17	5	<LD	94.06%	
K19-2290	13	63	<LD	<LD	27.7	325.6	11.4	196.5	9.0	8460	64	23	<LD	<LD	87.91%	
K19-2300	11	49	4	<LD	34.3	292.7	13.7	228.2	10.3	5857	67	26	<LD	<LD	93.31%	
K19-2320	11	77	7	<LD	48.6	306.5	19.2	312.8	14.9	5771	74	25	<LD	<LD	95.76%	
Rankin cuttings																
F04-2960	33.55	52.80	11.43	8.80	104.37	365.57	19.19	172.86	16.98	16748	96.99	19.62	9.13	4.33	93.81%	
F04-2965	29.08	33.65	<LD	16.89	61.84	408.35	16.82	275.31	13.52	16528	25.42	10.29	5.75	5.08	100.93%	
F04-2970	24.77	13.51	2.40	15.57	54.12	349.66	21.36	398.08	15.18	14515	62.62	6.79	6.69	4.02	102.34%	
F04-2975	73.92	12.81	<LD	16.58	44.56	354.55	18.73	355.61	14.27	12106	74.09	4.02	0.95	1.23	117.29%	
F04-2980	24.59	15.29	<LD	11.04	42.41	403.97	20.22	435.17	15.12	15236	65.17	4.46	5.24	4.87	102.78%	
F04-2985	24.72	18.42	<LD	7.77	59.11	339.37	23.33	380.10	16.11	13440	62.98	4.50	4.91	5.07	101.56%	

	Na2O wt%	MgO wt%	Al2O3 wt%	SiO2 wt%	P2O5 wt%	S ppm	Cl ppm	K2O wt%	CaO wt%	Sc ppm	TiO2 wt%	V ppm	Cr ppm	MnO wt%	Fe2O3T wt%	Ni ppm
Rankin Cuttings																
F04-2990	2.86%	0.76%	8.57%	69.15%	0.04%	12649	38535	3.06%	3.56%	7	0.71%	96	68	0.02%	3.72%	22.15
Ben Nevis cuttings																
A17-3050	0.40%	0.62%	2.20%	65.31%	0.05%	1782	18095	1.99%	26.98%	12	0.27%	26	38	0.02%	1.97%	10
A17-3055	0.49%	0.28%	2.04%	87.39%	0.03%	819	20960	2.19%	9.28%	<LD	0.29%	21	54	0.01%	1.10%	12
A17-3060	0.42%	0.42%	1.62%	72.04%	0.03%	1306	20272	1.90%	19.69%	12	0.28%	23	46	0.01%	1.66%	<LD
A17-3065	0.38%	0.31%	1.34%	63.36%	0.03%	1118	19536	1.72%	22.41%	<LD	0.25%	27	31	0.02%	1.52%	<LD
A17-3070	0.39%	0.35%	1.57%	65.95%	0.04%	1475	18483	1.73%	21.95%	13	0.25%	29	49	0.02%	1.59%	<LD
A17-3075	0.34%	0.40%	1.13%	50.85%	0.04%	2579	15111	1.21%	33.40%	13	0.23%	22	41	0.02%	1.32%	<LD
A17-3080	0.32%	0.45%	1.29%	54.37%	0.03%	2028	17409	1.52%	32.41%	16	0.21%	24	31	0.02%	1.31%	<LD
A17-3085	0.70%	1.06%	7.00%	63.99%	0.05%	3478	17576	2.66%	15.43%	17	0.70%	62	59	0.03%	2.71%	14
J22-1-2880	0.48%	0.40%	2.98%	70.83%	0.03%	5006	12726	0.60%	16.41%	<LD	0.41%	31	58	0.01%	1.86%	6
J22-1-2885	0.69%	0.39%	2.41%	61.55%	0.04%	9370	19316	0.49%	22.62%	<LD	0.34%	34	44	0.01%	1.67%	8
F04-2875	3.02%	1.19%	10.23%	57.74%	0.04%	9692	59815	5.00%	2.95%	5	0.64%	157	85	0.01%	3.93%	29.42
F04-2880	2.50%	1.42%	11.61%	62.37%	0.05%	7556	50953	4.67%	1.52%	8	0.66%	156	90	0.01%	4.17%	27.95
F04-2885	1.44%	1.03%	8.98%	72.37%	0.04%	9245	27982	3.26%	2.09%	4	0.53%	119	64	0.01%	3.01%	24.15
F04-2890	2.26%	1.17%	11.80%	58.68%	0.05%	13033	41711	4.37%	1.61%	7	0.60%	163	92	0.01%	3.91%	32.90
F04-2895	2.81%	0.97%	8.50%	67.75%	0.04%	9139	38086	3.24%	4.08%	2	0.52%	131	57	0.01%	3.15%	22.62

	Cu ppm	Zn ppm	Ga ppm	As ppm	Rb ppm	Sr ppm	Y ppm	Zr ppm	Nb ppm	Ba ppm	Ce ppm	Pb ppm	Th ppm	U ppm	total wt%
Rankin cuttings															
F04-2990	22.65	16.50	<LD	7.73	64.41	338.45	21.03	372.74	15.43	13755	24.95	10.81	7.42	4.90	101.13%
Ben Nevis cuttings															
A17-3050	18	378	<LD	<LD	14.1	187.7	6.5	116.6	3.8	1798	<LD	13	5	<LD	102.38%
A17-3055	7	104	<LD	<LD	14.7	105.7	9.1	211.0	5.1	420	<LD	7	5	<LD	105.51%
A17-3060	5	65	<LD	<LD	11.7	288.4	8.3	168.8	4.2	404	<LD	6	<LD	<LD	100.56%
A17-3065	7	170	<LD	<LD	10.8	206.1	7.2	135.5	3.8	355	54	8	<LD	<LD	93.72%
A17-3070	6	45	<LD	<LD	11.1	181.7	7.6	160.8	4.1	420	68	6	<LD	<LD	96.16%
A17-3075	5	93	<LD	<LD	8.7	282.7	6.0	120.4	2.9	377	<LD	6	<LD	<LD	91.21%
A17-3080	6	24	<LD	<LD	9.5	240.0	6.7	125.1	3.5	347	<LD	6	<LD	<LD	94.30%
A17-3085	10	22	7	<LD	44.6	176.3	20.2	412.8	12.5	356	58	9	6	<LD	97.11%
J22-1-2880	9	4	<LD	<LD	16.3	346.9	10.7	244.8	6.2	14242	<LD	8	<LD	<LD	98.21%
J22-1-2885	13	6	<LD	<LD	13.5	616.5	10.3	234.5	5.4	31989	<LD	10	<LD	<LD	98.15%
F04-2875	30.01	32.27	1.84	16.18	81.42	384.99	16.68	192.49	13.45	17559	41.08	10.25	7.17	2.53	95.26%
F04-2880	19.85	36.44	8.35	<LD	82.34	272.36	16.12	180.45	13.38	10753	85.93	10.67	7.89	0.69	97.30%
F04-2885	25.10	25.56	<LD	14.77	61.31	369.29	14.34	194.61	11.09	16775	1.55	11.00	3.60	2.37	99.87%
F04-2890	30.14	39.99	<LD	11.27	79.80	659.41	15.48	172.83	13.21	28376	<LD	7.36	2.99	3.44	95.23%
F04-2895	22.62	22.18	<LD	10.43	59.62	418.98	13.63	165.09	10.82	16380	23.37	5.83	3.83	2.73	99.11%

	Na2O wt%	MgO wt%	Al2O3 wt%	SiO2 wt%	P2O5 wt%	S ppm	Cl ppm	K2O wt%	CaO wt%	Sc ppm	TiO2 wt%	V ppm	Cr ppm	MnO wt%	Fe2O3T wt%	Ni ppm
Ben Nevis cuttings																
F04-2900	2.63%	0.77%	6.83%	68.78%	0.04%	10240	37803	2.99%	5.29%	4	0.46%	96	63	0.00%	2.64%	18.89
F04-2905	1.76%	1.98%	17.24%	60.52%	0.07%	11652	25584	4.33%	1.96%	9	0.71%	202	107	0.01%	5.21%	35.60
F04-2910	3.10%	0.92%	8.70%	69.64%	0.04%	9751	39338	3.41%	1.60%	3	0.53%	127	71	0.01%	3.19%	24.13
F04-2915	3.16%	0.65%	6.16%	77.11%	0.03%	7714	37238	2.62%	5.65%	3	0.43%	88	52	0.01%	2.20%	12.73
F04-2920	2.56%	0.96%	8.43%	65.16%	0.04%	8454	36917	3.14%	9.02%	8	0.51%	128	67	0.01%	3.19%	22.31
F04-2930	3.21%	0.83%	7.01%	58.70%	0.04%	9039	41748	2.90%	13.41%	17	0.46%	126	78	0.01%	3.24%	17.78
F04-2935	2.92%	0.41%	3.26%	50.82%	0.03%	13411	44267	2.27%	26.27%	9	0.31%	73	52	0.03%	2.69%	14.75
F04-2940	2.94%	0.48%	4.11%	52.20%	0.03%	10052	42592	2.35%	25.60%	4	0.32%	69	37	0.03%	2.26%	31.20
F04-2945	1.55%	0.74%	6.07%	47.65%	0.04%	9209	38566	3.08%	26.22%	17	0.41%	101	51	0.03%	2.96%	17.00
F04-2950	1.81%	0.77%	7.99%	47.99%	0.04%	9113	36761	3.06%	23.73%	6	0.44%	103	69	0.03%	3.13%	22.90
F04-2955	1.35%	1.34%	12.86%	52.73%	0.05%	11532	23092	3.55%	11.83%	21	0.62%	178	87	0.03%	4.72%	34.82
C17-2025	3.23%	0.53%	4.77%	52.90%	0.05%	4959	45234	2.59%	21.98%	8	0.42%	69	37	0.02%	2.93%	11.14
C17-2035	3.17%	0.31%	2.02%	41.88%	0.03%	4435	48689	1.88%	38.17%	18	0.28%	40	14	0.01%	1.36%	4.86
L08-3077.5	4.70%	0.29%	3.15%	59.41%	0.03%	3299	57807	2.05%	17.92%	11	0.31%	38	89	0.02%	2.29%	7.01
L08-3087.5	7.51%	0.00%	1.69%	48.66%	0.02%	1195	140154	5.04%	15.54%	8	0.21%	25	47	0.02%	2.02%	6.74
L08-3097.5	20.52%	0.00%	0.77%	11.45%	0.01%	2831	294297	6.92%	34.35%	13	0.12%	46	70	0.03%	2.11%	6

	Cu ppm	Zn ppm	Ga ppm	As ppm	Rb ppm	Sr ppm	Y ppm	Zr ppm	Nb ppm	Ba ppm	Ce ppm	Pb ppm	Th ppm	U ppm	total wt%
Ben Nevis cuttings															
F04-2900	28.67	18.04	<LD	10.37	50.37	665.26	11.26	145.11	9.65	26501	<LD	2.45	2.68	5.98	99.87%
F04-2905	35.56	46.18	6.71	9.42	95.24	396.87	19.36	223.96	20.79	17565	69.66	13.70	9.54	5.10	101.41%
F04-2910	33.10	24.39	<LD	5.24	62.54	362.07	14.61	182.49	11.26	16533	49.20	6.31	3.53	4.02	99.48%
F04-2915	24.21	14.56	<LD	12.39	42.95	341.43	10.54	149.01	8.61	12846	15.44	3.00	2.33	2.20	105.20%
F04-2920	26.65	24.44	2.96	18.72	59.27	349.38	13.78	152.34	12.23	13000	49.88	9.21	4.98	0.05	100.39%
F04-2930	24.16	19.24	<LD	20.66	52.74	393.80	12.00	129.11	9.29	14644	51.77	7.70	2.94	2.04	97.99%
F04-2935	24.47	8.20	<LD	11.07	24.83	539.80	7.15	96.20	5.38	16623	<LD	4.61	<LD	4.39	98.76%
F04-2940	22.10	8.90	<LD	20.96	27.13	539.49	7.07	103.58	5.74	16527	19.09	5.24	<LD	4.06	99.04%
F04-2945	22.76	14.96	<LD	7.22	39.02	520.37	8.31	98.17	6.96	17145	12.87	4.21	3.99	1.76	96.94%
F04-2950	41.83	17.23	<LD	12.33	43.02	521.47	10.03	109.77	7.60	19121	<LD	5.26	0.94	4.05	97.19%
F04-2955	51.29	35.35	4.46	11.09	74.80	399.51	14.24	131.36	12.42	15697	75.08	8.81	4.89	2.44	96.16%
C17-2025	14.48	8.70	<LD	14.54	35.72	483.25	10.55	204.22	7.31	10399	18.91	1.71	<LD	1.10	96.45%
C17-2035	9.97	1.89	<LD	<LD	15.92	562.29	6.10	103.89	4.08	9953	5.89	3.40	2.46	2.95	96.31%
L08-3077.5	16.76	394.94	1.15	7.70	19.60	228.96	8.36	160.86	4.97	849	55.49	16.26	4.90	0.45	97.00%
L08-3087.5	18.19	69.27	1.24	1.25	14.42	255.89	8.01	149.07	4.00	639	75.93	12.45	4.00	1.37	95.19%
L08-3097.5	66.17	99.85	<LD	20.89	13.40	485.02	7.81	48.38	1.99	605.78	57.89	14.70	5.94	<LD	106.18%

	Na2O wt%	MgO wt%	Al2O3 wt%	SiO2 wt%	P2O5 wt%	S ppm	Cl ppm	K2O wt%	CaO wt%	Sc ppm	TiO2 wt%	V ppm	Cr ppm	MnO wt%	Fe2O3T wt%	Ni ppm
Ben Nevis cuttings																
F20-2220	0.75%	0.91%	9.92%	71.96%	0.05%	3071	7111	1.86%	7.47%	15	0.78%	95	65	0.01%	4.06%	18
F20-2230	0.57%	0.99%	8.24%	57.47%	0.04%	3142	6309	1.71%	19.02%	17	0.69%	86	65	0.02%	3.97%	17
F20-2240	0.38%	0.55%	4.21%	51.59%	0.06%	2433	5499	0.90%	30.92%	13	0.48%	45	36	0.02%	2.60%	8
F20-2250	0.40%	0.94%	7.17%	52.21%	0.07%	3023	3818	1.45%	24.65%	13	0.63%	98	70	0.02%	4.16%	16
F20-2260	0.44%	0.93%	7.58%	52.14%	0.18%	3629	4047	1.55%	23.63%	13	0.68%	104	76	0.02%	4.54%	20
F20-2270	0.83%	1.39%	11.74%	55.12%	0.08%	3800	9968	2.33%	10.75%	17	0.85%	137	94	0.02%	5.49%	30
K19-2170	1.54%	1.47%	12.09%	55.32%	0.06%	4653	10047	2.22%	11.35%	15	0.77%	123	92	0.02%	5.22%	22
K19-2180	1.67%	1.38%	11.30%	54.38%	0.06%	4580	11597	2.11%	13.21%	16	0.74%	112	93	0.03%	5.05%	25
K19-2190	1.38%	1.49%	10.85%	54.94%	0.06%	4606	8330	2.03%	13.61%	16	0.70%	123	102	0.02%	6.57%	27
K19-2200	1.39%	1.49%	10.35%	50.26%	0.06%	5169	9711	1.90%	15.29%	17	0.67%	127	93	0.02%	6.38%	30
K19-2210	1.49%	1.36%	9.02%	48.53%	0.07%	5069	10675	1.63%	19.84%	12	0.60%	112	89	0.02%	4.92%	63
E09-2830	0.72%	1.27%	12.78%	73.76%	0.04%	3334	2564	2.18%	4.61%	4	0.80%	90	69	0.02%	3.60%	19.97
E09-2835	0.66%	1.27%	12.55%	70.05%	0.06%	3340	2341	2.16%	6.05%	5	0.81%	93	72	0.02%	3.63%	20.64
E09-2840	0.59%	1.02%	9.52%	75.86%	0.07%	3265	3150	1.73%	6.67%	7	0.67%	76	62	0.02%	3.60%	15.74
E09-2845	0.56%	1.11%	10.47%	72.35%	0.04%	4558	2430	1.87%	9.59%	4	0.69%	74	60	0.01%	3.24%	16.49
E09-2850	0.75%	0.91%	8.28%	71.68%	0.03%	4012	7917	1.55%	12.57%	10	0.63%	75	56	0.02%	2.86%	13.15

	Cu ppm	Zn ppm	Ga ppm	As ppm	Rb ppm	Sr ppm	Y ppm	Zr ppm	Nb ppm	Ba ppm	Ce ppm	Pb ppm	Th ppm	U ppm	total wt%
Ben Nevis cuttings															
F20-2220	9.15	11.88	7.14	25.17	64.27	208.03	21.27	416.42	13.58	1080.55	54.72	18.04	7.27	<LD	99.51%
F20-2230	7.97	13.58	6.42	<LD	62.43	310.60	18.74	304.47	12.30	1620.97	99.62	20.87	5.59	<LD	94.45%
F20-2240	6.07	5.45	4.13	<LD	28.75	408.23	13.50	223.03	6.84	1768.99	<LD	18.24	4.63	<LD	93.16%
F20-2250	11.03	11.91	5.22	19.64	44.89	360.00	15.74	264.35	9.81	1525.28	<LD	16.50	7.14	<LD	93.15%
F20-2260	12.74	18.04	6.36	<LD	52.84	417.89	19.39	271.26	10.23	1516.92	89.90	18.67	9.59	4.68	93.32%
F20-2270	17.09	25.88	13.03	<LD	83.65	283.94	21.84	299.66	14.99	1323.20	91.08	22.64	8.56	<LD	90.84%
K19-2170	13.82	32.99	10.33	<LD	73.50	330.42	19.65	279.00	12.98	987.43	102.46	23.99	4.69	<LD	92.51%
K19-2180	9.41	32.30	8.05	<LD	68.81	336.82	19.61	288.46	12.08	961.64	75.54	14.33	5.14	<LD	92.50%
K19-2190	13.44	24.32	8.72	18.66	64.43	353.29	18.68	299.75	11.67	865.44	59.29	20.23	5.13	<LD	93.89%
K19-2200	18.83	60.40	7.90	19.32	60.01	359.43	16.96	261.64	11.09	1250.01	97.23	25.24	6.66	<LD	90.38%
K19-2210	11.85	26.52	6.17	<LD	50.37	372.45	14.26	220.48	9.57	1159.43	90.54	16.62	7.16	<LD	90.08%
E09-2830	14.24	19.73	9.86	13.94	77.92	289.59	22.80	362.56	15.32	4404	70.69	39.41	10.06	3.47	101.51%
E09-2835	12.43	19.54	8.09	8.23	78.53	325.99	21.39	338.99	15.70	3676	92.92	40.21	9.26	1.73	98.88%
E09-2840	8.78	11.73	5.81	5.62	55.32	347.13	19.62	336.92	11.89	3455	77.06	32.26	6.08	3.84	101.40%
E09-2845	11.58	12.62	6.33	13.51	63.39	514.74	18.44	315.04	12.69	3965	99.20	35.72	6.72	0.45	101.91%
E09-2850	11.01	12.80	4.34	19.62	49.94	548.18	17.40	328.58	10.95	3922	73.65	40.07	5.01	0.10	101.67%

	Na2O wt%	MgO wt%	Al2O3 wt%	SiO2 wt%	P2O5 wt%	S ppm	Cl ppm	K2O wt%	CaO wt%	Sc ppm	TiO2 wt%	V ppm	Cr ppm	MnO wt%	Fe2O3T wt%	Ni ppm
Ben Nevis cuttings																
E09-2855	0.56%	1.08%	9.48%	68.99%	0.06%	3503	2642	1.74%	12.10%	11	0.68%	80	61	0.02%	3.05%	16.11
E09-2860	0.49%	0.92%	7.25%	67.98%	0.06%	4380	4969	1.42%	16.31%	11	0.58%	65	53	0.01%	2.67%	14.54
E09-2865	0.65%	1.11%	9.27%	68.22%	0.05%	4004	6565	1.75%	11.91%	6	0.66%	79	62	0.02%	3.26%	19.47
E09-2870	0.69%	0.90%	8.06%	73.99%	0.05%	4419	8009	1.62%	10.40%	11	0.62%	76	66	0.02%	2.74%	16.80
E09-2875	0.55%	0.90%	7.80%	72.82%	0.05%	4268	4731	1.59%	12.19%	13	0.63%	72	64	0.02%	3.41%	16.25
E09-2880	0.72%	0.87%	8.56%	81.23%	0.06%	4064	7301	1.73%	5.78%	10	0.64%	70	54	0.01%	2.56%	11.45
E09-2885	0.59%	0.86%	8.36%	81.87%	0.04%	4694	4374	1.64%	7.51%	9	0.62%	65	57	0.01%	2.42%	15.40
E09-2895	0.61%	0.87%	8.63%	83.30%	0.03%	3751	3930	1.74%	4.89%	8	0.63%	67	57	0.02%	2.81%	13.73
E09-2900	0.68%	0.98%	9.12%	80.03%	0.06%	4224	5989	1.75%	7.80%	11	0.64%	83	53	0.01%	2.78%	14.69
E09-2905	0.60%	1.00%	9.53%	81.33%	0.03%	3839	5593	1.91%	4.75%	9	0.68%	71	60	0.01%	2.87%	17.50
E09-2910	0.58%	0.85%	8.83%	84.46%	0.02%	3553	4631	1.80%	3.96%	7	0.65%	64	73	0.01%	2.42%	16.69
E09-2915	0.59%	0.85%	8.58%	84.40%	0.03%	4154	6768	1.71%	4.11%	11	0.66%	66	52	0.02%	2.68%	16.13
E09-2920	0.52%	0.83%	8.19%	83.46%	0.04%	3308	2916	1.64%	6.05%	7	0.65%	66	56	0.01%	2.52%	12.26
E09-2925	0.53%	0.83%	7.93%	81.41%	0.04%	3357	3719	1.61%	8.28%	10	0.64%	59	56	0.01%	2.66%	14.24
E09-2930	0.65%	0.85%	6.98%	74.46%	0.05%	5561	9449	1.44%	11.34%	16	0.57%	63	60	0.02%	3.46%	14.91
E09-2935	0.76%	1.05%	9.37%	75.04%	0.10%	4496	7575	1.94%	5.62%	7	0.77%	93	79	0.02%	4.25%	19.37

	Cu ppm	Zn ppm	Ga ppm	As ppm	Rb ppm	Sr ppm	Y ppm	Zr ppm	Nb ppm	Ba ppm	Ce ppm	Pb ppm	Th ppm	U ppm	total wt%
Ben Nevis cuttings															
E09-2855	11.84	12.30	5.84	4.68	59.87	559.14	18.41	299.97	12.12	3971	108.12	33.96	8.19	0.04	99.51%
E09-2860	11.52	10.59	2.48	18.84	45.56	652.60	14.81	266.65	10.25	4905	75.68	40.87	6.08	3.56	100.01%
E09-2865	13.88	13.53	6.19	17.83	62.67	480.73	19.97	306.02	12.64	4764	86.63	41.88	9.30	0.64	99.24%
E09-2870	10.20	13.35	2.99	11.76	51.78	447.45	18.92	298.73	11.03	5881	90.99	47.87	5.10	1.15	101.80%
E09-2875	11.45	11.42	2.88	7.87	51.59	413.16	16.26	271.51	11.46	4942	73.13	43.15	6.82	0.77	102.18%
E09-2880	9.02	10.74	6.13	19.95	53.24	252.57	18.27	336.69	11.68	3880	81.96	39.23	7.64	0.83	104.47%
E09-2885	8.20	9.92	5.19	7.74	51.09	275.70	17.03	305.21	10.83	3811	73.84	42.14	8.53	1.79	106.08%
E09-2895	11.32	12.74	5.19	8.58	55.60	235.86	17.86	303.12	11.65	3980	68.62	38.25	6.00	0.07	105.41%
E09-2900	13.70	11.96	4.64	9.34	56.06	330.50	17.33	272.54	11.90	4882	72.91	43.03	6.66	0.32	106.18%
E09-2905	8.88	12.93	6.35	7.13	61.34	242.99	18.70	336.85	12.62	4338	59.91	40.30	7.98	1.09	104.83%
E09-2910	11.13	10.30	7.42	9.01	57.43	215.73	18.96	312.09	11.66	3775	56.38	33.41	4.89	2.66	105.48%
E09-2915	11.52	11.52	5.19	11.33	53.64	259.60	17.43	308.95	12.04	5677	33.47	47.91	8.62	5.78	106.08%
E09-2920	10.05	10.24	4.62	3.58	51.70	223.31	17.29	309.03	11.54	3142	72.18	33.29	5.87	4.03	105.49%
E09-2925	8.21	10.32	5.83	15.15	50.26	289.63	17.20	306.27	11.55	4095	70.91	41.64	5.20	1.53	105.73%
E09-2930	12.73	11.02	4.13	11.59	44.37	455.14	15.24	234.12	9.90	9846	46.90	69.63	7.39	3.96	103.38%
E09-2935	11.58	14.33	3.63	6.32	62.62	292.08	21.73	339.37	14.21	5282	47.33	45.88	9.24	3.29	101.53%

	Na2O wt%	MgO wt%	Al2O3 wt%	SiO2 wt%	P2O5 wt%	S ppm	Cl ppm	K2O wt%	CaO wt%	Sc ppm	TiO2 wt%	V ppm	Cr ppm	MnO wt%	Fe2O3T wt%	Ni ppm
Ben Nevis cuttings																
E09-2940	0.70%	1.09%	10.46%	80.84%	0.07%	4479	5283	2.09%	3.96%	14	0.77%	72	62	0.01%	3.22%	20.86
E09-2955	0.86%	1.60%	12.02%	56.28%	0.10%	5975	7825	2.03%	5.31%	12	0.72%	171	105	0.02%	5.62%	40.54
E09-2960	0.76%	1.40%	10.07%	64.12%	0.05%	5718	6524	1.70%	12.05%	7	0.59%	105	226	0.04%	5.94%	45.19
E09-2965	0.40%	0.50%	4.50%	85.04%	0.02%	2184	4225	0.99%	5.00%	5	0.38%	33	55	0.01%	1.87%	9.60
E09-2970	0.44%	0.52%	4.84%	80.33%	0.02%	2105	3162	1.04%	5.08%	9	0.42%	37	95	0.01%	1.28%	4.36
E09-2975	0.38%	0.49%	4.90%	85.14%	0.02%	2254	3492	1.09%	4.26%	5	0.46%	38	41	0.01%	1.58%	6.23
E09-2980	0.45%	0.47%	4.55%	77.09%	0.02%	2139	4434	1.03%	6.45%	6	0.41%	27	59	0.01%	1.22%	4.42
E09-2985	0.30%	0.38%	3.33%	84.64%	0.01%	1842	2804	0.81%	7.41%	7	0.37%	26	30	0.01%	1.22%	6.98
E09-2990	0.26%	0.38%	2.91%	75.25%	0.02%	1649	2620	0.72%	9.24%	3	0.36%	25	71	0.01%	1.26%	6.09
E09-2995	0.30%	0.33%	2.65%	82.00%	0.04%	1646	3794	0.66%	9.42%	7	0.31%	23	39	0.01%	1.15%	5.75
E09-3000	0.30%	0.32%	2.88%	81.37%	0.02%	1992	4509	0.74%	9.09%	2	0.32%	24	38	0.01%	1.14%	4.81
E09-3005	0.31%	0.41%	3.60%	77.70%	0.02%	1457	2139	0.82%	8.81%	5	0.36%	23	73	0.01%	1.04%	5.29
E09-3010	0.28%	0.54%	4.22%	71.02%	0.03%	1905	1424	0.92%	15.54%	3	0.42%	38	48	0.01%	1.69%	6.10
E09-3015	0.33%	0.57%	4.76%	64.74%	0.02%	2087	2050	1.01%	15.32%	9	0.42%	41	100	0.01%	1.52%	5.55
E09-3020	0.34%	0.67%	4.83%	71.87%	0.02%	2320	2158	0.98%	11.25%	6	0.39%	36	39	0.01%	1.88%	6.09
E09-3025	0.35%	0.52%	4.40%	74.66%	0.03%	2498	2646	0.98%	9.80%	10	0.38%	42	81	0.01%	1.47%	5.28

	Cu ppm	Zn ppm	Ga ppm	As ppm	Rb ppm	Sr ppm	Y ppm	Zr ppm	Nb ppm	Ba ppm	Ce ppm	Pb ppm	Th ppm	U ppm	total wt%
Ben Nevis cuttings															
E09-2940	9.63	12.17	6.35	9.82	66.90	228.58	21.76	394.16	16.38	4085	89.73	44.46	10.11	2.84	105.46%
E09-2955	30.15	38.82	15.06	10.34	90.45	238.63	19.51	192.05	14.75	3538	101.49	32.45	9.61	3.32	87.37%
E09-2960	38.93	24.08	5.03	5.26	57.54	393.66	13.35	179.05	12.05	5838	43.23	65.82	6.65	3.13	99.62%
E09-2965	5.64	4.22	2.32	8.34	24.83	140.78	9.48	161.92	6.16	3316	33.01	20.24	3.63	0.91	100.12%
E09-2970	4.82	1.32	1.01	1.94	23.02	131.78	9.00	188.99	5.98	2992	45.35	11.93	3.74	1.33	95.23%
E09-2975	4.84	3.30	2.70	5.00	26.06	150.87	11.02	228.84	6.88	3634	48.57	18.13	4.00	1.86	99.73%
E09-2980	6.80	1.54	1.19	7.09	21.79	152.58	9.06	201.59	6.26	3267	29.97	15.57	3.22	1.76	93.10%
E09-2985	5.49	<LD	1.04	5.33	18.06	148.10	8.64	199.61	4.82	3063	13.01	18.03	3.06	1.18	99.62%
E09-2990	5.57	0.85	<LD	2.10	15.74	155.97	7.23	164.89	4.99	3409	66.97	15.67	3.19	1.05	91.53%
E09-2995	3.78	<LD	0.19	7.91	15.20	173.68	7.41	141.64	4.65	3575	73.15	15.47	0.45	<LD	98.12%
E09-3000	3.43	<LD	0.21	12.76	16.42	177.23	7.01	135.26	4.26	4040	33.08	17.16	2.46	2.57	97.65%
E09-3005	3.27	<LD	1.93	4.92	17.68	148.73	9.10	168.08	5.72	2219	9.54	11.66	4.29	<LD	93.97%
E09-3010	5.15	1.63	1.27	5.62	21.93	302.63	8.62	177.13	5.34	2201	40.35	11.19	4.28	2.95	95.61%
E09-3015	5.05	<LD	1.72	7.25	22.42	289.57	9.09	170.21	5.17	2258	36.51	8.91	2.10	1.83	89.80%
E09-3020	4.53	1.44	0.19	8.99	21.41	234.48	7.93	161.30	4.97	3374	53.44	26.24	4.78	2.07	93.50%
E09-3025	4.19	<LD	1.31	11.97	21.37	205.65	8.41	168.57	5.06	2194	48.17	14.35	3.68	0.83	93.81%

	Na2O wt%	MgO wt%	Al2O3 wt%	SiO2 wt%	P2O5 wt%	S ppm	Cl ppm	K2O wt%	CaO wt%	Sc ppm	TiO2 wt%	V ppm	Cr ppm	MnO wt%	Fe2O3T wt%	Ni ppm
Ben Nevis cuttings																
E09-3030	0.37%	0.56%	5.02%	78.19%	0.03%	2145	1626	1.15%	10.01%	2	0.41%	42	66	0.01%	1.43%	8.46
E09-3035	0.32%	0.42%	3.64%	77.82%	0.02%	1776	2170	0.84%	11.14%	9	0.34%	33	50	0.01%	1.18%	3.88
E09-3040	0.36%	0.41%	3.70%	90.48%	0.02%	1755	3216	0.86%	7.42%	4	0.43%	28	36	0.01%	1.19%	10.05
Avalon cuttings																
H20-3180	0.42%	0.45%	3.87%	73.97%	0.05%	4235	13807	1.90%	12.15%	<LD	0.37%	44	63	0.01%	2.02%	12
H20-3185	0.47%	0.35%	1.88%	65.84%	0.03%	2063	21655	1.79%	19.39%	13	0.24%	30	118	0.02%	1.76%	10
H20-3190	0.80%	0.49%	2.98%	62.33%	0.04%	1665	23835	2.16%	15.86%	<LD	0.31%	42	99	0.02%	2.14%	32
H20-3195	0.40%	0.43%	2.74%	63.99%	0.03%	1635	11385	1.42%	15.40%	<LD	0.28%	29	92	0.02%	1.90%	28
H20-3200	0.48%	0.50%	3.56%	67.82%	0.03%	1595	15451	1.80%	11.93%	<LD	0.31%	32	115	0.02%	2.05%	51
H20-3205	0.46%	0.57%	4.07%	68.53%	0.03%	1761	14274	1.95%	14.92%	11	0.38%	48	95	0.02%	2.52%	73
H20-3210	0.29%	0.33%	2.05%	64.03%	0.02%	1424	10044	1.19%	20.95%	<LD	0.26%	21	63	0.02%	1.54%	22
H20-3215	0.39%	0.35%	2.50%	71.13%	0.02%	1377	12982	1.40%	12.76%	<LD	0.27%	27	97	0.02%	1.81%	92
H20-3220	0.46%	0.37%	1.98%	68.45%	0.02%	1256	17277	1.58%	14.33%	<LD	0.23%	16	101	0.02%	1.85%	28
H20-3225	0.63%	0.39%	2.88%	68.11%	0.02%	1107	18549	1.65%	10.63%	<LD	0.26%	30	140	0.02%	2.11%	52
H20-3230	0.54%	0.40%	2.46%	67.18%	0.03%	1616	13199	1.30%	16.07%	11	0.27%	25	122	0.02%	2.32%	153
H20-3235	0.68%	0.52%	3.66%	65.91%	0.03%	1596	17789	1.93%	11.88%	<LD	0.32%	29	173	0.03%	2.76%	184
	Cu ppm	Zn ppm	Ga ppm	As ppm	Rb ppm	Sr ppm	Y ppm	Zr ppm	Nb ppm	Ba ppm	Ce ppm	Pb ppm	Th ppm	U ppm	total wt%	
Ben Nevis cuttings																
E09-3030	4.96	0.41	1.94	8.81	26.42	225.97	9.87	198.12	5.64	1886	36.45	12.13	2.33	1.80	98.17%	
E09-3035	4.32	<LD	<LD	1.99	18.67	223.46	7.98	173.23	4.94	2502	65.30	11.53	4.33	3.07	96.75%	
E09-3040	4.88	1.97	1.83	4.79	21.81	200.85	11.35	243.30	6.36	2705	28.87	16.74	1.87	2.09	106.02%	
Avalon cuttings																
H20-3180	18	74	<LD	<LD	23.6	233.8	10.8	210.6	6.3	291	72	10	5	<LD	97.79%	
H20-3185	43	40	<LD	<LD	12.5	250.5	6.5	105.0	3.3	496	68	12	<LD	<LD	94.59%	
H20-3190	40	2033	<LD	<LD	16.4	193.7	6.9	127.6	4.0	903	59	89	<LD	<LD	90.37%	
H20-3195	34	474	<LD	<LD	14.8	197.7	7.0	110.3	4.0	671	68	24	<LD	<LD	88.36%	
H20-3200	19	229	<LD	<LD	19.5	158.6	8.5	124.3	4.9	655	<LD	11	<LD	<LD	90.63%	
H20-3205	39	181	<LD	<LD	23.8	215.4	10.7	162.0	6.3	922	<LD	12	5	<LD	95.53%	
H20-3210	16	60	<LD	<LD	12.3	279.4	8.0	132.1	3.8	311	<LD	6	<LD	<LD	92.15%	
H20-3215	99	121	<LD	<LD	12.9	158.8	8.5	150.3	4.5	429	<LD	11	<LD	<LD	92.45%	
H20-3220	53	241	<LD	<LD	10.3	304.3	5.6	105.1	3.4	727	<LD	16	<LD	<LD	91.52%	
H20-3225	52	243	<LD	<LD	15.9	132.0	7.0	128.9	4.5	399	<LD	12	<LD	<LD	89.00%	
H20-3230	157	383	<LD	<LD	15.7	194.7	7.0	122.8	5.0	516	<LD	17	<LD	<LD	92.56%	
H20-3235	43	1881	5	<LD	20.3	179.9	8.2	161.4	6.2	628	71	28	<LD	<LD	90.32%	

	Na2O wt%	MgO wt%	Al2O3 wt%	SiO2 wt%	P2O5 wt%	S ppm	Cl ppm	K2O wt%	CaO wt%	Sc ppm	TiO2 wt%	V ppm	Cr ppm	MnO wt%	Fe2O3T wt%	Ni ppm
Avalon cuttings																
H20-3240	0.50%	0.33%	2.52%	69.04%	0.02%	1847	23020	1.98%	12.41%	<LD	0.30%	25	134	0.02%	1.70%	48
H20-3245	0.37%	0.37%	2.94%	67.87%	0.02%	2977	13045	1.54%	14.17%	<LD	0.32%	28	100	0.01%	1.50%	25
H20-3250	0.38%	0.40%	2.92%	62.86%	0.04%	3875	13519	1.65%	18.77%	<LD	0.35%	29	83	0.01%	1.62%	25
H20-3255	0.36%	0.41%	3.10%	66.18%	0.04%	3981	11801	1.58%	16.44%	11	0.33%	30	73	0.02%	1.59%	16
H20-3260	0.51%	0.38%	2.54%	64.91%	0.03%	3483	15823	1.54%	19.78%	11	0.29%	24	87	0.02%	1.60%	15
H20-3265	0.41%	0.46%	4.09%	71.93%	0.03%	3985	13321	1.80%	9.96%	12	0.36%	34	139	0.01%	1.69%	13
H20-3270	0.48%	0.45%	4.05%	73.72%	0.02%	3999	12496	1.83%	9.39%	<LD	0.37%	37	66	0.01%	1.70%	15
H20-3275	0.55%	0.46%	4.17%	78.10%	0.02%	4173	14159	1.91%	6.61%	<LD	0.37%	33	81	0.01%	1.63%	11
H20-3280	0.48%	0.43%	3.14%	73.97%	0.03%	2476	15143	1.70%	10.14%	<LD	0.30%	23	97	0.02%	1.54%	16
H20-3285	0.50%	0.34%	1.92%	73.61%	0.03%	1532	17091	1.47%	13.14%	<LD	0.21%	17	69	0.01%	1.29%	14
H20-3290	0.44%	0.28%	1.75%	75.53%	0.02%	1097	18810	1.50%	10.28%	<LD	0.20%	12	110	0.01%	1.02%	12
H20-3295	0.42%	0.31%	1.90%	72.99%	0.02%	989	16313	1.45%	10.22%	<LD	0.20%	16	94	0.01%	1.06%	7
H20-3300	0.36%	0.36%	1.93%	67.11%	0.02%	1143	13631	1.30%	17.02%	<LD	0.23%	22	91	0.01%	1.45%	12
H20-3305	0.49%	0.31%	2.17%	77.74%	0.02%	1110	19539	1.65%	8.76%	<LD	0.23%	17	90	0.01%	1.11%	11
H20-3310	0.48%	0.32%	2.06%	71.86%	0.02%	1030	17879	1.51%	11.49%	<LD	0.23%	18	107	0.01%	1.19%	11
	Cu ppm	Zn ppm	Ga ppm	As ppm	Rb ppm	Sr ppm	Y ppm	Zr ppm	Nb ppm	Ba ppm	Ce ppm	Pb ppm	Th ppm	U ppm	total wt%	
Avalon cuttings																
H20-3240	59	99	<LD	<LD	15.1	174.8	8.2	154.0	4.7	365	<LD	6	<LD	<LD	91.73%	
H20-3245	35	44	<LD	<LD	19.3	239.2	9.7	180.7	5.8	399	<LD	6	<LD	<LD	91.28%	
H20-3250	24	36	<LD	<LD	19.1	322.8	10.1	213.1	5.9	313	<LD	9	<LD	<LD	91.46%	
H20-3255	67	67	<LD	<LD	18.5	279.2	8.7	173.5	5.1	324	69	7	<LD	<LD	92.35%	
H20-3260	72	60	<LD	<LD	14.7	332.3	7.9	155.2	4.7	343	86	10	<LD	<LD	94.20%	
H20-3265	90	25	<LD	<LD	20.9	153.8	9.3	176.2	5.7	287	<LD	7	5	<LD	93.20%	
H20-3270	104	46	<LD	<LD	23.4	145.2	11.0	198.3	6.9	314	61	7	<LD	<LD	94.41%	
H20-3275	26	18	<LD	<LD	21.1	108.8	10.9	193.8	6.6	296	67	9	5	<LD	96.40%	
H20-3280	39	113	<LD	<LD	16.1	127.8	8.0	145.1	5.2	310	<LD	9	<LD	<LD	93.99%	
H20-3285	33	57	<LD	<LD	11.1	161.3	6.0	85.7	3.6	363	<LD	<LD	<LD	<LD	94.71%	
H20-3290	36	17	<LD	<LD	9.1	105.6	6.6	72.1	3.2	302	<LD	<LD	<LD	<LD	93.27%	
H20-3295	30	20	<LD	<LD	9.7	113.9	6.0	89.1	3.6	357	<LD	<LD	<LD	<LD	90.57%	
H20-3300	24	15	<LD	18	10.1	201.8	6.4	96.1	3.3	323	<LD	9	<LD	<LD	91.56%	
H20-3305	19	15	<LD	<LD	11.3	109.2	6.1	98.0	3.8	316	<LD	<LD	<LD	<LD	94.82%	
H20-3310	32	87	<LD	<LD	11.2	126.0	6.1	102.1	3.8	377	<LD	8	<LD	<LD	91.35%	

	Na2O wt%	MgO wt%	Al2O3 wt%	SiO2 wt%	P2O5 wt%	S ppm	Cl ppm	K2O wt%	CaO wt%	Sc ppm	TiO2 wt%	V ppm	Cr ppm	MnO wt%	Fe2O3T wt%	Ni ppm
Avalon cuttings																
H20-3315	0.39%	0.34%	1.76%	62.29%	0.02%	1302	15588	1.33%	21.25%	11	0.22%	26	86	0.02%	1.39%	<LD
H20-3320	0.35%	0.37%	1.18%	40.85%	0.03%	1719	15390	1.23%	36.11%	18	0.15%	23	109	0.04%	2.01%	8
J22-1-2890	0.97%	0.39%	3.01%	59.93%	0.06%	10225	20592	0.58%	22.43%	17	0.35%	42	46	0.01%	1.98%	9
J22-1-2895	2.04%	0.44%	5.19%	68.08%	0.02%	8466	40398	0.99%	6.36%	<LD	0.48%	57	116	0.01%	2.92%	14
J22-1-2900	1.08%	0.53%	5.27%	78.33%	0.09%	5817	19025	0.95%	6.26%	<LD	0.49%	66	42	0.01%	3.36%	13
J22-1-2905	0.85%	0.53%	6.14%	85.00%	0.03%	5061	12388	1.04%	2.33%	<LD	0.52%	48	49	0.00%	2.61%	9
J22-1-2910	0.61%	0.55%	7.40%	75.96%	0.02%	5679	10935	1.27%	3.90%	<LD	0.69%	57	58	0.01%	2.49%	16
J22-1-2920	0.73%	1.06%	7.99%	46.35%	0.20%	4812	12580	1.53%	9.32%	14	0.65%	354	164	0.03%	17.86%	49
A mrk mbr cuttings																
H20-3335	0.88%	1.93%	11.32%	43.70%	0.06%	4482	16378	3.58%	15.70%	21	0.74%	134	114	0.05%	5.97%	31
H20-3340	0.49%	1.19%	5.20%	32.66%	0.04%	5120	16747	2.33%	39.20%	22	0.44%	58	60	0.04%	3.19%	12
H20-3345	0.43%	1.22%	5.25%	33.53%	0.04%	5194	8100	1.73%	40.20%	18	0.44%	63	82	0.04%	3.01%	19
H20-3350	0.36%	0.87%	3.20%	25.82%	0.03%	5129	17080	1.91%	45.10%	27	0.25%	49	67	0.03%	2.60%	11
H20-3355	0.35%	0.90%	3.17%	25.91%	0.04%	4406	13958	1.67%	44.88%	24	0.26%	65	72	0.03%	2.90%	9
H20-3360	0.36%	0.77%	1.95%	20.88%	0.03%	4400	21111	1.72%	49.06%	17	0.18%	70	47	0.03%	2.88%	10
H20-3365	0.30%	0.78%	2.18%	22.62%	0.03%	5172	12721	1.33%	49.97%	21	0.20%	58	55	0.03%	2.53%	8
	Cu ppm	Zn ppm	Ga ppm	As ppm	Rb ppm	Sr ppm	Y ppm	Zr ppm	Nb ppm	Ba ppm	Ce ppm	Pb ppm	Th ppm	U ppm	total wt%	
Avalon cuttings																
H20-3315	19	37	<LD	<LD	10.1	240.6	6.1	84.2	3.5	461	56	7	<LD	<LD	91.03%	
H20-3320	23	18	<LD	<LD	7.5	340.8	6.9	59.7	2.4	312	69	<LD	<LD	<LD	84.39%	
J22-1-2890	16	6	<LD	<LD	17.3	746.5	10.9	224.6	6.4	33982	<LD	6	<LD	<LD	98.24%	
J22-1-2895	18	9	<LD	<LD	37.3	566.9	14.1	290.6	9.5	26819	<LD	10	<LD	<LD	95.81%	
J22-1-2900	11	7	<LD	<LD	34.0	386.0	16.7	298.1	9.1	13908	<LD	10	<LD	<LD	101.40%	
J22-1-2905	11	7	<LD	<LD	39.4	323.2	17.5	333.4	10.8	12433	<LD	9	<LD	<LD	103.06%	
J22-1-2910	15	8	<LD	<LD	53.5	360.2	23.9	467.3	14.7	13575	<LD	12	6	<LD	97.08%	
J22-1-2920	17	50	<LD	72	60.5	397.3	21.0	333.5	13.3	15945	<LD	38	11	<LD	90.18%	
A mrk mbr cuttings																
H20-3335	26	39	12	42	95.1	426.3	22.6	184.4	14.0	381	104	18	9	<LD	86.90%	
H20-3340	34	18	5	27	37.8	800.0	13.3	133.3	5.9	386	83	12	6	<LD	87.94%	
H20-3345	66	16	<LD	20	35.6	709.5	13.7	137.3	6.7	247	61	10	5	<LD	88.20%	
H20-3350	93	15	<LD	28	24.0	847.6	8.9	53.0	3.2	303	<LD	10	5	<LD	83.36%	
H20-3355	53	50	<LD	30	22.3	954.6	10.5	68.6	4.0	271	<LD	9	<LD	<LD	82.80%	
H20-3360	77	14	<LD	25	14.4	1046.5	8.3	42.0	2.5	271	<LD	11	<LD	<LD	81.27%	
H20-3365	71	13	<LD	23	18.1	1163.9	8.4	46.1	3.5	281	<LD	7	<LD	<LD	82.76%	

	Na2O wt%	MgO wt%	Al2O3 wt%	SiO2 wt%	P2O5 wt%	S ppm	Cl ppm	K2O wt%	CaO wt%	Sc ppm	TiO2 wt%	V ppm	Cr ppm	MnO wt%	Fe2O3T wt%	Ni ppm
A-mrk mbr cuttings																
H20-3370	0.62%	1.15%	4.55%	31.82%	0.03%	6193	19542	2.19%	39.11%	26	0.37%	60	70	0.03%	2.81%	14
H20-3375	0.38%	1.30%	4.85%	34.52%	0.04%	6013	8295	1.81%	39.65%	19	0.39%	48	65	0.03%	2.63%	13
E09-3045	0.29%	0.33%	3.22%	92.19%	0.02%	1586	1873	0.78%	6.82%	5	0.40%	30	41	0.01%	1.13%	9.15
E09-3050	0.23%	0.40%	2.90%	80.90%	0.03%	2074	3318	0.66%	12.61%	10	0.31%	38	146	0.02%	2.48%	10.20
E09-3055	0.24%	0.26%	1.76%	79.98%	0.03%	1617	4772	0.46%	16.73%	4	0.25%	17	29	0.01%	1.04%	4.61
E09-3060	0.24%	0.30%	2.25%	81.78%	0.02%	1875	2781	0.56%	15.20%	4	0.29%	21	70	0.01%	1.77%	6.12
E09-3065	0.38%	0.41%	2.93%	69.04%	0.03%	1779	4212	0.70%	16.83%	11	0.34%	23	78	0.01%	1.17%	4.60
E09-3070	0.50%	0.25%	2.56%	92.62%	0.02%	1612	6496	0.63%	5.44%	6	0.33%	25	36	0.01%	0.94%	5.10
E09-3075	0.33%	0.32%	2.35%	79.48%	0.02%	1778	4644	0.56%	14.30%	9	0.29%	24	49	0.01%	1.13%	4.66
E09-3080	0.23%	0.44%	2.20%	70.06%	0.03%	3009	3843	0.50%	22.95%	1	0.28%	41	44	0.01%	1.85%	4.93
E09-3085	0.20%	0.35%	1.93%	73.53%	0.03%	1725	2066	0.48%	20.92%	7	0.31%	34	41	0.01%	1.52%	1.46
E09-3090	0.36%	0.36%	1.97%	77.25%	0.03%	1618	5807	0.49%	17.11%	8	0.28%	40	35	0.01%	1.48%	6.04
E09-3095	0.36%	0.46%	1.84%	74.58%	0.02%	1993	7645	0.47%	17.80%	2	0.31%	31	58	0.02%	1.53%	4.04
E09-3100	0.21%	0.35%	1.86%	77.95%	0.03%	1436	2298	0.46%	17.38%	11	0.30%	30	43	0.01%	1.36%	0.39
E09-3105	0.15%	0.23%	1.36%	73.31%	0.03%	1425	2738	0.33%	21.38%	1	0.24%	24	34	0.01%	1.10%	3.83
E09-3110	0.17%	0.27%	1.46%	71.47%	0.02%	1295	2741	0.37%	21.55%	7	0.25%	23	53	0.01%	1.06%	0.72
	Cu ppm	Zn ppm	Ga ppm	As ppm	Rb ppm	Sr ppm	Y ppm	Zr ppm	Nb ppm	Ba ppm	Ce ppm	Pb ppm	Th ppm	U ppm	total wt%	
A-mrk mbr cuttings																
H20-3370	106	23	<LD	<LD	33.5	978.5	11.4	113.7	4.9	395	<LD	17	<LD	<LD	86.42%	
H20-3375	160	14	<LD	19	34.5	826.6	11.1	119.6	5.2	282	<LD	13	<LD	<LD	88.14%	
E09-3045	2.89	1.13	0.15	<LD	18.96	168.50	9.31	211.00	6.00	2462	45.21	18.31	4.07	1.42	106.12%	
E09-3050	26.81	5.87	1.10	10.68	17.42	262.01	7.22	140.44	4.70	4032	20.18	32.03	2.72	0.58	101.93%	
E09-3055	4.57	<LD	<LD	16.51	11.14	279.98	5.73	131.06	3.52	3051	19.18	17.18	1.14	<LD	102.04%	
E09-3060	7.87	1.91	0.49	6.27	14.53	322.76	9.33	159.17	4.10	3003	47.19	23.68	2.47	2.46	103.61%	
E09-3065	4.84	<LD	0.17	8.13	15.59	285.39	8.18	179.00	5.50	2586	14.19	13.47	3.29	<LD	93.09%	
E09-3070	3.20	0.34	0.70	2.94	16.66	152.72	9.47	229.92	5.35	2739	45.02	19.24	3.91	1.43	104.73%	
E09-3075	5.82	<LD	1.89	7.20	13.90	243.65	8.35	185.61	4.01	2709	27.43	13.63	2.86	0.18	100.07%	
E09-3080	6.09	1.38	<LD	17.97	12.98	372.59	8.27	172.77	3.64	3290	<LD	20.57	3.14	0.37	100.14%	
E09-3085	3.41	<LD	<LD	10.48	12.18	289.20	8.32	215.06	4.75	2348	28.53	14.84	4.88	0.29	100.27%	
E09-3090	5.01	<LD	<LD	7.45	12.37	231.81	9.78	197.38	4.28	2607	44.27	17.49	3.97	1.65	100.69%	
E09-3095	6.90	0.68	1.03	8.23	12.01	241.66	9.81	209.00	4.89	2916	40.32	20.67	2.66	<LD	99.06%	
E09-3100	4.21	0.34	0.06	1.30	12.37	243.68	8.37	210.85	4.43	2304	54.28	18.14	4.62	1.21	100.83%	
E09-3105	6.76	<LD	1.40	3.84	8.94	328.72	7.29	140.33	3.72	2577	26.56	14.62	3.14	<LD	99.15%	
E09-3110	5.50	<LD	<LD	0.69	8.99	285.89	6.98	173.70	4.01	1902	54.61	11.43	1.92	<LD	97.52%	

	Na2O wt%	MgO wt%	Al2O3 wt%	SiO2 wt%	P2O5 wt%	S ppm	Cl ppm	K2O wt%	CaO wt%	Sc ppm	TiO2 wt%	V ppm	Cr ppm	MnO wt%	Fe2O3T wt%	Ni ppm
A-mrk mbr cuttings																
E09-3115	0.25%	0.56%	3.21%	63.80%	0.02%	4741	3433	0.71%	24.87%	14	0.34%	30	54	0.01%	1.63%	9.36
E09-3120	0.23%	0.57%	3.09%	61.50%	0.06%	4670	3468	0.66%	23.81%	19	0.33%	25	49	0.01%	1.44%	7.50
E09-3125	0.29%	0.74%	2.71%	71.18%	0.05%	1631	1410	0.59%	18.18%	11	0.32%	26	52	0.01%	1.68%	3.13
E09-3130	0.33%	0.55%	2.50%	71.02%	0.03%	2077	3796	0.56%	19.43%	11	0.33%	28	51	0.02%	1.91%	6.24
E09-3135	0.20%	0.35%	1.84%	77.50%	0.02%	1071	1792	0.41%	19.16%	7	0.29%	21	24	0.01%	1.06%	4.09
E09-3140	0.15%	0.40%	1.75%	59.20%	0.02%	2251	1300	0.43%	28.98%	18	0.25%	19	30	0.01%	1.02%	3.91
E09-3145	0.14%	1.44%	2.71%	25.42%	0.04%	6781	1903	0.68%	50.04%	29	0.22%	38	28	0.02%	1.66%	3.95
E09-3150	0.10%	1.30%	2.22%	13.91%	0.03%	8199	903	0.55%	59.85%	44	0.16%	52	17	0.02%	1.64%	1.18
E09-3155	0.15%	1.28%	2.26%	13.73%	0.03%	8352	2700	0.56%	59.61%	40	0.17%	52	18	0.01%	1.78%	7.26
E09-3160	0.17%	1.14%	2.66%	16.25%	0.02%	8789	2005	0.62%	57.39%	40	0.20%	47	14	0.02%	1.77%	3.33
E09-3165	0.34%	1.56%	8.92%	34.63%	0.03%	8398	1702	1.66%	38.15%	24	0.54%	89	59	0.02%	3.08%	16.74
E09-3170	0.26%	1.14%	5.67%	23.91%	0.03%	6482	2338	1.16%	49.45%	28	0.37%	65	39	0.03%	2.13%	11.47
E09-3175	0.14%	0.85%	3.24%	16.64%	0.03%	7043	1665	0.73%	57.44%	39	0.22%	47	25	0.02%	1.62%	5.84
E09-3180	0.09%	0.70%	2.06%	11.34%	0.03%	5360	1356	0.49%	62.57%	37	0.13%	36	21	0.02%	1.21%	6.65

	Cu ppm	Zn ppm	Ga ppm	As ppm	Rb ppm	Sr ppm	Y ppm	Zr ppm	Nb ppm	Ba ppm	Ce ppm	Pb ppm	Th ppm	U ppm	total wt%
A-mrk mbr cuttings															
E09-3115	11.67	4.57	<LD	6.00	18.88	407.42	9.79	189.94	5.24	2727	31.93	30.12	5.25	<LD	97.34%
E09-3120	6.82	<LD	1.42	8.73	16.94	360.48	9.10	168.23	5.01	2021	51.63	15.81	5.40	1.69	93.53%
E09-3125	4.80	0.96	2.18	11.81	14.08	253.44	10.68	198.04	5.59	1528	46.90	10.40	3.06	<LD	96.55%
E09-3130	4.87	0.99	<LD	12.92	13.82	263.14	10.04	180.64	4.81	1868	43.89	17.55	6.46	0.80	97.86%
E09-3135	4.58	<LD	0.51	9.21	11.19	262.42	7.44	184.65	4.89	1822	9.45	19.89	4.34	1.13	101.58%
E09-3140	4.96	<LD	0.55	10.88	10.94	280.10	6.72	126.77	3.88	1751	52.62	11.41	2.40	0.41	93.16%
E09-3145	7.80	1.30	1.46	16.53	19.65	524.60	7.31	71.90	3.09	1449	35.82	13.79	1.32	2.34	84.50%
E09-3150	7.70	0.77	1.27	15.14	16.20	639.44	6.05	36.56	2.69	792	10.31	10.29	5.19	<LD	82.10%
E09-3155	9.17	<LD	1.58	15.19	16.66	633.11	6.42	43.15	2.19	833	31.76	12.57	2.74	1.72	82.13%
E09-3160	7.92	1.10	1.90	7.01	18.89	602.09	6.48	51.58	3.08	985	33.37	16.15	4.14	2.88	82.86%
E09-3165	13.21	22.96	8.95	15.12	60.33	504.02	11.59	90.63	7.46	1456	74.13	20.33	5.94	1.80	91.49%
E09-3170	13.89	3.89	5.27	21.29	40.88	480.34	7.70	52.57	4.58	1235	19.34	15.31	4.61	2.04	86.23%
E09-3175	6.13	2.25	1.59	12.06	25.20	517.18	4.12	33.37	3.34	1466	2.43	18.06	4.80	1.81	83.12%
E09-3180	8.08	<LD	<LD	3.76	16.03	541.23	4.32	19.02	1.68	1870	<LD	15.25	3.68	<LD	80.43%

	Na2O wt%	MgO wt%	Al2O3 wt%	SiO2 wt%	P2O5 wt%	S ppm	Cl ppm	K2O wt%	CaO wt%	Sc ppm	TiO2 wt%	V ppm	Cr ppm	MnO wt%	Fe2O3T wt%	Ni ppm
A-mrk mbr cuttings																
E09-3185	0.09%	0.66%	1.92%	10.86%	0.03%	4994	1475	0.45%	63.41%	44	0.13%	34	5	0.02%	1.09%	7.04
E09-3190	0.11%	0.77%	1.58%	12.04%	0.03%	6024	2888	0.36%	62.17%	30	0.10%	39	9	0.02%	1.29%	5.59
E09-3195	0.10%	0.74%	1.82%	12.58%	0.02%	5442	1745	0.41%	60.50%	34	0.12%	37	9	0.02%	1.23%	3.79
E09-3200	0.12%	0.92%	1.87%	22.57%	0.03%	6253	1681	0.40%	55.61%	15	0.17%	39	15	0.02%	1.36%	6.49
E09-3205	0.28%	1.28%	3.51%	28.90%	0.03%	7306	3214	0.72%	49.14%	35	0.26%	51	38	0.02%	1.59%	8.52
E09-3210	0.26%	1.50%	3.79%	28.58%	0.03%	7444	2255	0.76%	48.45%	23	0.26%	50	29	0.02%	1.75%	9.02
E09-3215	0.47%	2.17%	6.54%	40.99%	0.03%	8704	3175	1.29%	35.34%	26	0.46%	67	47	0.02%	2.40%	12.44
L08-3102.5	24.74%	<LD	1.39%	12.67%	0.02%	5662	382873	15.24%	33.95%	11	0.20%	48	59	0.03%	2.38%	6.87
L08-3127.5	3.83%	1.34%	16.91%	60.44%	0.47%	935	623	2.81%	4.86%	12	1.03%	120	2	0.10%	6.68%	18.53
B-mrk mbr cuttings																
F20-2275	0.20%	0.46%	2.18%	22.64%	0.04%	3204	3700	0.52%	52.53%	30	0.26%	40	36	0.04%	2.06%	8
F20-2285	0.09%	0.41%	1.05%	5.09%	0.03%	3338	1593	0.21%	65.42%	40	0.08%	36	13	0.03%	1.10%	2
F20-2295	0.28%	3.05%	4.25%	19.15%	0.04%	8519	4330	0.88%	46.30%	26	0.30%	68	39	0.06%	3.12%	10
F20-2305	0.34%	1.95%	7.88%	34.70%	0.05%	7856	2418	1.63%	34.47%	26	0.54%	82	54	0.05%	3.77%	16
	Cu ppm	Zn ppm	Ga ppm	As ppm	Rb ppm	Sr ppm	Y ppm	Zr ppm	Nb ppm	Ba ppm	Ce ppm	Pb ppm	Th ppm	U ppm	total wt%	
A-mrk mbr cuttings																
E09-3185	7.42	1.43	<LD	<LD	13.80	544.43	3.45	23.72	1.38	1650	<LD	11.62	0.82	2.04	80.32%	
E09-3190	8.88	<LD	<LD	15.80	11.81	585.72	4.91	16.63	2.01	1879	<LD	16.53	3.74	0.18	80.56%	
E09-3195	10.06	<LD	0.35	23.08	13.00	560.65	4.33	16.86	1.55	1320	<LD	13.28	2.81	3.75	79.31%	
E09-3200	5.41	<LD	<LD	18.51	11.63	602.02	6.18	62.50	2.74	1887	6.47	14.85	2.54	<LD	85.11%	
E09-3205	8.25	0.22	1.49	22.77	23.41	630.10	6.31	57.95	3.90	2140	<LD	18.76	5.37	2.04	88.22%	
E09-3210	7.55	2.38	0.28	6.57	25.05	642.60	7.89	66.81	3.58	2051	13.71	14.70	4.24	<LD	87.82%	
E09-3215	9.02	6.51	5.55	10.07	45.97	616.13	9.94	108.55	6.56	2624	23.21	17.49	6.13	4.15	92.63%	
L08-3102.5	18.61	46.68	4.18	23.86	26.73	471.55	10.88	100.31	3.70	455	2.33	17.49	3.92	0.64	129.71%	
L08-3127.5	58.90	69.59	20.20	3.93	68.69	671.39	17.64	245.57	16.23	1248	77.35	33.95	7.54	2.72	99.08%	
B-mrk mbr cuttings																
F20-2275	10	4	2	<LD	18.0	512.3	8.3	98.0	4.1	3135	<LD	22	<LD	<LD	82.55%	
F20-2285	7	20	<LD	<LD	6.7	645.7	4.1	19.8	1.5	1177	<LD	14	<LD	<LD	74.73%	
F20-2295	5	5	<LD	30	29.7	504.5	8.7	56.5	4.3	1055	<LD	13	<LD	<LD	80.22%	
F20-2305	9	11	8	20	61.2	558.8	14.1	124.2	9.2	1155	100	17	6	<LD	87.85%	

Appendix 5  
Samples that were re-run (due to contamination)

well - depth	Na2O wt%	MgO wt%	Al2O3 wt%	SiO2 wt%	P2O5 wt%	S ppm	Cl ppm	K2O wt%	CaO wt%	Sc ppm	TiO2 wt%	V ppm	Cr ppm	MnO wt%	Fe2O3T wt%	Ni ppm
F04-2945	1.55%	0.74%	6.07%	47.65%	0.04%	9209	38566	3.08%	26.22%	17	0.41%	101	51	0.03%	2.96%	17.00
F04-2950	1.81%	0.77%	7.99%	47.99%	0.04%	9113	36761	3.06%	23.73%	6	0.44%	103	69	0.03%	3.13%	22.90
F04-2955	1.35%	1.34%	12.86%	52.73%	0.05%	11532	23092	3.55%	11.83%	21	0.62%	178	87	0.03%	4.72%	34.82
F04-2960	1.26%	1.90%	17.14%	54.64%	0.07%	12202	17333	4.05%	1.65%	18	0.77%	221	110	0.01%	5.49%	37.83
F04-2965	2.62%	1.04%	8.86%	65.06%	0.05%	9499	40454	3.40%	6.73%	12	0.68%	125	82	0.02%	4.04%	25.42
F04-2970	3.88%	0.59%	7.68%	60.52%	0.03%	7217	115068	7.24%	3.22%	1	0.69%	72	70	0.02%	3.39%	19.07
F04-2975	7.70%	-0.26%	2.27%	22.62%	0.01%	9857	428118	31.75%	2.60%	0	0.52%	68	47	0.02%	3.28%	14.98
F04-2980	1.29%	0.64%	7.83%	74.27%	0.04%	10565	21932	2.27%	5.95%	2	0.73%	73	59	0.02%	3.05%	17.79
F04-2985	3.09%	0.76%	9.45%	67.55%	0.05%	11249	42417	3.14%	4.04%	11	0.76%	98	70	0.02%	4.01%	19.83
F04-2990	2.86%	0.76%	8.57%	69.15%	0.04%	12649	38535	3.06%	3.56%	7	0.71%	96	68	0.02%	3.72%	22.15
F04-2895	2.81%	0.97%	8.50%	67.75%	0.04%	9139	38086	3.24%	4.08%	2	0.52%	131	57	0.01%	3.15%	22.62
F04-2900	2.63%	0.77%	6.83%	68.78%	0.04%	10240	37803	2.99%	5.29%	4	0.46%	96	63	0.00%	2.64%	18.89
F04-2905	1.76%	1.98%	17.24%	60.52%	0.07%	11652	25584	4.33%	1.96%	9	0.71%	202	107	0.01%	5.21%	35.60
F04-2910	3.10%	0.92%	8.70%	69.64%	0.04%	9751	39338	3.41%	1.60%	3	0.53%	127	71	0.01%	3.19%	24.13
F04-2915	3.16%	0.65%	6.16%	77.11%	0.03%	7714	37238	2.62%	5.65%	3	0.43%	88	52	0.01%	2.20%	12.73
F04-2920	2.56%	0.96%	8.43%	65.16%	0.04%	8454	36917	3.14%	9.02%	8	0.51%	128	67	0.01%	3.19%	22.31

240

	Cu ppm	Zn ppm	Ga ppm	As ppm	Rb ppm	Sr ppm	Y ppm	Zr ppm	Nb ppm	Ba ppm	Ce ppm	Pb ppm	Th ppm	U ppm	total wt%
F04-2945	22.76	14.96	-3.93	7.22	39.02	520.37	8.31	98.17	6.96	17145	12.87	4.21	3.99	1.76	96.94%
F04-2950	41.83	17.23	-0.84	12.33	43.02	521.47	10.03	109.77	7.60	19121	-4.01	5.26	0.94	4.05	97.19%
F04-2955	51.29	35.35	4.46	11.09	74.80	399.51	14.24	131.36	12.42	15697	75.08	8.81	4.89	2.44	96.16%
F04-2960	33.55	52.80	11.43	8.80	104.37	365.57	19.19	172.86	16.98	16748	96.99	19.62	9.13	4.33	93.81%
F04-2965	29.08	33.65	-0.71	16.89	61.84	408.35	16.82	275.31	13.52	16528	25.42	10.29	5.75	5.08	100.93%
F04-2970	24.77	13.51	2.40	15.57	54.12	349.66	21.36	398.08	15.18	14515	62.62	6.79	6.69	4.02	102.34%
F04-2975	73.92	12.81	-4.42	16.58	44.56	354.55	18.73	355.61	14.27	12106	74.09	4.02	0.95	1.23	117.29%
F04-2980	24.59	15.29	-4.05	11.04	42.41	403.97	20.22	435.17	15.12	15236	65.17	4.46	5.24	4.87	102.78%
F04-2985	24.72	18.42	-0.95	7.77	59.11	339.37	23.33	380.10	16.11	13440	62.98	4.50	4.91	5.07	101.56%
F04-2990	22.65	16.50	-0.50	7.73	64.41	338.45	21.03	372.74	15.43	13755	24.95	10.81	7.42	4.90	101.13%
F04-2895	22.62	22.18	-2.33	10.43	59.62	418.98	13.63	165.09	10.82	16380	23.37	5.83	3.83	2.73	99.11%
F04-2900	28.67	18.04	-15.01	10.37	50.37	665.26	11.26	145.11	9.65	26501	-11.90	2.45	2.68	5.98	99.87%
F04-2905	35.56	46.18	6.71	9.42	95.24	396.87	19.36	223.96	20.79	17565	69.66	13.70	9.54	5.10	101.41%
F04-2910	33.10	24.39	-0.82	5.24	62.54	362.07	14.61	182.49	11.26	16533	49.20	6.31	3.53	4.02	99.48%
F04-2915	24.21	14.56	-2.27	12.39	42.95	341.43	10.54	149.01	8.61	12846	15.44	3.00	2.33	2.20	105.20%
F04-2920	26.65	24.44	2.96	18.72	59.27	349.38	13.78	152.34	12.23	13000	49.88	9.21	4.98	0.05	100.39%

	Na2O	MgO	Al2O3	SiO2	P2O5	S	Cl	K2O	CaO	Sc	TiO2	V	Cr	MnO	Fe2O3T	Ni
	wt%	wt%	wt%	wt%	wt%	ppm	ppm	wt%	wt%	ppm	wt%	ppm	ppm	wt%	wt%	ppm
F04-2930	3.21%	0.83%	7.01%	58.70%	0.04%	9039	41748	2.90%	13.41%	17	0.46%	126	78	0.01%	3.24%	17.78
F04-2935	2.92%	0.41%	3.26%	50.82%	0.03%	13411	44267	2.27%	26.27%	9	0.31%	73	52	0.03%	2.69%	14.75
F04-2940	2.94%	0.48%	4.11%	52.20%	0.03%	10052	42592	2.35%	25.60%	4	0.32%	69	37	0.03%	2.26%	31.20
C17-2025	3.23%	0.53%	4.77%	52.90%	0.05%	4959	45234	2.59%	21.98%	8	0.42%	69	37	0.02%	2.93%	11.14
C17-2035	3.17%	0.31%	2.02%	41.88%	0.03%	4435	48689	1.88%	38.17%	18	0.28%	40	14	0.01%	1.36%	4.86
C17-2060	1.97%	0.65%	8.60%	76.36%	0.06%	4770	28917	2.82%	1.36%	6	1.06%	61	67	0.05%	2.66%	17.13
C17-2070	3.73%	0.44%	4.55%	49.28%	0.03%	10568	55510	2.95%	22.82%	15	0.54%	73	47	0.08%	3.09%	11.12
C17-2080	2.14%	0.66%	5.40%	52.56%	0.05%	7200	40301	3.09%	22.60%	11	0.51%	84	40	0.08%	2.88%	16.13
C17-2090	3.06%	0.67%	8.18%	59.86%	0.07%	8279	43046	3.24%	10.27%	13	0.78%	80	64	0.05%	3.24%	19.43
F04-2875	3.02%	1.19%	10.23%	57.74%	0.04%	9692	59815	5.00%	2.95%	5	0.64%	157	85	0.01%	3.93%	29.42
F04-2880	2.50%	1.42%	11.61%	62.37%	0.05%	7556	50953	4.67%	1.52%	8	0.66%	156	90	0.01%	4.17%	27.95
F04-2885	1.44%	1.03%	8.98%	72.37%	0.04%	9245	27982	3.26%	2.09%	4	0.53%	119	64	0.01%	3.01%	24.15
F04-2890	2.26%	1.17%	11.80%	58.68%	0.05%	13033	41711	4.37%	1.61%	7	0.60%	163	92	0.01%	3.91%	32.90
L08-3077.5	4.70%	0.29%	3.15%	59.41%	0.03%	3299	57807	2.05%	17.92%	11	0.31%	38	89	0.02%	2.29%	7.01
L08-3087.5	7.51%	0.00%	1.69%	48.66%	0.02%	1195	140154	5.04%	15.54%	8	0.21%	25	47	0.02%	2.02%	6.74
	Cu	Zn	Ga	As	Rb	Sr	Y	Zr	Nb	Ba	Ce	Pb	Th	U	total	
	ppm	ppm	ppm	ppm	ppm	ppm	ppm	ppm	ppm	ppm	ppm	ppm	ppm	ppm	wt%	
F04-2930	24.16	19.24	-1.11	20.66	52.74	393.80	12.00	129.11	9.29	14644	51.77	7.70	2.94	2.04	97.99%	
F04-2935	24.47	8.20	-5.65	11.07	24.83	539.80	7.15	96.20	5.38	16623	-8.31	4.61	-3.26	4.39	98.76%	
F04-2940	22.10	8.90	-6.47	20.96	27.13	539.49	7.07	103.58	5.74	16527	19.09	5.24	-1.92	4.06	99.04%	
C17-2025	14.48	8.70	-1.61	14.54	35.72	483.25	10.55	204.22	7.31	10399	18.91	1.71	-0.09	1.10	96.45%	
C17-2035	9.97	1.89	-5.26	-1.37	15.92	562.29	6.10	103.89	4.08	9953	5.89	3.40	2.46	2.95	96.31%	
C17-2060	13.42	25.11	3.43	8.52	64.55	176.15	34.83	454.81	29.69	6396	90.58	8.78	8.73	2.60	100.53%	
C17-2070	10.67	7.20	0.53	14.69	40.57	433.82	16.71	167.13	11.90	8906	27.10	5.46	4.96	-0.86	96.80%	
C17-2080	14.03	9.96	0.24	4.16	44.24	411.65	12.93	133.62	9.48	9913	38.88	7.56	4.81	-0.80	97.01%	
C17-2090	10.77	16.99	6.00	10.02	67.77	280.55	18.84	229.14	16.57	8163	40.53	7.92	7.16	2.71	96.81%	
F04-2875	30.01	32.27	1.84	16.18	81.42	384.99	16.68	192.49	13.45	17559	41.08	10.25	7.17	2.53	95.26%	
F04-2880	19.85	36.44	8.35	-4.17	82.34	272.36	16.12	180.45	13.38	10753	85.93	10.67	7.89	0.69	97.30%	
F04-2885	25.10	25.56	-0.60	14.77	61.31	369.29	14.34	194.61	11.09	16775	1.55	11.00	3.60	2.37	99.87%	
F04-2890	30.14	39.99	-8.78	11.27	79.80	659.41	15.48	172.83	13.21	28376	-5.45	7.36	2.99	3.44	95.23%	
L08-3077.5	16.76	394.94	1.15	7.70	19.60	228.96	8.36	160.86	4.97	849	55.49	16.26	4.90	0.45	97.00%	
L08-3087.5	18.19	69.27	1.24	1.25	14.42	255.89	8.01	149.07	4.00	639	75.93	12.45	4.00	1.37	95.19%	

Appendix 6  
Chemical Index of alteration

	Na <sub>2</sub> O wt%	Al <sub>2</sub> O <sub>3</sub> wt%	SiO <sub>2</sub> wt%	P <sub>2</sub> O <sub>3</sub> wt%	K <sub>2</sub> O wt%	CaO wt%	CO <sub>2</sub> wt%	Mol Na <sub>2</sub> O	mol Al <sub>2</sub> O <sub>3</sub>	mol P <sub>2</sub> O <sub>5</sub>	mol K <sub>2</sub> O	mol CaO	Mol CO <sub>2</sub>	CaO*( corect ed)	CIA	A%	CN%	K%	
<b>Ben Nevis Cuttings</b>																			
F04 2831.08	0.62	21.28	55.58	0.03	3.45	1.84	3.64	0.01	0.21	0.00	0.04	0.03	0.08	-0.09	0.00	81.75%	81.75%	3.92%	14.33%
F04 2-1	0.45	2.61	87.36	0.01	0.81	1.17	0.72	0.01	0.03	0.00	0.01	0.02	0.02	0.00	0.00	61.75%	61.75%	17.51%	20.73%
F04 2-2	0.34	2.98	83.42	0.02	0.86	1.56	0.97	0.01	0.03	0.00	0.01	0.03	0.02	-0.01	0.00	66.60%	66.60%	12.51%	20.89%
F04 2-3	0.48	2.72	90.16	0.01	0.86	0.47	0.47	0.01	0.03	0.00	0.01	0.01	0.01	-0.01	0.00	61.31%	61.31%	17.81%	20.88%
F04 2-4	0.32	2.68	88.23	0.01	0.72	0.42	0.46	0.01	0.03	0.00	0.01	0.01	0.01	-0.01	0.00	67.18%	67.18%	13.19%	19.62%
F04 2-5	0.55	3.11	85.84	0.01	0.86	1.06	0.99	0.01	0.03	0.00	0.01	0.02	0.02	-0.02	0.00	62.89%	62.89%	18.31%	18.80%
F04 2-6	0.34	3.50	89.63	0.01	0.93	1.89	1.11	0.01	0.03	0.00	0.01	0.03	0.03	0.00	0.00	69.02%	69.02%	11.04%	19.94%
F04 2-7	2.69	2.83	82.08	0.01	2.49	0.82	1.04	0.04	0.03	0.00	0.03	0.01	0.02	-0.02	0.00	28.42%	28.42%	44.46%	27.11%
F04 2-8	0.48	3.11	84.05	0.01	0.94	3.47	2.17	0.01	0.03	0.00	0.01	0.06	0.05	-0.01	0.00	63.32%	63.32%	16.07%	20.62%
F04 2-9	0.39	2.80	90.92	0.01	0.73	0.78	0.69	0.01	0.03	0.00	0.01	0.01	0.02	-0.01	0.00	66.15%	66.15%	15.17%	18.69%
F04 2-10	0.54	4.62	85.01	0.01	1.15	3.53	2.41	0.01	0.05	0.00	0.01	0.06	0.05	-0.02	0.00	68.39%	68.39%	13.14%	18.47%
L08 2861.06	0.45	3.17	91.42	0.01	0.81	2.01	1.34	0.01	0.03	0.00	0.01	0.04	0.03	-0.01	0.00	66.15%	66.15%	15.45%	18.39%
L08 2871.23	0.51	3.13	85.71	0.01	0.83	0.98	0.87	0.01	0.03	0.00	0.01	0.02	0.02	-0.01	0.00	64.25%	64.25%	17.22%	18.53%
L08 2881.08	0.46	2.95	81.25	0.02	0.83	3.63	2.40	0.01	0.03	0.00	0.01	0.06	0.05	-0.02	0.00	64.03%	64.03%	16.45%	19.52%
L08 2993.48	0.47	2.83	93.01	0.01	0.79	0.64	0.63	0.01	0.03	0.00	0.01	0.01	0.01	-0.01	0.00	63.40%	63.40%	17.35%	19.26%
L08 2905.26	0.52	3.42	85.50	0.01	0.94	1.34	1.03	0.01	0.03	0.00	0.01	0.02	0.02	-0.01	0.00	64.61%	64.61%	16.17%	19.22%
L08 2915.88	0.55	3.40	89.35	0.01	0.98	0.74	0.82	0.01	0.03	0.00	0.01	0.01	0.02	-0.02	0.00	63.35%	63.35%	16.85%	19.81%
L08 2927.26	0.39	2.36	85.04	0.04	0.76	2.05	1.10	0.01	0.02	0.00	0.01	0.04	0.02	0.00	0.00	61.81%	61.81%	16.77%	21.42%
L08 2938.08	0.46	2.02	77.80	0.01	0.79	5.00	3.10	0.01	0.02	0.00	0.01	0.09	0.07	-0.02	0.00	55.53%	55.53%	20.85%	23.62%
L08 2945.35	0.44	3.23	83.22	0.29	0.91	2.92	1.71	0.01	0.03	0.00	0.01	0.05	0.04	-0.01	0.00	65.44%	65.44%	14.66%	19.90%
L08 2953.55	0.52	3.25	86.57	0.01	0.94	2.12	1.38	0.01	0.03	0.00	0.01	0.04	0.03	-0.01	0.00	63.40%	63.40%	16.69%	19.91%
L08 2962.95	0.45	2.60	87.32	0.01	0.82	2.13	1.43	0.01	0.03	0.00	0.01	0.04	0.03	-0.01	0.00	61.52%	61.52%	17.53%	20.95%
L08 2972.38	0.46	2.99	83.73	0.02	0.90	4.92	2.84	0.01	0.03	0.00	0.01	0.09	0.06	-0.01	0.00	63.39%	63.39%	16.04%	20.57%
L08 2981.88	0.31	2.24	86.02	0.02	0.69	2.63	1.44	0.01	0.02	0.00	0.01	0.05	0.03	0.00	0.00	64.14%	64.14%	14.60%	21.26%
L08 2991.54	0.47	3.08	86.42	0.02	0.84	1.93	1.23	0.01	0.03	0.00	0.01	0.03	0.03	-0.01	0.00	64.74%	64.74%	16.25%	19.02%
L08 3000.23	0.39	2.41	84.13	0.03	0.70	2.67	1.51	0.01	0.02	0.00	0.01	0.05	0.03	0.00	0.00	63.36%	63.36%	16.85%	19.79%
L08 3010.05	0.28	2.04	84.54	0.01	0.63	3.69	1.98	0.00	0.02	0.00	0.01	0.07	0.04	0.00	0.00	64.10%	64.10%	14.47%	21.43%
L08 3021.08	0.32	3.11	85.80	0.02	0.77	2.77	1.77	0.01	0.03	0.00	0.01	0.05	0.04	-0.01	0.00	69.59%	69.59%	11.79%	18.62%
L08 3032.0	0.50	2.94	90.61	0.01	0.80	2.49	1.69	0.01	0.03	0.00	0.01	0.04	0.04	-0.01	0.00	63.50%	63.50%	17.74%	18.76%
L08 3050.2	0.31	2.02	82.54	0.01	0.55	2.70	1.80	0.01	0.02	0.00	0.01	0.05	0.04	-0.01	0.00	64.57%	64.57%	16.31%	19.12%
L08 3060.	0.75	2.48	84.17	0.01	0.79	3.25	2.07	0.01	0.02	0.00	0.01	0.06	0.05	-0.01	0.00	54.31%	54.31%	26.97%	18.72%
J22-1 1-1	0.20	2.37	84.15	0.01	0.43	1.07	0.88	0.00	0.02	0.00	0.00	0.02	0.02	-0.01	0.00	74.89%	74.89%	10.40%	14.72%
J22-1 1-2	0.18	2.27	88.16	0.01	0.46	1.06	0.79	0.00	0.02	0.00	0.00	0.02	0.02	-0.01	0.00	74.16%	74.16%	9.68%	16.16%
J22-1 1-3	0.19	2.49	85.38	0.01	0.53	1.46	1.05	0.00	0.02	0.00	0.01	0.03	0.02	-0.01	0.00	73.69%	73.69%	9.27%	17.04%
J22-1 1-4	0.21	2.44	89.99	0.01	0.47	1.16	0.94	0.00	0.02	0.00	0.00	0.02	0.02	-0.01	0.00	74.08%	74.08%	10.48%	15.45%

	Na <sub>2</sub> O wt%	Al <sub>2</sub> O <sub>3</sub> wt%	SiO <sub>2</sub> wt%	P <sub>2</sub> O <sub>3</sub> wt%	K <sub>2</sub> O wt%	CaO wt%	CO <sub>2</sub> wt%	Mol Na <sub>2</sub> O	mol Al <sub>2</sub> O <sub>3</sub>	mol P <sub>2</sub> O <sub>5</sub>	mol K <sub>2</sub> O	mol CaO	Mol CO <sub>2</sub>	CaO*( corect ed)	CIA	A%	CN%	K%	
BenNevis Core con't.																			
J22-1 1-5	0.18	1.91	71.35	0.02	0.38	3.10	4.45	0.00	0.02	0.00	0.00	0.06	0.10	-0.10	0.00	72.92%	72.92%	11.29%	15.80%
A17 2942.22	0.29	3.31	84.88	0.01	0.92	4.50	2.63	0.00	0.03	0.00	0.01	0.08	0.06	-0.01	0.00	69.23%	69.23%	9.97%	20.80%
A17 2962.11	0.24	2.92	90.39	0.01	0.81	1.09	0.96	0.00	0.03	0.00	0.01	0.02	0.02	-0.01	0.00	69.71%	69.71%	9.43%	20.85%
A17 2974.91	0.24	3.20	86.94	0.02	0.87	2.18	1.58	0.00	0.03	0.00	0.01	0.04	0.04	-0.02	0.00	70.50%	70.50%	8.71%	20.80%
A17 2982.56	0.17	2.12	86.33	0.04	0.65	1.54	1.03	0.00	0.02	0.00	0.01	0.03	0.02	-0.01	0.00	68.27%	68.27%	9.00%	22.72%
A17 2993.89	0.21	3.07	90.33	0.01	0.88	0.48	0.57	0.00	0.03	0.00	0.01	0.01	0.01	-0.01	0.00	70.34%	70.34%	7.91%	21.75%
A17 3002.13	0.18	2.19	88.40	0.01	0.68	1.31	0.68	0.00	0.02	0.00	0.01	0.02	0.02	0.00	0.00	67.87%	67.87%	9.18%	22.95%
A17 3013.34	0.21	2.31	86.64	0.01	0.70	0.65	0.90	0.00	0.02	0.00	0.01	0.01	0.02	-0.02	0.00	67.66%	67.66%	10.10%	22.25%
A17 3023.07	0.24	2.40	89.12	0.01	0.74	1.80	0.98	0.00	0.02	0.00	0.01	0.03	0.02	0.00	0.00	66.66%	66.66%	10.97%	22.37%
A17 3033.33	0.28	2.38	91.52	0.01	0.90	1.20	1.00	0.00	0.02	0.00	0.01	0.02	0.02	-0.01	0.00	62.42%	62.42%	12.08%	25.50%
A17 3045.54	0.27	1.74	84.43	0.01	0.64	5.52	3.20	0.00	0.02	0.00	0.01	0.10	0.07	-0.01	0.00	60.38%	60.38%	15.43%	24.19%
H20-2161.3	0.59	8.12	76.90	0.02	1.54	2.24	1.45	0.01	0.08	0.00	0.02	0.04	0.03	-0.01	0.00	75.48%	75.48%	9.02%	15.49%
H20-2972.5	0.25	4.75	51.93	0.03	1.02	26.46	14.57	0.00	0.05	0.00	0.01	0.47	0.33	-0.03	0.00	75.81%	75.81%	6.56%	17.62%
H20-2983.7	0.40	5.57	78.21	0.01	1.15	4.49	2.36	0.01	0.05	0.00	0.01	0.08	0.05	0.00	0.00	74.54%	74.54%	8.81%	16.66%
H20-2995.7	0.46	7.88	73.76	0.02	1.47	3.08	1.69	0.01	0.08	0.00	0.02	0.05	0.04	0.00	0.00	77.04%	77.04%	7.40%	15.56%
H20-3007.8	0.33	4.10	83.99	0.01	0.89	7.02	3.32	0.01	0.04	0.00	0.01	0.13	0.08	0.01	0.01	60.19%	60.19%	25.67%	14.14%
H20-3024	0.37	3.72	85.18	0.01	0.89	5.83	2.95	0.01	0.04	0.00	0.01	0.10	0.07	0.00	0.00	66.31%	66.31%	16.52%	17.17%
H20-3031	0.22	2.36	85.71	0.01	0.76	1.59	1.00	0.00	0.02	0.00	0.01	0.03	0.02	-0.01	0.00	66.58%	66.58%	10.21%	23.21%
<b>Avg</b>	<b>0.42</b>	<b>3.43</b>	<b>84.34</b>	<b>0.02</b>	<b>0.90</b>	<b>2.76</b>	<b>1.81</b>	<b># 0.01</b>	<b>0.03</b>	<b>0.00</b>	<b>0.01</b>	<b>0.05</b>	<b>0.04</b>	<b>-0.01</b>	<b>0.00</b>	<b>66.05%</b>	<b>66.05%</b>	<b>14.31%</b>	<b>19.64%</b>
Hibernia core																			
G57-3985.3	0.48	4.78	73.07	0.03	0.44	6.71	2.44	0.01	0.05	0.00	0.00	0.12	0.06	0.04	0.04	49.31%	49.31%	45.78%	4.91%
G57-3990	0.26	2.17	60.51	0.03	0.24	19.43	11.13	0.00	0.02	0.00	0.00	0.35	0.25	-0.03	0.00	75.94%	75.94%	14.97%	9.09%
G57-3995.2	0.44	5.68	60.41	0.03	0.38	14.04	6.85	0.01	0.06	0.00	0.00	0.25	0.16	0.02	0.02	67.12%	67.12%	28.01%	4.86%
<b>Avg</b>	<b>0.39</b>	<b>4.21</b>	<b>64.66</b>	<b>0.03</b>	<b>0.35</b>	<b>13.39</b>	<b>6.80</b>	<b># 0.01</b>	<b>0.04</b>	<b>0.00</b>	<b>0.00</b>	<b>0.24</b>	<b>0.15</b>	<b>0.01</b>	<b>0.02</b>	<b>64.12%</b>	<b>64.12%</b>	<b>29.59%</b>	<b>6.29%</b>
Terra Nova core																			
G57-4029.3	0.13	2.80	77.41	0.03	0.17	8.65	5.73	0.00	0.03	0.00	0.00	0.15	0.13	-0.04	0.00	87.56%	87.56%	6.69%	5.75%
G57-4035.0	0.25	3.41	77.85	0.03	0.24	7.41	4.68	0.00	0.03	0.00	0.00	0.13	0.11	-0.03	0.00	83.56%	83.56%	10.08%	6.37%
C73- 4123	0.18	2.46	72.06	0.05	0.18	14.27	7.91	0.00	0.02	0.00	0.00	0.25	0.18	-0.02	0.00	83.36%	83.36%	10.03%	6.60%
C73-4129	0.07	1.47	48.93	0.03	0.14	29.60	11.83	0.00	0.01	0.00	0.00	0.53	0.27	0.12	0.12	10.22%	10.22%	88.73%	1.05%
<b>Avg</b>	<b>0.16</b>	<b>2.54</b>	<b>69.06</b>	<b>0.03</b>	<b>0.18</b>	<b>14.98</b>	<b>7.54</b>	<b># 0.00</b>	<b>0.02</b>	<b>0.00</b>	<b>0.00</b>	<b>0.27</b>	<b>0.17</b>	<b>0.01</b>	<b>0.03</b>	<b>66.17%</b>	<b>66.17%</b>	<b>28.88%</b>	<b>4.94%</b>
Lower Tempest core																			
G57-4594.25	0.10	0.57	79.13	0.03	0.12	12.60	7.64	0.00	0.01	0.00	0.00	0.22	0.17	-0.04	0.00	65.94%	65.94%	19.03%	15.03%
G57-4598	0.12	0.69	80.58	0.02	0.15	12.27	6.13	0.00	0.01	0.00	0.00	0.22	0.14	0.01	0.01	34.60%	34.60%	57.25%	8.14%
<b>Avg</b>	<b>0.11</b>	<b>0.63</b>	<b>79.86</b>	<b>0.03</b>	<b>0.14</b>	<b>12.43</b>	<b>6.89</b>	<b># 0.00</b>	<b>0.01</b>	<b>0.00</b>	<b>0.00</b>	<b>0.22</b>	<b>0.16</b>	<b>-0.01</b>	<b>0.00</b>	<b>0.50</b>	<b>0.50</b>	<b>0.38</b>	<b>0.12</b>

	Na <sub>2</sub> O	Al <sub>2</sub> O <sub>3</sub>	SiO <sub>2</sub>	P <sub>2</sub> O <sub>3</sub>	K <sub>2</sub> O	CaO	CO <sub>2</sub>	Mol	mol	mol	mol	mol	Mol	CaO*(	corect	CIA	A%	CN%	K%	
	wt%	wt%	wt%	wt%	wt%	wt%	wt%	Na <sub>2</sub> O	Al <sub>2</sub> O <sub>3</sub>	P <sub>2</sub> O <sub>5</sub>	K <sub>2</sub> O	CaO	CO <sub>2</sub>	CaO*	ed)					
Eastern shoals cuttings																				
N30-3075	0.73	11.20	60.65	0.05	3.80	6.16	7.04	0.01	0.11	0.00	0.04	0.11	0.16	-0.13	0.00	67.83%	67.83%	7.23%	24.94%	
N30-3080	0.76	8.76	55.91	0.06	4.29	12.89	8.34	0.01	0.09	0.00	0.05	0.23	0.19	-0.06	0.00	59.77%	59.77%	8.58%	31.65%	
N30-3085	0.74	7.18	67.49	0.04	3.36	7.20	6.02	0.01	0.07	0.00	0.04	0.13	0.14	-0.08	0.00	59.67%	59.67%	10.14%	30.19%	
N30-3090	0.82	8.29	67.14	0.03	3.99	9.92	7.86	0.01	0.08	0.00	0.04	0.18	0.18	-0.09	0.00	59.40%	59.40%	9.71%	30.89%	
N30-3095	0.78	8.82	67.70	0.04	3.51	7.30	6.22	0.01	0.09	0.00	0.04	0.13	0.14	-0.08	0.00	63.45%	63.45%	9.24%	27.32%	
N30-3100	0.73	8.01	66.19	0.04	3.34	10.47	8.99	0.01	0.08	0.00	0.04	0.19	0.20	-0.12	0.00	62.47%	62.47%	9.37%	28.16%	
N30-3105	0.66	5.80	57.57	0.04	3.96	17.90	12.62	0.01	0.06	0.00	0.04	0.32	0.29	-0.11	0.00	51.94%	51.94%	9.74%	38.32%	
N30-3110	0.70	7.77	61.43	0.03	3.84	12.95	8.60	0.01	0.08	0.00	0.04	0.23	0.20	-0.06	0.00	59.47%	59.47%	8.76%	31.78%	
N30-3115	0.62	10.68	46.05	0.05	4.13	17.87	13.07	0.01	0.10	0.00	0.04	0.32	0.30	-0.13	0.00	66.04%	66.04%	6.29%	27.67%	
H20-3325	0.63	13.39	51.17	0.06	3.94	12.29	10.93	0.01	0.13	0.00	0.04	0.22	0.25	-0.15	0.00	71.61%	71.61%	5.55%	22.84%	
H20-3330	0.83	12.65	47.75	0.05	3.81	10.85	9.36	0.01	0.12	0.00	0.04	0.19	0.21	-0.13	0.00	69.77%	69.77%	7.50%	22.73%	
J22-1-2935	1.87	14.50	55.58	0.06	2.90	1.93	4.31	0.03	0.14	0.00	0.03	0.03	0.10	-0.11	0.00	69.98%	69.98%	14.88%	15.14%	
J22-1-2940	0.94	13.28	69.22	0.07	2.27	2.84	3.68	0.02	0.13	0.00	0.02	0.05	0.08	-0.08	0.00	76.88%	76.88%	8.92%	14.21%	
J22-1-2945	0.67	7.42	82.87	0.03	1.34	3.42	3.03	0.01	0.07	0.00	0.01	0.06	0.07	-0.04	0.00	74.33%	74.33%	11.12%	14.55%	
J22-1-2950	0.80	7.38	81.51	0.03	1.36	3.11	2.62	0.01	0.07	0.00	0.01	0.06	0.06	-0.03	0.00	72.60%	72.60%	12.94%	14.46%	
J22-1-2955	0.82	14.06	63.74	0.03	2.68	1.69	2.71	0.01	0.14	0.00	0.03	0.03	0.06	-0.06	0.00	76.81%	76.81%	7.37%	15.83%	
J22-1-2960	0.80	9.53	72.91	0.03	1.79	4.98	3.82	0.01	0.09	0.00	0.02	0.09	0.09	-0.04	0.00	74.58%	74.58%	10.25%	15.17%	
J22-1-2965	0.75	8.21	62.18	0.03	1.62	11.08	7.99	0.01	0.08	0.00	0.02	0.20	0.18	-0.08	0.00	73.37%	73.37%	11.00%	15.64%	
J22-1-2970	0.94	11.49	67.75	0.05	2.15	2.66	2.98	0.02	0.11	0.00	0.02	0.05	0.07	-0.06	0.00	74.73%	74.73%	10.10%	15.17%	
<b>Avg</b>	<b>0.82</b>	<b>9.92</b>	<b>63.41</b>	<b>0.04</b>	<b>3.06</b>	<b>8.29</b>	<b>6.85</b>	<b>#</b>	<b>0.01</b>	<b>0.10</b>	<b>0.00</b>	<b>0.03</b>	<b>0.15</b>	<b>0.16</b>	<b>-0.09</b>	<b>0.00</b>	<b>67.62%</b>	<b>67.62%</b>	<b>9.40%</b>	<b>22.98%</b>
Whiterose cuttings																				
E87-2150	0.78	12.34	54.88	0.08	4.13	1.97	4.04	0.01	0.12	0.00	0.04	0.04	0.09	-0.10	0.00	68.18%	68.18%	7.13%	24.70%	
E87-2160	0.50	14.60	58.59	0.08	3.98	4.17	4.00	0.01	0.14	0.00	0.04	0.07	0.09	-0.06	0.00	74.01%	74.01%	4.18%	21.81%	
E87-2170	0.67	12.51	48.61	0.08	3.73	5.70	3.86	0.01	0.12	0.00	0.04	0.10	0.09	-0.03	0.00	70.85%	70.85%	6.26%	22.89%	
E87-2180	0.58	14.53	57.37	0.06	3.16	1.82	3.66	0.01	0.14	0.00	0.03	0.03	0.08	-0.09	0.00	76.87%	76.87%	5.07%	18.07%	
E87-2190	0.68	11.83	56.30	0.06	3.16	5.08	3.89	0.01	0.12	0.00	0.03	0.09	0.09	-0.04	0.00	72.26%	72.26%	6.83%	20.91%	
E87-2200	0.86	12.69	57.84	0.06	3.56	3.18	3.90	0.01	0.12	0.00	0.04	0.06	0.09	-0.08	0.00	70.67%	70.67%	7.89%	21.44%	
E09-3220	0.52	6.03	39.27	0.03	1.21	35.95	23.58	0.01	0.06	0.00	0.01	0.64	0.54	-0.16	0.00	73.54%	73.54%	10.45%	16.01%	
E09-3225	0.40	7.77	34.80	0.04	1.58	35.93	24.45	0.01	0.08	0.00	0.02	0.64	0.56	-0.19	0.00	76.70%	76.70%	6.42%	16.87%	
E09-3230	0.47	8.87	38.03	0.07	1.77	33.29	22.88	0.01	0.09	0.00	0.02	0.59	0.52	-0.19	0.00	76.73%	76.73%	6.69%	16.58%	
E09-3235	0.47	10.81	40.91	0.06	1.96	27.18	19.27	0.01	0.11	0.00	0.02	0.48	0.44	-0.17	0.00	78.82%	78.82%	5.69%	15.50%	
E09-3240	0.45	10.35	39.01	0.05	1.97	30.18	21.47	0.01	0.10	0.00	0.02	0.54	0.49	-0.19	0.00	78.24%	78.24%	5.62%	16.14%	
E09-3245	0.60	11.21	41.15	0.05	2.10	25.67	18.80	0.01	0.11	0.00	0.02	0.46	0.43	-0.18	0.00	77.46%	77.46%	6.85%	15.70%	
E09-3250	0.43	9.13	36.37	0.05	1.73	32.31	22.69	0.01	0.09	0.00	0.02	0.58	0.52	-0.20	0.00	77.98%	77.98%	5.99%	16.03%	

	Na <sub>2</sub> O wt%	Al <sub>2</sub> O <sub>3</sub> wt%	SiO <sub>2</sub> wt%	P <sub>2</sub> O <sub>3</sub> wt%	K <sub>2</sub> O wt%	CaO wt%	CO <sub>2</sub> wt%	Mol Na <sub>2</sub> O	mol Al <sub>2</sub> O <sub>3</sub>	mol P <sub>2</sub> O <sub>5</sub>	mol K <sub>2</sub> O	mol CaO	Mol CO <sub>2</sub>	CaO*( corect ed)	CIA	A%	CN%	K%	
Whiterose cuttings con't.																			
E09-3255	0.57	10.36	42.63	0.05	2.00	27.95	17.76	0.01	0.10	0.00	0.02	0.50	0.40	-0.11	0.00	76.92%	76.92%	7.02%	16.06%
E09-3260	0.61	9.82	38.53	0.05	1.93	29.20	21.53	0.01	0.10	0.00	0.02	0.52	0.49	-0.21	0.00	76.07%	76.07%	7.77%	16.16%
E09-3265	0.47	9.68	39.26	0.05	1.92	29.57	19.91	0.01	0.09	0.00	0.02	0.53	0.45	-0.15	0.00	77.32%	77.32%	6.11%	16.57%
E09-3270	0.80	10.34	44.62	0.05	1.76	22.61	13.01	0.01	0.10	0.00	0.02	0.40	0.30	-0.04	0.00	76.21%	76.21%	9.72%	14.07%
E09-3275	0.50	9.35	39.78	0.05	1.80	29.30	19.01	0.01	0.09	0.00	0.02	0.52	0.43	-0.13	0.00	77.18%	77.18%	6.74%	16.08%
E09-3280	0.54	9.76	38.03	0.06	2.02	29.36	19.49	0.01	0.10	0.00	0.02	0.52	0.44	-0.14	0.00	76.02%	76.02%	6.97%	17.01%
E09-3285	0.58	8.46	34.47	0.05	1.86	32.89	22.26	0.01	0.08	0.00	0.02	0.59	0.51	-0.17	0.00	74.10%	74.10%	8.29%	17.61%
E09-3290	0.49	9.00	35.67	0.07	1.90	30.99	22.11	0.01	0.09	0.00	0.02	0.55	0.50	-0.20	0.00	75.88%	75.88%	6.83%	17.29%
E09-3295	0.61	10.78	44.59	0.08	2.12	22.29	15.72	0.01	0.11	0.00	0.02	0.40	0.36	-0.14	0.00	76.60%	76.60%	7.08%	16.31%
E09-3300	0.72	13.32	52.48	0.06	2.42	14.21	10.01	0.01	0.13	0.00	0.03	0.25	0.23	-0.09	0.00	77.76%	77.76%	6.94%	15.30%
<b>Avg</b>	<b>0.58</b>	<b>10.59</b>	<b>44.05</b>	<b>0.06</b>	<b>2.34</b>	<b>22.21</b>	<b>15.54</b>	<b># 0.01</b>	<b>0.10</b>	<b>0.00</b>	<b>0.02</b>	<b>0.40</b>	<b>0.35</b>	<b>-0.13</b>	<b>0.00</b>	<b>75.49%</b>	<b>75.49%</b>	<b>6.89%</b>	<b>17.61%</b>
Hibernia cuttings																			
A17-3090	0.72	7.34	66.28	0.18	2.89	14.46	9.89	0.01	0.07	0.00	0.03	0.26	0.22	-0.08	0.00	63.01%	63.01%	10.12%	26.87%
A17-3095	0.67	7.51	77.37	0.07	2.71	8.16	6.88	0.01	0.07	0.00	0.03	0.15	0.16	-0.09	0.00	65.05%	65.05%	9.54%	25.41%
A17-3100	0.77	10.37	69.53	0.05	3.33	8.16	6.54	0.01	0.10	0.00	0.04	0.15	0.15	-0.08	0.00	68.04%	68.04%	8.30%	23.66%
A17-3105	0.71	9.50	67.34	0.07	3.01	9.27	7.23	0.01	0.09	0.00	0.03	0.17	0.16	-0.08	0.00	68.24%	68.24%	8.37%	23.39%
A17-3110	0.69	10.04	62.77	0.07	3.59	12.34	7.81	0.01	0.10	0.00	0.04	0.22	0.18	-0.05	0.00	66.70%	66.70%	7.50%	25.80%
A17-3115	0.61	8.23	65.29	0.04	3.09	14.32	9.44	0.01	0.08	0.00	0.03	0.26	0.21	-0.07	0.00	65.45%	65.45%	8.00%	26.55%
A17-3120	0.62	9.30	55.64	0.04	3.78	16.98	13.97	0.01	0.09	0.00	0.04	0.30	0.32	-0.17	0.00	64.54%	64.54%	7.05%	28.41%
A17-3125	0.57	9.04	49.32	0.04	3.37	20.85	16.68	0.01	0.09	0.00	0.04	0.37	0.38	-0.20	0.00	66.32%	66.32%	6.93%	26.74%
A17-3130	0.54	7.71	53.38	0.04	3.19	18.88	14.28	0.01	0.08	0.00	0.03	0.34	0.32	-0.15	0.00	63.97%	63.97%	7.38%	28.65%
A17-3135	0.56	8.97	58.22	0.05	3.51	15.24	10.62	0.01	0.09	0.00	0.04	0.27	0.24	-0.09	0.00	65.56%	65.56%	6.69%	27.74%
A17-3140	0.52	12.53	55.93	0.05	3.94	10.70	6.70	0.01	0.12	0.00	0.04	0.19	0.15	-0.04	0.00	71.00%	71.00%	4.87%	24.14%
A17-3145	0.50	7.61	74.29	0.04	2.81	8.95	5.80	0.01	0.07	0.00	0.03	0.16	0.13	-0.04	0.00	66.35%	66.35%	7.16%	26.50%
A17-3155	0.66	10.79	66.76	0.04	3.22	6.52	4.89	0.01	0.11	0.00	0.03	0.12	0.11	-0.05	0.00	70.24%	70.24%	7.04%	22.72%
A17-3160	0.68	8.67	72.56	0.04	2.80	7.52	5.23	0.01	0.09	0.00	0.03	0.13	0.12	-0.04	0.00	67.61%	67.61%	8.75%	23.64%
A17-3165	0.79	9.92	70.94	0.05	3.06	7.46	5.96	0.01	0.10	0.00	0.03	0.13	0.14	-0.07	0.00	68.27%	68.27%	8.94%	22.79%
A17-3175	0.36	3.21	69.66	0.02	1.57	13.19	7.08	0.01	0.03	0.00	0.02	0.24	0.16	-0.01	0.00	58.34%	58.34%	10.77%	30.88%
E87-2210	0.61	12.75	61.28	0.06	3.03	4.75	4.15	0.01	0.13	0.00	0.03	0.08	0.09	-0.06	0.00	74.83%	74.83%	5.90%	19.26%
E87-2220	0.58	13.11	62.49	0.05	2.83	3.82	4.35	0.01	0.13	0.00	0.03	0.07	0.10	-0.08	0.00	76.53%	76.53%	5.59%	17.88%
E87-2230	0.77	12.12	61.98	0.06	2.99	2.34	3.83	0.01	0.12	0.00	0.03	0.04	0.09	-0.09	0.00	72.90%	72.90%	7.66%	19.44%
E87-2240	0.54	11.80	65.41	0.05	3.44	1.76	7.76	0.01	0.12	0.00	0.04	0.03	0.18	-0.23	0.00	71.91%	71.91%	5.39%	22.70%
E87-2250	0.53	11.65	70.16	0.04	2.96	1.24	3.55	0.01	0.11	0.00	0.03	0.02	0.08	-0.10	0.00	74.05%	74.05%	5.57%	20.38%
E87-2260	0.59	11.06	56.66	0.05	3.09	8.40	7.35	0.01	0.11	0.00	0.03	0.15	0.17	-0.10	0.00	71.89%	71.89%	6.35%	21.76%

	Na <sub>2</sub> O wt%	Al <sub>2</sub> O <sub>3</sub> wt%	SiO <sub>2</sub> wt%	P <sub>2</sub> O <sub>3</sub> wt%	K <sub>2</sub> O wt%	CaO wt%	CO <sub>2</sub> wt%	Mol Na <sub>2</sub> O	mol Al <sub>2</sub> O <sub>3</sub>	mol P <sub>2</sub> O <sub>5</sub>	mol K <sub>2</sub> O	mol CaO	Mol CO <sub>2</sub>	CaO*( corect ed)	CIA	A%	CN%	K%	
Hibernia cuttings con't.																			
E87-2270	0.47	7.72	67.68	0.04	3.03	2.95	6.54	0.01	0.08	0.00	0.03	0.05	0.15	-0.17	0.00	65.56%	65.56%	6.62%	27.82%
E87-2280	0.54	8.96	74.68	0.04	2.19	4.03	3.79	0.01	0.09	0.00	0.02	0.07	0.09	-0.06	0.00	73.30%	73.30%	7.31%	19.39%
E87-2290	0.58	11.36	61.81	0.07	3.09	5.11	4.94	0.01	0.11	0.00	0.03	0.09	0.11	-0.08	0.00	72.56%	72.56%	6.10%	21.34%
E87-2300	0.54	12.91	55.86	0.04	3.11	2.27	3.53	0.01	0.13	0.00	0.03	0.04	0.08	-0.08	0.00	75.21%	75.21%	5.20%	19.59%
C17-2060	1.97	8.60	76.36	0.06	2.82	1.36	3.72	0.03	0.08	0.00	0.03	0.02	0.08	-0.10	0.00	57.76%	57.76%	21.75%	20.50%
C17-2070	3.73	4.55	49.28	0.03	2.95	22.82	13.89	0.06	0.04	0.00	0.03	0.41	0.32	-0.07	0.00	32.78%	32.78%	44.21%	23.01%
C17-2080	2.14	5.40	52.56	0.05	3.09	22.60	14.23	0.03	0.05	0.00	0.03	0.40	0.32	-0.08	0.00	44.00%	44.00%	28.75%	27.25%
C17-2090	3.06	8.18	59.86	0.07	3.24	10.27	8.08	0.05	0.08	0.00	0.03	0.18	0.18	-0.09	0.00	48.91%	48.91%	30.12%	20.97%
K19-2230	1.23	8.96	51.63	0.05	1.67	19.76	13.32	0.02	0.09	0.00	0.02	0.35	0.30	-0.10	0.00	70.04%	70.04%	15.87%	14.09%
K19-2240	1.36	9.56	54.87	0.10	1.62	16.60	11.30	0.02	0.09	0.00	0.02	0.30	0.26	-0.09	0.00	70.55%	70.55%	16.49%	12.96%
K19-2250	1.31	8.55	57.30	0.05	1.39	16.49	11.53	0.02	0.08	0.00	0.01	0.29	0.26	-0.10	0.00	70.04%	70.04%	17.68%	12.28%
K19-2260	1.12	9.12	60.34	0.09	1.47	14.73	11.16	0.02	0.09	0.00	0.02	0.26	0.25	-0.12	0.00	72.60%	72.60%	14.73%	12.67%
K19-2270	1.30	7.51	58.41	0.05	1.20	16.32	13.29	0.02	0.07	0.00	0.01	0.29	0.30	-0.16	0.00	68.62%	68.62%	19.51%	11.87%
K19-2280	1.10	6.30	54.89	0.13	1.00	22.96	13.92	0.02	0.06	0.00	0.01	0.41	0.32	-0.07	0.00	68.61%	68.61%	19.66%	11.72%
K19-2290	1.56	7.10	51.07	0.04	1.19	17.92	9.33	0.03	0.07	0.00	0.01	0.32	0.21	0.00	0.00	64.47%	64.47%	23.84%	11.69%
K19-2300	1.58	8.20	59.82	0.04	1.34	14.01	6.70	0.03	0.08	0.00	0.01	0.25	0.15	0.02	0.02	57.18%	57.18%	32.71%	10.11%
K19-2320	1.48	10.94	61.03	0.05	1.63	11.66	8.27	0.02	0.11	0.00	0.02	0.21	0.19	-0.07	0.02	63.61%	63.61%	26.11%	10.28%
<b>Avg</b>	<b>0.99</b>	<b>9.16</b>	<b>62.07</b>	<b>0.06</b>	<b>2.67</b>	<b>11.21</b>	<b>8.40</b>	<b># 0.02</b>	<b>0.09</b>	<b>0.00</b>	<b>0.03</b>	<b>0.20</b>	<b>0.19</b>	<b>-0.09</b>	<b>0.00</b>	<b>66.07%</b>	<b>66.07%</b>	<b>12.83%</b>	<b>21.10%</b>
Rankin cuttings																			
F04-2960	1.26	17.14	62.07	0.07	4.05	1.65	6.92	0.02	0.17	0.00	0.04	0.03	0.16	-0.21	0.00	72.64%	72.64%	8.79%	18.58%
F04-2965	2.62	8.86	54.64	0.05	3.40	6.73	7.33	0.04	0.09	0.00	0.04	0.12	0.17	-0.13	0.00	52.56%	52.56%	25.60%	21.83%
F04-2970	3.88	7.68	65.06	0.03	7.24	3.22	5.32	0.06	0.08	0.00	0.08	0.06	0.12	-0.12	0.00	35.06%	35.06%	29.17%	35.77%
F04-2975	7.70	2.27	60.52	0.01	31.75	2.60	5.55	0.12	0.02	0.00	0.34	0.05	0.13	-0.14	0.00	4.60%	4.60%	25.70%	69.70%
F04-2980	1.29	7.83	22.62	0.04	2.27	5.95	5.15	0.02	0.08	0.00	0.02	0.11	0.12	-0.07	0.00	63.10%	63.10%	17.11%	19.80%
F04-2985	3.09	9.45	74.27	0.05	3.14	4.04	4.26	0.05	0.09	0.00	0.03	0.07	0.10	-0.07	0.00	52.70%	52.70%	28.35%	18.95%
F04-2990	2.86	8.57	67.55	0.04	3.06	3.56	4.52	0.05	0.08	0.00	0.03	0.06	0.10	-0.09	0.00	51.67%	51.67%	28.37%	19.97%
<b>Avg</b>	<b>3.24</b>	<b>8.83</b>	<b>58.10</b>	<b>0.04</b>	<b>7.84</b>	<b>3.97</b>	<b>5.58</b>	<b># 0.05</b>	<b>0.09</b>	<b>0.00</b>	<b>0.08</b>	<b>0.07</b>	<b>0.13</b>	<b>-0.12</b>	<b>0.00</b>	<b>47.47%</b>	<b>47.47%</b>	<b>23.30%</b>	<b>29.23%</b>
Ben Nevis cuttings																			
A17-3050	0.40	2.20	65.31	0.05	1.99	26.98	19.36	0.01	0.02	0.00	0.02	0.48	0.44	-0.18	0.00	43.87%	43.87%	13.25%	42.89%
A17-3055	0.49	2.04	87.39	0.03	2.19	9.28	6.39	0.01	0.02	0.00	0.02	0.17	0.15	-0.05	0.00	39.17%	39.17%	15.36%	45.47%
A17-3060	0.42	1.62	72.04	0.03	1.90	19.69	12.86	0.01	0.02	0.00	0.02	0.35	0.29	-0.09	0.00	37.14%	37.14%	15.83%	47.03%
A17-3065	0.38	1.34	63.36	0.03	1.72	22.41	13.53	0.01	0.01	0.00	0.02	0.40	0.31	-0.06	0.00	34.96%	34.96%	16.33%	48.71%
A17-3070	0.39	1.57	65.95	0.04	1.73	21.95	12.43	0.01	0.02	0.00	0.02	0.39	0.28	-0.03	0.00	38.57%	38.57%	15.61%	45.82%
A17-3075	0.34	1.13	50.85	0.04	1.21	33.40	19.15	0.01	0.01	0.00	0.01	0.60	0.44	-0.06	0.00	37.79%	37.79%	18.51%	43.70%

	Na <sub>2</sub> O	Al <sub>2</sub> O <sub>3</sub>	SiO <sub>2</sub>	P <sub>2</sub> O <sub>3</sub>	K <sub>2</sub> O	CaO	CO <sub>2</sub>	Mol	mol	mol	mol	mol	Mol	CaO*(	CaO*(	CIA	A%	CN%	K%
	wt%	wt%	wt%	wt%	wt%	wt%	wt%	Na <sub>2</sub> O	Al <sub>2</sub> O <sub>3</sub>	P <sub>2</sub> O <sub>5</sub>	K <sub>2</sub> O	CaO	CO <sub>2</sub>	CaO*	correct				
Ben Nevis cuttings con't.																			
A17-3080	0.32	1.29	54.37	0.03	1.52	32.41	18.62	0.01	0.01	0.00	0.02	0.58	0.42	-0.06	0.00	37.24%	37.24%	15.18%	47.58%
A17-3085	0.70	7.00	63.99	0.05	2.66	15.43	11.44	0.01	0.07	0.00	0.03	0.28	0.26	-0.12	0.00	63.53%	63.53%	10.39%	26.07%
J22-1-2880	0.48	2.98	70.83	0.03	0.60	16.41	8.76	0.01	0.03	0.00	0.01	0.29	0.20	-0.01	0.00	67.42%	67.42%	17.91%	14.67%
J22-1-2885	0.69	2.41	61.55	0.04	0.49	22.62	12.78	0.01	0.02	0.00	0.01	0.40	0.29	-0.03	0.00	59.34%	59.34%	27.73%	12.93%
F04-2875	3.02	10.23	57.74	0.04	5.00	2.95	5.89	0.05	0.09	0.00	0.05	0.05	0.13	-0.15	0.00	46.40%	46.40%	25.64%	27.96%
F04-2880	2.50	11.61	62.37	0.05	4.67	1.52	5.12	0.04	0.11	0.00	0.05	0.03	0.12	-0.15	0.00	55.87%	55.87%	19.80%	24.33%
F04-2885	1.44	8.98	72.37	0.04	3.26	2.09	4.53	0.02	0.09	0.00	0.03	0.04	0.10	-0.12	0.00	60.34%	60.34%	15.95%	23.71%
F04-2890	2.26	11.80	58.68	0.05	4.37	1.61	6.84	0.04	0.12	0.00	0.05	0.03	0.16	-0.21	0.00	58.27%	58.27%	18.37%	23.36%
F04-2895	2.81	8.50	67.75	0.04	3.24	4.08	5.71	0.05	0.08	0.00	0.03	0.07	0.13	-0.12	0.00	51.12%	51.12%	27.79%	21.09%
F04-2900	2.63	6.83	68.78	0.04	2.99	5.29	6.46	0.04	0.07	0.00	0.03	0.09	0.15	-0.13	0.00	47.47%	47.47%	30.03%	22.49%
F04-2905	1.76	17.24	60.52	0.07	4.33	1.96	6.57	0.03	0.17	0.00	0.05	0.04	0.15	-0.19	0.00	69.46%	69.46%	11.65%	18.88%
F04-2910	3.10	8.70	69.64	0.04	3.41	1.60	4.54	0.05	0.09	0.00	0.04	0.03	0.10	-0.13	0.00	49.76%	49.76%	29.13%	21.11%
F04-2915	3.16	6.16	77.11	0.03	2.62	5.65	6.03	0.05	0.06	0.00	0.03	0.10	0.14	-0.11	0.00	43.39%	43.39%	36.63%	19.98%
F04-2920	2.56	8.43	65.16	0.04	3.14	9.02	7.59	0.04	0.08	0.00	0.03	0.16	0.17	-0.10	0.00	52.57%	52.57%	26.23%	21.20%
F04-2930	3.21	7.01	58.70	0.04	2.90	13.41	10.41	0.05	0.07	0.00	0.03	0.24	0.24	-0.12	0.00	45.43%	45.43%	34.22%	20.34%
F04-2935	2.92	3.26	50.82	0.03	2.27	26.27	16.40	0.05	0.03	0.00	0.02	0.47	0.37	-0.09	0.00	30.99%	30.99%	45.65%	23.36%
F04-2940	2.94	4.11	52.20	0.03	2.35	25.60	16.58	0.05	0.04	0.00	0.02	0.46	0.38	-0.11	0.00	35.76%	35.76%	42.10%	22.13%
F04-2945	1.55	6.07	47.65	0.04	3.08	26.22	16.19	0.02	0.06	0.00	0.03	0.47	0.37	-0.09	0.00	50.81%	50.81%	21.28%	27.91%
F04-2950	1.81	7.99	47.99	0.04	3.06	23.73	14.38	0.03	0.08	0.00	0.03	0.42	0.33	-0.07	0.00	55.98%	55.98%	20.81%	23.21%
F04-2955	1.35	12.86	52.73	0.05	3.55	11.83	9.31	0.02	0.13	0.00	0.04	0.21	0.21	-0.11	0.00	67.97%	67.97%	11.72%	20.31%
C17-2025	3.23	4.77	52.90	0.05	2.59	21.98	14.12	0.05	0.05	0.00	0.03	0.39	0.32	-0.09	0.00	37.04%	37.04%	41.20%	21.77%
C17-2035	3.17	2.02	41.88	0.03	1.88	38.17	24.09	0.05	0.02	0.00	0.02	0.68	0.55	-0.14	0.00	21.77%	21.77%	56.29%	21.93%
L08-3077.5	4.70	3.15	59.41	0.03	2.05	17.92	12.16	0.08	0.03	0.00	0.02	0.32	0.28	-0.10	0.00	24.05%	24.05%	59.00%	16.94%
L08-3087.5	7.51	1.69	48.66	0.02	5.04	15.54	14.72	0.12	0.02	0.00	0.05	0.28	0.33	-0.23	0.00	8.67%	8.67%	63.36%	27.97%
L08-3097.5	20.52	0.77	11.45	0.01	6.92	34.35	30.09	0.33	0.01	0.00	0.07	0.61	0.68	-0.41	0.00	1.83%	1.83%	80.34%	17.83%
F20-2220	0.75	9.92	71.96	0.05	1.86	7.47	5.15	0.01	0.10	0.00	0.02	0.13	0.12	-0.04	0.00	75.36%	75.36%	9.33%	15.31%
F20-2230	0.57	8.24	57.47	0.04	1.71	19.02	11.93	0.01	0.08	0.00	0.02	0.34	0.27	-0.07	0.00	74.70%	74.70%	8.51%	16.78%
F20-2240	0.38	4.21	51.59	0.06	0.90	30.92	18.87	0.01	0.04	0.00	0.01	0.55	0.43	-0.09	0.00	72.51%	72.51%	10.67%	16.81%
F20-2250	0.40	7.17	52.21	0.07	1.45	24.65	14.92	0.01	0.07	0.00	0.02	0.44	0.34	-0.07	0.00	76.22%	76.22%	7.07%	16.71%
F20-2260	0.44	7.58	52.14	0.18	1.55	23.63	14.66	0.01	0.07	0.00	0.02	0.42	0.33	-0.08	0.00	75.97%	75.97%	7.23%	16.80%
F20-2270	0.83	11.74	55.12	0.08	2.33	10.75	8.49	0.01	0.12	0.00	0.02	0.19	0.19	-0.10	0.00	75.13%	75.13%	8.75%	16.12%
K19-2170	1.54	12.09	55.32	0.06	2.22	11.35	9.79	0.02	0.12	0.00	0.02	0.20	0.22	-0.13	0.00	70.99%	70.99%	14.91%	14.10%
K19-2180	1.67	11.30	54.38	0.06	2.11	13.21	11.35	0.03	0.11	0.00	0.02	0.24	0.26	-0.15	0.00	69.16%	69.16%	16.83%	14.01%
K19-2190	1.38	10.85	54.94	0.06	2.03	13.61	11.09	0.02	0.11	0.00	0.02	0.24	0.25	-0.14	0.00	70.85%	70.85%	14.82%	14.34%

	Na <sub>2</sub> O	Al <sub>2</sub> O <sub>3</sub>	SiO <sub>2</sub>	P <sub>2</sub> O <sub>3</sub>	K <sub>2</sub> O	CaO	CO <sub>2</sub>	Mol	mol	mol	mol	mol	Mol	CaO*(					
	wt%	wt%	wt%	wt%	wt%	wt%	wt%	Na <sub>2</sub> O	Al <sub>2</sub> O <sub>3</sub>	P <sub>2</sub> O <sub>5</sub>	K <sub>2</sub> O	CaO	CO <sub>2</sub>	CaO*	corect	CIA	A%	CN%	K%
Ben Nevis cuttings con't.																			
K19-2200	1.39	10.35	50.26	0.06	1.90	15.29	11.94	0.02	0.10	0.00	0.02	0.27	0.27	-0.14	0.00	70.41%	70.41%	15.58%	14.01%
K19-2210	1.49	9.02	48.53	0.07	1.63	19.84	13.62	0.02	0.09	0.00	0.02	0.35	0.31	-0.11	0.00	68.16%	68.16%	18.52%	13.31%
E09-2830	0.72	12.78	73.76	0.04	2.18	4.61	3.57	0.01	0.13	0.00	0.02	0.08	0.08	-0.04	0.00	78.31%	78.31%	7.22%	14.47%
E09-2835	0.66	12.55	70.05	0.06	2.16	6.05	4.72	0.01	0.12	0.00	0.02	0.11	0.11	-0.05	0.00	78.61%	78.61%	6.77%	14.62%
E09-2840	0.59	9.52	75.86	0.07	1.73	6.67	4.84	0.01	0.09	0.00	0.02	0.12	0.11	-0.05	0.00	77.01%	77.01%	7.88%	15.11%
E09-2845	0.56	10.47	72.35	0.04	1.87	9.59	6.80	0.01	0.10	0.00	0.02	0.17	0.15	-0.06	0.00	78.02%	78.02%	6.89%	15.09%
E09-2850	0.75	8.28	71.68	0.03	1.55	12.57	8.15	0.01	0.08	0.00	0.02	0.22	0.19	-0.05	0.00	73.98%	73.98%	11.05%	14.96%
E09-2855	0.56	9.48	68.99	0.06	1.74	12.10	8.03	0.01	0.09	0.00	0.02	0.22	0.18	-0.06	0.00	77.16%	77.16%	7.53%	15.31%
E09-2860	0.49	7.25	67.98	0.06	1.42	16.31	10.37	0.01	0.07	0.00	0.02	0.29	0.24	-0.06	0.00	75.51%	75.51%	8.45%	16.05%
E09-2865	0.65	9.27	68.22	0.05	1.75	11.91	8.09	0.01	0.09	0.00	0.02	0.21	0.18	-0.06	0.00	75.76%	75.76%	8.76%	15.48%
E09-2870	0.69	8.06	73.99	0.05	1.62	10.40	7.09	0.01	0.08	0.00	0.02	0.19	0.16	-0.06	0.00	73.57%	73.57%	10.40%	16.03%
E09-2875	0.55	7.80	72.82	0.05	1.59	12.19	8.31	0.01	0.08	0.00	0.02	0.22	0.19	-0.07	0.00	74.76%	74.76%	8.75%	16.48%
E09-2880	0.72	8.56	81.23	0.06	1.73	5.78	4.51	0.01	0.08	0.00	0.02	0.10	0.10	-0.05	0.00	73.72%	73.72%	10.17%	16.11%
E09-2885	0.59	8.36	81.87	0.04	1.64	7.51	5.03	0.01	0.08	0.00	0.02	0.13	0.11	-0.04	0.00	75.33%	75.33%	8.68%	16.00%
E09-2895	0.61	8.63	83.30	0.03	1.74	4.89	3.60	0.01	0.08	0.00	0.02	0.09	0.08	-0.04	0.00	75.01%	75.01%	8.65%	16.34%
E09-2900	0.68	9.12	80.03	0.06	1.75	7.80	3.91	0.01	0.09	0.00	0.02	0.14	0.09	0.00	0.00	72.43%	72.43%	12.52%	15.05%
E09-2905	0.60	9.53	81.33	0.03	1.91	4.75	4.38	0.01	0.09	0.00	0.02	0.08	0.10	-0.07	0.00	75.73%	75.73%	7.83%	16.44%
E09-2910	0.58	8.83	84.46	0.02	1.80	3.96	3.67	0.01	0.09	0.00	0.02	0.07	0.08	-0.05	0.00	75.26%	75.26%	8.17%	16.57%
E09-2915	0.59	8.58	84.40	0.03	1.71	4.11	2.48	0.01	0.08	0.00	0.02	0.07	0.06	-0.01	0.00	75.22%	75.22%	8.55%	16.23%
E09-2920	0.52	8.19	83.46	0.04	1.64	6.05	5.18	0.01	0.08	0.00	0.02	0.11	0.12	-0.07	0.00	75.72%	75.72%	7.88%	16.40%
E09-2925	0.53	7.93	81.41	0.04	1.61	8.28	4.97	0.01	0.08	0.00	0.02	0.15	0.11	-0.02	0.00	75.24%	75.24%	8.25%	16.50%
E09-2930	0.65	6.98	74.46	0.05	1.44	11.34	4.13	0.01	0.07	0.00	0.02	0.20	0.09	0.06	0.06	44.39%	44.39%	45.72%	9.89%
E09-2935	0.76	9.37	75.04	0.10	1.94	5.62	6.01	0.01	0.09	0.00	0.02	0.10	0.14	-0.11	0.00	73.68%	73.68%	9.82%	16.50%
E09-2940	0.70	10.46	80.84	0.07	2.09	3.96	3.19	0.01	0.10	0.00	0.02	0.07	0.07	-0.04	0.00	75.35%	75.35%	8.32%	16.33%
E09-2955	0.86	12.02	56.28	0.10	2.03	5.31	4.59	0.01	0.12	0.00	0.02	0.09	0.10	-0.06	0.00	76.95%	76.95%	9.01%	14.04%
E09-2960	0.76	10.07	64.12	0.05	1.70	12.05	5.80	0.01	0.10	0.00	0.02	0.21	0.13	0.02	0.02	68.00%	68.00%	19.61%	12.39%
E09-2965	0.40	4.50	85.04	0.02	0.99	5.00	2.60	0.01	0.04	0.00	0.01	0.09	0.06	0.00	0.00	71.94%	71.94%	10.90%	17.16%
E09-2970	0.44	4.84	80.33	0.02	1.04	5.08	2.19	0.01	0.05	0.00	0.01	0.09	0.05	0.02	0.02	58.67%	58.67%	27.71%	13.62%
E09-2975	0.38	4.90	85.14	0.02	1.09	4.26	2.40	0.01	0.05	0.00	0.01	0.08	0.05	-0.01	0.00	73.08%	73.08%	9.32%	17.60%
E09-2980	0.45	4.55	77.09	0.02	1.03	6.45	3.30	0.01	0.04	0.00	0.01	0.11	0.07	0.00	0.00	68.69%	68.69%	14.53%	16.78%
E09-2985	0.30	3.33	84.64	0.01	0.81	7.41	3.32	0.00	0.03	0.00	0.01	0.13	0.08	0.02	0.02	50.45%	50.45%	36.32%	13.23%
E09-2990	0.26	2.91	75.25	0.02	0.72	9.24	4.25	0.00	0.03	0.00	0.01	0.16	0.10	0.02	0.02	47.91%	47.91%	39.36%	12.74%
E09-2995	0.30	2.65	82.00	0.04	0.66	9.42	4.39	0.00	0.03	0.00	0.01	0.17	0.10	0.02	0.02	47.13%	47.13%	40.11%	12.76%
E09-3000	0.30	2.88	81.37	0.02	0.74	9.09	4.38	0.00	0.03	0.00	0.01	0.16	0.10	0.01	0.01	52.81%	52.81%	32.49%	14.70%

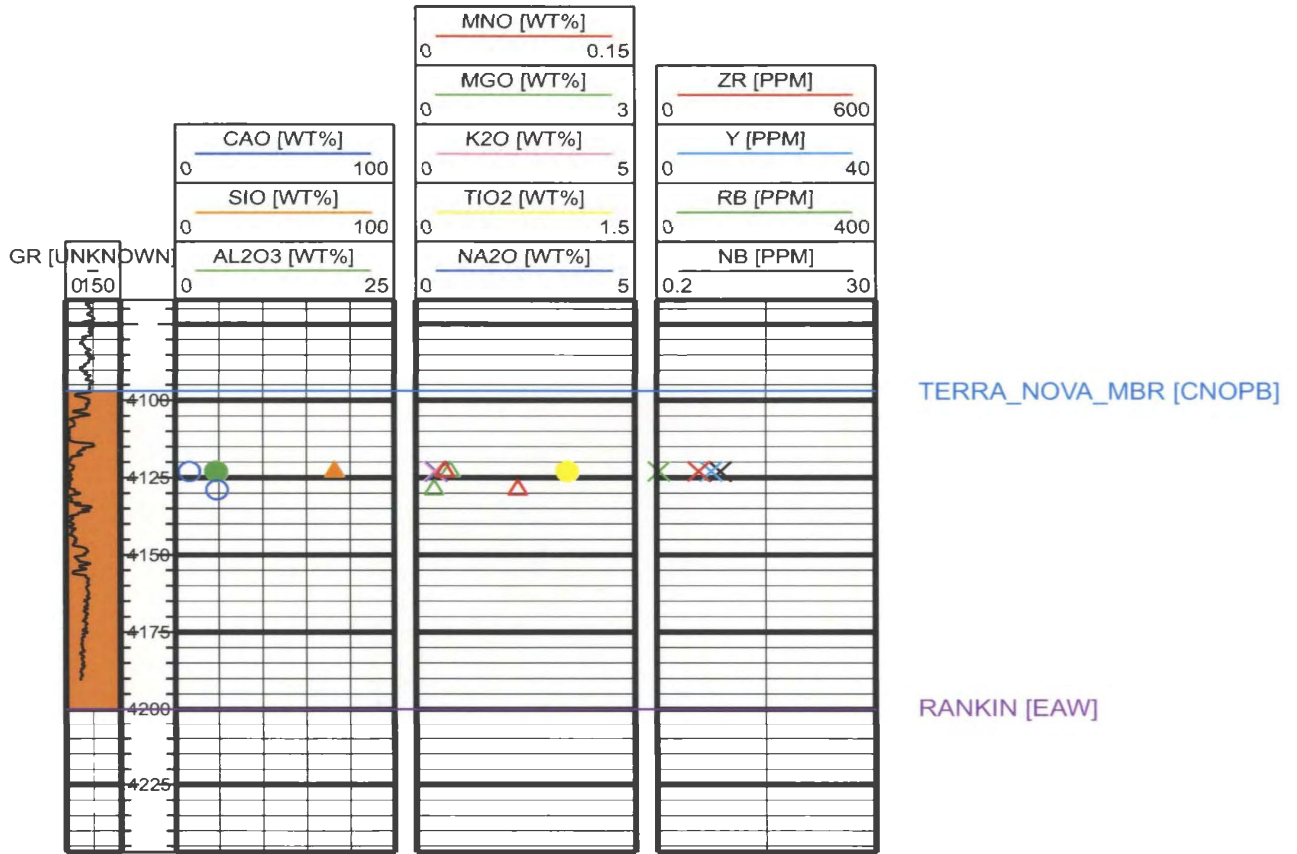
	Na <sub>2</sub> O	Al <sub>2</sub> O <sub>3</sub>	SiO <sub>2</sub>	P <sub>2</sub> O <sub>3</sub>	K <sub>2</sub> O	CaO	CO <sub>2</sub>	Mol	mol	mol	mol	mol	Mol	CaO*	CaO*( correct ed)	CIA	A%	CN%	K%
	wt%	wt%	wt%	wt%	wt%	wt%	wt%	Na <sub>2</sub> O	Al <sub>2</sub> O <sub>3</sub>	P <sub>2</sub> O <sub>5</sub>	K <sub>2</sub> O	CaO	CO <sub>2</sub>	CaO*					
Ben Nevis cuttings con't.																			
E09-3005	0.31	3.60	77.70	0.02	0.82	8.81	4.32	0.00	0.04	0.00	0.01	0.16	0.10	0.01	0.01	60.49%	60.49%	24.58%	14.93%
E09-3010	0.28	4.22	71.02	0.03	0.92	15.54	7.20	0.00	0.04	0.00	0.01	0.28	0.16	0.03	0.03	47.80%	47.80%	40.94%	11.26%
E09-3015	0.33	4.76	64.74	0.02	1.01	15.32	7.00	0.01	0.05	0.00	0.01	0.27	0.16	0.03	0.03	48.07%	48.07%	40.86%	11.07%
E09-3020	0.34	4.83	71.87	0.02	0.98	11.25	4.52	0.01	0.05	0.00	0.01	0.20	0.10	0.05	0.05	43.39%	43.39%	47.08%	9.53%
E09-3025	0.35	4.40	74.66	0.03	0.98	9.80	2.64	0.01	0.04	0.00	0.01	0.17	0.06	0.08	0.08	30.09%	30.09%	62.66%	7.25%
E09-3030	0.37	5.02	78.19	0.03	1.15	10.01	4.19	0.01	0.05	0.00	0.01	0.18	0.10	0.03	0.03	48.14%	48.14%	39.92%	11.95%
E09-3035	0.32	3.64	77.82	0.02	0.84	11.14	4.24	0.01	0.04	0.00	0.01	0.20	0.10	0.05	0.05	34.56%	34.56%	56.84%	8.59%
E09-3040	0.36	3.70	90.48	0.02	0.86	7.42	3.80	0.01	0.04	0.00	0.01	0.13	0.09	0.00	0.00	67.79%	67.79%	15.18%	17.03%
<b>Avg</b>	<b>1.40</b>	<b>6.89</b>	<b>67.19</b>	<b>0.04</b>	<b>2.02</b>	<b>12.68</b>	<b>8.55</b>	<b># 0.02</b>	<b>0.07</b>	<b>0.00</b>	<b>0.02</b>	<b>0.23</b>	<b>0.19</b>	<b>-0.07</b>	<b>0.01</b>	<b>58.53%</b>	<b>58.53%</b>	<b>22.09%</b>	<b>19.38%</b>
Avalon cuttings																			
H20-3180	0.42	3.87	73.97	0.05	1.90	12.15	6.89	0.01	0.04	0.00	0.02	0.22	0.16	-0.02	0.00	58.51%	58.51%	10.42%	31.07%
H20-3185	0.47	1.88	65.84	0.03	1.79	19.39	10.03	0.01	0.02	0.00	0.02	0.35	0.23	0.00	0.00	38.31%	38.31%	22.16%	39.53%
H20-3190	0.80	2.98	62.33	0.04	2.16	15.86	8.04	0.01	0.03	0.00	0.02	0.28	0.18	0.01	0.01	40.02%	40.02%	28.58%	31.40%
H20-3195	0.40	2.74	63.99	0.03	1.42	15.40	7.37	0.01	0.03	0.00	0.02	0.27	0.17	0.02	0.02	37.74%	37.74%	41.07%	21.19%
H20-3200	0.48	3.56	67.82	0.03	1.80	11.93	6.21	0.01	0.03	0.00	0.02	0.21	0.14	0.00	0.00	56.38%	56.38%	12.68%	30.93%
H20-3205	0.46	4.07	68.53	0.03	1.95	14.92	7.88	0.01	0.04	0.00	0.02	0.27	0.18	0.00	0.00	58.58%	58.58%	10.96%	30.46%
H20-3210	0.29	2.05	64.03	0.02	1.19	20.95	10.38	0.00	0.02	0.00	0.01	0.37	0.24	0.02	0.02	35.53%	35.53%	42.24%	22.23%
H20-3215	0.39	2.50	71.13	0.02	1.40	12.76	6.31	0.01	0.02	0.00	0.01	0.23	0.14	0.01	0.01	42.50%	42.50%	31.78%	25.72%
H20-3220	0.46	1.98	68.45	0.02	1.58	14.33	7.32	0.01	0.02	0.00	0.02	0.26	0.17	0.01	0.01	39.74%	39.74%	26.03%	34.23%
H20-3225	0.63	2.88	68.11	0.02	1.65	10.63	7.10	0.01	0.03	0.00	0.02	0.19	0.16	-0.05	0.00	50.50%	50.50%	18.15%	31.35%
H20-3230	0.54	2.46	67.18	0.03	1.30	16.07	8.37	0.01	0.02	0.00	0.01	0.29	0.19	0.00	0.00	51.71%	51.71%	18.67%	29.63%
H20-3235	0.68	3.66	65.91	0.03	1.93	11.88	6.94	0.01	0.04	0.00	0.02	0.21	0.16	-0.03	0.00	53.30%	53.30%	16.33%	30.37%
H20-3240	0.50	2.52	69.04	0.02	1.98	12.41	7.68	0.01	0.02	0.00	0.02	0.22	0.17	-0.04	0.00	45.87%	45.87%	15.04%	39.08%
H20-3245	0.37	2.94	67.87	0.02	1.54	14.17	8.19	0.01	0.03	0.00	0.02	0.25	0.19	-0.03	0.00	56.34%	56.34%	11.67%	31.99%
H20-3250	0.38	2.92	62.86	0.04	1.65	18.77	10.38	0.01	0.03	0.00	0.02	0.33	0.24	-0.02	0.00	54.72%	54.72%	11.78%	33.50%
H20-3255	0.36	3.10	66.18	0.04	1.58	16.44	10.15	0.01	0.03	0.00	0.02	0.29	0.23	-0.05	0.00	57.51%	57.51%	10.88%	31.61%
H20-3260	0.51	2.54	64.91	0.03	1.54	19.78	11.16	0.01	0.02	0.00	0.02	0.35	0.25	-0.03	0.00	50.36%	50.36%	16.52%	33.12%
H20-3265	0.41	4.09	71.93	0.03	1.80	9.96	5.28	0.01	0.04	0.00	0.02	0.18	0.12	0.00	0.00	60.97%	60.97%	10.05%	28.98%
H20-3270	0.48	4.05	73.72	0.02	1.83	9.39	4.91	0.01	0.04	0.00	0.02	0.17	0.11	0.00	0.00	59.35%	59.35%	11.59%	29.05%
H20-3275	0.55	4.17	78.10	0.02	1.91	6.61	3.79	0.01	0.04	0.00	0.02	0.12	0.09	-0.01	0.00	58.42%	58.42%	12.58%	29.00%
H20-3280	0.48	3.14	73.97	0.03	1.70	10.14	5.50	0.01	0.03	0.00	0.02	0.18	0.12	-0.01	0.00	54.46%	54.46%	13.63%	31.91%
H20-3285	0.50	1.92	73.61	0.03	1.47	13.14	7.01	0.01	0.02	0.00	0.02	0.23	0.16	-0.01	0.00	44.23%	44.23%	19.01%	36.76%
H20-3290	0.44	1.75	75.53	0.02	1.50	10.28	5.00	0.01	0.02	0.00	0.02	0.18	0.11	0.01	0.01	32.76%	32.76%	36.96%	30.29%
H20-3295	0.42	1.90	72.99	0.02	1.45	10.22	4.79	0.01	0.02	0.00	0.02	0.18	0.11	0.02	0.02	31.44%	31.44%	42.53%	26.03%

	Na <sub>2</sub> O	Al <sub>2</sub> O <sub>3</sub>	SiO <sub>2</sub>	P <sub>2</sub> O <sub>3</sub>	K <sub>2</sub> O	CaO	CO <sub>2</sub>	Mol	mol	mol	mol	mol	Mol	CaO*(	corect	CIA	A%	CN%	K%
	wt%	wt%	wt%	wt%	wt%	wt%	wt%	Na <sub>2</sub> O	Al <sub>2</sub> O <sub>3</sub>	P <sub>2</sub> O <sub>3</sub>	K <sub>2</sub> O	CaO	CO <sub>2</sub>	CaO*	ed)				
Avalon cuttings con't.																			
H20-3300	0.36	1.93	67.11	0.02	1.30	17.02	8.79	0.01	0.02	0.00	0.01	0.30	0.20	0.00	0.00	45.13%	45.13%	22.01%	32.86%
H20-3305	0.49	2.17	77.74	0.02	1.65	8.76	4.98	0.01	0.02	0.00	0.02	0.16	0.11	-0.01	0.00	45.59%	45.59%	16.80%	37.61%
H20-3310	0.48	2.06	71.86	0.02	1.51	11.49	6.07	0.01	0.02	0.00	0.02	0.20	0.14	0.00	0.00	45.92%	45.92%	17.63%	36.44%
H20-3315	0.39	1.76	62.29	0.02	1.33	21.25	11.62	0.01	0.02	0.00	0.01	0.38	0.26	-0.02	0.00	45.72%	45.72%	16.81%	37.47%
H20-3320	0.35	1.18	40.85	0.03	1.23	36.11	20.26	0.01	0.01	0.00	0.01	0.64	0.46	-0.05	0.00	38.24%	38.24%	18.55%	43.21%
J22-1-2890	0.97	3.01	59.93	0.06	0.58	22.43	13.74	0.02	0.03	0.00	0.01	0.40	0.31	-0.07	0.00	57.49%	57.49%	30.54%	11.96%
J22-1-2895	2.04	5.19	68.08	0.02	0.99	6.36	5.00	0.03	0.05	0.00	0.01	0.11	0.11	-0.06	0.00	54.00%	54.00%	34.83%	11.17%
J22-1-2900	1.08	5.27	78.33	0.09	0.95	6.26	4.80	0.02	0.05	0.00	0.01	0.11	0.11	-0.05	0.00	65.25%	65.25%	22.07%	12.68%
J22-1-2905	0.85	6.14	85.00	0.03	1.04	2.33	2.42	0.01	0.06	0.00	0.01	0.04	0.05	-0.04	0.00	70.95%	70.95%	16.07%	12.98%
J22-1-2910	0.61	7.40	75.96	0.02	1.27	3.90	4.35	0.01	0.07	0.00	0.01	0.07	0.10	-0.08	0.00	75.64%	75.64%	10.32%	14.04%
J22-1-2920	0.73	7.99	46.35	0.20	1.53	9.32	9.41	0.01	0.08	0.00	0.02	0.17	0.21	-0.16	0.00	73.63%	73.63%	11.10%	15.28%
<b>Avg</b>	<b>0.57</b>	<b>3.25</b>	<b>68.33</b>	<b>0.03</b>	<b>1.53</b>	<b>13.51</b>	<b>7.66</b>	<b># 0.01</b>	<b>0.03</b>	<b>0.00</b>	<b>0.02</b>	<b>0.24</b>	<b>0.17</b>	<b>-0.02</b>	<b>0.00</b>	<b>51.05%</b>	<b>51.05%</b>	<b>20.23%</b>	<b>28.72%</b>
A mrk mbr cuttings																			
H20-3335	0.88	11.32	43.70	0.06	3.58	15.70	13.98	0.01	0.11	0.00	0.04	0.28	0.32	-0.20	0.00	68.01%	68.01%	8.74%	23.25%
H20-3340	0.49	5.20	32.66	0.04	2.33	39.20	25.97	0.01	0.05	0.00	0.02	0.70	0.59	-0.19	0.00	61.00%	61.00%	9.44%	29.57%
H20-3345	0.43	5.25	33.53	0.04	1.73	40.20	25.89	0.01	0.05	0.00	0.02	0.72	0.59	-0.17	0.00	67.00%	67.00%	9.04%	23.96%
H20-3350	0.36	3.20	25.82	0.03	1.91	45.10	29.81	0.01	0.03	0.00	0.02	0.80	0.68	-0.21	0.00	54.61%	54.61%	10.16%	35.24%
H20-3355	0.35	3.17	25.91	0.04	1.67	44.88	29.97	0.01	0.03	0.00	0.02	0.80	0.68	-0.22	0.00	57.12%	57.12%	10.37%	32.51%
H20-3360	0.36	1.95	20.88	0.03	1.72	49.06	32.83	0.01	0.02	0.00	0.02	0.87	0.75	-0.24	0.00	44.26%	44.26%	13.37%	42.37%
H20-3365	0.30	2.18	22.62	0.03	1.33	49.97	31.66	0.00	0.02	0.00	0.01	0.89	0.72	-0.19	0.00	52.99%	52.99%	12.11%	34.89%
H20-3370	0.62	4.55	31.82	0.03	2.19	39.11	27.38	0.01	0.04	0.00	0.02	0.70	0.62	-0.24	0.00	57.31%	57.31%	12.82%	29.87%
H20-3375	0.38	4.85	34.52	0.04	1.81	39.65	26.15	0.01	0.05	0.00	0.02	0.71	0.59	-0.19	0.00	65.20%	65.20%	8.40%	26.40%
E09-3045	0.29	3.22	92.19	0.02	0.78	6.82	2.56	0.00	0.03	0.00	0.01	0.12	0.06	0.03	0.03	40.23%	40.23%	49.23%	10.54%
E09-3050	0.23	2.90	80.90	0.03	0.66	12.61	6.03	0.00	0.03	0.00	0.01	0.22	0.14	0.02	0.02	49.30%	49.30%	38.61%	12.08%
E09-3055	0.24	1.76	79.98	0.03	0.46	16.73	7.03	0.00	0.02	0.00	0.00	0.30	0.16	0.06	0.06	20.55%	20.55%	73.63%	5.81%
E09-3060	0.24	2.25	81.78	0.02	0.56	15.20	7.80	0.00	0.02	0.00	0.01	0.27	0.18	0.00	0.00	59.98%	59.98%	23.74%	16.27%
E09-3065	0.38	2.93	69.04	0.03	0.70	16.83	5.44	0.01	0.03	0.00	0.01	0.30	0.12	0.11	0.11	18.40%	18.40%	76.83%	4.78%
E09-3070	0.50	2.56	92.62	0.02	0.63	5.44	2.65	0.01	0.03	0.00	0.01	0.10	0.06	0.01	0.01	54.49%	54.49%	31.09%	14.42%
E09-3075	0.33	2.35	79.48	0.02	0.56	14.30	7.30	0.01	0.02	0.00	0.01	0.26	0.17	0.01	0.01	57.71%	57.71%	27.54%	14.75%
E09-3080	0.23	2.20	70.06	0.03	0.50	22.95	12.51	0.00	0.02	0.00	0.01	0.41	0.28	-0.02	0.00	70.66%	70.66%	11.94%	17.40%
E09-3085	0.20	1.93	73.53	0.03	0.48	20.92	11.30	0.00	0.02	0.00	0.01	0.37	0.26	-0.01	0.00	69.60%	69.60%	11.76%	18.64%
E09-3090	0.36	1.97	77.25	0.03	0.49	17.11	9.15	0.01	0.02	0.00	0.01	0.31	0.21	-0.01	0.00	63.84%	63.84%	18.95%	17.21%
E09-3095	0.36	1.84	74.58	0.02	0.47	17.80	9.71	0.01	0.02	0.00	0.00	0.32	0.22	-0.01	0.00	62.67%	62.67%	19.95%	17.38%
E09-3100	0.21	1.86	77.95	0.03	0.46	17.38	9.59	0.00	0.02	0.00	0.00	0.31	0.22	-0.02	0.00	68.75%	68.75%	12.99%	18.26%

	Na <sub>2</sub> O wt%	Al <sub>2</sub> O <sub>3</sub> wt%	SiO <sub>2</sub> wt%	P <sub>2</sub> O <sub>3</sub> wt%	K <sub>2</sub> O wt%	CaO wt%	CO <sub>2</sub> wt%	Mol Na <sub>2</sub> O	mol Al <sub>2</sub> O <sub>3</sub>	mol P <sub>2</sub> O <sub>5</sub>	mol K <sub>2</sub> O	mol CaO	Mol CO <sub>2</sub>	CaO*( corect ed)	CIA	A%	CN%	K%	
A mrk mbr cuttings con't.																			
E09-3105	0.15	1.36	73.31	0.03	0.33	21.38	9.20	0.00	0.01	0.00	0.00	0.38	0.21	0.07	0.07	15.45%	15.45%	80.44%	4.10%
E09-3110	0.17	1.46	71.47	0.02	0.37	21.55	11.26	0.00	0.01	0.00	0.00	0.38	0.26	0.00	0.00	67.80%	67.80%	13.51%	18.69%
E09-3115	0.25	3.21	63.80	0.02	0.71	24.87	13.35	0.00	0.03	0.00	0.01	0.44	0.30	-0.01	0.00	73.24%	73.24%	9.25%	17.52%
E09-3120	0.23	3.09	61.50	0.06	0.66	23.81	11.86	0.00	0.03	0.00	0.01	0.42	0.27	0.02	0.02	50.28%	50.28%	38.02%	11.69%
E09-3125	0.29	2.71	71.18	0.05	0.59	18.18	9.32	0.00	0.03	0.00	0.01	0.32	0.21	0.01	0.01	61.96%	61.96%	23.50%	14.54%
E09-3130	0.33	2.50	71.02	0.03	0.56	19.43	10.59	0.01	0.02	0.00	0.01	0.35	0.24	-0.02	0.00	68.64%	68.64%	14.77%	16.59%
E09-3135	0.20	1.84	77.50	0.02	0.41	19.16	10.41	0.00	0.02	0.00	0.00	0.34	0.24	-0.01	0.00	70.23%	70.23%	12.74%	17.03%
E09-3140	0.15	1.75	59.20	0.02	0.43	28.98	12.73	0.00	0.02	0.00	0.00	0.52	0.29	0.08	0.00	71.23%	71.23%	9.81%	18.95%
E09-3145	0.14	2.71	25.42	0.04	0.68	50.04	32.04	0.00	0.03	0.00	0.01	0.89	0.73	-0.20	0.00	73.88%	73.88%	6.07%	20.05%
E09-3150	0.10	2.22	13.91	0.03	0.55	59.85	36.45	0.00	0.02	0.00	0.01	1.07	0.83	-0.18	0.00	74.72%	74.72%	5.33%	19.96%
E09-3155	0.15	2.26	13.73	0.03	0.56	59.61	36.30	0.00	0.02	0.00	0.01	1.06	0.82	-0.17	0.00	72.54%	72.54%	7.86%	19.60%
E09-3160	0.17	2.66	16.25	0.02	0.62	57.39	34.49	0.00	0.03	0.00	0.01	1.02	0.78	-0.15	0.00	73.56%	73.56%	7.87%	18.56%
E09-3165	0.34	8.92	34.63	0.03	1.66	38.15	27.51	0.01	0.09	0.00	0.02	0.68	0.63	-0.26	0.00	79.14%	79.14%	4.90%	15.96%
E09-3170	0.26	5.67	23.91	0.03	1.16	49.45	31.90	0.00	0.06	0.00	0.01	0.88	0.72	-0.21	0.00	77.18%	77.18%	5.81%	17.01%
E09-3175	0.14	3.24	16.64	0.03	0.73	57.44	34.73	0.00	0.03	0.00	0.01	1.02	0.79	-0.16	0.00	76.04%	76.04%	5.47%	18.48%
E09-3180	0.09	2.06	11.34	0.03	0.49	62.57	36.04	0.00	0.02	0.00	0.01	1.12	0.82	-0.11	0.00	74.95%	74.95%	5.63%	19.42%
E09-3185	0.09	1.92	10.86	0.03	0.45	63.41	37.98	0.00	0.02	0.00	0.00	1.13	0.86	-0.16	0.00	75.25%	75.25%	5.62%	19.13%
E09-3190	0.11	1.58	12.04	0.03	0.36	62.17	36.94	0.00	0.02	0.00	0.00	1.11	0.84	-0.15	0.00	73.38%	73.38%	8.31%	18.31%
E09-3195	0.10	1.82	12.58	0.02	0.41	60.50	37.62	0.00	0.02	0.00	0.00	1.08	0.85	-0.20	0.00	74.94%	74.94%	6.58%	18.48%
E09-3200	0.12	1.87	22.57	0.03	0.40	55.61	32.27	0.00	0.02	0.00	0.00	0.99	0.73	-0.11	0.00	74.47%	74.47%	8.10%	17.43%
E09-3205	0.28	3.51	28.90	0.03	0.72	49.14	31.00	0.00	0.03	0.00	0.01	0.88	0.70	-0.18	0.00	74.00%	74.00%	9.58%	16.43%
E09-3210	0.26	3.79	28.58	0.03	0.76	48.45	31.47	0.00	0.04	0.00	0.01	0.86	0.72	-0.21	0.00	75.22%	75.22%	8.43%	16.34%
E09-3215	0.47	6.54	40.99	0.03	1.29	35.34	24.76	0.01	0.06	0.00	0.01	0.63	0.56	-0.21	0.00	75.03%	75.03%	8.91%	16.07%
L08-3102.5	24.74	1.39	12.67	0.02	15.24	33.95	27.12	0.40	0.01	0.00	0.16	0.61	0.62	-0.32	0.00	2.37%	2.37%	69.47%	28.16%
L08-3127.5	3.83	16.91	60.44	0.47	2.81	4.86	31.43	0.06	0.17	0.00	0.03	0.09	0.71	-1.00	0.00	64.41%	64.41%	24.00%	11.59%
<b>Avg</b>	<b>0.89</b>	<b>3.40</b>	<b>46.85</b>	<b>0.04</b>	<b>1.26</b>	<b>34.18</b>	<b>21.38</b>	<b># 0.01</b>	<b>0.03</b>	<b>0.00</b>	<b>0.01</b>	<b>0.61</b>	<b>0.49</b>	<b>-0.12</b>	<b>0.01</b>	<b>61.60%</b>	<b>61.60%</b>	<b>19.36%</b>	<b>19.04%</b>
B mrk mbr cuttings																			
F20-2275	0.20	2.18	22.64	0.04	0.52	52.53	30.49	0.00	0.02	0.00	0.01	0.94	0.69	-0.10	0.00	71.13%	71.13%	10.56%	18.31%
F20-2285	0.09	1.05	5.09	0.03	0.21	65.42	39.60	0.00	0.01	0.00	0.00	1.17	0.90	-0.18	0.00	73.84%	73.84%	9.92%	16.24%
F20-2295	0.28	4.25	19.15	0.04	0.88	46.30	32.98	0.00	0.04	0.00	0.01	0.83	0.75	-0.30	0.00	74.94%	74.94%	8.19%	16.87%
F20-2305	0.34	7.88	34.70	0.05	1.63	34.47	23.49	0.01	0.08	0.00	0.02	0.61	0.53	-0.19	0.00	77.20%	77.20%	5.47%	17.34%
<b>Avg</b>	<b>0.23</b>	<b>3.84</b>	<b>20.40</b>	<b>0.04</b>	<b>0.81</b>	<b>49.68</b>	<b>31.64</b>	<b># 0.00</b>	<b>0.04</b>	<b>0.00</b>	<b>0.01</b>	<b>0.89</b>	<b>0.72</b>	<b>-0.19</b>	<b>0.00</b>	<b>74.28%</b>	<b>74.28%</b>	<b>8.53%</b>	<b>17.19%</b>

Appendix 7  
Gamma Ray Logs with immobile element values for all samples

# C73



# G57



FORTUNE\_BAY [EAW]  
 JEANNE\_D'ARC\_FRM [AFD]  
 TERRA\_NOVA\_MBR [CNOPB]

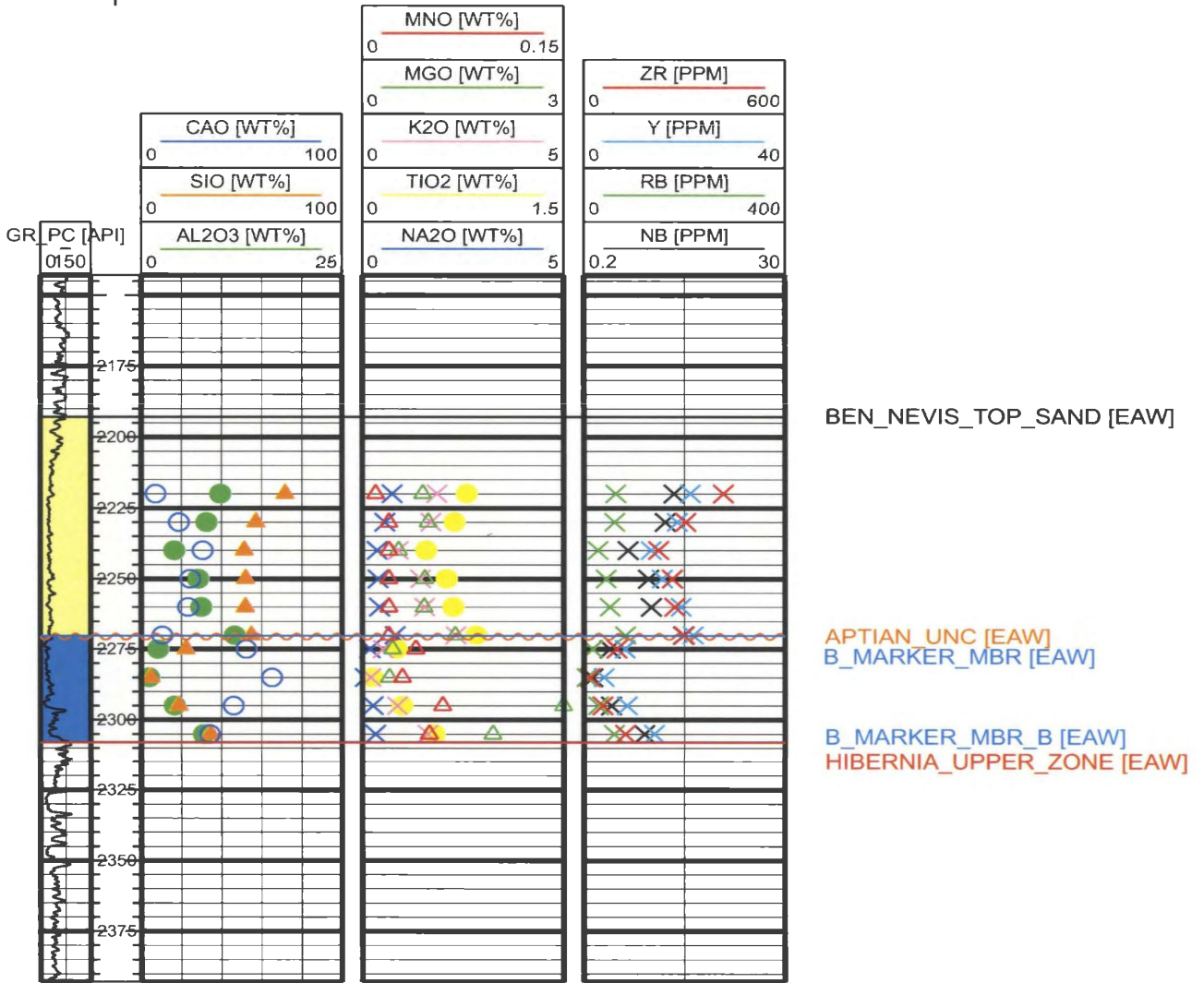
RANKIN [EAW]

VOYAGER [EAW]  
 L\_TEMPEST\_TOP [CNOPB]  
 L\_TEMPEST\_BASE [CNOPB]

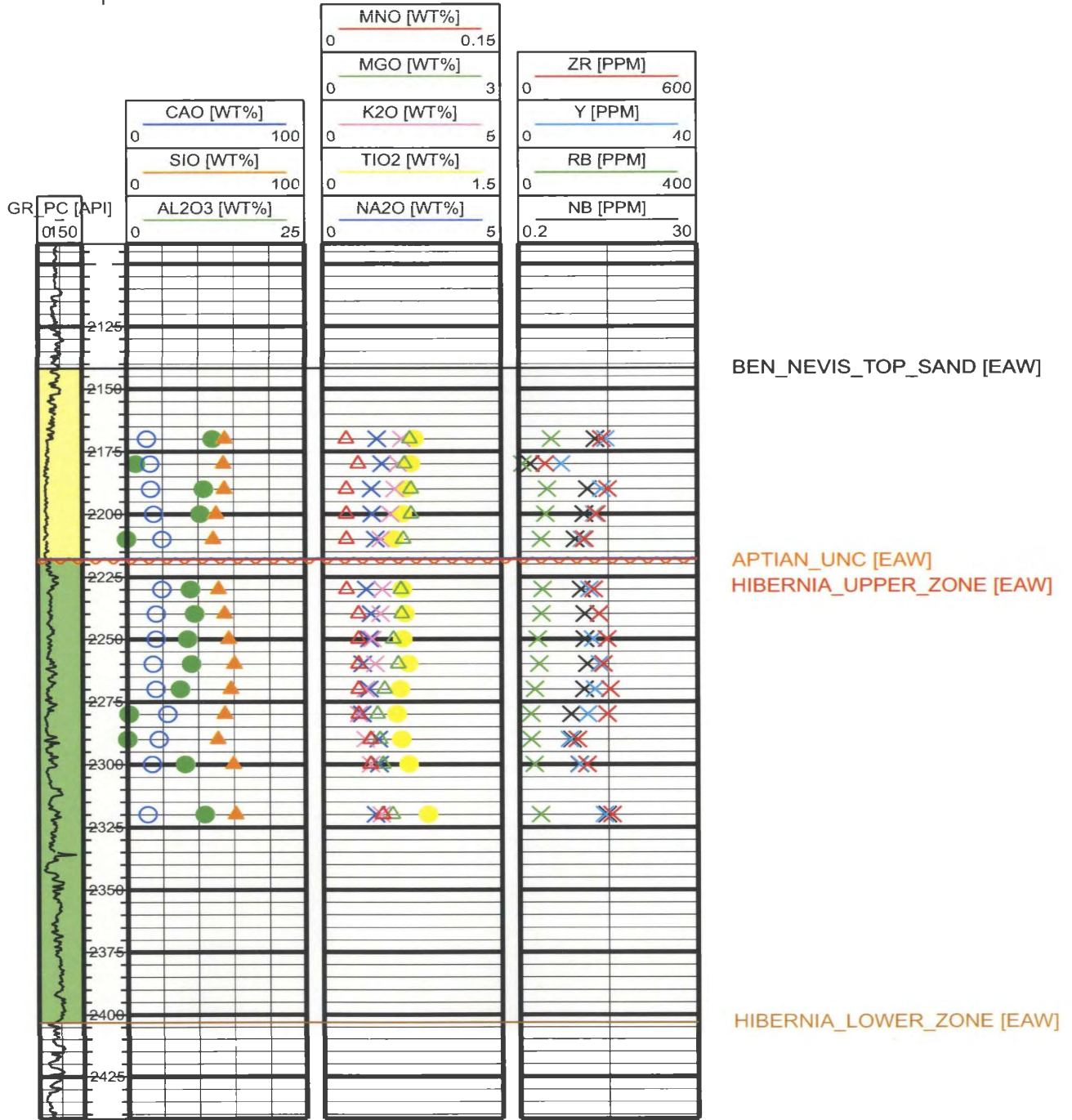
# C-17



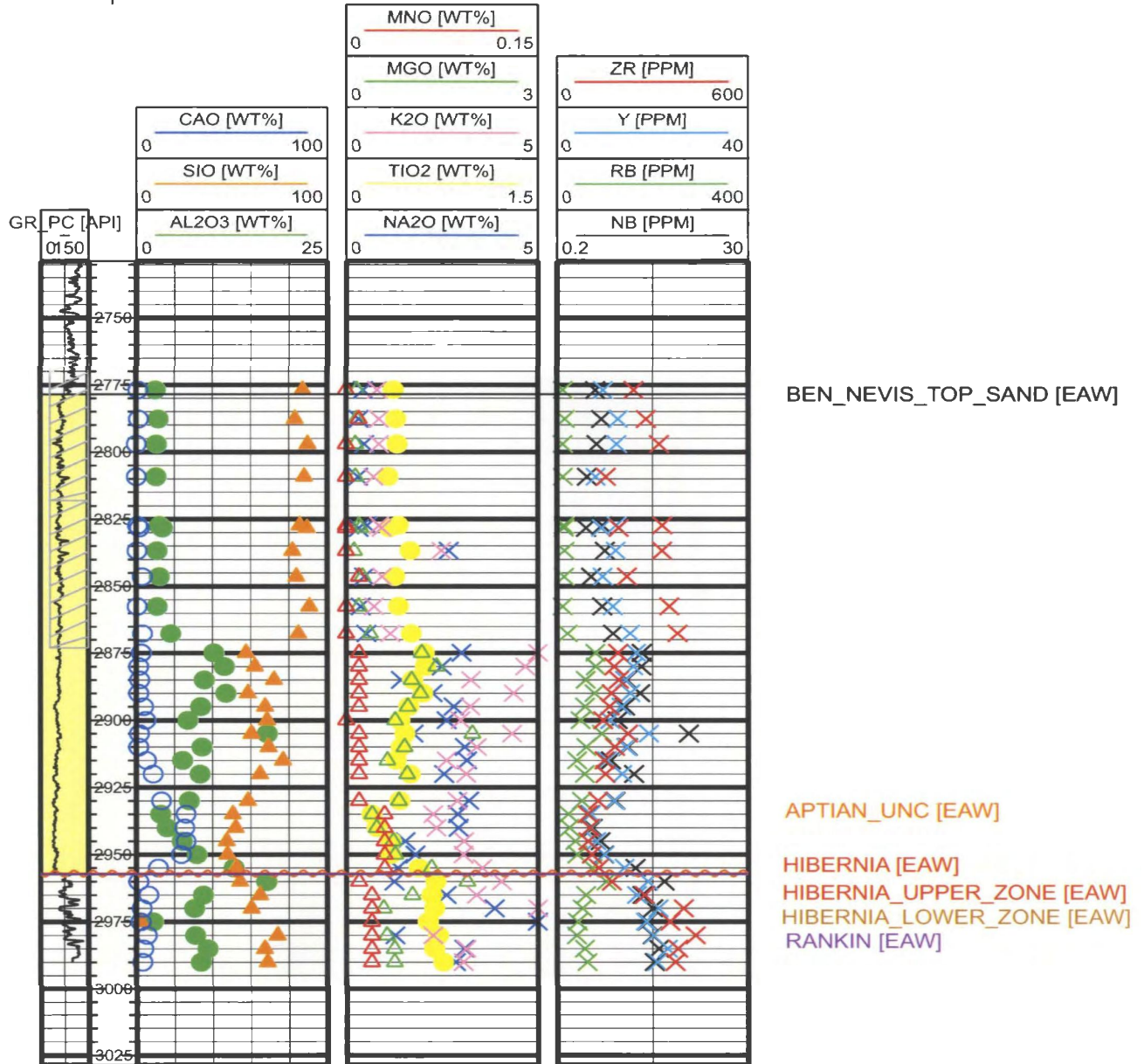
# F-20



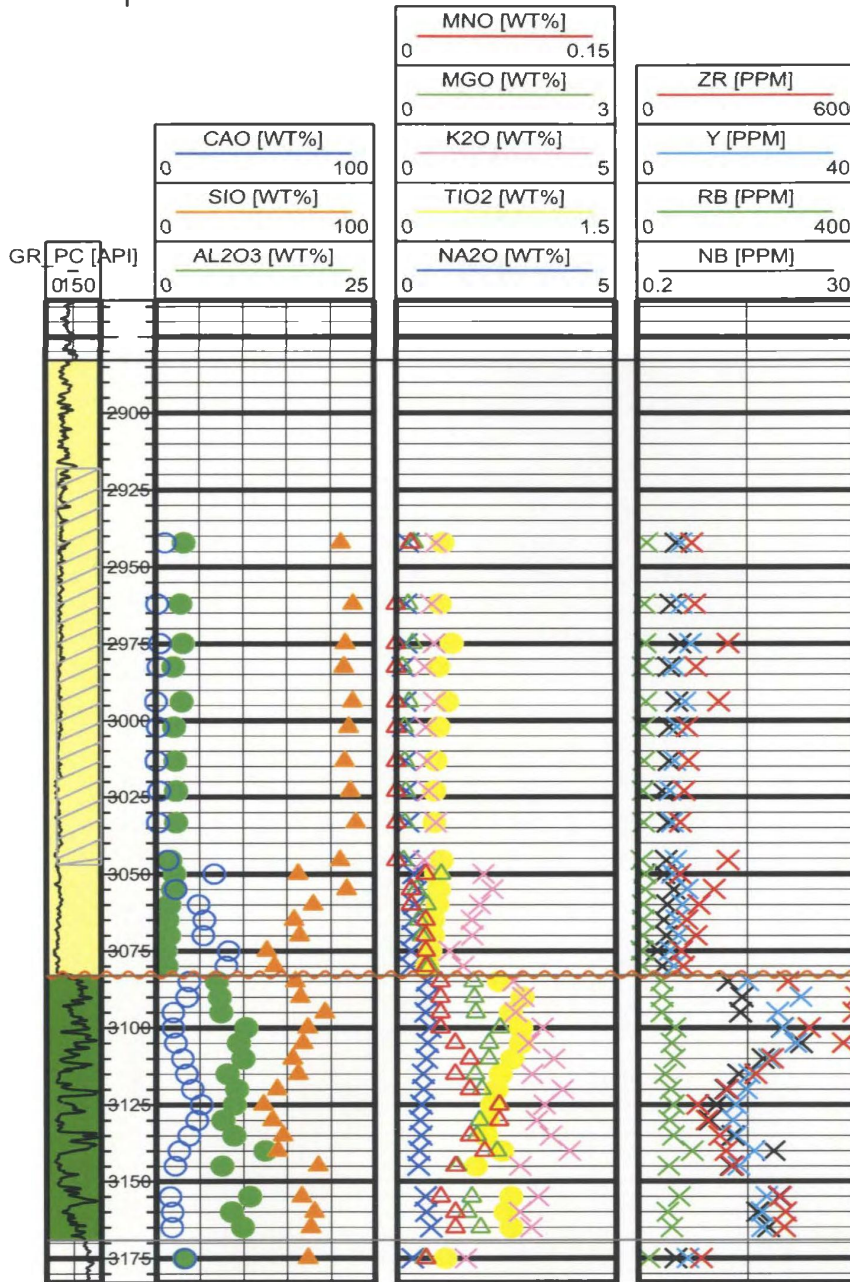
# K-19



# F-04



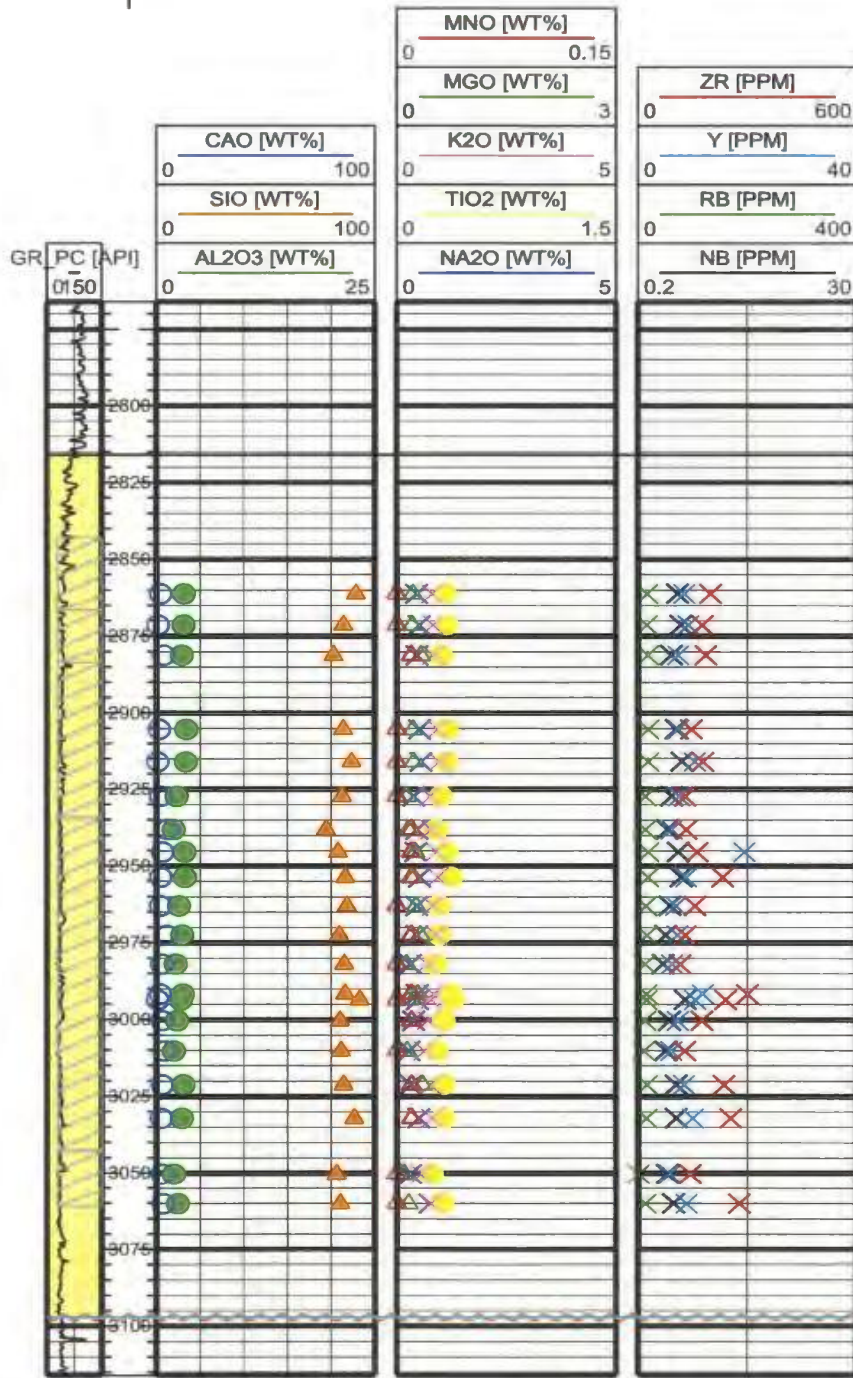
# A-17



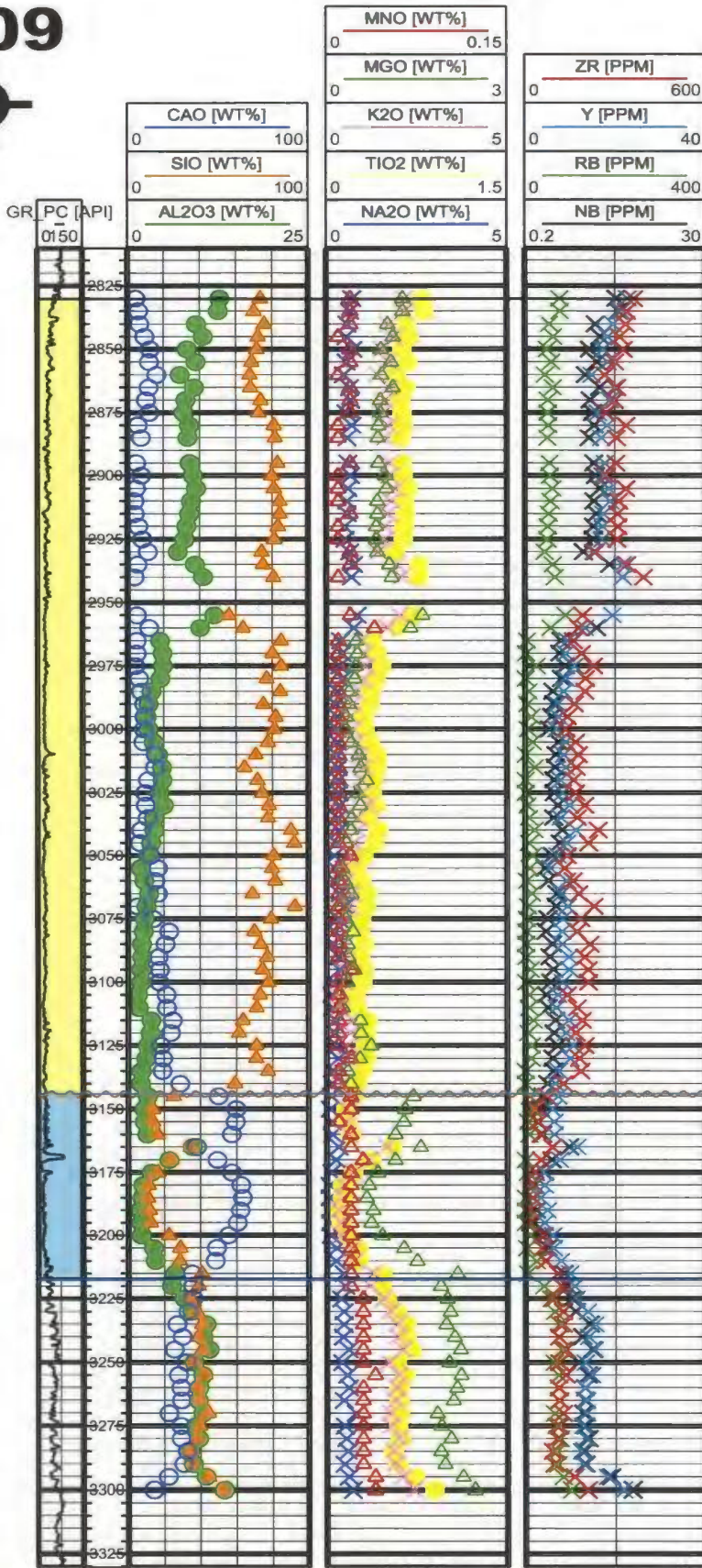
BEN\_NEVIS\_TOP\_SAND [EAW]

APTIAN UNC [EAW]  
HIBERNIA\_LOWER\_ZONE [EAW]

# L-08



# E-09



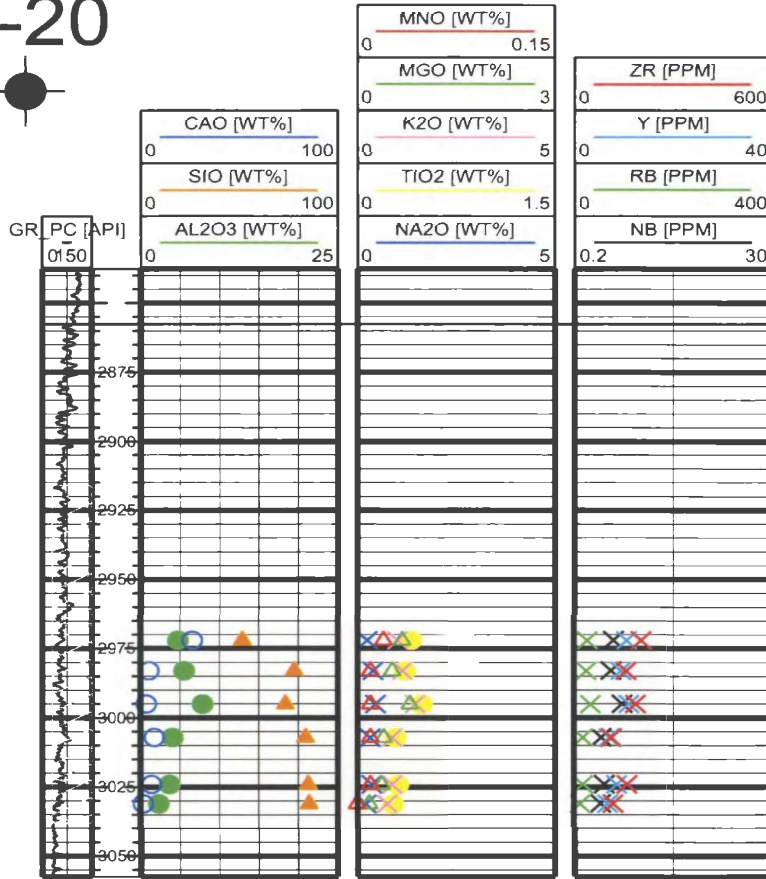
BEN\_NEVIS\_TOP\_SAND [EAW]

EASTERN\_SHOALS [EAW]  
APTIAN\_UNC [EAW]

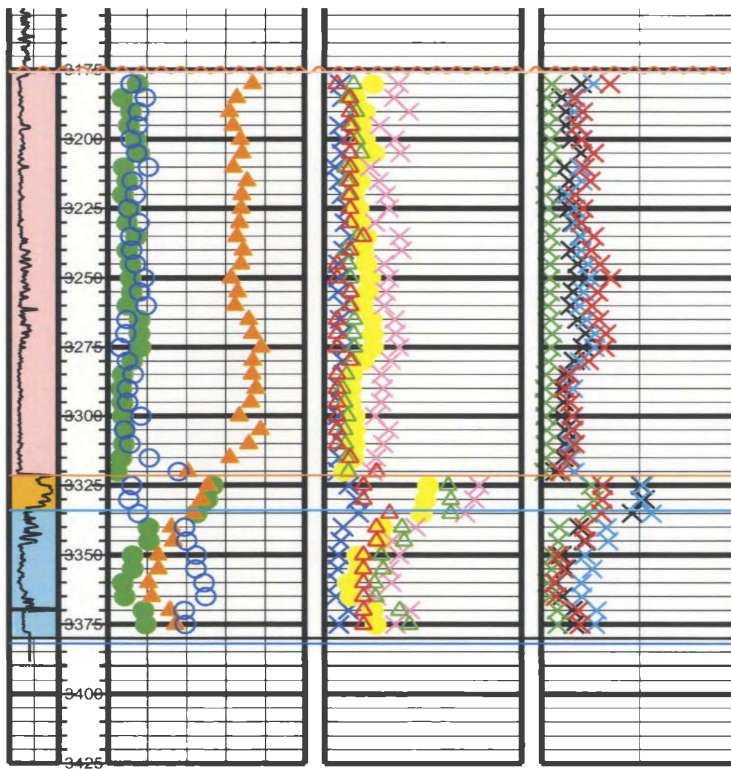
A\_MARKER\_MBR [EAW]

A\_MRK\_MBR\_B [EAW]  
WHITEROSE [EAW]

# H-20



BEN\_NEVIS\_TOP\_SAND [EAW]



APTIAN UNC [EAW]

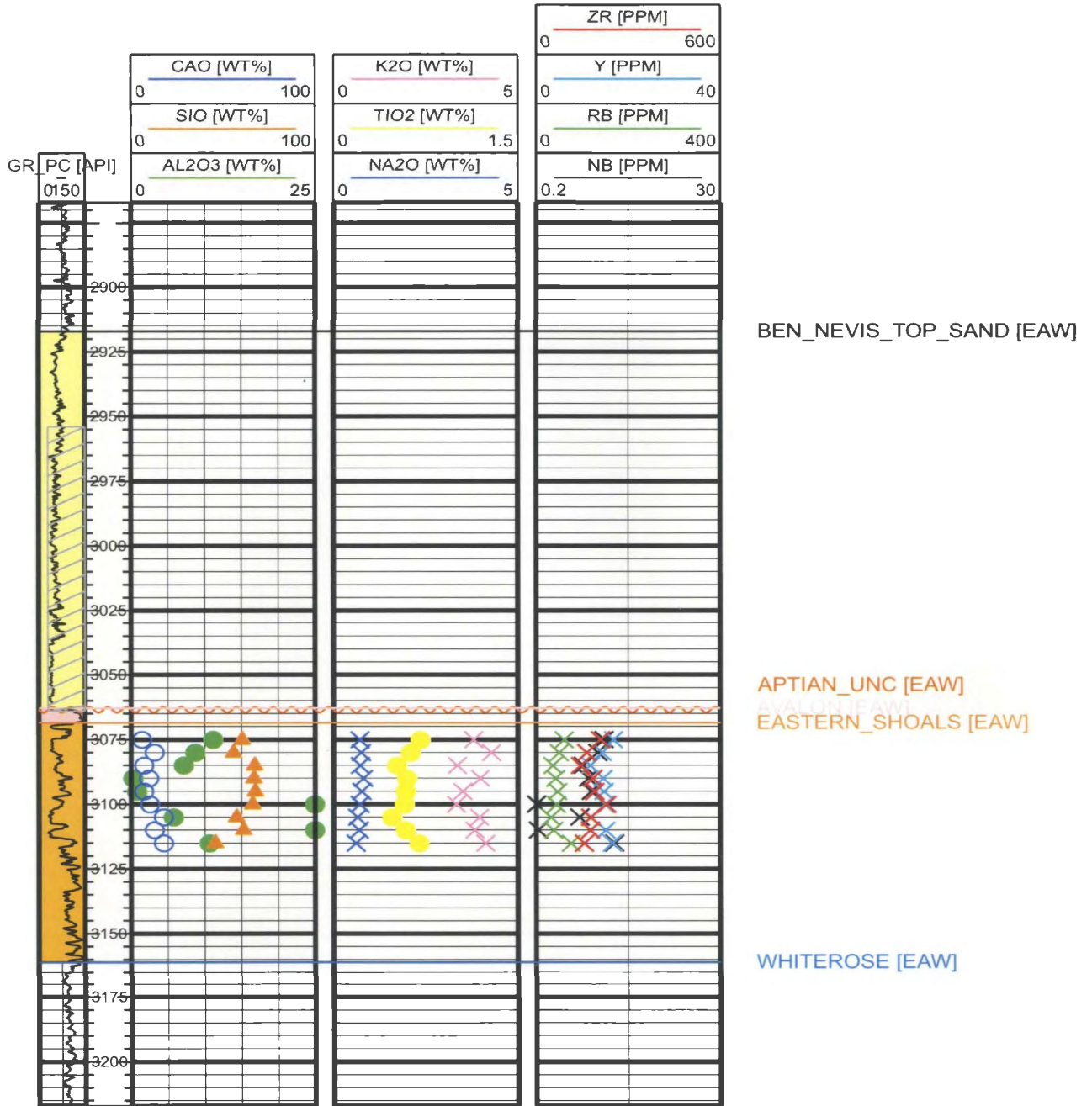
EASTERN\_SHOALS [EAW]

A\_MARKER\_MBR [EAW]

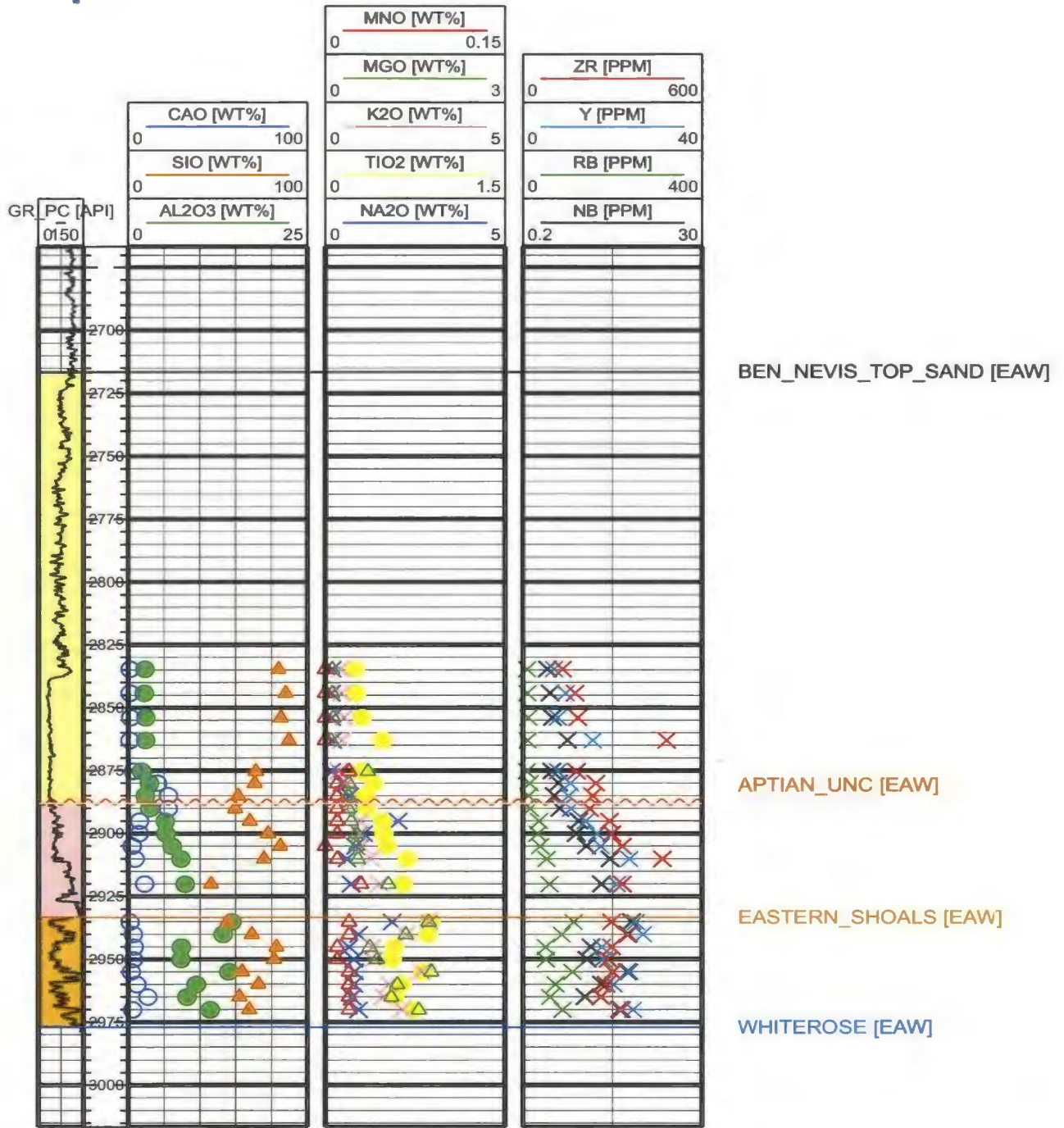
A\_MRK\_MBR\_B [EAW]

WHITEROSE [EAW]

# N-30



# J-22-1



# E-87

